UNIVERSITY OF SOUTHAMPTON

FACULTY OF NATURAL AND ENVIRONMENTAL SCIENCES

School of Ocean and Earth Science

Volume 1 of 1

A high-resolution environmental and climate record of change in the Holocene sediments of Windermere, UK

by

John James Fielding

Thesis for the degree of Doctor of Philosophy

November 2017

UNIVERSITY OF SOUTHAMPTON

ABSTRACT

The Holocene (11,750 Yrs. B.P. – present day) provides valuable examples of climate change in response to natural and anthropogenic forcing, by which future forecasting models can be validated. However, reliable climate and environmental observations rarely extend beyond the past 200 years. In this case proxy-based reconstructions can extend the record further.

The sediments and water of Windermere, NW England, have been studied since the 1930s. These studies show the potential of the sediments to create a record of environment and climate change which extends from the Pleistocene to the present day. It's location in the NE Atlantic region means it is ideally suited to record changes in climate and environment which are affected by globally important systems such as the North Atlantic Oscillation, Atlantic sea surface temperatures and the North Atlantic Currents.

This thesis aims to firstly provide preliminary results of a multiproxy study of the whole Holocene sediment sequence from Windermere's North Basin. A combination of organic, geochemical, and sediment microfabric analysis complemented by a chironomid inferred mean July temperature and pollen community reconstruction show the potential for the Holocene sediments of Windermere to record major climate events such as the 4.2 k. Yrs. B.P. cooling event. More detailed analysis has identified mass transport deposits (MTDs) in the early Holocene, likely caused by seismic instability induced by isostatic readjustment following deglaciation.

The sediments of Windermere have also been impacted by anthropogenic activities since at least the beginning of the industrial revolution. However, the full impact of this activity is as yet unknown. With this in mind this thesis aims to provide a detailed history of anthropogenic impacts on the water column and sediments. Using gravity cores collected from Windermere in 2014 this thesis presents a novel combination of techniques to relate microscopic sediment fabric features to lake-basin scale processes. Together microfabric and geochemical methods enabled the identification of MTDs which, despite bioturbational mixing, can be dated to 1979 and 1979-1980 respectively. The timing of these features make a likely trigger the 4.7 ML 1979 Carlisle earthquake. Slope failure was likely to be the result of preconditioning principally by increased sediment in-wash as a result of anthropogenic activities. This study constitutes the first evidence of seismic activity-induced MTDs

preserved in lake sediments in the UK and is published in the Journal of the Geological Society of London.

Further to this, this study presents the results of a multi-method organic- and geochemical, and sediment fabric analysis, applied to reconstruct the history of eutrophication and pollution in Windermere. Eutrophication developed in the late 19th and earliest 20th centuries and is marked by changes in the sediment microfabric, organic chemistry and geochemistry. Δ13C values show increased lake productivity is coeval with Pb, Zn, Cu, Hg, and As enrichment. Δ15N values in the South Basin sediment correlate with Zn, Hg and Cu, suggesting a major source of pollution to be from human sewage or farm runoff marked by isotopically heavy nitrate. In peak eutrophic conditions, a strongly reducing environment promoted Fe dissolution and the formation of anglesite-barite mineralisation, hitherto undescribed in lake sediments. Partial recovery is shown to occur after 1980 across both basins, but elevated $\delta^{15}N$ in the South Basin shows the continued impacts of sewage discharge. Results also show elevated concentrations of Mn, Fe, Ba, and As in the surficial sediment.

Scanning Electron Microscope (SEM)-led methods additionally identified preserved diatom algae seasonal blooms, some of which may be matched with bloom occurrence record from Windermere. Millimetre-scale laminations of Fe and Mn minerals are also further analysed from the surface and pre-eutrophication intervals, and are shown to record seasonal cycles of lake ventilation. Results also show tight coupling of Fe and P, which indicates the potential redox-driven release of P to the water column with implications for lake eutrophication.

This study highlights the power of microstratigraphic techniques in the recognition and characterisation of event layers in sediments where bioturbative disruption has occurred.

FACULTY OF NATURAL AND ENVIRONMENTAL SCIENCES

Palaeolimnology

Thesis for the degree of Doctor of Philosophy

A HIGH-RESOLUTION ENVIRONMENTAL AND CLIMATE RECORD OF CHANGE IN THE HOLOCENE SEDIMENTS OF WINDERMERE, UK

By John James Fielding

Table of Contents

Table of Tables

Table of Figures

Academic Thesis: Declaration Of Authorship

I, ...

declare that this thesis and the work presented in it are my own and has been generated by me as the result of my own original research.

A high-resolution environmental and climate record of change in the Holocene sediments of Windermere, UK

I confirm that:

1. This work was done wholly or mainly while in candidature for a research degree at this University;
2. Where any part of this thesis has previously been submitted for a degree or any other qualification at this University or any other institution, this has been clearly stated;
3. Where I have consulted the published work of others, this is always clearly attributed;
4. Where I have quoted from the work of others, the source is always given. With the exception of such quotations, this thesis is entirely my own work;
5. I have acknowledged all main sources of help;
6. Where the thesis is based on work done by myself jointly with others, I have made clear exactly what was done by others and what I have contributed myself;
7. None of this work has been published before submission

Signed: .....

Date: .....

Acknowledgements

Acknowledgements: We thank the British Ocean Sediment Core Research Facility for use of the facilities and support. This work was supported by the NERC Radiocarbon Facility NRCF010001 (allocation numbers 1856.1014 and 1736.1013). Funding: This research was supported by a University of Southampton Studentship Grant and a Natural Environmental Research Council Studentship Grant (NE/L50161X/1).

It is with a heavy heart I dedicate this text to Barrie Edmund Dakers, a much loved Great Grandad, Grandad, Dad, Husband and friend whose generous support, kind advice and love made this study possible.

I would like to deeply thank my academic supervisors Alan Kemp, Jon Bull, Pete Langdon, Carol Cotterill, and support staff Richard Pearce, Dan, Matt and John, Megan Spencer, Cath Langdon and Robert Scaife whose support has ensured my completion and without the help of which this study would be impossible. I would like to thank Professor Ian Croudace for his contribution of the bulk WD-XRF, ^{137}Cs and ^{210}Pb data, and help in interpretation.

It is with much joy that I also dedicate this study to beloved friends and family whose help advice and support are invaluable. While enumerable, many of the most import contributors to this study (fifty shades of brown) include; Mam and Dad, Lol, Nana, Tom and Jonny, Adeline Dutrieux, Dr. Rachael X. Avery, Dr. Manon P.L. Durret, Dr. Cat Burd, Frenchies, Dr. Tim Van Peer (Dr. Magneto), Padwell road buoyz (Drs. Stu, Josh, Matt, Amy, Sara, Nico, Millie), lunch time crew and a seagull.

Glossary of Terms

Allochthonous: Sedimentary material with origins outside the lake, this includes from within the catchment and beyond.

Authigenic minerals: Minerals which were generated in situ.

Autochthonous: Sedimentary material with origins within the lake or lake sediments, this includes remains of aquatic insects.

Cultural Eutrophication: Eutrophication caused by, or enhanced by anthropogenic activity.

Gyttja: An organic rich sediment which has been deposited in eutrophic waters. As the sediments are formed in typically dysoxic or anoxic conditions they can also be sulphur rich.

Hypolimnetic: Deeper water in a stratified lake that can be chemically and/or thermally distinct from the upper (**epilimnion)** waters. In thermally stratified lakes **Hypolimnetic** waters lie beneath the thermocline.

Mass Transport Deposit: Sedimentary formations within a stratigraphic successions that were formed by remobilized sediment transported downslope by gravitational processes.

Microlithostratigraphy: The stratigraphy of sediments considered on µm scales.

Redox: Oxidation and reduction reactions as complementary processes.

Sediment Quality Standard: Quantifiable figure of a substance in sediments above which quantities are harmful to health or have adverse biological effects. Sediment Quality Standards are normally advisory but exceedance of these values in some countries can be met with mandatory remediation measures.

Turbidites: Sedimentary deposits formed after material settles from a turbidity current.

Warm Monomictic Lake: Standing bodies of water that become thermally stratified during summer. Stratification is caused by a density difference between the warm surface waters (the epilimnion) and the colder bottom waters (the hypolimnion). Cooling of the surface waters in winter leads to the breakdown of the thermal stratification and mixing once a year.

List of abbreviations

(μ)XRF	X-Ray Fluorescence analysis (on a μm scale)
BOSCORF	British Ocean Sediment Core Facility
BSEI	BackScatter Electron Image
CEH	Centre for Ecology and Hydrology
CF:CS	Constant Flux: Constant Supply
CIS	Core Imaging System
C-IT	Chironomid Inferred mean July Temperature
CTS	Covered Thin Section
EDS	Energy Dispersive X-ray Spectroscopy
ED-XRF	Energy Dispersive X-Ray Fluorescence
EMS	European Macroseismic Scale
LIA	Little Ice Age
LSR	Linear Sedimentation Rate
ML	Local magnitude
MTD	Mass Transport Deposit
NAO	North Atlantic Oscillation
NERC	Natural Environmental Research Council
PTS	Polished Thin Section
SEM	Scanning Electron Microscope
SQS	Sediment Quality Standards
TOC	Total Organic Carbon
WD-XRF	Wavelength Dispersive X-Ray Fluorescence

WFD	Water Framework Directive
WSI	Water Sediment Interface
Yrs. (cal.) B.P.	(calibrated) Years before present (relative to 1950 A.D.)

Chapter 1 Introduction

1.1 Palaeolimnology

Sediments typically comprise of a mineral and organic component, changes in which are heavily influenced by a suite of environmental and climatic drivers. As such the measurement of geochemical, organic, or physical properties of sediments with depth (palaeolimnology) has the potential to serve as sensitive recorders of environmental changes and events driven by climatic, anthropogenic, or even tectonic processes (Smol 2010; Naeher et al. 2013; Schlolaut et al. 2014). Due to their proximity to major sedimentary inputs such as rivers, and high productivity, sedimentation rates in lakes, or restricted marine basins such as fjords, are typically two orders of magnitude higher in comparison to marine sedimentary archives. This allows for the preservation of higher resolution records (Johnson 1984; Piovano et al. 2014). In such cases, the study of ancient lake sediments can yield annual or even seasonal-resolution records of past lake conditions (Zolitschka 1998; Zolitschka et al. 2015a; Schimmelmann et al. 2016). In addition, because sediments can originate from both within the lake catchment or beyond (allochthonous) and from within the lake (autochthonous), palaeolimnological studies have the potential to reconstruct both basin wide and regional scale process. Depending on a number of factors including the latitude, altitude, catchment size and nutrient input the balance of allochthonous input compared to autochthonous input can vary from lake to lake, and in many lakes can even vary seasonally (Pickering & Sutcliffe 2001; Rautio et al. 2011). Thus a careful understanding of the lakes setting and seasonal regime is needed to understand and interpret proxy palaeolimnological records accurately (Birks & Birks 2006).

Within lake sediments robust multi-technique chronologies can be built using a range of dating methods which include, but are not limited to, radioisotope (^{14}C, ^{137}Cs, ^{210}Pb), tephra, annual lamination (varve), palaeomagnetism and pollen based chronologies, which can be verified by comparing event stratigraphy to archival records where available. However, erosional processes such as terrestrial ice flow (especially at high latitudes or in mountainous areas), or simply the comparatively young age of a lakes formation when compared to sea floor can mean that very few lakes contain records on a time scale in excess of thousands of year (Zolitschka et al. 2015a)

1.2 Holocene climate and environment palaeolimnology

The Holocene, ~11,700 years before present (y. b.p.) to the present day, represents a period of relative climate stability in comparison to the last glacial period (Johnsen et al. 2001). The Pleistocene-Holocene boundary represents the last large, orbitally derived climatic change, where abrupt warming, especially at high latitudes, lead to the end of persistent glacial conditions (Walker et al. 2009). However, particularly in the early Holocene, stable climate was punctuated by short-lived and abrupt climate events, such as the cold events at 11.3–11.1, 9.3, and 8.2 k. y. B.P. (Björck et al. 1997; Rohling & Pälike 2005; Rasmussen et al. 2007). These short lived decadal to centennial scale events have often been linked with the disruption of ocean circulation brought about by the abrupt release of melt water to the North Atlantic following the collapse of large ice sheets (Elmore et al. 2015). Proxy records in Britain show that temperatures during these events could be 1.6 °C cooler than the Early Holocene average (Lang et al. 2010), making their understanding crucial. Prominent centennial and multi-millennial scale climate shifts have also occurred during this period, such as the Holocene Thermal Maximum (HTM) (Renssen et al. 2009) and the Little Ice Age (LIA) (Mann et al. 2009).

The Holocene provides valuable examples of climate change in response to natural and anthropogenic forcing, by which future forecasting models can be validated (McCarroll et al. 2013; IPCC 2014). However, particularly concerning climate events and shifts there is ambiguity in the timing, geographical extent and even the nature of the climate change (Wanner et al. 2011). Reliable instrumental climate observations and environmental records rarely extend further than the past 200 years (Barker et al. 2004), making proxy-based climate and environmental reconstructions necessary to extend climate records through the Holocene. Palaeolimnology has been successfully applied in a range of locations worldwide in recording Holocene climate change (Catalan et al. 2013), including but not limited to Europe (Magny et al. 2003; Baier et al. 2004; Langdon et al. 2004), the Near East (Eastwood et al. 2007), Central Asia (Horiuchi et al. 2000) the near Arctic (Axford et al. 2013) and the Antarctic (Jones et al. 2000).

1.3 Recording anthropogenic change

Lakes and freshwater systems provide a crucial natural resource and a wide range of services such as a municipal water source (Fowler et al. 2007), flood mitigation (Thampapillai & Musgrave 1985), fisheries and refuge for rare and protected species

(Dudgeon et al. 2006; Maberly & Elliott 2012). Despite this many freshwater lakes and catchments are under increasing pressure from anthropogenic activities. Among these is cultural eutrophication, caused predominantly by excess Phosphorus (P) and Nitrogen (N) enrichment (Richardson & Jørgensen 1996), and driven by population increase, agricultural intensification and industrialisation. Eutrophication has caused a major shift in abundance and diversity of aquatic species with major implications for the above services (Correll 1998). In addition, and often in conjunction with other stressors such as eutrophication, lakes can also been left with a legacy toxic heavy metal enrichment from industrial point and diffuse sources (Förstner & Wittmann 2012), the economic impact of which is estimated to be £75-114 million per year in England and Wales alone (Pretty et al. 2003; Harvey et al. 2012). Further amplification and increased impact of these stressors is also caused by anthropogenic climate change (Williamson et al. 2009), for example through prolonged thermal stratification or additional productivity. All these elements make the restoration of freshwater lakes a priority.

The European Union Water Framework Directive (WFD) (2000/06/EC) legally obliges stakeholders to return waterbodies to "good ecological and chemical status" with reference to pre-anthropogenic chemical, ecological and environmental conditions. However, in areas with freshwater bodies affected by anthropogenic stressors records of climate, environment or hydrology rarely extend beyond the recent past (Barker et al. 2004; Winfield & Fletcher 2014). In addition, chemical and ecological data is often unavailable, and even where archival records exist, the time range covered is typically only a few decades (Winfield & Fletcher 2014). Due to their potential for robust chronologies and their multi-proxy nature, palaeolimnological studies have been put at the forefront of reconstructing accurate chemical and ecological status beyond the age range of archival records (Sirocko et al. 2013).

1.4 Windermere

Windermere in the Lake District National Park is England's largest natural lake being approximately 17 km long with a maximum width of *ca.* 1.5 km. The lake is divided into a North Basin (max. depth 64 m) and a South Basin (max. depth 42 m) by a basement high (10 m average) within a glacial ribbon valley, which effectively separates the two basins into two distinct hydrological systems (Figure 1-1 Map of Windermere (1:220,000 map). Map of Windermere (1:220,000 map): The Windermere catchment with 200 m contour lines,

multibeam lake bathymetry, and sediment sample locations. Thick black line represents catchment boundaries of 1: Esthwaite Water, 2: Brathay River, 3: Rothay River and 4: Troutbeck, and blue lines the major water ways and lake boundaries. Major lakes are labelled in blue: 1 Windermere North Basin, 2 Windermere South Basin, 3 Esthwaite Water, 4 Rydal Water, and 5 Grasmere. Urban centres are highlighted in light brown. Inset: Location of Windermere in the British Isles (black box). Co-ordinates given in UTM. (Pearsall & Pennington 1973; Pickering & Sutcliffe 2001).

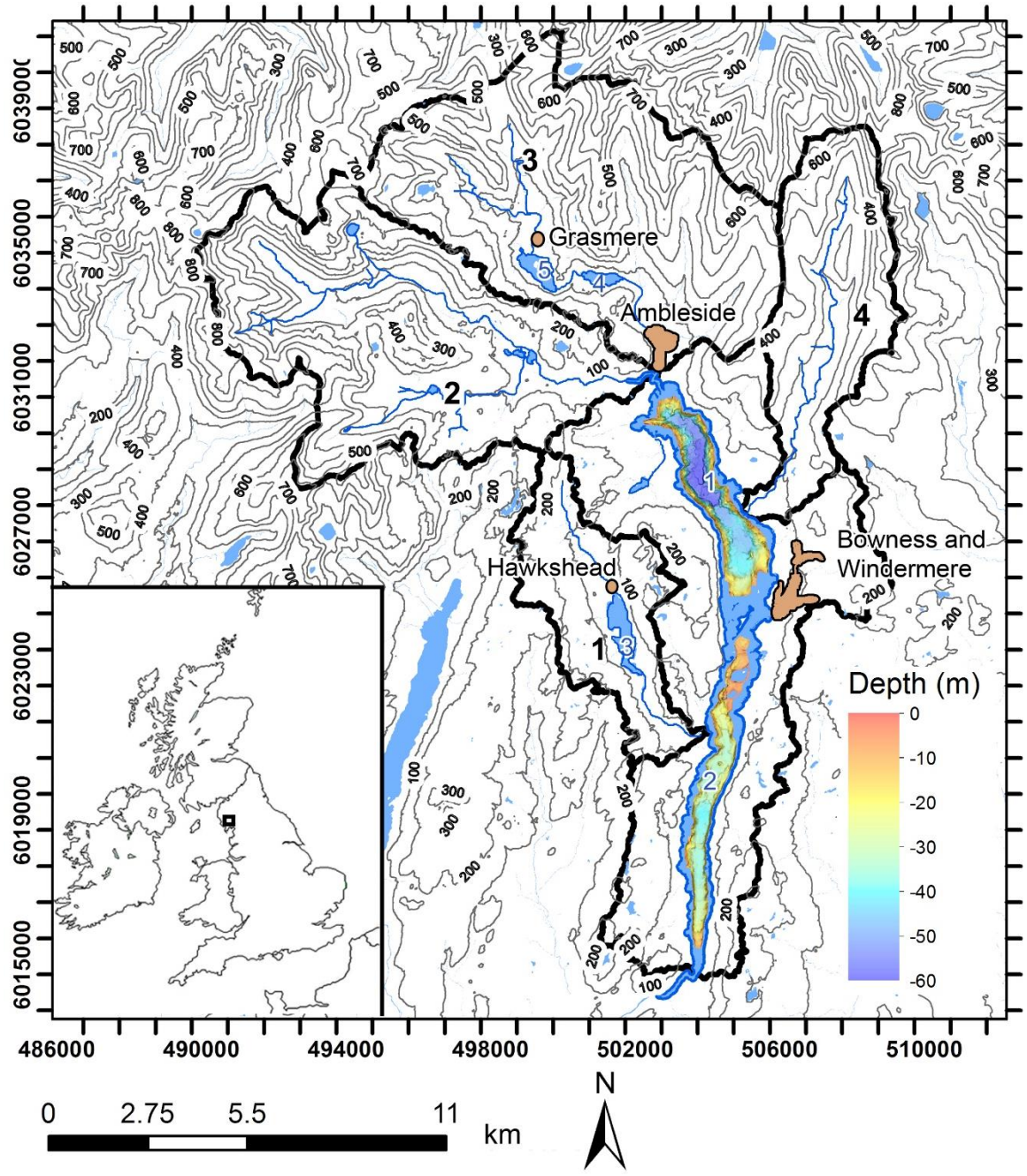

Figure 1-1 Map of Windermere (1:220,000 map). Map of Windermere (1:220,000 map): The Windermere catchment with 200 m contour lines, multibeam lake bathymetry, and sediment sample locations. Thick black line represents catchment

boundaries of 1: Esthwaite Water, 2: Brathay River, 3: Rothay River and 4: Troutbeck, and blue lines the major water ways and lake boundaries. Major lakes are labelled in blue: 1 Windermere North Basin, 2 Windermere South Basin, 3 Esthwaite Water, 4 Rydal Water, and 5 Grasmere. Urban centres are highlighted in light brown. Inset: Location of Windermere in the British Isles (black box). Co-ordinates given in UTM.

The mountainous, westerly maritime location of the Windermere catchment means that the climate is characterised by variations in globally important North Atlantic oceanic and atmospheric systems such as the Azores High and Icelandic Low giving the North Atlantic Oscillation (NAO), Atlantic sea surface temperature changes and the North Atlantic Currents (Wilby et al., 1997; Barker et al, 2004). Previous palaeolimnological studies have shown Windermere has an intermittently laminated sedimentary record extending from G-S 1 to the present day, with changes in sediment input closely reflect drivers such as climate and land use change, giving it the potential to create a high resolution climate and environment reconstruction (Table 7) (Pennington 1943, 1947, 1953, 1991, 1973; Barker et al, 2012; Miller, 2014).

1.4.1 Windermere anthropogenic change and time line

Human activity on Windermere and the catchment has a long history and has left a legacy of waterways and bodies impacted by heavy metal pollution and excess nutrient loading (

Table 1) (McGowan et al. 2012; Miller et al. 2014b).

The water column of Windermere has been regularly monitored and sampled for its physical properties, chemistry and biology since the 1940's by the Freshwater Biological Association and the Centre for Ecology and Hydrology (Pickering & Sutcliffe 2001; McGowan et al. 2012).

These long-term records along with previous palaeolimnological studies (outlined in table 7) have already recorded a wealth of information. Since the mid-19th century, development of population centres have led to increases in sewage discharge, and pastoral farming have resulted in eutrophication and associated contamination (McGowan et al. 2012). In addition, it is thought that a combination of sewage discharge and fossil fuel burning have left the sediments of Windermere enriched in heavy metals. Enrichments in some heavy metals (Pb, Zn, Cu) have been reported from analysis of a single core from the South Basin taken in 1975 (Hamilton-Taylor 1979).

Table 1: Time line of human impact on the catchment of Windermere (Pennington 1973; Claris et al. 1989; Wimble et al. 2000; Barker et al. 2005; Coombes et al. 2009; Dong et al. 2012; McGowan et al. 2012; Miller et al. 2014b; Woodbridge et al. 2014)

Age	Human activity and land use
Neolithic	• In the Windermere catchment as seen in evidence from sites such as the Langdale Axe Factory, phases of forest clearances for agriculture reduces tree cover and increase open land.
Iron age - Roman	• Continued expansion of agricultural is seen in pollen stratigraphies in Southern Cumbria.
7th – 11th centuries	• Saxon and Norse settlers continue phases of forest clearance and mixed agriculture.
16th and 17th centuries	

	• Following a period of relative stability in vegetation cover, changes in social and agricultural practices led to further upland clearances in Southern Cumbria. • These phase in clearance leads to high levels of soil erosion. • Mineral mining expanded significantly in Cumbria but remained limited in the Windermere catchment
18th century	
	• Expansion of agriculture, and industry reduces woodland cover further. • Soil erosion remains high • 1778 'a guide to the Lakes' is written and coincides with the beginning of small scale tourism to the Lake District. This along with increases in industry leads to population increase. • Pine plantations are introduced and expand in the latter half of the century and continue to grow into the early 19th century
19th century	
	• The population of the Windermere catchment expands from 3800 to 14 700 between 1801 and 1921. • Agricultural practices move to be dominated by pastoral farming and improved grassland, increasing the use of fertilisers through the 19th and 20th centuries • Railway reaches Windermere in 1847 • Establishment of the towns of Bowness and Windermere • Population expansion and agricultural intensification causes excess nutrient loading and eutrophication in Grasmere ~1850s • Mining operations in the head waters of the Windermere catchment significantly expand and some small scale mine workings are opened nearer to the North Basin at Place Fell with peak production in the 1850s and 60s. However, most are closed by the end of the 19th century • 1870 installation of sewage pipes and piped water in Bowness and Ambleside with gradual continued expansion thereafter.

20th century	• Sewage treatment works opened in Ambleside in 1886 (North Basin) and Beemire in 1888 (South Basin) • 1910 UK fertiliser manufacturing begins • Inadequate sewage treatment lead to the upgrade of the Ambleside site in 1914 • 1920s resident population stabilises at ~14000 in the catchment • Tower Wood sewage treatment works opened in the South Basin in 1924 • Hawkshead sewage treatment works opens ~1930s • 1951 Lakes District National Park designated • 1950s Tower Wood site is described as 'overwhelmed', and is upgraded in 1967 • Grasmere, Elter Water and Hawkshead sewage treatment works upgraded in early 1970s • In response to persistent eutrophication in Windermere, P stripping was introduced at the Ambleside and Tower Wood sewage treatment works in the early 1990s

1.5 Gaps in the knowledge and research aims

Windermere's location between the well-established Greenland ice core proxy climate records (North Greenland Ice Core Project, 2004) and Central Europe palaeolimnological proxy-record (Goslar et al, 1993), means a high resolution proxy climate record here would provide a bridge between the records which show diachroneity for major climate events and shifts of the Holocene (Schwander et al, 2000; Grove, 2001; Juckes et al., 2006; Dong et al, 2011). In addition, as discussed the climate and environment of Windermere are driven by globally important climate systems. To the authors' knowledge no such entire Holocene climate and environment record is available from lake sediments in the UK. As such this thesis will aim to develop a preliminary record and show the potential using well dated sediment sequences that extend to beyond the beginning of the Holocene.

Even with a comparatively long-term monitoring record, and previous palaeolimnological studies the timing and scale of anthropogenic activities effects on the water column and sediment of Windermere is not yet full constrained. In order for the water quality of Windermere to be restored and meet newly emplaced laws a full understanding of this is

necessary (Bennion & Battarbee 2007). In 2012 a joint BGS and University of Southampton project recovered piston cores taken from both basins (Miller et al. 2014), with the aim of investigating recent anthropogenic effects on the water column and sediments of Windermere. However, it was later discovered that these cores were missing the near-surface sediments (top 10-20 cm). The purpose of this study is to perform a comprehensive chemical and physical analysis of the near-surface sediments and water sediment interface (WSI) in four cores taken from mid-depths and deep basinal locations in both the North and South Basin of Windermere in 2014.

By applying techniques such as stable isotope analysis at higher resolution and by combining these with techniques such as microscopic sediment fabric analysis and µm scale geochemical analysis, this thesis will better assess the timing of anthropogenic activity such as nutrient and heavy metal loading in the Windermere catchments. Using the same methods the thesis will also better asses the scale of the influence of these activities on the water column and sediment. It is also not yet fully understood how sediments with a legacy of anthropogenic pollutants can effect water quality on Windermere, and investigation of this may help to shed light on freshwater bodies facing the same history of anthropogenic pollution.

Bathometric surveys conducted before the coring also identified several recent subaquatic slope failures and mass movements (Miller et al. 2013). Very little work has been conducted on lacustrine sub-aquatic mass movement events in the UK. With this in mind gravity cores will be used to investigate the nature, age and cause of these mass movement events.

1.6 Outline of thesis

Chapter 2 presents details of the methods and materials used in this thesis. These include physical details of Windermere and the catchment. It also presents the novel combination of techniques used for the analysis of sediment cores. Also included are a brief stratigraphy of the gravity cores taken in 2014, and specifics of the age depth model methods and results.

Chapter 3 presents preliminary results of a multi-proxy study of the well-dated Holocene sediments of Windermere. Sediments are investigated using a range of geochemical (itrax, and EDS lines scan and elemental map analysis) and organic and stable isotopes (TOC, TN, C:N, and $\delta^{13}C$) analyses. In addition, a chironomid inferred mean July temperature record and pollen community reconstructions are presented. To complement these findings,

199 microlithostratigraphic analyses of thin section optical and backscatter electron imagery are
200 presented. Results show that in the Holocene redox driven process controlled Mn
201 distribution, and that this can possibly be linked to changes in allochthonous carbon input
202 to the lake and phases of cooling. The chapter also identifies at least two mass transport
203 deposits in the Early Holocene.

204 Chapter 4 presents the use of a novel combination of techniques to relate microscopic
205 sediment fabric features to lake-basin scale processes for the identification of seismically
206 generated mass transport deposits (MTD) in the North Basin of Windermere. Results show
207 that two cores SC64 (shallow North Basin) and SC68 (deep North Basin) with robust
208 radionuclide chronologies contain correlative clay rich layers dated to 1979 and 1979-1980
209 respectively. More detailed microlithostratigraphic analyses identify the clay rich layers to
210 be a MTD consisting of a 'classic' debrite – turbidite structure, despite bioturbational mixing
211 of the original facies. The paper uses comparison with multibeam swath bathymetry and
212 sediment grab sampling to identify the origin for the mass flow as a distal slope failure of
213 the Troutbeck delta fan. The study uses further comparison with historic records to give a
214 likely trigger as the 4.7 ML 1979 Carlisle earthquake. Evidence for preconditioned failure
215 by increased sedimentary biogenic gas production and sediment in-wash as a result of
216 anthropogenic activities, coupled with sediment disruption and dredging is discussed. The
217 paper highlights the power of microstratigraphic techniques in the recognition and
218 characterisation of event layers in sediments where bioturbative disruption has occurred.
219 It is also, to the author's knowledge, the first evidence of seismic activity-induced MTD
220 preserved in lake sediments in the UK. The paper is due to be published in Journal of the
221 Geological Society of London.

222 Chapter 5 reports the results of a multi-method geochemical and sediment fabric analysis
223 applied to reconstruct the history of eutrophication and pollution of Windermere. Organic
224 geochemistry is coupled with sediment microfabric analysis to show the timing and impact
225 of cultural eutrophication in Windermere since the 19th century. Furthermore, using WD-
226 XRF and itrax core scanning techniques the chapter investigates trace element enrichment
227 as both a result of anthropogenic pollutants (Pb, Zn, Cu, Hg, and As) as well as a result of
228 redox driven geochemical focusing (Mn, Fe). Sedimentary Pb and As are shown to be
229 significantly higher through early and mid-20th century in the North Basin and late 19th to
230 mid-20th century in the South Basin, coinciding with lows in redox sensitive metals Fe and
231 Mn. Findings also highlight the importance of redox driven cycling of elements, in
232 particular As, to maintaining lake 'health' with reference to sediment quality standards and

current European legislation. As and Pb both exceed the upper legal limit of sediment quality standards set by the Netherlands and Canadian Governments in a least one of the core sites. Findings showed that the incidence of sediment anoxia increased and was most intense in the deep basin, where microscope analysis of sediment fabrics showed that benthic activity intermittently ceased. Strongly reducing conditions in the sediment promoted Fe-reduction and the formation of unusual Pb-bearing barite mineralisation, hitherto only described from toxic mine wastes and contaminated soils. From the late 20th century (1980) there is a partial recovery but elevated $\delta^{15}N$ of organic matter shows the continued impacts of sewage discharge to the South Basin.

Chapter 6 showcases the use of a Scanning Electron Microscope (SEM)-led approach to reconstructing seasonal-scale processes in lake basins. Using a combination of macro and micro scale sediment fabric analysis the study shows how individual historic diatom blooms can be identified and matched with historic phytoplankton record from the Freshwater Biology Association. On a broader scale a shift in the dominance of species *asterionella* to *aulacoseira* around the 1990s could be tracked in the sediment. The study also highlights the analysis of µm scale Mn and Fe mineral laminae from the surface sediments and from a pre-eutrophication interval from the deep North Basin. This more detailed analysis showed that laminae, which when compared to the sedimentation rate were likely to be annual or multi annual in resolution, can be used to record seasonal cycles of lake ventilation. Analysis of the sediment water interface shows the coupling of Fe and P at the modern lake bed of Windermere. Furthermore, the chapter shows the potential redox driven release of P along with Fe during phases of bottom water dysoxia. In addition, Mn, Fe, Ba, and As in the surficial sediment provide evidence for dynamic redox mobilisation of potentially toxic elements that may also be released to the lake waters.

Chapter 7 summarises the main conclusions that can be drawn from this study as well as outlining areas of future work.

Chapter 2 **Materials and Methods**

2.1 Study site

Windermere in the Lake District National Park is England's largest natural lake and has long been a popular tourist attraction (Figure 2-1**Error! Reference source not found.**). The lake is 17 km long with a maximum width of *ca.* 1.5 km, and is divided into a North Basin (max. depth 64 m) and a South Basin (max. depth 42 m) by a basement high (10 m average) within a glacial ribbon valley, which effectively separates the two basins into two distinct hydrological systems (Pearsall & Pennington 1973; Pickering & Sutcliffe 2001).

The larger North Basin has a surface area of 8.1 km^2 and volume of 202.1 x 10^6 m^3 while the South Basin has a surface area of 6.7 km^2 and a volume just over half that of the North at 112.2 x 10^6 m^3 (Maberly et al. 2011). The Windermere catchment is characterised by high levels of precipitation, with 4000 – 5500 mm per year in the most elevated parts of the catchment (CEH, 2012). The catchment is 247 km^2 (catchment ratio: lake = 16.7:1) and the main inflows are from the rivers Rothay and Brathay at the northern end of the North Basin. Primary inflow to the South Basin comes from the North Basin and from Cunsey Beck that drains the small seasonally anoxic lake, Esthwaite Water. Outflow is at the south end via the River Leven, with retention times in the North and South Basin of 185 and 100 days respectively (Maberly et al. 2011). The catchment geology includes part of the Borrowdale Volcanic Group comprising of andesites, with some basalts, rhyolites, tuffs and agglomerates to the north and the Windermere Group (Silurian slates and flags) to the South, separated by the Coniston limestone (Miller et al. 2013). Land cover is largely grass (62.9%) and woodland (19.7%), other coverage types are mountain/ upland heath/ bog (4.6%), arable and horticultural (4.3%), and urban (0.6%) (Rowland 2015). Small urban centres in the catchment include Ambleside, Grasmere, Elterwater, Bowness, Windermere and Hawkshead.

The lake is classified as warm monomictic, becoming stratified in early summer with re-mixing usually in late October/ early November in the South Basin and a little later (November/ December) in the North Basin (Pickering & Sutcliffe 2001; McGowan et al. 2012). At present anthropogenic nutrient loading has led to Windermere's North Basin seasonally fluctuating between mesotrophic – meso-eutrophic, and the South Basin between mesotrophic – eutrophic (Maberly et al. 2011). The larger volume and depth, (table

290 2) of the North basin mean that the nutrient loading is more dilute when compared to the
291 smaller and shallower South Basin, causing the South Basin to be more productive, and the
292 minimum oxygen concentrations to be lower (table 2).
293

294 Table 2: Physical and hydrological characteristics of Windermere North and South Basin,
295 *George et al. (2004), **Trophic classification for 2010 (Maberly et al. 2011),
296 ***Annual minimum concentrations of oxygen at depth in 2010 (Maberly et al.
297 2011).

	North Basin	**South Basin**
Length (km)*	7	10
Area (km^3)*	8.05	6.72
Max depth (m)*	62	44
Volume (10^6 m^3)*	201.8	112.7
Retention time (days)*	185	100
Trophic state**	Mesotrophic – Meso - eutrophic	Mesotrophic – Eutrophic
Minimum oxygen concentration at depth (g m^{-3})***	7.19	3.07

298

299 2.2 Previous Windermere study

300 The sediments of Windermere have been extensively studied in the past (Table 7) Table 7:
301 a compilation of previous palaeolimnological work from the Windermere catchment.and
302 these sediments showed the potential for proxy climate and environment reconstruction
303 extending back to at least GS-1 (Pennington 1943). Of these investigation those done by the
304 FBA and in particular Winnifred Pennington are the best known. These classic works were
305 among the first to discuss the chronological extent and climate characteristics of the Bølling-
306 Allerød climate event in Britain where it is still known as the Windermere Interstadial
307 (Pennington 1947; Coope & Pennington 1977). Other works have investigated the
308 sediments potential to record the anthropogenic effects on the lake (Pennington 1973;
309 Hamilton-Taylor 1979).

Work in 2011 and 2012 on the lake bed and subsurface studies included single- and multi-channel Boomer profiles and 3D seismic reflection surveys (Vardy et al. 2010; Lowag et al. 2012; Pinson et al. 2013), as well as a detailed lake bed survey using multibeam swath bathymetry complemented by ROV bottom photography and sediment grab sampling (Miller et al. 2013). This work identified well preserved laminated sediments (Miller et al. 2013) and led to the initial aim of collecting a full Holocene and late glacial record of climate and environment.

2.3 Coring

2.3.1 Piston core locations (rationale for location)

With this in mind cores were located at points which were shown through ultrasound and bathymetry to be least likely affected by erosion from mass movement events. Locations were as near to the centre of depositional basins placing them away from steeper sided slopes which are more likely to fail and at the centre of gravity driven accumulation. Bathymetry also showed that anthropogenic activity like dredging had disturbed sediments in some parts of the lake and so these areas were also avoided (Miller et al. 2013; Miller 2014).

2.3.2 Piston coring methods

In April 2012 a joint British Geological Survey (BGS) and University of Southampton sediment coring field survey retrieved 9 piston cores from the North and South basin using a Uwitec piston corer and anchored platform with A-frame (table 3).

The Uwitec piston corer was deployed from the platform by lowering the ground plate, guide shaft and re- entry cone as a single unit to the sediment surface (http://www.uwitec.at/). The piston corer retrieved up to 10 m of sediment in 2 m x 9 cm section. Sections were end to end and the depth of each section was calculated from the number of piston rods fitted between the piston retainer and the piston head (i.e. below the sediment surface). Each 2 m section was retrieved by hammering the corer tube and core liner into the sediment. As the corer descended the piston forced pressurised water between the core liner and corer tube. At 2 m intervals a rubber hydraulic core catcher was deployed at the base of the corer tube, retaining the sediment, extra core liners and piston rods were added and the core hammered further into the sediment.

Recovery of the core followed the reverse of deployment, and sediment was raised in 2 m sections, with extension tubes and rods removed in stages. Following retrieval sediment cores were placed horizontally, the core catcher removed and the core liner capped and sealed. Cores were labelled in 1 m sections with core number (ranging from 49 - 68), corer type (PC for piston core) and section number (labelled alphabetically from shallowest to deepest). A more detailed description of the coring is found in Miller (2014).

This thesis focuses on PC68 collected from the deep North Basin site, but also includes results from PC64, PC67 and PC 57 (Figure 2-1).

Table 3: Piston cores collected in 2012.

Core code	Location	Easting	Northing	Core length (m)
PC68	**North Basin (Deep)**	**502902**	**6029135**	**10**
PC64	North Basin (Shallow)	504184	6024639	8
PC67	South Basin (Shallow)	503764	6020856	8
PC57	South Basin (Deep)	503288	6018757	6

2.3.3 Grab samples

In addition to the four piston cores retrieved in the 2012 coring campaign several gravity cores and grab samples were also retrieved. A full list of these are shown in Miller (2014). With reference to chapter 4 owing to their proximity to the Troutbeck delta failure scarp, high resolution photographic data from a gravity core (core 53), and a grab sample taken were also used (Figure 2-1).

2.3.4 Gravity coring

It was first determined that the WSI and an unknown amount of sediment had not been collected by comparison of radionuclide results in the PC. Caesium -137 is only generated during nuclear fission and is present in the environment due to weapons testing or releases from nuclear reactors (Ritchie & McHenry 1990). In sediments in Britain, and in those of previous studies in the Windermere catchment (Pennington 1973; Ritchie & McHenry 1990), the greatest peaks in ^{137}Cs were found to correspond to 1963 peak bomb testing and the 1986 Chernobyl accident (see chronology section for more detailed method). The ^{137}Cs data

364 presented in Miller et al. (2014b) showed no peaks in ^{137}Cs in the core tops, possibly
365 indicating the loss of sediment from later than at least 1963. Furthermore, closer inspection
366 of resin embedded thin sections form the core tops of PC 57 and PC68 showed evidence for
367 heavily disturbed sediments including disjointed lamina and fluid escape structures.

368 Since piston coring had removed an unknown amount of sediment at the core tops, a series
369 of gravity cores were used to recover the WSI and up to 46 cm of sediment. Retrieval of a
370 full record from the modern sediment surface to beyond the industrial revolution was vital
371 to completing the aim of assessing the anthropogenic impact of sediments and water
372 quality at Windermere.

373

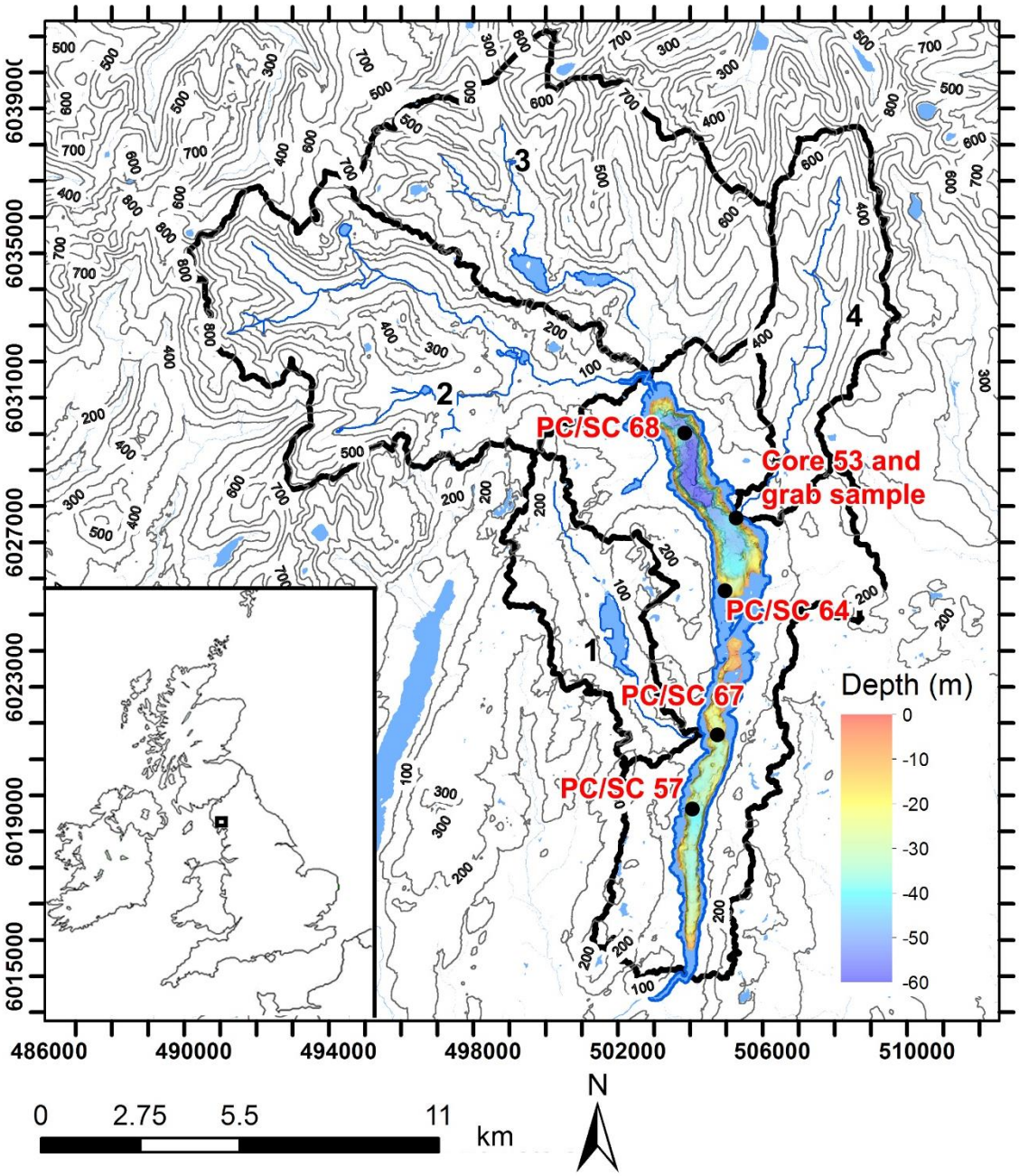

Figure 2-1: Map of core locations. 1:220,000 map of the Windermere catchments labelled: 1 Cunsey Beck, 2 Braythay, 3 Rothay, and 4 Trout Beck. Also shown 100 m contour lines, multibeam lake bathymetry, and core, and grab sample, locations. Co-ordinates given in UTM. Inset: Location of Windermere in the British Isles (black box), and Carlisle Earthquake epicentre (black star).

2.3.5 Gravity coring method

With the assistance of the Freshwater Biology Association (FBA) aboard the FBA's John Lund two gravity cores were collected from each of the four PC sites using (Figure 2-1, Table 4: 2013 gravity core locations, water depth and amount of sediment recovered. Cores

analysed in this study are in bold.**Error! Reference source not found.Error! Reference source not found.**) a Uwitec 86 mm diameter gravity corer and a clear core liner. A hand held GPS system and on board GPS system was used to verify and record the position of the cores. The gravity cores recovered the water-sediment interface and up to 46 cm of sediment. Core liners were cleaned down and the core was assessed for disturbance during sampling. If disturbance was considered minimal the core length and a basic stratigraphy were recorded. Following this sodium polyacrylate was added to the captured water overlaying the surface sediments in order to solidify the water and preserve the water-sediment interface. Here care was taken to only add the sodium polyacrylate in small aliquots until the point that all the water is solidified. Adding to much can cause the solidified water to expand and push down on the water sediment interface potentially damaging the original water-sediment interface. Cores were capped, sealed and stored upright for transport back to the National Oceanography Centre (NOC).

Table 4: 2013 gravity core locations, water depth and amount of sediment recovered. Cores analysed in this study are in bold.

Core code	Location	Water Depth	Easting	Northing	Core length
SC 68 – 1	North Basin	53.7	502913	6029123	0.42
SC 68 – 2	**North Basin**	**53.7**	**502902**	**6029135**	**0.45**
SC 64 – 1	**North Basin**	**25.6**	**504170**	**6024651**	**0.37**
SC 64 – 2	North Basin	25.6	504184	6024639	0.28
SC 67 – 1	**South Basin**	**29**	**0503736**	**6020840**	**0.37**
SC 67 – 2	South Basin	29	503764	6020856	0.35
SC 57 – 1	**South Basin**	**39.1**	**503288**	**6018757**	**0.39**
SC 57 – 2	South Basin	38.1	503288	6018757	0.36

2.3.6 Gravity core splitting

Gravity cores were split and processed at the British Ocean Sediment Core Facility (BOSCORF). Before splitting, cores were measured, followed by an assessment and recording of the stratigraphy and any post sampling shrinkage or slumping. Following the packing of the core to reduce disturbance to the sediments the core liner was split using low speed vibrating blades. To split the sediment into two work halves first a cheese wire

was run through the length of the core. Two metal sheets, one on top of the other, were then inserted and the two halves gently separated. Split core surfaces were then cleaned and excess sediment removed. Immediately after this both core halves were imaged using the GeotekTM MSCL-CIS and then a more detailed stratigraphy recorded.

2.4 Piston and gravity core processing

2.4.1 Microfabric analysis sampling

While typically avoided many lacustrine sequences contain MTDs and turbidites. Where included, these deposits can be used to reconstruct past events including seismic activity and floods (Schlolaut et al. 2014). Equally, sediments can also contain varves or other seasonal to decadal scale structures (Zolitschka et al. 2015b). These can include features such as palaeo-redox fronts in the form of ferromanganese rich lamina (Naeher et al. 2013). In order to interpret these features and build an accurate record of past climate or environment, careful analysis of the microfabric and structure of well-preserved sediments is sometimes necessary using microscopy and/ or µm-scale geochemistry (Kemp et al. 2001; Schlolaut et al. 2014; Zolitschka et al. 2015b). Ideally, this involves the analysis of annually laminated or varved records (Van Daele et al. 2014), but sediments are often subject to disturbance by biota even in environments with reduced water column turnover and resultant limited levels of bottom water oxygenation (Reynoldson 1987). Where sediments are disturbed by bioturbation the original structure may be obscured (McCall & Tevesz 1982). In particular, conventional optical microscopy of resin-embedded sediment may lack the necessary resolution to interpret microfabrics. An example comes from Hage et al. (2017) who found it difficult to distinguish burrows from fluid escape features using optical microscopy. To aid microfabric analysis by optical microscopy Back Scattered Electron Imagery (BSEI) can also be used (Krinsley et al. 2005). BSEI is effectively an ultra-thin section image showing a porosity and composition signal in resin embedded sediment, and so is more informative than the optical image that contains optical "noise" from the entire thickness of the thin section. While BSEI has been extensively used in the study of varved sediments (Dean et al. 1999), studies of other sediment features such as MTDs have primarily only used optical microscopy for the highest resolution observations (Schlolaut et al. 2014; Hage et al. 2017).

Sediments from both the gravity cores and piston cores were prepared for high-resolution microfabric analysis using the method outlined in Kemp et al. (1998), Dean et al. (1999) and

Kemp et al. (2001). In this method one of the split core halves was slab sampled (25.5 – 15 – 5 cm x 1cm x 10 cm) continuously with overlapping sections. The 1 cm-thick slabs were then digitally imaged using a GeotekTM MSCL-CIS. To further aid thin section microfabric analysis an x-radiograph of the slab was taken using a Hewlett Packard Faxitron X-radiography cabinet at 35 kVe for 10 seconds. A 2 cm section was then taken down the length of the slab, and underwent fluid-displacive resin embedding. To avoid sediment expansion or distortion during this process, subsamples were placed in muslin cloth and bound with stainless steel chicken wire. Care was also taken to avoid sediment disturbance by fluids replacement, by firstly the stepped replacement of water by ethanol over a two week period, and then the replacement of ethanol by resin over a minimum four week period. To this end sediment disturbance is calculated to be negligible. From these resin embedded samples 3.5 x 1 cm covered thin sections (CTS) for optical microscopy and 3.5-4 x 1 cm polished thin sections (PTS) for backscatter electron imagery were prepared.

Carbon coated PTS were imaged and analysed using a Carl Zeiss LEO 1450VP Scanning Electron Microscope (SEM). Using a combination of the photomosaic back scatter electron images (BSEI), higher magnification BSEI and optical thin section microscopy, sediment fabrics and mineral, and organic components were documented. Bioturbation was assessed by the degree of pelleting of the sediment and the percentage of pelletisation of individual microfacies was quantified by assigning the following designations <25% low or un-pelleted, 25- 75% partially pelleted, >75% pervasively pelleted.

In addition, gold coated stub samples for the analysis of diatom remains and sediment mineralogy were taken from the WSI and black organic sediments in all cores, and from selected diatom and mineral rich lamina in SC68. ~ 1mg samples directly from the slab surface were mounted using adhesive carbon tabs to 12mm specimen stubs, and gold coated.

For BSEI the SEM operating conditions were 20kV at a working distance (WD) of 19mm (focal length).

2.4.2 Geochemical analysis

In achieving the aim of creating a climate and environment record for the Holocene, geochemical analysis of sediments is crucial in tracking changes in input through K-rich clays, and in tracking changes in lake bottom water ventilation through changes in redox sensitive metals such as Mn and Fe. In more recent sediments geochemistry can also shed

469 light on the extent of anthropogenic pollution from heavy metals such as Pb or As, and in
470 tracking changes in excess nutrient loading (P) (Table 5).

471 Table 5: drivers of changes in sedimentary geochemistry and associated studies.

Element	Environmental or climatic driver	Study
K, Ti, Si	Terrestrial sediment input: Weathered clays from the Borrowdale volcanic group are K and Ti rich (Miller et al. 2013). Si is also common in durable minerals weathered from both the igneous and metamorphic-sedimentary (Silurian flags and slates) geology.	(Schlolaut et al. 2014; Plaza-Morlote et al. 2017)
Fe, Mn, Ba, As, S	Redox conditions of the water sediment interface: Mn, Fe reduced in anoxic condition and (re)precipitate in oxic conditions. Fe oxidises more rapidly (and reduces more slowly) than Mn. Increased Mn accretion can only occur under prolonged oxic conditions. Ba and As is often sequestered by Fe and Mn oxyhydroxides. Sulphide formation occurs in lakes sediments due to the brake down of organic matter in anoxic conditions.	(Sugiyama et al. 1992; Davison 1993; Farmer et al. 1999; Burke & Kemp 2004; Fakhraee et al. 2017)
Pb, Zn, As, Hg, Cu	Anthropogenic pollution: Enrichment of Pb, Zn, As, Hg and Cu to be associated with Mining, fossil fuel combustion and sewage treatment output.	(Miller et al. 2014b)

P	Excess nutrient loading: Increased levels of P are often found in excess in lake sediments affected by excess nutrient loading. P, along with N, is usually lacking in natural freshwater ecosystems, and thus is typically a controlling nutrient of productivity. Introduction of excess P can cause primary production to increase and lead to eutrophication.	(Correll 1998)

2.4.3 Itrax

Even in lake sediments with relatively high accumulation rates seasonal – annual scale changes can occur over <1mm (Naeher et al. 2013). To achieve the highest possible temporal resolution it is therefore important to measure geochemical changes over intervals equal to or less than the calculated annual sedimentation rate. The itrax Energy Dispersive X-Ray Fluorescence (ED-XRF) core scanner is able to achieve a 200µm sampling resolution. The core archive-half surface was analysed using an itrax ED-XRF core scanner (Croudace et al. 2006) with a scanning step size of 200 µm, and a scanning window of 22 mm – 0.002 mm (Croudace et al. 2006). Data points were excluded from the analysis where surface discontinuities caused the total number of counts to drop below 20,000 kcps. Data points with zero validity or a mean standard error of >5 were also excluded from analysis following recommended procedures. Elemental data (counts) was normalised by dividing it by total kilocounts per second (kcps) for each interval to account for changes in the core density and surface high between sample points and cores (Croudace et al. 2006).

2.4.4 Bulk WD-XRF

In the gravity cores in order to calibrate and complement the itrax ED-XRF semi-quantitative analysis, continuous 1 cm thick bulk samples were analysed via fully quantitative WD-XRF. Approximately 10g of sample was homogenised by grinding and powdering, and then compressed into pellets in accordance with the methodology in Croudace & Williams-Thorpe (1988). Results were obtained using a Philips Magix-Pro Sequential Wavelength Dispersive XRF Spectrometer (Almelo – Holland), fitted with a 4 kW rhodium anode x-ray tube.

The XRF was calibrated by Prof. Ian Croudace (GAU-Radioanalytical) using International Geochemical Reference Samples (GRS) obtained from the USGS (USA), CANMET (Canada), NIM (South Africa), CRPG-ANRT (France), JGS (Japan), and an external monitor (high stability doped glass) was used to ensure that calibrations remain robust and stable over long periods (years). Philips calibration software (SuperQ 4.0) was used to correct for interferences, inter-element effects and to calibrate the instrument. Assessments of accuracy are contributed to international intercomparison exercises (International Geochemical Proficiency Testing Scheme: GeoPT) for which samples are measured blind and subsequent reports produced. Accuracy and precision are typically 5% relative or better (2 σ). Detection Limits can be found in appendix D.

2.4.5 Fine scale geochemistry

To link the coarser scale XRF geochemical analysis, the PTS for selected intervals were analysed in the SEM by energy dispersive X-ray spectroscopy microanalysis (EDS) using an Oxford Instruments X-Act 10mm^2 area Silicon Drift Detector. In addition to the analysis of individual grains, elemental maps and line scans were generated. Chemical characterisation of mineralogy was aided by use of the AZtec Energy software system (v.3.1). Line scans were run at 20kV, a WD of 19mm, and a dwell time per analysis site of 60 seconds, with EDS data collected at ~5,000 cps. The calculated data have been acquired using standardless analysis, hence all results are normalized to 100%. Minimum detection limits are 0.195% for Na Kα and decreasing to 0.085% for Ca Kα (Goldstein et al. 2003). For direct comparison with SEM EDS at key intervals, the relevant PTS were also analysed by ED-XRF. To validate the mineral component of the debris lamina a 0.6 x 1 x 1cm sample was taken from 5.5 and 6.1 cm in SC64 and analysed by XRD using a Panalytical X'Pert Pro diffractometer with a Cu tube. Samples were ground for 8 minutes with 25% corundum in a McCrone micronizer in 5 ml of propan-2-ol. Samples were run from 2-76° θ and were compared with the ICDD 2016 mineral database.

2.4.6 TOC, TN, $\delta^{13}C$, $\delta^{15}N$

The molecular, elemental and isotopic compositions of organic matter in lake sediments has the potential to preserve palaeoenvironmental information and identify the provenance of organic material (Meyers & Lallier-Vergès 1999). Productivity in the lake or catchment, for example, is related to the sedimentary total organic carbon (TOC) and total nitrogen (TN). The ratio of these can be used to distinguish between an algal and a land-plant origin of

sedimentary organic material. Owing to the lack of cellulose (carbon poor) lacustrine algae typically have C/N values of 4-10, whereas plant matter will be much higher at >20 (Meyers 1994). The carbon isotope ratio is also useful in distinguishing source and even productivity due to the preferential uptake of ^{12}C by algae. However, due to the complex nature of photosynthetic pathways it is often necessary to interpret $\delta^{13}C$ in conjunction with other organic matter measurements (Meyers 1994; Hodell & Schelske 1998; Meyers & Teranes 2002).

Cores SC68 from the North Basin and SC57 from the South Basin were analysed for TOC, TN, $\delta^{13}C$ and $\delta^{15}N$. 1g samples were taken continuously at a frequency of 2cm and freeze dried for 48 hours. Between 13 to 15 mg were taken from 6 samples representing end member sediment types in both cores and were analysed for calcium carbonate ($CaCO_3$) content at the University of Southampton on an AutoMate + CM5015 coulometer. All samples were analysed for TOC, TN, $\delta^{13}C$ and $\delta^{15}N$ using a Elementar Vario Isotope Cube Elemental Analyser equipped with a TCD (Thermal conductivity detector) which is interfaced with an Isoprime 100 continuous flow isotope ratio mass spectrometer (IRMS). Acetanilide was used as an elemental standard for C and N and USGS40 and USGS41 as international reference materials for the normalisation of the isotope ratios.

PC68 was also analysed for TOC, TN and $\delta^{13}C$. 1g samples were taken at intervals and analysed by M. Leng, British Geological Survey using the same method as above.

2.4.7 Chironomid inferred mean July temperature (C-IT)

Chironomidae (*Insecta: Diptera*) are a diverse group of non-biting midges (~1000 European species) found throughout freshwater systems globally. Communities react to changes in environmental and climatic variables (Langdon et al. 2004; Langdon et al. 2008). By comparing changes in chironomid communities preserved in lake sediments with contemporary instrumental climate data, transfer functions have been developed, and have been successfully used to reconstruct quantitative July air temperature in the Late glacial and Holocene (Langdon et al. 2004; Lang et al. 2010). In multi-proxy palaeolimnology studies, chironomids can provide an air temperature record independent of sedimentary processes. Subsamples of 2x2x2cm were taken from archive halves of one core in each basin (+54-03/68 PC (north) and +54-03/67 PC (south)). Higher resolution sample spacing (4cm) was done through the key time periods of the late Holocene (0-150 cm in core 68; 0-35 cm in core 57), early Holocene and Pleistocene-Holocene transition (500-510cm in core 68; 180-210 cm in core 57), and was lower (16 cm) in the Mid Holocene (150-500 cm in core 68; 35-

180 cm), with the scope for return sampling if necessary. Chironomid extraction, slide mounting, identification and statistical and quantitative mean July air temperature reconstructions follows the method set out in Langdon et al. (2004).

2.4.8 Pollen

Pollen assemblages preserved in sediments are crucial to understanding past environmental and climate change as many vegetation types have very specific ranges in temperature and moisture (Bradley 1999). Evidence for cultural landscape change is also preserved in pollen assemblages. For example in the UK pollen has been integral in tracing phases of forest clearance and agricultural expansion throughout the Holocene (Woodbridge et al. 2014). Furthermore, because of the short lived nature of plant life cycles plant communities can respond very quickly to changes in climate and environment, and as such they are extremely effective in providing annual to decadal scale palaeoenvironment or climate reconstructions (Davis et al. 2003).

To this end a 27 sample pollen community study was conducted on PC68 by R. Scaife, University of Southampton. <1g samples were removed from the split core surface. Where there was insufficient pollen to complete even a preliminary community study (<40 individual gains) sites were resampled.

2.4.9 Archival data

Instrumental data includes a mean daily river flow record for the period 1939-2014 from four different sites at Newby Bridge at the outflow of Windermere. A combined annually resolved mean over-winter maximum phosphorus concentration for the period 1946–2007 was developed from an annually resolved phosphorus concentration (PO_4-P meaning orthophosphate as phosphorus) record for the period 1946 – 1997 from South Basin of Windermere (Parker & Maberly 2000), and a phosphorus concentration (PO_4-P, PO_4^{3-}) record from Windermere Tower Wood sewage treatment works outfall for the period 1979 – 2007 (Maberly 2008). Total monthly and annual precipitation (mm) for the period 1788-1795, 1802, and 1806-2000 came from the Central Lake district Precipitation record shown in Barker et al. (2004). From 2000-2014 total monthly and annual precipitation data (mm) came from Laurel Bank, Ambleside, was collected by Mr Bernard Tebay, and was provided by Stephen Maberly, Centre for Ecology and Hydrology. North Atlantic Oscillation index data for the period 1821-2014 came from Jones et al. (1997) (online record extended to 2016/17). Seasonal and annual mean air temperature (1932-2014) and wind speed (1950-

2014) was provided by Steven Maberly, Centre for Ecology and Hydrology, and was developed by combining records from Ambleside Sewage Works (1932 -1969) and a record collected by Mr Bernard Tebay at Laurel Bank, Ambleside (1969 – 2014). Seasonally (Summer - JJA, Autumn - SON, Winter - DJF, Spring - MAM) and annually resolved mean lake surface temperature (°C) for the period 1946 – 2012 collected at Far Sawrey/ Ferry House (OS map: SD393960) was provided by the NERC Centre for Ecology and Hydrology and the Freshwater Biological Association (Winfield & Fletcher 2014). Phyto- and Zooplankton concentrations from the deepest point of both the North (NY383006) and South Basins (SD382914) are at weekly-biweekly resolution for 1977 – 2003 (Burthe et al. 2016). All instrumental data, where not already, were averaged, or totalled on an annual resolution for statistical analysis.

2.4.10 Statistical analyses

Ordination analysis orders multivariate data sets and shows (dis)similarity in 2 or 3 D multidimensional plots. Of the many ordination analyses Canonical Correspondence Analysis (CCA) is particularly useful as multivariate comparison is done with multiple regressions allowing for hypothesis testing (Legendre & Legendre 1998). The technique compares linear combinations of explanatory variables (often environmental data) with other variables allowing comparison of 'drivers' and 'responses'. This method was therefore employed to identify if environment conditions could be drive changes in the geochemistry of the sediment. However, this technique is only applicable where data sets have unimodal distribution.

Geochemical (K, Mn:Fe, Pb, As) data and archival environmental/climatic data was tested firstly for model distribution using a Direct Correspondence Analysis (DCA). The relationship between selected geochemical data and archival environmental/climatic data was then tested in all cores, using CCA. Selected geochemical data was averaged to an annual scale using the ^{137}Cs – ^{210}Pb age depth model average age for the depth interval. CCA was undertaken using PAST v.3.1 (Hammer et al. 2001) a for all climate and environment instrumental data between 1950 – 2014. Data was also grouped by lithology.

2.4.11 Freshwater Biology Association diatom record comparison

The timing of diatom bloom laminae in the sediments was compared with Freshwater Biology association (FBA) diatom abundance records taken near to the FBA site in the North Basin (nearest core SC64). Using the FBA diatom abundance records, a 'bloom' in either

Aulacoseira spp. or *Asterionella Formosa* occurred where the total counts for a species in a given week exceeded the average weekly total for the same year by more than 10x.

2.5 Chronology

2.5.1 ^{210}Pb and ^{137}Cs

Lead-210 is a naturally occurring radionuclide and is part of the radioactive decay chain of ^{238}U with a half-life of 22.26 years. Its short half-life and even shorter typical atmospheric residence of 5 - 10 days makes it a far more affective dating tool than radio-carbon for recent sediments. As such it has been extensively used to date marine and freshwater sediments sequences, including some previous studies of sediments from Windermere (Appleby 2008). Lead-210 is incorporated into lake waters and then sediments from atmospheric fall-out usually via precipitation. By measuring the vertical distribution of atmospherically deposited ^{210}Pb (excess 210Pb) and comparing it to the known decay rate ages can be attributed to sedimentary layers down core. Excess ^{210}Pb is determined in sediments as ^{210}Pb above background levels or the value at which ^{210}Pb remains constant down core.

Caesium -137 is a non-natural isotope being generated during nuclear fission. It's presence in the environment began in 1945 with the first testing of nuclear devices but increased with the testing of thermo-nuclear devices from 1952 peaking in 1963. More localised sources can be from nuclear reactors, with a notable example in the northern Hemisphere coming from the 1986 Chernobyl accident (Ritchie & McHenry 1990). Atmospheric ^{137}Cs can enters lake sediments via direct atmospheric fallout or by reworked ^{137}Cs deposited in the catchment. In lacustrine sediments in Britain, and in those of previous studies of sediments in the Windermere catchment, the greatest peaks in ^{137}Cs are found to correspond to 1963 peak bomb testing and the 1986 Chernobyl accident (Ritchie & McHenry 1990; McDougall et al. 1991; Davison et al. 1993). In addition, some nearby coastal sediments also contain peaks corresponding to peak periods of nuclear waste discharge from the Sellafield nuclear power and processing facility (Oldfield et al. 1993).

Bulk samples were taken at 1 - 2 cm (2-3g of sediment) intervals and analysed for ^{210}Pb and ^{137}Cs in all gravity cores except core 53. Initially every other sample was analysed, and the sampling resolution was increased where activity was highest. Caesium-137 activities were determined by gamma spectrometry using a Canberra well-type HPGe spectrometer counting for 100,000 seconds and evaluating the 661 keV peaks of the spectra as outlined in Ritchie & McHenry (1990). Errors were ~4% (1σ). Lead-210 was measured by proxy

656 through the granddaughter ^{210}Po by alpha spectrometry. Yield was measured by the
657 addition of 0.15 Bq of the yield tracer ^{209}Po (original certified source National Physical
658 Laboratories). Each activity was corrected for sample mass and volume. The method, based
659 on Flynn (1968), uses a double acid leaching and auto-deposition onto silver discs
660 methodology to determine ^{210}Pb activities of the samples. The linear sedimentation rates
661 (LSR) and subsequent age estimates reported below are generated from ^{210}Pb activity and
662 validated using ^{137}Cs.

663 A chronology was generated from excess ^{210}Pb activity data by applying the constant flux:
664 constant sedimentation (CF:CS) model (Robbins 1978). The CF:CS model was chosen as it
665 allows the extrapolation of the mean LSR beyond 120 years, the lower limit for other
666 methods of ^{210}Pb sedimentation models. The model generates a LSR that is extrapolated
667 down core. Outliers in natural log (Ln) excess ^{210}Pb, for example those affected by redox
668 processes at the water sediment interface, or that were not deposited by background
669 sedimentation, were excluded from the analysis. Values of 0 ^{210}Pb activity were also
670 excluded from the analysis. Age error was calculated by applying the CF:CS model to the
671 upper and lower machine error ^{210}Pb values to produce LSRs which were extrapolated
672 down core to give an upper and lower age depth error estimate. All ages stated in this paper
673 are given in years A.D. and are the median probable ages followed by machine error in
674 brackets. ^{137}Cs was used to estimate dates of peak atmospheric nuclear weapons testing
675 (1963) and the Chernobyl nuclear reactor incident (1986) (Ritchie & McHenry 1990).

676 **2.5.1.1 Radiocarbon dating**

677 PC68 radiocarbon sampling was done following an inspection of the core for macrofossils
678 from within the top and bottom 10 cm of each core section, to minimise the risk of carbon
679 contamination entrained in the coring process, from split core surfaces where possible.
680 Macrofossils and bulk samples (1 cm) were taken under clean conditions, weighed and
681 stored in either foil or glass containers for transport.

682 In total 13 samples were analysed by the Natural Environment Research Council
683 Radiocarbon Facility (NRCF) in East Kilbride. The method followed turned samples to
684 graphite and passed to the SUERC laboratory for accelerator mass spectrometry (AMS) ^{14}C
685 analysis (Damon et al. 1989).

686 Radiocarbon dates were processed and calibrated using Calib 7.1 (Stuiver & Reimer 1993)
687 and the Intcal 13 calibration curve (Reimer et al. 2013). The radiocarbon results are reported

688 with ages given as the calibrated median probability age, and 2σ calibrated ages. Two dates
689 were later found to have been extracted from MTD and so were excluded from the analysis.

690 Table 6: Radiocarbon sample details.

Depth in core (cm)	Radio carbon age	Median prob. age	1 σ	Probability	2 σ	Probability
70.5	1114	1020	975 - 1057	1	1109 - 1125	0.022
					1109 - 1125	0.02
					1160 - 1172	0.011
102.5	1708	1614	1561 - 1626	0.776	1548 - 1702	1
			1669 - 1691	0.224		
151.5	2242	2232	2178 - 2244	0.664	2153 - 2277	0.717
			2301 - 2330	0.279	2288 - 2342	0.283
			2161 - 2169	0.057		
238	3499	3771	3720 - 3802	0.793	3690 - 3866	0.981
			3810 - 3831	0.207	3649 - 3659	0.019
330	5124	5862	5762 - 5809	0.512	5843 - 5939	0.523

			5887	-	0.488	5748	-	0.477
			5923			5830		
378.5	6468	7337	7329	-	0.428	7293	-	0.005
			7359			7298		
			7367	-	0.342	7305	-	0.995
			7395			7439		
			7412	-	0.23			
			7428					
428	8653	9600	9545	-	0.983	9539	-	1
			9629			9688		
			9649	-	0.017			
			9651					
456	9061	10225	10205	-	1	10180	-	1
			10241			10260		
492.7-493.8	9308	Not used						
523	9708	11160	11127	-	1	10881	-	0.072
			11202			10929		
						11082	-	0.928
						11225		

2.6 Age depth model

2.6.1 ^{137}Cs and ^{210}Pb Age depth model

The Ln excess ^{210}Pb activity in SC68 and SC64 showed good correlation over the whole sampling interval indicating a near constant linear sedimentation rate (LSR) (Figure 2-2). SC67 and SC57 had a segmented regression trend in the Ln excess ^{210}Pb data with the partition in both cores corresponding to a change in sediment type at 10.5 and 9.5 cm respectively (Figure 2-2). As a result the CF:CS model was applied piecewise to each interval (Appleby 2002; Tylmann et al. 2016). Both South Basin cores showed a lower LSR in the lower sediments compared with the upper sediments.

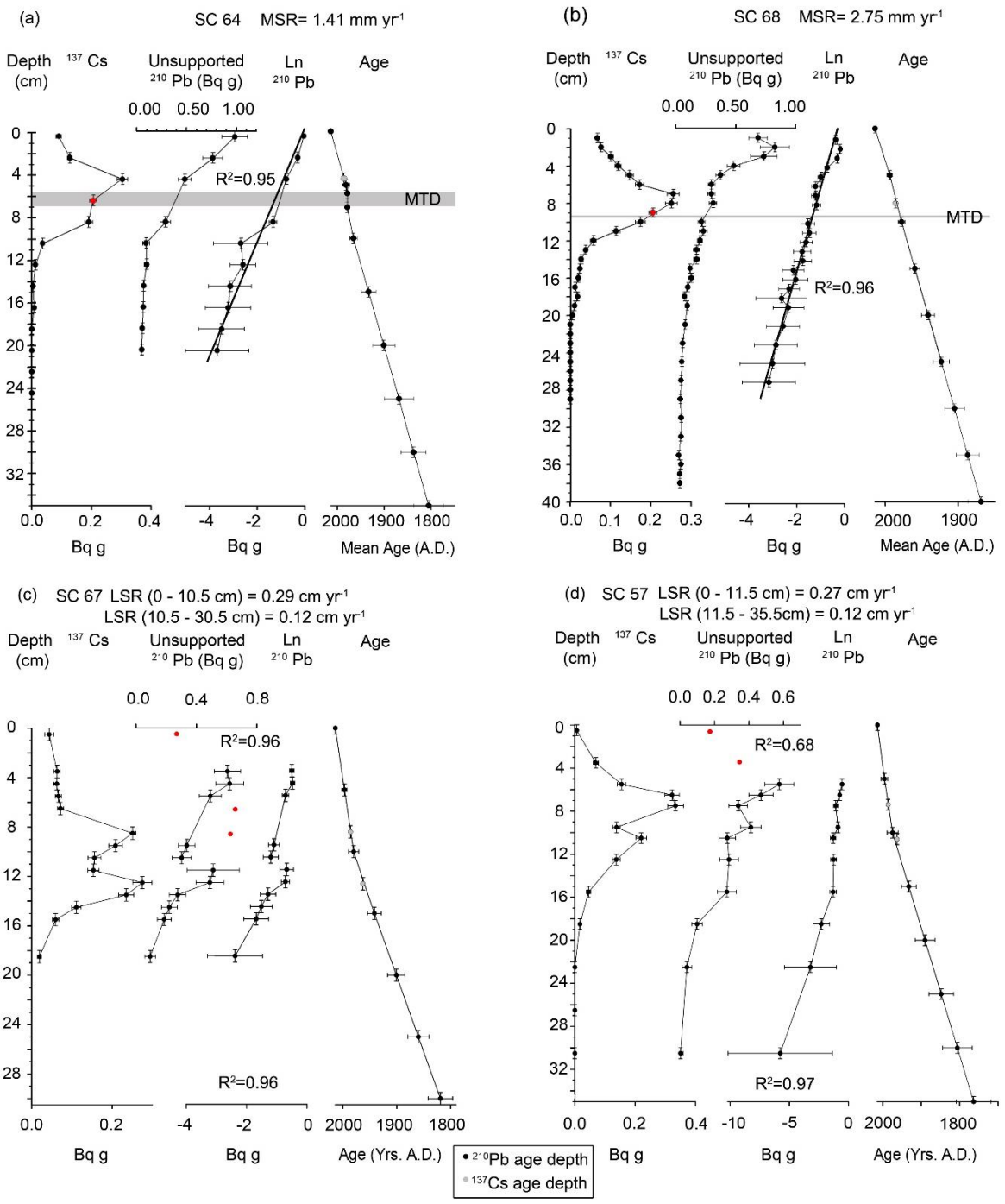

Figure 2-2: ^{137}Cs and ^{210}Pb Age Depth Model. Measurements of artificial radionuclides for cores SC68 (a), SC64 (b), SC67 (c), SC57 (d) and calculated linear sedimentation rates (LSR). R2 shows the linear trend for the LN ^{210}Pb data. Black circles show the ^{210}Pb CF:CS LSR age depth model at 10 cm intervals. Vertical error indicates bulk sample interval and horizontal error represents the extent of the maximum and minimum age depth based on machine measurement error. Red circles indicate data removed from analysis. Grey circles show the ^{137}Cs based age depth at 1986 and 1963 with vertical error also indicating the bulk sample interval.

The SC68 excess ^{210}Pb CF:CS model (Figure 2-2) gave a constant LSR of 0.28 cm yr-1 (0.25 - 0.30 cm yr^{-1}) and an age of 1868 (1850 – 1879) for the base of the core. A ^{137}Cs peak of 0.25 Bq/g at 8cm was attributed to the 1986 Chernobyl nuclear reactor incident. No further clear peak in ^{137}Cs was observed down core, however, the increase at 14 cm was attributed to the 1963 peak atmospheric bomb testing. This gave a linear sedimentation rate based on ^{137}Cs of 0.27-0.29 cm yr^{-1} and validated the ^{210}Pb age depth model to within 2 years.

The SC64 excess ^{210}Pb CF:CS model (Figure 2-2) gave a constant LSR of 0.14 cm yr^{-1} (0.12 - 0.16 cm yr^{-1}) and an age estimate for the base of the core of 1793 (1757 – 1809). A ^{137}Cs peak of 0.3 Bq/g at 4.5 cm was attributed to the 1986 Chernobyl nuclear reactor incident. As in SC68 no clear peak in ^{137}Cs was observed down core, and so the increase in ^{137}Cs at 8.5 cm was attributed to the 1963 peak atmospheric bomb testing. This gave a ^{137}Cs LSR of 0.16-0.17 cm yr^{-1} and validated the ^{210}Pb age depth model to within 3 years.

In SC67 data (Figure 2-2) from 0-3, 6-7 and 8-9 cm was outlaying and excluded from the analysis (see below). The CF:CS model gave an LSR of 0.29 cm yrs^{-1} (0.23 - 0.37 cm yrs^{-1}) between 0 and 10.5 cm, and 0.12 cm yrs^{-1} (0.11 - 0.13 cm yrs^{-1}) between 10.5cm and the base of the core. A ^{137}Cs peak of 0.25 Bq/g at 8.5 cm was attributed to the 1986 Chernobyl nuclear reactor incidents. A ^{137}Cs peak of 0.27 Bq/g at 12.5cm was attributed to the 1963 peak atmospheric bomb testing. This gave a LSR based on ^{137}Cs of 0.25 - 0.28 cm yrs^{-1} agreeing to within 1 year of the ^{210}Pb age depth model. SC67 has a maximum age of 1814 (1791 – 1829).

Outlying data points in SC57 data from between the top of the core and 3cm were excluded from the analysis. ^{210}Pb data between the base of the core and 18.5 with no activity was removed from the final age depth calculations. The ^{210}Pb CF:CS gave an LSR of 0.26 cm yrs-1 (0.19 - 0.27 cm yrs^{-1}) between 0 and 11.5 cm, and 0.13 cm yrs^{-1} (0.10 - 0.18 cm yrs^{-1}) between 11.5cm and the base of the core (Figure 2-2). A ^{137}Cs peak of 0.33 Bq/g at 7.5 cm depth was attributed to the 1986 Chernobyl nuclear reactor incidents. A ^{137}Cs peak of 0.21Bq/g was observed at 10.5cm depth and attributed to the 1963 peak atmospheric bomb testing. This gave a ^{137}Cs LSR of 0.21 - 0.27 cm yrs^{-1} between 2014 and 1963. In this case the ^{137}Cs age estimate matched the CF:CS ^{210}Pb age depth model for 1986, and the ^{137}Cs age estimate of 1963 lagged the ^{210}Pb CF:CS age depth model estimate by 6 years. This small discrepancy in ages could be caused by the sampling resolution being insufficient to locate the exact change in LSR. SC57 has a maximum age of 1760 (1714 – 1838).

2.6.2 Evidence for ^{137}Cs and ^{210}Pb mobility

In all four cores ^{137}Cs is observed at depths below the ^{210}Pb CF:CS model estimated depth for 1954, the earliest date of atmospheric ^{137}Cs fallout, despite agreeing well with ^{137}Cs in the upper core. The mobility of ^{137}Cs down core has been observed in other studies (Baskaran et al. 2016) and can occur due to smearing during the sediment sampling process, bioturbation or soft sediment mixing, or dissolution and diffusion in pore waters (Klaminder et al. 2012). Pelleting of the sediment in some intervals does suggest some bioturbation has occurred, however, the presence of sub-mm scale sediment structures suggest that sediment has not been disturbed beyond this scale therefore ^{137}Cs dissolution is more likely.

In contrast to the South Basin cores both North Basin cores lack a clear 1963 peak bomb testing ^{137}Cs profile which could also be explained by ^{137}Cs diffusion. In areas that received high levels of ^{137}Cs from the Chernobyl nuclear reactor incidents, downward diffusion has been shown to overwrite the 1963 peak bomb testing ^{137}Cs profile (Appleby et al. 1990; Appleby et al. 1991; Klaminder et al. 2012). The larger upland catchment of the North Basin would mean that potentially more ^{137}Cs could be delivered by overland flow after atmospheric deposition over a larger area, when compared to the South Basin. Both a muted 1963 peak bomb testing ^{137}Cs profile and diffusion of ^{137}Cs to sediments below 1954 have been observed at Grasmere, also in in the North Basin catchment (Barker et al. 2005).

Decreases in ^{137}Cs away from the expected trend in the North basin (especially in SC64) at the clay horizon are likely due to the entrainment of old remobilised clay rich material as part of a MTD (see chapter 4).

In SC67 ^{210}Pb data from 0-3 cm showed values that were lower than the exponential trend in the rest ^{210}Pb of the core. Equally in SC57 ^{210}Pb values between 0-3 cm were lower than the expected for the ^{210}Pb deposition and decay history suggesting that redistribution had occurred. A similar pattern has also been observed in excess ^{210}Pb in sediment in other lakes in the Windermere catchment (Pennington et al. 1976), and other areas (Appleby & Oldfield 1978; Putyrskaya et al. 2015). This could be due to one of a number of reasons: (i) Low compaction rates in the upper most sediments could cause relatively low ^{210}Pb activity concentration (Putyrskaya et al. 2015), (ii) post depositional redistribution as a result of bioturbation or sampling, or (iii) ^{210}Pb loss due to redox processes and organic matter decomposition (Appleby & Oldfield 1978; Von Gunten & Moser 1993).

While it is possible that low compaction of the upper most sediments could account for lower concentration of ^{210}Pb, low density sediments are present in upper sediments of all four cores and so would not explain why only sediments in the South Basin are affected by this. Post depositional redistribution is also unlikely as while the sediments are pelleted, the presence of sub-mm scale sediment structures suggest bioturbation beyond this scale has not occurred. Furthermore, ^{137}Cs profiles in both cores have well defined peaks at 1986 and 1963, and so appear to be unaffected. Similarly, analysis of the core by microscopy shows the sediment water interface of both SC67 and SC57 is intact and so sampling error is an unlikely source of the lower than expected concentrations.

Pb and in particular ^{210}Pb has been shown to undergo diffusive migration in response to redox gradients within sediments. Many studies have found that sedimentary ^{210}Pb becomes mobilised under reducing conditions and migrate into the overlying water column depleting the upper most sediments. This has typically been shown to be in association with the redox sensitive metals Fe and Mn (Davison 1993) which scavenge divalent Pb (Benoit & Hemond 1990, 1991; Von Gunten & Moser 1993; Putyrskaya et al. 2015). SC67 and SC57 were collected in April when the South Basin bottom waters are typically considered to be leading in to a phase of sub-oxia and anoxia (Simpson et al. 2015) caused by thermal stratification of the lake between early Spring (March-April) and early Autumn (September – November) (Woolway et al. 2014). However, the presence of peaks in Mn and Fe in the core tops of SC67 and SC57 (Figure 4-2) would suggest that oxygen conditions were not low enough to mobilise these redox sensitive metals or ^{210}Pb. Although, Balistrieri et al. (1995) observe that in a monomictic lake during the latter part of oxygenated period even slightly declining levels of dissolved oxygen in the water column caused redox driven ^{210}Pb dissolution and migrate to the water column, and that lake water ^{210}Pb was highest leading into a period of sub-oxia.

2.6.3 Combined ^{210}Pb, ^{137}Cs and radiocarbon model

For the piston core – gravity core age depth a combined model and sedimentation rate was developed by linear interpolation between radionuclide derived mean date points. Hiatuses were inserted where MTD were identified and sediment was assumed to have been deposited instantaneously.

803

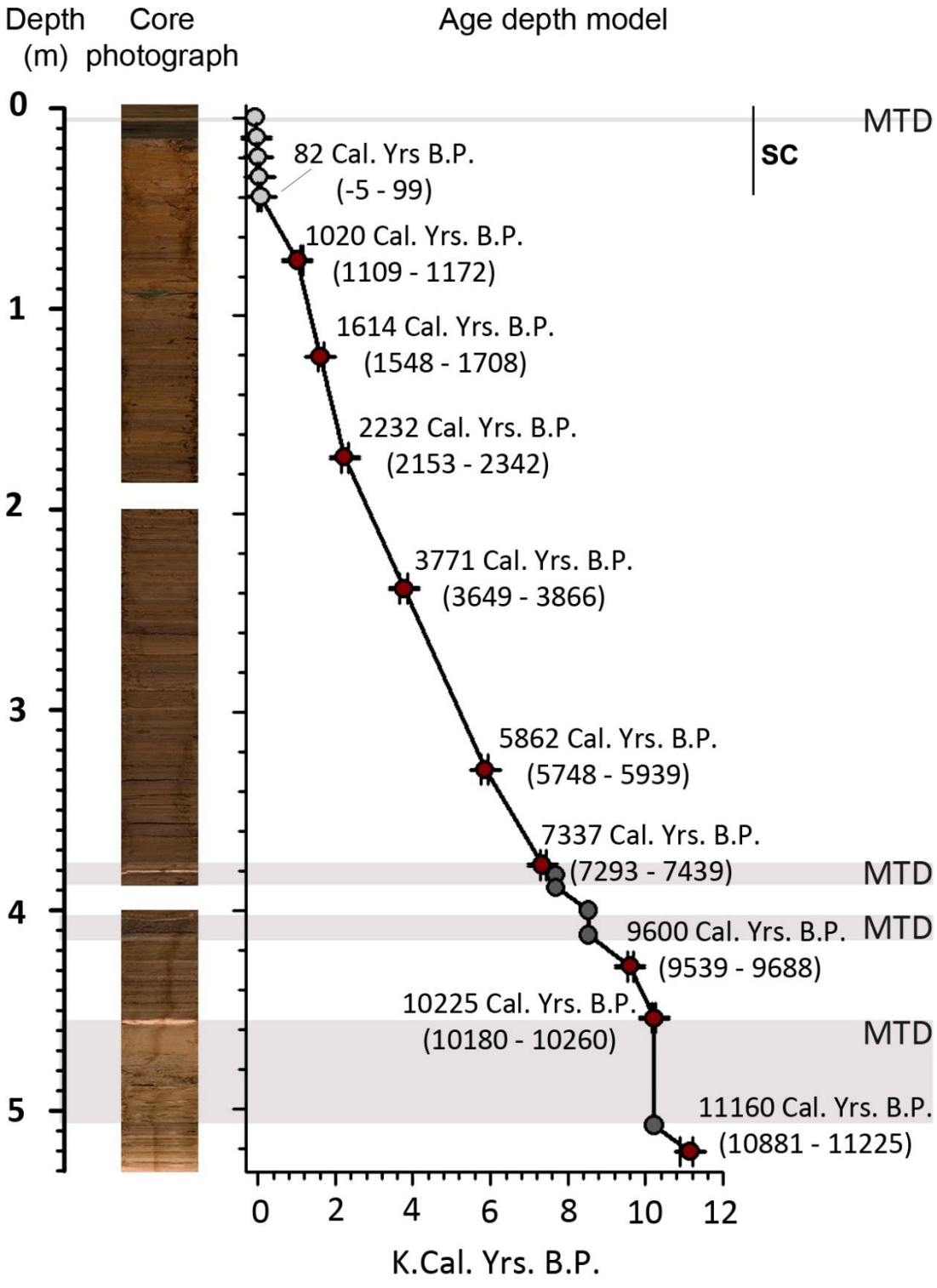

804

805 Figure 2-3 age depth model for core PC68 with core photography. The position of MTDs
806 are highlighted in light grey with estimated ages given as dark grey dots. Mean probable
807 radiocarbon ages are given with a corresponding 2 σ range date estimate, in addition to red
808 dots which show radiocarbon ages with vertical error bars showing sampling interval and
809 horizontal error bars showing 2 σ range date estimate. In the upper sediments light grey

dots and corresponding labels show ^{210}Pb derived age estimates, machine derived error (horizontal error bar) and sample interval (vertical error bar). SC marks the extent of the short core within the sequence.

2.6.4 Lithostratigraphy of the gravity cores

The overall lithostratigraphy determined from optical and backscatter electron microscopy for both the North and South Basin short cores shows a tripartite structure with a lower pale brown mud overlain by a dark grey mud, which is in turn succeeded by an upper pale brown mud (SC68, SC67) or a less dark mud (SC64, SC57) (**Error! Reference source not ound.**). This tripartite structure is broadly consistent with the descriptions of earlier cores taken from Windermere (Pennington 1973; Hamilton-Taylor 1979) with the main difference being the thicker upper pale brown interval in the modern cores, the transition to the paler brown apparently having been around 1970 – 1975. In the North Basin, the dark grey and upper paler mud are separated by a paler clay rich interval dated to 1980 and 1979-1980 in the North Basin deep and shallow core respectively. The transition from the lower pale brown mud to the dark grey mud occurs earlier in the South Basin cores (1904 in SC67; 1882 in SC57) than in those from the North Basin (1916 in SC64; 1920 in SC68).

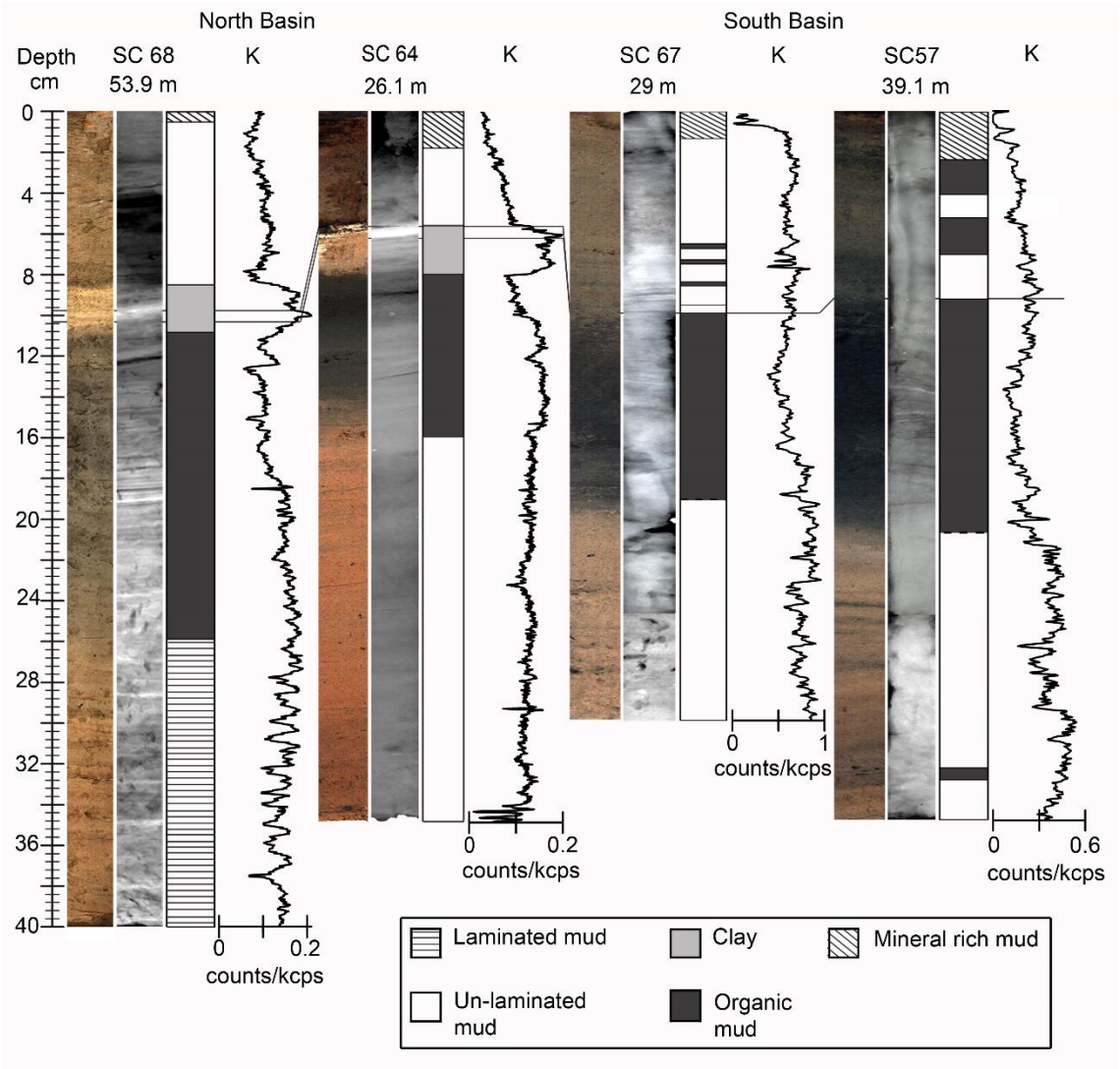

Figure 2-4: Overall stratigraphy for all cores. Core depth in cm, core photograph, core x-radiograph, lithostratigraphic classification (based on optical and backscatter electron microscope observations), and ED-XRF K for all four gravity cores collected from Windermere. Water depths of each coring site is shown above the corresponding core. The grey lines shows correlation between the clay K rich facies (mass transport deposit) in the North Basin cores and contemporary facies boundary in the South Basin cores, demonstrating the absence of the pale clay horizon from the South Basin.

Chapter 3 A high resolution Holocene environmental and climate change record from Windermere

3.1 Introduction

To better predict how future climate and environments will change with increasing anthropogenic pressures, forecasting models need to be extensively validated with past environmental and climate information (Overpeck et al. 2006; McCarroll et al. 2013; IPCC 2014). The Holocene commenced roughly 11,750 cal. yrs. B.P. and extends to the present day represents a period of relative climate stability in comparison to the last glacial period (Johnsen et al. 2001; Rasmussen et al. 2007). However, it has been punctuated by short-lived and abrupt climate events, such as the cooling at 8.2 k. yrs. B.P. and 4.2 k. yrs. B.P. (Alley et al. 1997; Walker et al. 2012; Roland et al. 2014), where temperatures were on average 1-3 °C cooler in Northern Britain. Prominent centennial and multi-millennial scale climate shifts have also occurred, such as the Holocene Thermal Maximum (HTM) (Renssen et al. 2009) and the Little Ice Age (LIA) (McCarroll et al. 2013; Joannin et al. 2014).

The study of ancient lake sediments (palaeolimnology) allows for high resolution seasonal to decadal reconstructions based on multiple proxies (Birks & Birks 2006; Smol 2010; Battarbee & Bennion 2011). Lake sediments typically comprise of a mineral and organic component deposited from either allochthonous (external) or autochthonous (internal) sources, and are highly sensitive to environmental and climate drivers. The quantification of fine scale changes in the sedimentary, geochemical, or organic components, can provide reconstructions of past environmental and climatic conditions on a centennial or even annual basis (Smol 2010; Lowe & Walker 2014).

Palaeolimnological studies show Windermere in the Lake District National Park, UK, to have an intermittently laminated sedimentary record extending from Greenland Stadial 1 to the present day. This gives it the potential to provide high resolution climate and environment reconstructions (Pennington 1943; Pennington 1973; Pennington et al. 1976; Miller et al. 2014b). The mountainous, westerly maritime location of the Windermere catchment results in high levels of precipitation, with 4000 – 5500 mm per year in the most elevated parts of the catchment (Centre for Ecology and Hydrology records). Changes in precipitation are influenced by variations in North Atlantic oceanic and atmospheric

systems, particularly the North Atlantic Oscillation (NAO); Atlantic sea surface temperature changes; and the North Atlantic Currents (Wilby et al. 1997; Barker et al. 2005). Windermere's location between the well-established Greenland ice core proxy climate records (Rasmussen et al. 2007) and Central Europe palaeolimnological proxy-records (Goslar et al. 1993), gives the potential for a high resolution proxy climate record that would provide a bridge between these records which show diachroneity for major climate events and shifts during the Holocene (Grove 2001; Juckes et al. 2007)

The purpose of this chapter is to provide a preliminary account of the Holocene stratigraphy including pilot proxy studies of a piston core in the deep North Basin of Windermere together with a more detailed analysis of early Holocene mass transport deposits.

3.2 Results

3.2.1 Pollen stratigraphy

Pollen stratigraphy (Figure 3-1) can be divided into six clear zones of community change: Zone I is characterised by high grass pollen (*poaceae* and *cyperaceae*) counts reflecting the late glacial sub-arctic tundra type vegetation and consistent with the presence of glacial clays (Kelly et al. 2017). Zone II shows peak abundance of *juniperus* consistent with more tundra like conditions common in upland areas of Britain at around 10000 cal. yrs. B.P. (Ince 1996; Kelly et al. 2017). The presence of *Pinus* and *Betula* also shows the development of forests and is consistent with other pollen communities from the time (Kelly et al. 2017). Zone III begins with the pine and hazel maxima, comparatively earlier than has been suggested elsewhere (Tallantire 2002). Oak and Elm also begin to become significant through this period reflecting warmer temperatures but predominantly sub-boreal conditions. Zone IV is marked by an Alder rise, and Oak and Elm maximum, which has been identified in other pollen stratigraphies in the Britain to date to 7 - 5 k. cal. yrs. B.P. (Bennett & Birks 1990), and reflects the radiocarbon age-depth well. Zone V begins with the classic Elm decline profile estimated in Britain to have occurred at 5.5-5 k. cal. yrs. B.P. (Parker et al. 2002). Furthermore, a rise in grass type pollen and the first occurrence of *plantago lanceolata* is indicative of early pastoral agriculture (Woodbridge et al. 2014) in this period. Finally, Zone VI is dominated by phases of decreasing woodland cover and increasing cereal pollen types, as well as grasses and sedges. This is indicative of an increasingly agricultural landscape starting in the Neolithic, with phases of cereal and

grassland expansion around 2150, 1250 cal. yrs. B.P. closely matching major expansions in agriculture in Romano-British, and early Medieval (Fell farming) recorded elsewhere in Britain (Tipping 1995). A slight increase in *Pinus* type pollen at the top of this zone is indicative of pine plantations over the past 200 years (Wood & Walton 2016).

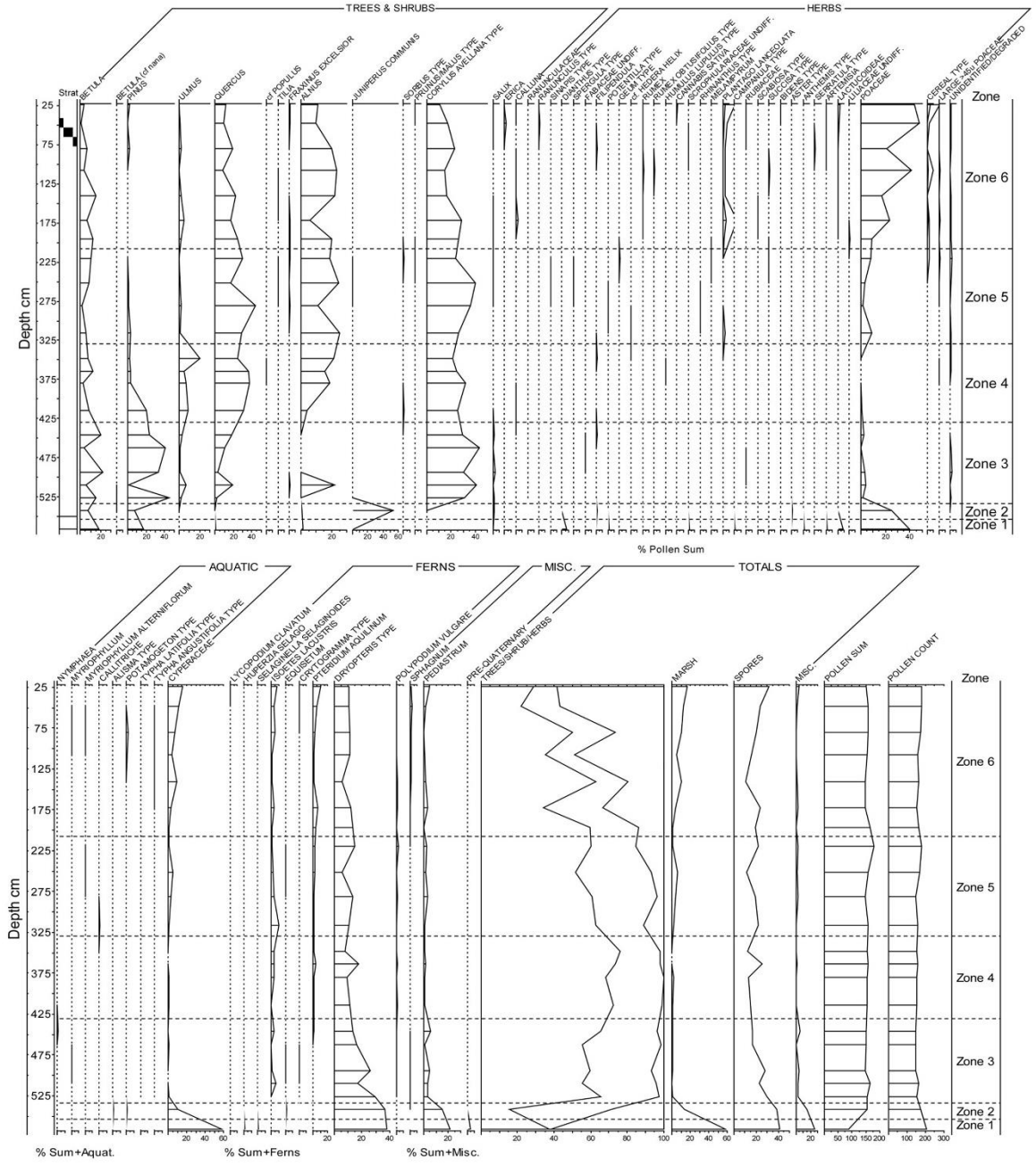

Figure 3-1: Pollen assemblage and zones

3.2.2 Lithostratigraphy

At 528 cm a sharp colour change from pink (5/4 10 YR Munsell) to brown (4/2 – 5/2 10 YR) denoting the change from clay to organic rich silts and muds above, and the appearance of organic matter, marks the beginning of the Holocene. This is followed by laminated cm-

mm scale clay rich organic muds with alternating pale Mn and Fe-rich laminae which make up the earliest Holocene sediments of Windermere. The early Holocene interval is marked by two prominent mass transport deposits (MTDs) (Figure 3-2) that are discussed in more detail below. Clay rich laminations increasing in thickness and frequency between 416.8cm and MTD 2 at 412.5cm (Figure 3-2).

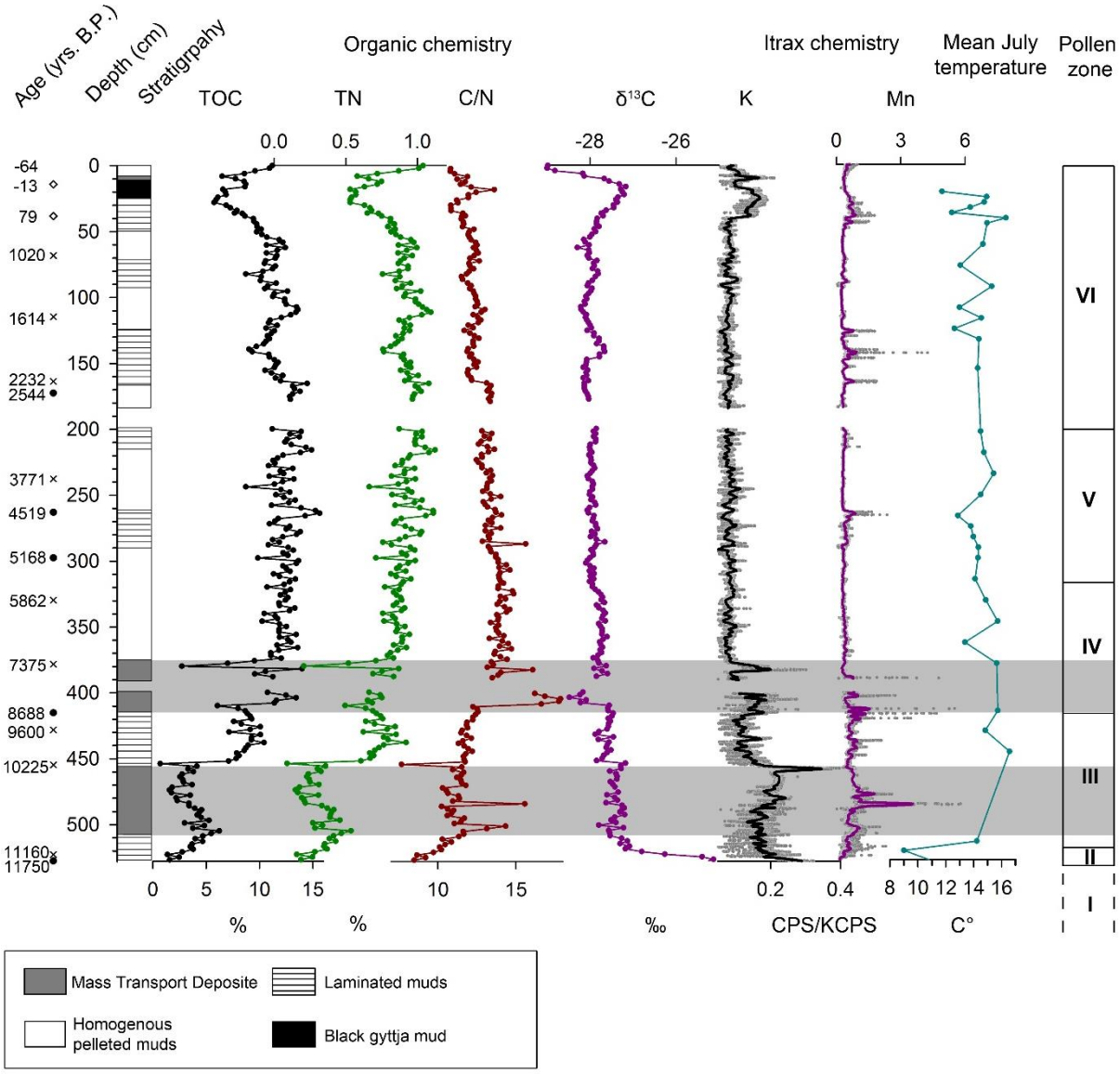

Figure 3-2: PC68 core stratigraphy with depth and mean probable radio carbon ages (black X), palaeomagnetic radiocarbon age tie points (black dot), and Pb210 derived ages (diamond). Total organic carbon (TOC) is shown in black, total nitrogen (TN) in green, carbon – nitrogen (C/N) in red, $\delta^{13}C$ organic chemistry in purple. In addition, itrax data for K (grey dots) 100 point running average is shown by the solid black line, and Mn (grey dots) 100 point running average is shown by the solid purple line. Chironomid derived mean July temperature is shown in blue (solid line and data points), as well as pollen zones I – VI with pollen zone I extending below the Holocene section.

After MTD 2, muds become more organic rich and show mm laminae scale variations in density, terrigenous detrital grains and organic fragments (Figure 3-2). Often these homogenous sediments are pervasively pelleted which is indicative of bioturbation by conveyor belt feeding benthic organisms such as tubificid oligochaetes. Sediments are periodically laminated through the mid-late Holocene with distinct decimetre-scale intervals of alternating mm scale detritus-rich and pale Mn – Fe mineral rich laminae.

3.2.3 Changes in terrestrial input

Both are K and Ti are commonly found in terrestrial detrital minerals and can serve as a proxy for the input of terrestrial material (Table 5), and highlight large input events such as floods or mass movement deposits (Schlolaut et al. 2014; Plaza-Morlote et al. 2017). Ti shows a high correlation with K (R2=0.98) suggesting these elements indeed share a common delivery process or source. As such both are interpreted as a proxy for terrestrial input but here only K data is presented. From 528 cm at the beginning of the Holocene a lowering of K content (Figure 3-2) is interpreted as decreasing terrestrial input. The increase above 533 cm in TOC is interpreted as increasing productivity and vegetation in the catchment and reflects the increase in diversity in the pollen assemblage as well as later seclusion type plants. As seen in chironomid inferred mean July temperatures (C-IT), the Early Holocene saw a rapid increase in temperature consistent with other palaeo proxy records from North West England which show a temperature increase of up to 5°C (Lang et al. 2010), and temperature increases regionally in Europe and the North Atlantic (Goslar et al. 1993). Higher temperatures would have allowed the return of vegetation (as seen in the pollen results) to the catchment, increasing the amount TOC in the lake sediments.

In the Early Holocene below and between the MTDs, K has higher amplitude variability, suggesting that terrestrial sediment input was highly variable, consistent with climatic and catchment vegetation instability. This is further reflected by cm scale alternating detrital rich laminae (Figure 3-2). The Early Holocene in North West England saw centennial and decadal fluctuations in average temperature of between 1-3°C (Lang et al. 2010), a pattern also seen in the Greenland Ice core $\delta^{18}O$ temperature records (Rasmussen et al. 2007), and reflected in part by C-IT. This climatic instability, marked by "major flood episodes" in British rivers (Macklin & Lewin 2003), would have periodically inhibited stable soil development, instigated flooding, and increased erosion and transport of terrestrial sediments into the lake over short periods, causing the highly fluctuating Ti, K, and clay content (Figure 3-2).

Above MTD 2, K shows lower amplitude variability indicating less extreme variability in terrestrial sediment input. This, combined with the increasing pollen from climax community final succession species such as Oak (Figure 3-1), is likely the result of a more stable climate in the mid Holocene when compared with the early Holocene (Davis et al. 2003), which would have allowed for more extensive vegetation groundcover, curtailing erosion. This is also seen in the declining sedimentation rate from 0.042 to 0.014 cm yrs. $^{-1}$ (Figure 2-3). From 5.8 cal. k. yrs. B.P. K remains relatively stable, however, the sedimentation rate increases through the rest of the Holocene up to 0.82 cm yrs. $^{-1}$ in around 1600 cal. yrs. B.P. This possibly reflects increasing deforestation, and associated increased sediment erosion in the wake of Neolithic, Bronze Age and Iron-Roman Age agricultural expansion (Edwards & Whittington 2001; Macklin & Lewin 2003; Woodbridge et al. 2014), which are in turn reflected by increasing cereal pollens over the same period (Figure 3-1).

3.2.4 Organic chemical indicators

The $\delta^{13}C$ drop in the first ~10cm (Figure 3-2) shows a change in input from an algal dominated carbon source to a terrestrial dominated source, as freshwater algal carbon tends to be lighter in $\delta^{13}C$ by up to 2‰ (McGowan et al. 2012). This is further supported by a coeval rise in C:N (Figure 3-2) with a transition from protein rich, lignin poor algal organic matter of phytoplankton, in the earliest Holocene, to values which shows a mix of protein poor, lignin rich terrestrial biomass and phytoplankton (Meyers & Teranes 2002).

Between MTD 2 and 290 cm in the mid-Holocene, TOC and TN have a high correlation (R^2=0.92) and are relatively stable with an overall slight increase suggesting a period of high stable catchment productivity, and reflecting the pollen record for the time (zone 4). $\delta^{13}C$ and C:N values also remain relatively stable over this interval and continue to show a mixed source of carbon (Meyers & Teranes 2002).

Between 290 and 177.5 cm TOC and TN remain relatively high, with TOC showing the highest value for the whole Holocene, but increase in variability. Δ13C remains relatively stable, while C/N values show an overall slight decrease. Fluctuating levels of TOC and TN could be indicative of fluctuations in carbon being delivered to the lake, possibly as a result of short lived changes in primary productivity in the catchment, with the C/N values showing a slight increase in the proportion of that carbon source coming from algal organic matter (Meyers 1994). This could reflect changes in climate associated with the globally recognised 4.2 k year climate event associated with cooler and wetter climates at high latitudes and potentially (Roland et al. 2014), shown in the Windermere chironomid record.

However, this would not go as far as to explain all variation during this interval. The pollen data shows phases of decreasing climax community plants and increasing grasses, and herbs. This is consistent with the emergence of agriculture in the UK at this time (Woodbridge et al. 2014), fluctuations in which could be responsible for changing productivity and delivery of TOC (and TN) to the lake sediments.

Throughout, this period, however, peaks in TOC (and TN) are found both during periods of decreasing climax vegetation, and so decreasing productivity (265 cm), and during periods of increased stable climax vegetation. Owing to the wide range of different species dispersal distances and mechanism, pollen stratigraphies do not always fully reflect plant and vegetation abundance on a local or even catchment scale (Prentice 1985). This problem becomes more exaggerated in mountainous areas where due to relief dependant changes in local climate vegetation communities can change over very short distances (Bradley 1999). Sedimentary carbon and nitrogen on the other hand is representative of a much smaller scale either being part of organic material generated within the lake or immediate catchment. In the case of Windermere the development of farming was most likely transitional, and may not have been as extensive in the steeper more elevated northern part of the catchment as elsewhere in the area. This would undoubtedly give a difference between the pollen record and changes in vegetation cover and productivity in the immediate catchment.

Through the Mid-Late Holocene, TOC shows a positive correlation with C:N (Figure 3-3). It also shows a negative correlation with $\delta^{13}C$ and Mn (Figure 3-3) which would suggest that increases in TOC are due to increases in allochthonous vegetation brought about by high runoff. While carbon from algal sources might remain constant the proportion of carbon from allochthonous vegetation would cause lower $\delta^{13}C$ and higher C:N values.

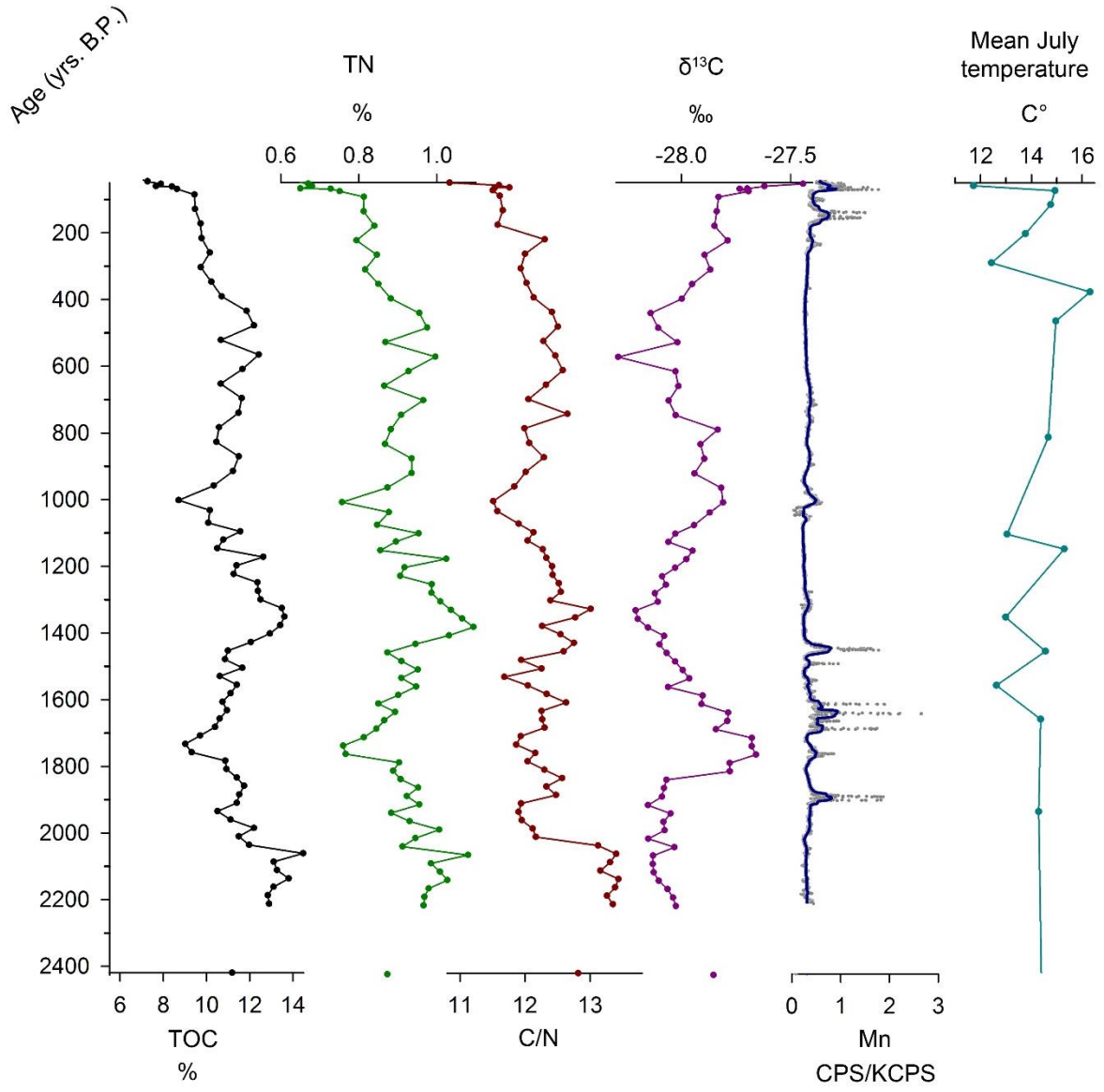

Figure 3-3: detail of organic chemistry, Mn (blue line 100 year running average, grey dots are counts) and C-IT in the Late Holocene of PC68

The $\delta^{13}C$ enrichment in the late Holocene above ~50 cm is likely the result of increased carbon input from phytoplankton source due to periodic eutrophication caused by agricultural fertilisers at this time (Barker et al. 2005) and resulting nutrient enrichment in run-off feeding algal growth (Pennington 1973; Dong et al. 2012).

3.2.5 Palaeo redox indicators

Sediments show periods of high Mn values from the onset of the Holocene up to the base of MTD 1, and Mn shows periodic episodes of high variability through the Mid and Late Holocene, with episodes of high Mn variability corresponding to Mn-Fe laminated sediments (Figure 3-2). As with the lower pale brown muds of the late 19th and early 20th

century in SC68 (See chapter 5), the Mn – Fe laminations in the mid to late Holocene are comprised of rhodochrosites above Fe-oxyhydroxides implying a similar formation process (Figure 3-4). The lower Holocene is dominated by cm scale laminated sediments similar in character to those found in the mid and late Holocene, with alternating detrital rich and Fe –rich laminae (Figure 3-5, Figure 3-4). Detrital rich laminae are more clay rich and thicker than mid-late Holocene (**Error! Reference source not found.**) laminations which could eflect a higher erosional activity in cooler temperatures (Table 5). Fe rich laminations occur on a multi – annual scale (LSR = 0.08 cm/ yrs.), and so are likely to reflect episodic stratification followed by ventilation on this time scale.

As discussed in chapters 5 and 6, a likely mechanism for the enrichment of Mn is the development of sediment anoxia promoted by hypoxia of bottom waters during the period of summer stratification resulting in reductive mobilisation of Mn followed by oxidation at a redox boundary that may have been enhanced seasonally by lake turnover. Thus, high Mn values (Figure 3-2: Position of slide 168 (black square) with in laminated Holocene sediments as by the slab photograph. Slide 168 optical thin section, back scatter electron image, and EDS map (Si, Mn and Fe) of alternating laminae. In addition to this a detailed image of the optical thin section and corresponding BSEI, elemental map for Fe (blue) and Mn (red) with the labelled mineral phases identified by EDS spot analysis, are shown for one of the mineral rich lamina.) are indicative of fluctuating redox conditions in the bottom waters. In turn low Mn variability are therefore interpreted to indicate persistent oxic conditions, as Mn is never reduced, and mobilised, and so unable to undergo geochemical focusing (Davison 1993; Müller 2001; Naeher et al. 2013). This is also consistent with more pervasive pelletisation in the intervals of low Mn variability.

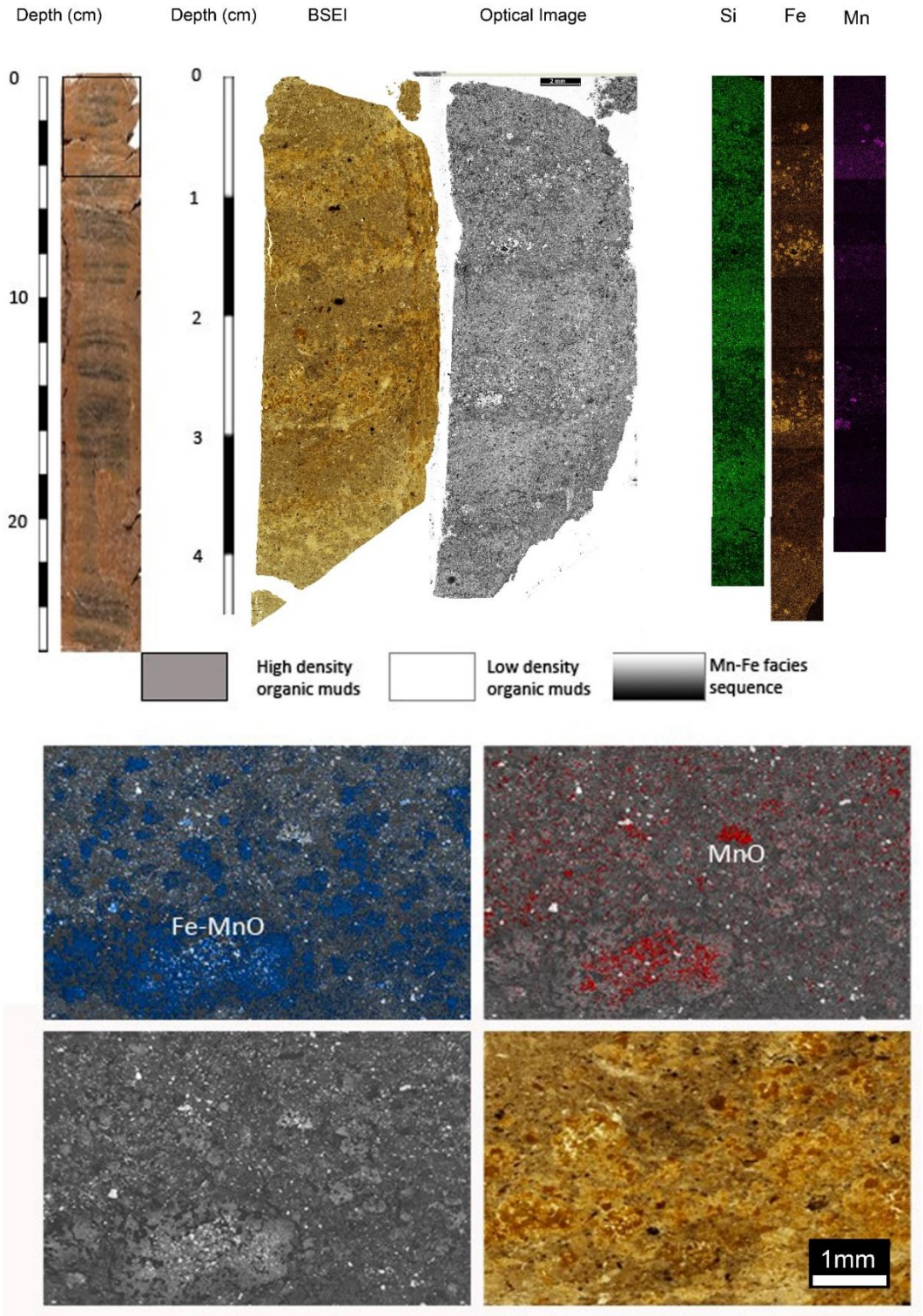

Figure 3-4: Position of slide 168 (black square) with in laminated Holocene sediments as by the slab photograph. Slide 168 optical thin section, back scatter electron image, and EDS map (Si, Mn and Fe) of alternating laminae. In addition to this a detailed image of the optical thin section and corresponding BSEI, elemental map for Fe (blue) and Mn (red) with the labelled mineral phases identified by EDS spot analysis, are shown for one of the mineral rich lamina.

High Mn laminae appear in the earliest Holocene with high amplitude variability in terrestrial sediments (Figure 3-2). This is evidence for increased lake productivity leading to flux of allochthonous material to the lake bed promoting anoxia within the sediment. These periods of fluctuating bottom water redox conditions are shown to occur more intensely during known periods of cooler climate especially in conjunction with cooling around 4.5 k. cal. yrs. B.P. shown by C-IT (Figure 3-2). In a modern setting Windermere is thermally stratified during the summer with warmer well mixed oxygenated waters at the surface (epilimnion) and cooler deep waters below (hypolimnion) (Jones et al. 2008).

Episodes of increased variability in Mn through the early Holocene may suggest increased seasonality with productive lake waters, enhanced summer stratification followed by more vigorous winter overturning. For example the highest amplitude variability in Mn is immediately below MTD 2 with an age range of 8650-8100 cal. yrs. B.P.. This timing is consistent with the well know 8.2 k. yrs. Cooling event. In warm monomictic lakes such as Windermere overturn normally occurs as a result of wind driven process, and surface cooling, in early autumn (Ambrosetti & Barbanti 1999). During observations of the overturning process at Windermere in 1931-32 A.D it was found that cooler winters increased overturning, but more importantly cooler summers curtailed thermal stratification allowing for more complete overturning to occur in winter (Jenkin 1942). Such a case could therefore result in higher enrichment of Mn in at the WSI. These periods may therefore represent a time when the epilimnion of Windermere was cooled to below 4°C (winter low of the bottom water recorded in 1932) for prolonged periods during the winter, and possibly also one of cooler summer temperatures.

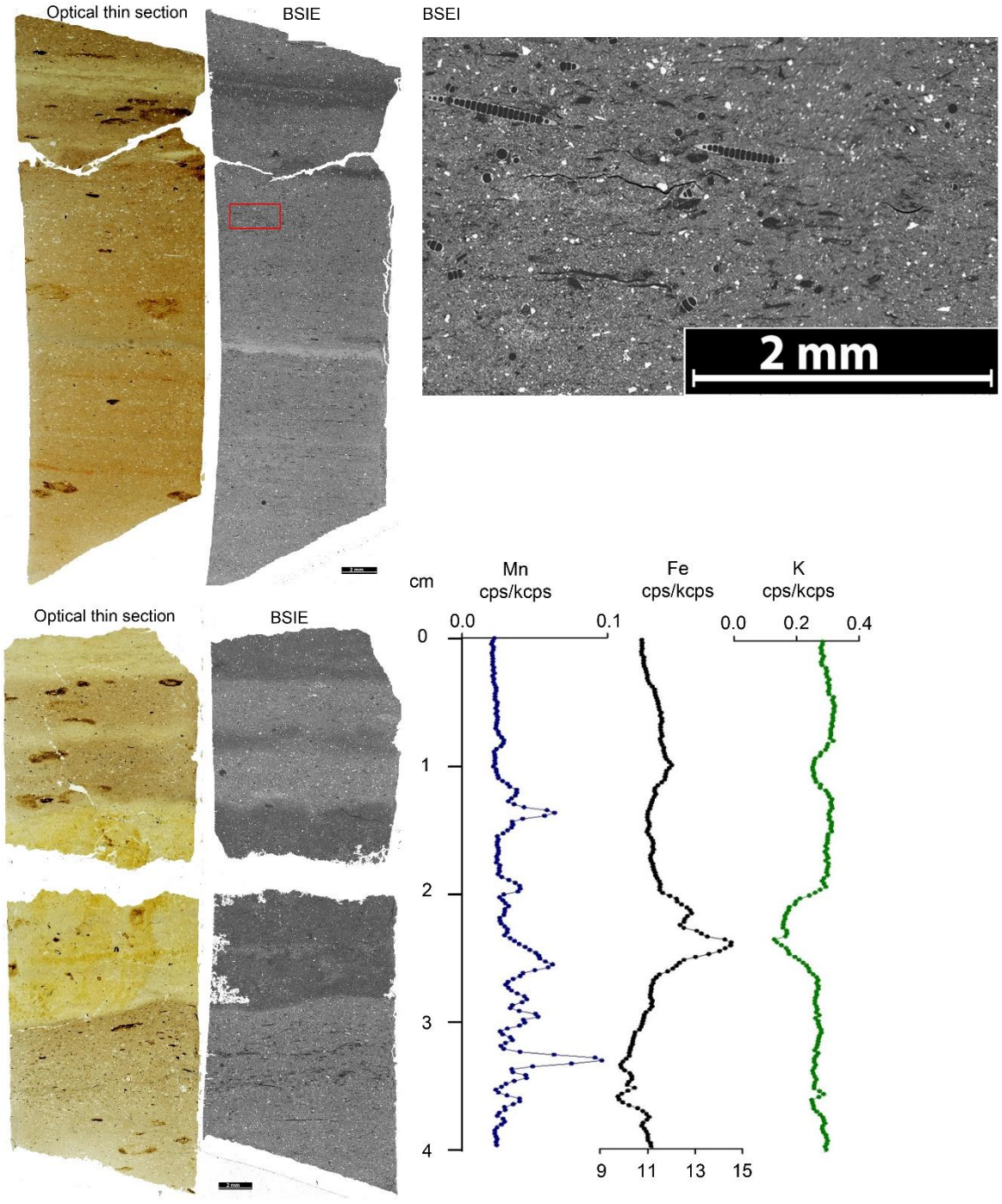

Figure 3-5: Optical thin section and backscatter electron image (BSEI) of glacial clay – organic laminated mud transition (upper panel), with BSEI enlargement showing macro organic and autochthonous organic fragments. The lower panel shows cm scale alternating detrital – Fe rich laminae typical of the early Holocene sediments, and corresponding itrax values for Mn, Fe and K.

3.2.6 Paleo-temperature reconstruction

Chironomid inferred mean July temperatures (C-IT) at the end of the glacial period (sample from clays taken at 530 cm depth, not shown in Figure 3-2) and the earliest part of the Holocene (11025 cal. yrs. B.P.) are 11.3 and 9 °C respectively. When compared with C-IT reconstruction at nearby Haws Water (Lang et al. 2010) for the late glacial and early Holocene (10.5 – 13°C) estimates at Windermere are slightly cooler, and instead compare better with estimates from Scotland (Brooks & Birks 2000a) and Western Norway of 10 – 12 °C (Brooks & Birks 2000b). This could be the result of the inclusion of chironomid remains from some of the higher relief areas of the catchment, which is reflected by high levels of in wash throughout this period. Continuing through the early Holocene mean C-IT begin to increase to a peak of 16 °C at 10 k. cal. yrs. B.P, fitting well with other nearby C-IT (Lang et al. 2010) records which show a similar temperature range during the regionally well documented Early Holocene Warm Period (EHWP) (Jansen et al. 2008). Although this study does not provide sufficient resolution to identify such short lived events in detail, a decrease at the beginning of the record at 11.3 k. cal. yrs. B.P., could correspond to the aforementioned pre boreal oscillation (figure 5.3). Equally, a decrease of 1.8 °C occurs at 9.6 k. cal. yrs. B.P. could reflect the short lived cool period at 9.3 k. cal. yrs. B.P. identified at nearby Haws Water (Lang et al. 2010) and in the wider region (Young et al. 2013) (figure 5.3).

Following recovery to around 15.5 °C C-IT show a short lived decrease at 6.4 k. yrs. B.P. which is identified as the peak of climate instability globally (Wanner et al. 2015), and as a major transition period from the Early to the Mid Holocene (Mayewski et al. 2004; Meyer-Jacob et al. 2017). Following a recovery to 15.7 °C C-IT gradually decrease to 12.8 °C at ~4.5 k. cal. yrs. B.P. This could relate to the widespread climate phenomenon at 4.2 k. cal. yrs. B.P. recorded in palaeo-proxy records particularly at mid-low latitudes. At higher latitudes this phenomenon often corresponds to cooling (Mayewski et al. 2004; Walker et al. 2012; Wanner et al. 2015). Furthermore this contradicts recent findings which suggest there was an un-coherent or muted impact of this phenomenon in Britain (Roland et al. 2014).

Following this C-IT remain relatively stable until 1650 cal. yrs. B.P. after which variability increases. Notable cooler periods occur at samples which correspond to 1351, 1103, 289, 58 cal. yrs. B.P. Cooling at 1351 cal. yrs. (Figure 3-3). B.P. also relates well to the regional record which shows a 'migration period' cooling phenomenon around this time (Wanner et al. 2015). Cooler temperatures at 289 cm could reflect the little ice age cool period (Mann et al. 2009). However one of the warmest C-IT for the entire Holocene record (16.31 °C) also

occurs during the LIA interval, possible hinting at a different driver in chironomid community assemblage on Windermere. The C-IT also shows a general cooling trend following the early Holocene warm period. This in part reflects other palaeoclimate records which show a downward trend in summer temperatures, linked to decreased summer insolation in the Northern Hemisphere, in Northern and Central Europe from 6 k. cal. yrs. B.P. (Figure 3-6) (Davis et al. 2003).

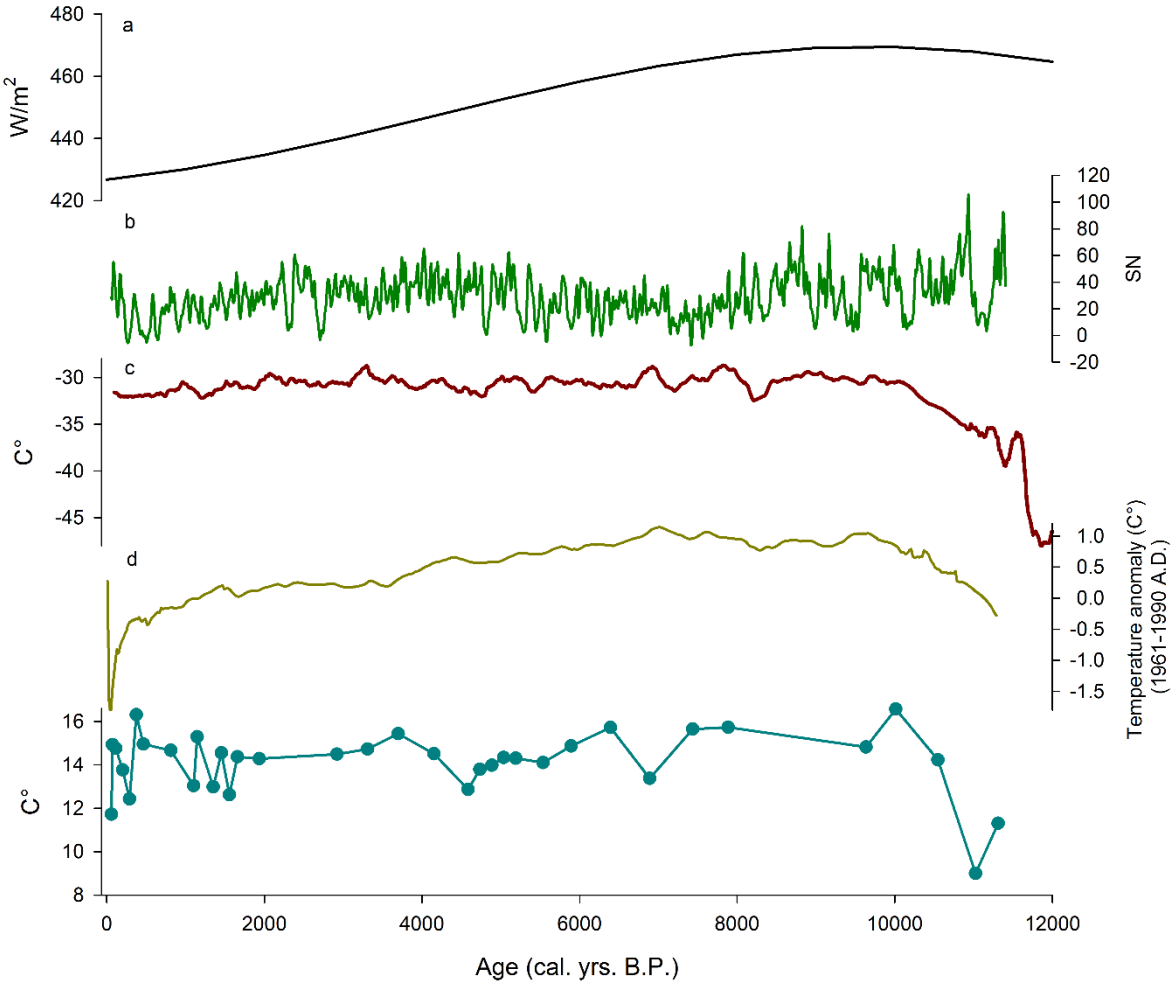

Figure 3-6: Comparison of chironomid inferred mean July temperature (C-IT) (C°) with a) July insolation (W/m²) at 65° N owing to eccentricity (Berger & Loutre 1991), b) reconstructed sunspot number (SN) (Solanki et al. 2004), c) Temperature (C°) interpretation based on stable isotope analysis, and ice accumulation data, from the GISP2 ice core, central Greenland (Alley 2000), and d) zonal mean temperature anomaly reconstruction stack for 90°-30° N (Marcott et al. 2013).

3.2.7 Mass Transport Deposits

Mass Transport Deposit (MTD) are typically caused by high-level water inflow (floods), river delta fan collapse and seismic activity (Schnellmann et al. 2005; Kremer et al. 2012; Strasser et al. 2013; Schlolaut et al. 2014). MTDs have been identified in +54-03/68 PC between 509.5 – 456 cm (MTD 1), 413.5 – 404 cm (MTD 2).

3.2.7.1 MTD 1

MTD 1 initiates with a layer of fine sand overlaid by organic rich and clay rich mud clasts in a fine sand matrix (Figure 3-7). This is interpreted as the redeposition of the laminated clay rich and organic rich lake muds probably from a higher elevated distal setting, which have become mixed in a debris flow. Debris flows constitutes concentrated, viscous sediment-fluid mix of clasts carried in a water sand-mud matrix which moves downslope under the influence of gravity (Stow 1984). The deposition of the sand size fraction first is interpreted as the settling from suspension of coarser sediment.

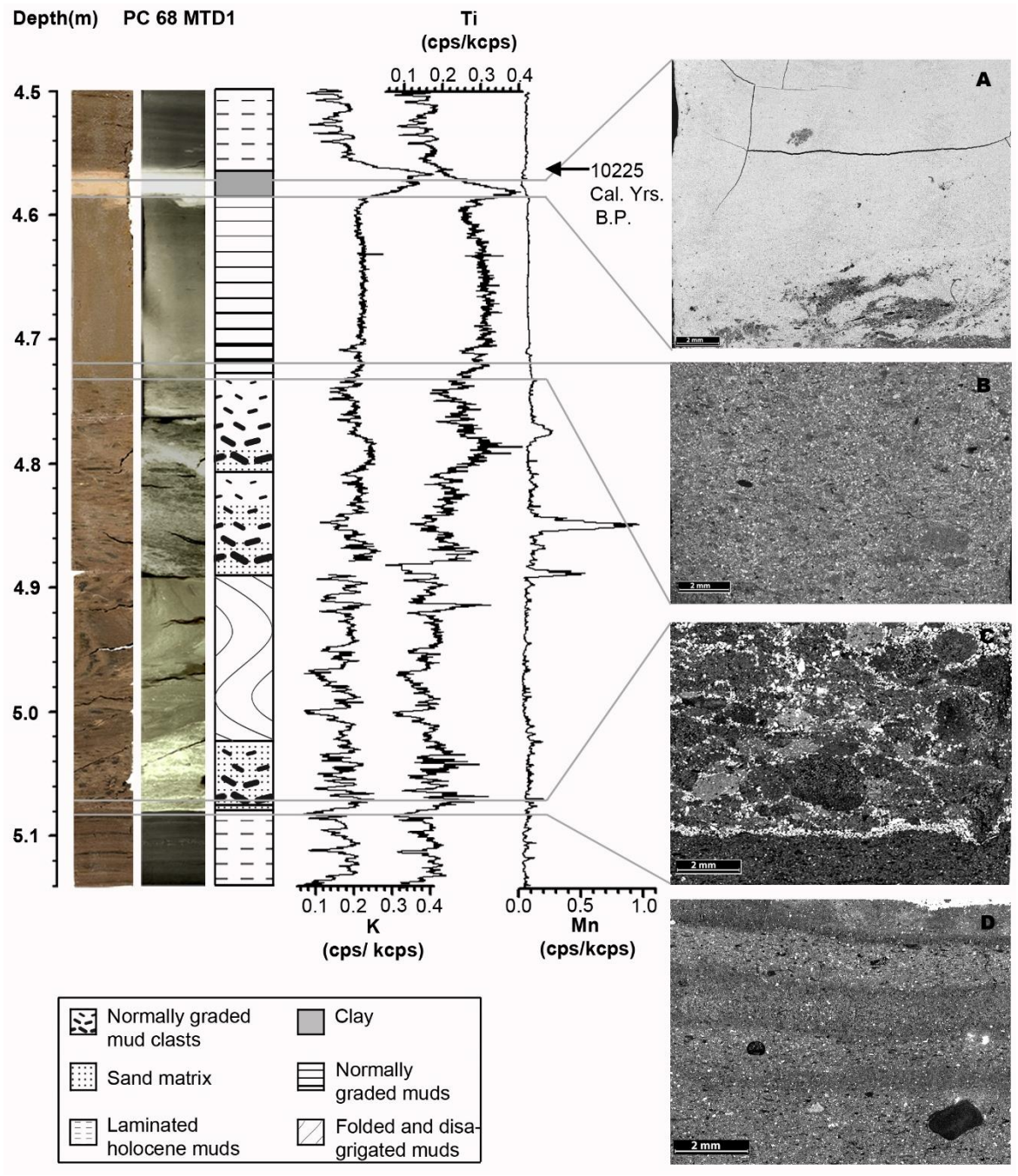

Figure 3-7: MTD 1 (509.5-456 cm) with photograph, x-radiograph and graphic log. Also shown are itrax K, Ti and Mn along with BSEI images of A the 'clay cap' with flame structure at the lower boundary, B graded detrital mud, C graded mud clast with sand matrix, and D Holocene laminated muds.

The debris flow is then overlain by slump folded sediments indicating a more cohesive movement, possibly folded by rotational sliding and slumping indicating a more plastic deformation rather than disintegration of sediments into clasts (Schnellmann et al. 2005;

Strasser et al. 2013). This is then followed by two graded organic and silty clay rich mud clast layers, which are interpreted as two further successive debris flows.

Above this are graded organic and silt rich muds lower amplitude variability in Ti and K reflecting the better sorted terrigenous silts with the grading marked by decreasing Ti. This is overlain by a graded clay cap with a distinct peak in Ti leading that in K (Figure 3-7). The clay cap also contains flame structures (Figure 3-7) at the base and mixing at the top which are interpreted as vertical deformation of the clays, silts and mud below as a result of loading of more dense material above (Mills 1983).

The graded silts, organic matter and clay cap sequence is interpreted as the fine sediment settling out of suspension from a turbidity current triggered by slumping. This geochemical pattern is strikingly similar to that observed in MTDs in sediments from Lake Suigestsu, Japan and Ledro, Italy which also shows the distinct low amplitude variability in terrigenous sediment indicators increasing and then decreasing before a peak in terrigenous sediment indicators in the clay cap (Figure 3-7) (Gilli et al. 2003; Schlolaut et al. 2014).

The sequences of debris flow deposit, overlain by folded sediments, graded debris flow and turbidites observed in Windermere has also been observed in Lake Zurich (Strasser et al. 2013). The Lake Zurich MTD is ascribed to the result of failures in the distal basins slopes causing sub-aqueous landslides, with the turbidite representing fine material suspended by a debris flow. The interpretation of MTD 1 as a resulting from a subaqueous land slide is supported by the organic rich mud clast being comprised of lake sediments with organic remains such as chironomids, and benthic diatoms.

The timing of MTD 1 between ~11000 and ~10100 cal. y. B.P. coincides with a period of increased landslide activity in formerly glaciated regions which is widely ascribed to more active seismicity in the late Glacial to early Holocene period due to combinations of isostatic crustal rebound and stress release (McColl 2012). Varve dating of palaeo-seismicity in Sweden shows a clear maximum in the interval 11,000 - 9,000 k yrs. B.P. corresponding to the period of maximum rates of glacial isostatic uplift (Morner 2005). Dating of rock slope failures in Scotland and NW Ireland by cosmogenic isotope exposure shows a period of frequent slope failure occurrence that spans a period of around 5,000 years through the Lateglacial to very early Holocene to around 11 k yrs. B.P. (Ballantyne et al. 2014).

Across the Lake District, 48 relict rock slope failures are identified, it is inferred that most post-date the Last Glacial Maximum with at least one probably post-dating the Younger

Dryas cold interval (Wilson 2005; Wilson & Smith 2006). Their origins are ascribed to a range of causes including redistribution of stresses during glaciation and subsequent stress release on deglaciation that may act in combination with the trigger of seismic activity resulting from glacio-isostatic crustal readjustment (Wilson & Smith 2006).

It is therefore likely that seismic activity following deglaciation is responsible for the triggering the MTD.

3.2.7.2 MTD2

As in MTD1, a 300µm sand layer is followed by large allochthonous well preserved organic fragments set in a fine – medium sand matrix, and succeeded by graded organic-rich silt with a clay cap, and so is similarly interpreted as the settling of coarse to fine material from suspension in a turbidity current. This is comparable with deposits from alpine lakes which show graded macro organic fragments, overlaid by organic rich silt and clay as turbidites (Gilli et al. 2003; Wilhelm et al. 2013). Ti and K shows enriched values with low amplitude variability between 409 and 406 cm after which values rise with the beginning of the clay cap before the data becomes unreliable, and falls again afterwards (Figure 3-8). This pattern is consistent with graded deposition from suspension in a turbidity current also observed in Ti and K values in MTD 1 (Figure 3-8).

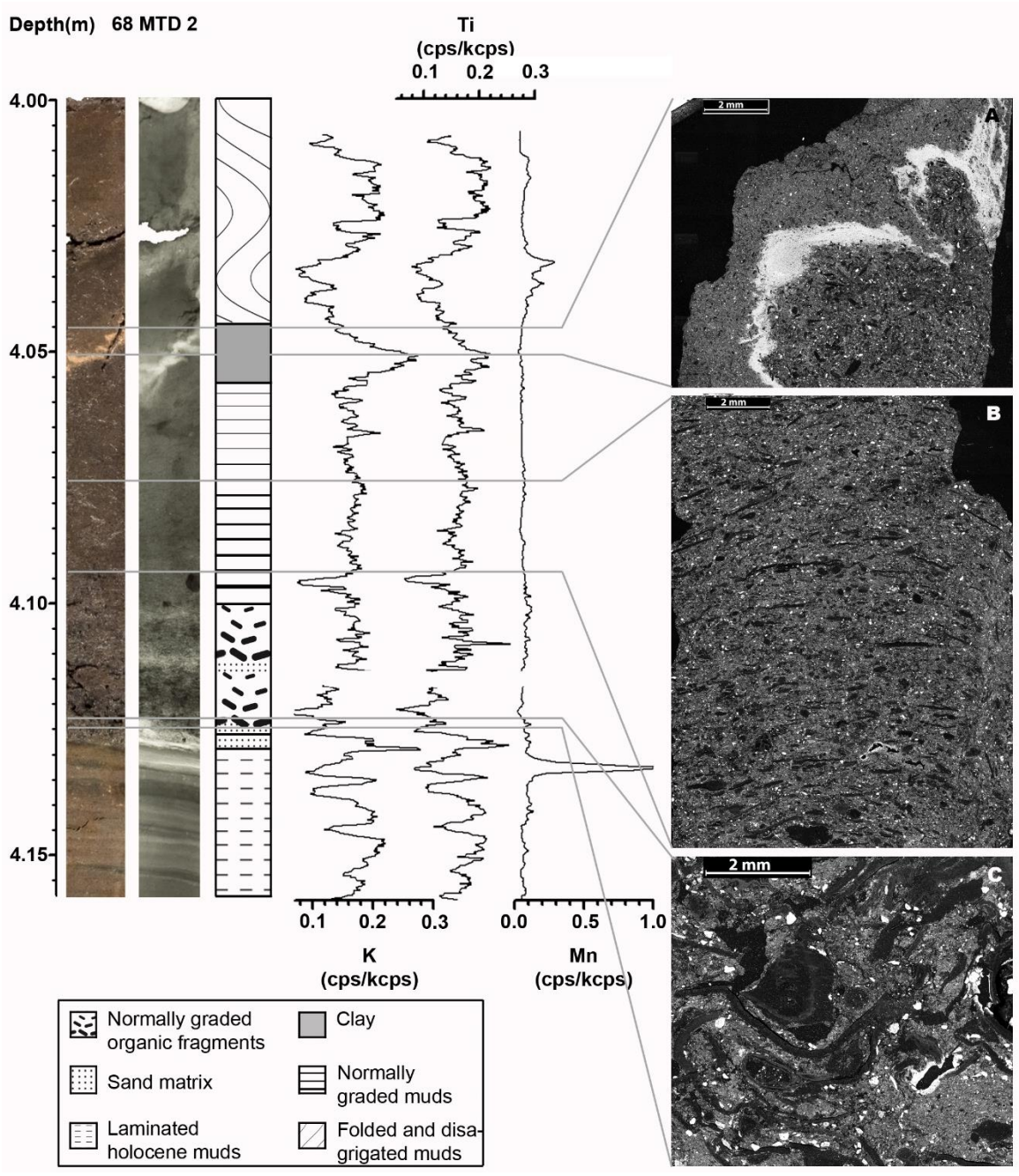

1204

1205 Figure 3-8: MTD 2 (412.5 - 400 cm) with photograph, x-radiograph and graphic log. Also
1206 shown are itrax K, Ti and Mn along with BSEI images of A the distorted 'clay
1207 cap', B graded organic rich detrital mud, and C graded organic fragments and
1208 sand matrix.

1209 The large allochthonous organic fragments suggest that it was associated with a period of
1210 in wash. The upper age estimate for MTD 2 is ~8100 cal. y. B.P. just after the abrupt climate
1211 cooling event at 8.2 k. y B.P. (Renssen et al. 2009; Young et al. 2013). There is evidence in
1212 Cumbria from loessic silts of increased snow accumulation, extended snowpack cover, and
1213 an increase in the magnitude and frequency of meltwater flooding during this time (Vincent
1214 et al. 2011). It is therefore feasible that a single precipitation event or snowmelt could be

the cause of large inflow (Sturm & Matter 1978; Gilli et al. 2003). However, despite documentary evidence for large flood events in 1635 AD during the LIA (Miller et al. 2014b), deposits of the same scale are not observed at any other interval in the sediments after MTD1 and so a different trigger mechanism needs to be considered. Outbursts of water from moraine- or rockfall- dammed lake, as a result of heavy rain and or snow melt, have been proposed for the deposition of large MTDs in Lake Constance, and Lucerne (Schnellmann et al. 2005). This could provide an appropriate mechanism for MTD 2.

3.3 Conclusion

A well preserved and complete Holocene sequence has been cored from Windermere. The earliest Holocene shows evidence for rapid warming, the onset of lake productivity and the colonisation of the catchment by vegetation. This period was marked by tectonic instability likely related to glacio-isostatic readjustment that led to slope failure and the deposition of MTDs in the lake. High amplitude variability in runoff to the lake in the early Holocene decreased from around 8 - 7.5 k B.P. alluding to greater climate stability and a more settled forested catchment. Episodes of high lake productivity associated with vigorous seasonal lake turnover marked by high Mn variability may be associated with colder climate episodes that punctuated the Holocene. These pilot studies show the potential for the Windermere cores to provide a definitive UK Holocene climate record.

Chapter 4 Palaeoseismology from microfabric and geochemical analysis of lacustrine sediment, Windermere, UK

4.1 Introduction

A major target in the analysis of the sedimentary records of lakes and marine margins has been to investigate the origins of slope-failures that produce scarps and generate mass transport deposits (MTD) and turbidites (Strasser et al. 2013). Increasingly, such event deposits are being related to historical records of seismic activity and these efforts have led to the development of a new interdisciplinary field of "subaquatic palaeoseismology" that integrates marine and lacustrine sedimentology with palaeoseismology (Gracia et al. 2013; Strasser et al. 2013). Most of these sedimentary palaeoseismic records are being constructed from more seismically active regions and while historically based palaeoseismic records exist for Britain (British Geological Survey 2010; Stucchi et al. 2013), there are no such sedimentary palaeoseismic records. Critical evidence to associate sedimentary deposits with specific earthquakes includes synchronicity tests that require well-dated and clearly correlated sequences.

Many lacustrine sequences contain MTDs and turbidites with similar sedimentary and geochemical profiles from a range of sources including flooding and seismic activity. In order to interpret these features and build an accurate record of past extreme events, careful analysis of the microfabric and structure of well-preserved sediments is needed (Schlolaut et al. 2014). Ideally, this involves the analysis of annually laminated or varved records, but sediments in these settings are often subject to disturbance by biota even in environments with reduced water column turnover and resultant limited levels of bottom water oxygenation (Reynoldson 1987). Where sediments are disturbed by bioturbation, the original structure may be obscured (McCall & Tevesz 1982) making interpretation difficult. Here we use a novel combination of techniques to study microscopic sediment fabric features in well-dated cores from Windermere to identify evidence for seismically generated MTD in sediments which have undergone disturbance by biota. This new approach may serve as an example for future development of subaquatic palaeoseismology.

4.1.1 Previous work

Recent lake bed and subsurface studies (Miller et al. 2013) have revealed evidence for several mass flow events characterised by scarps, transportation zones, and deposition zones (Miller et al. 2013). The largest and most recent of these is located on the distal shelf of the Trout Beck delta fan, extending 450 m into the lake to depths of 45 m (Figure 4-1). The exact date and trigger mechanism for the Trout Beck mass flow event deposit have hitherto not been established.

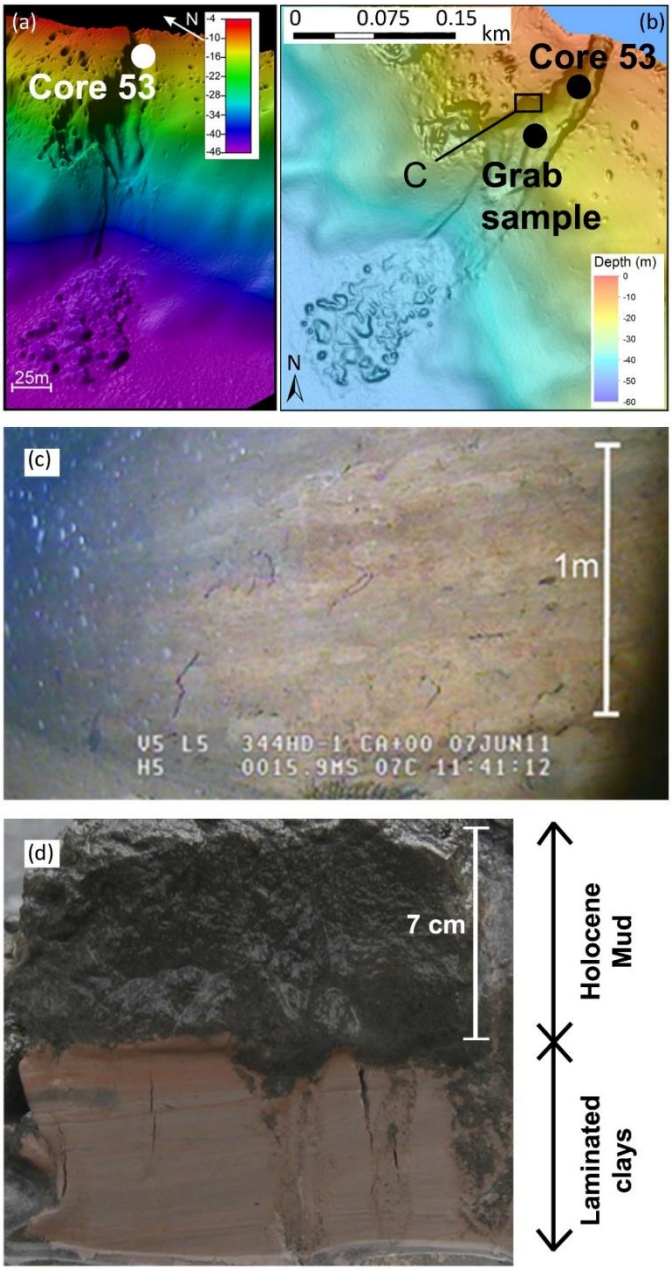

Figure 4-1: Trout Beck debris flow; (**a**) hillshade bathymetry (x5 vertically exaggerated), (**b**) bathymetric map of Trout Beck debris flow showing position of core 53 and a grab sample within the scarp and location of bottom photograph of

(c). (**c**) Photograph of exposed laminated glacial clay (taken with remotely operated vehicle) within the sidewall of the Troutbeck debris flow scarp. (**d**) Photograph of grab sample showing 7 cm of Holocene mud unconformably overlying laminated clays. The unconformity represents the debris flow failure plane. The top surface of the grab sample is the lakebed surface, indicating no mud was lost during collection of the sample.

4.2 Results

4.2.1 Clay rich lamina

In both SC68 and SC64 there is a distinct pale clay-rich layer above the dark gyttja that is entirely absent from the South Basin cores (**Error! Reference source not found.**). The clay-ich layer is marked by elevated potassium (K) and Titanium (Ti) (**Error! Reference source not found.**). In SC64 the upper part of this pale clay rich layer is marked by a peak in Mn (Figure 4-2).

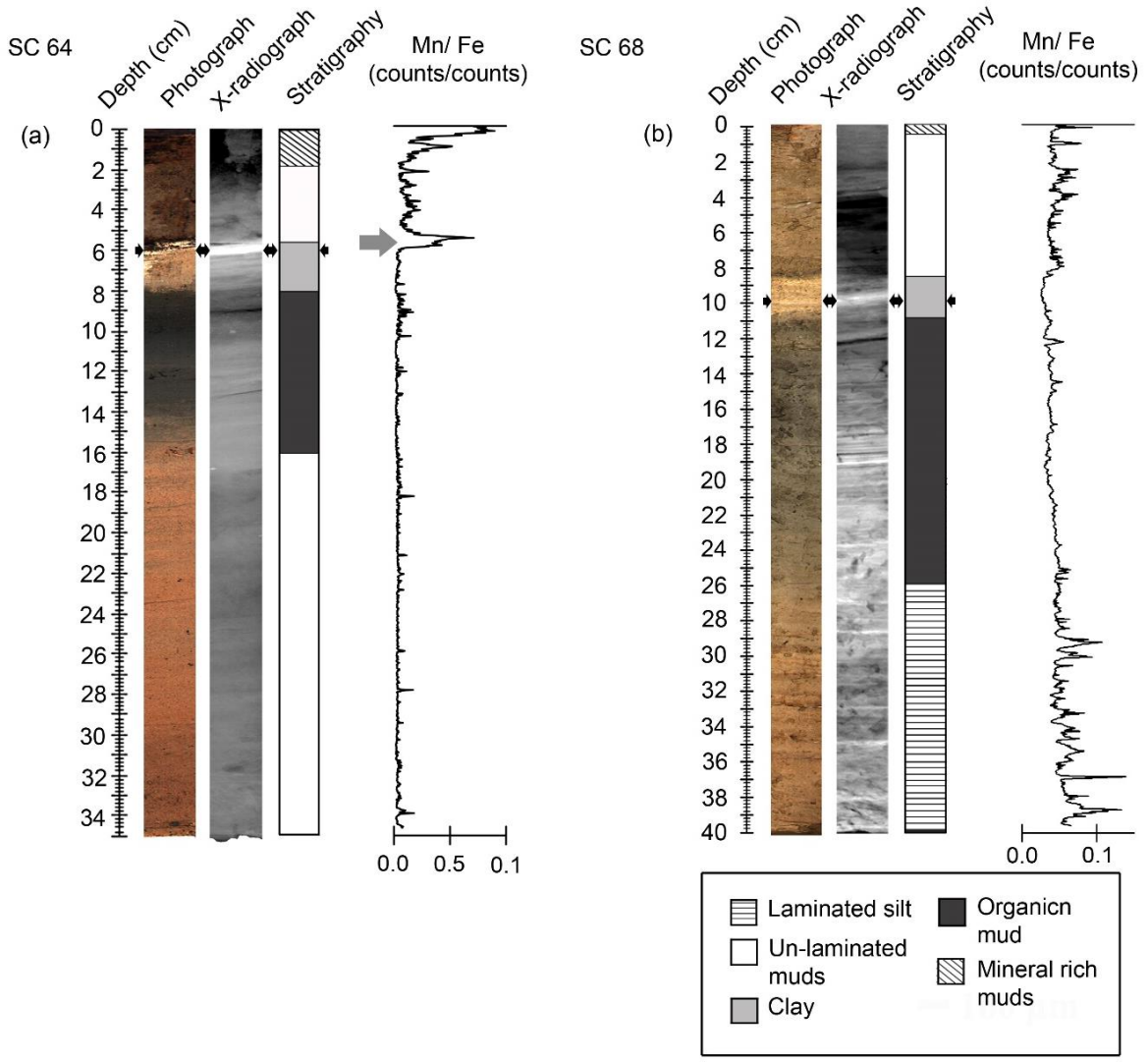

Figure 4-2**:** Post mass transport deposit (MTD) redox redistribution. Photography, x-radiograph and stratigraphy of cores SC64 (A) and SC68 (B). The black arrows mark the clay horizon (with in the MTD) and the grey arrow shows the peak ED-XRF (counts/ counts) Mn/Fe values in SC64 following the MTD.

Analysis of high resolution photography from core 53 (Figure 4-3) shows laminated glacial clay (Avery et al. 2017) ending with an erosional unconformity, followed by a mixed organic matter debris clay rich layer thought to represent a debris deposit. This is then overlain by massive organic rich muds.

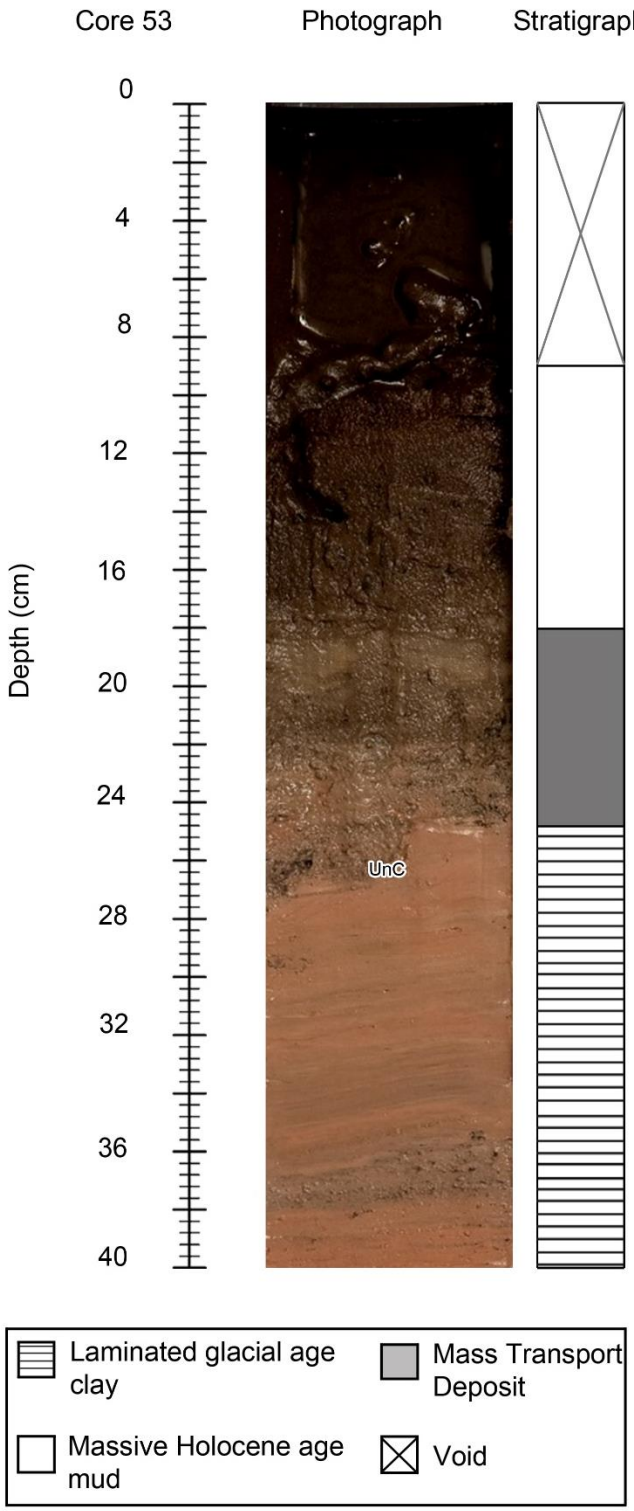

1300

1301 Figure 4-3: Core photograph and stratigraphy of core 53 taken from within the Trout
1302 Beck mass transport deposit (MTD). The figure shows laminated glacial ending with
1303 an erosional unconformity (UnC), followed by a mixed organic matter/clay rich
1304 layers (MTD), and finally massive Holocene age muds.

1305

4.2.2 Micro-lithostratigraphy of the clay rich interval

In core SC64 (Figure 4-4a) the sediment shows an abrupt change from grey (7.5Y 4/1) organic-rich mud to the light orange (7.5 YR 8/6) clay rich sediments at 8 cm. There is a further colour change to light yellow (7.5 YR 8/5) at 7.1 cm. The upper boundary at 5.6 cm is irregular and is marked by another abrupt change to overlying brown (10 YR 4/4) organic muds. The x-radiograph (Figure 4-4a) shows a clear two-part structure within the pale orange/ yellow horizon visible in the core with a very dense upper layer between 5.6 – 6.2 cm (as shown by higher x-ray scattering) and a more diffuse lower part with density decreasing downwards to 8 cm (as shown by gradually decreasing x-ray scattering). The BSEI (Figure 4-4a) shows the 0.5 cm dense layer in the X-radiograph to correspond to a 0.5 cm thick clay layer. The BSEI also reveals an underlying paler zone that is relatively enriched in clay. Small-scale redistribution of sediment due to zoobenthos burrowing, as well as some pelletisation, is also evident from the BSEI (Figure 4-4a). The ED-XRF Ti and K increase sharply at 8cm (K also shown in Figure 4-4), corroborated by increased values also in WD-XRF (Figure 4-4a). Ti and K from ED-XRF both remain elevated to 6.5 cm, peak at 6 cm then decrease to 5.5 cm where values decrease in variability and remain low (Figure 4-4a). At 6 cm, Mn/Fe values increase abruptly to peak at 5.5 cm, the highest value in the core (Figure 4-2).

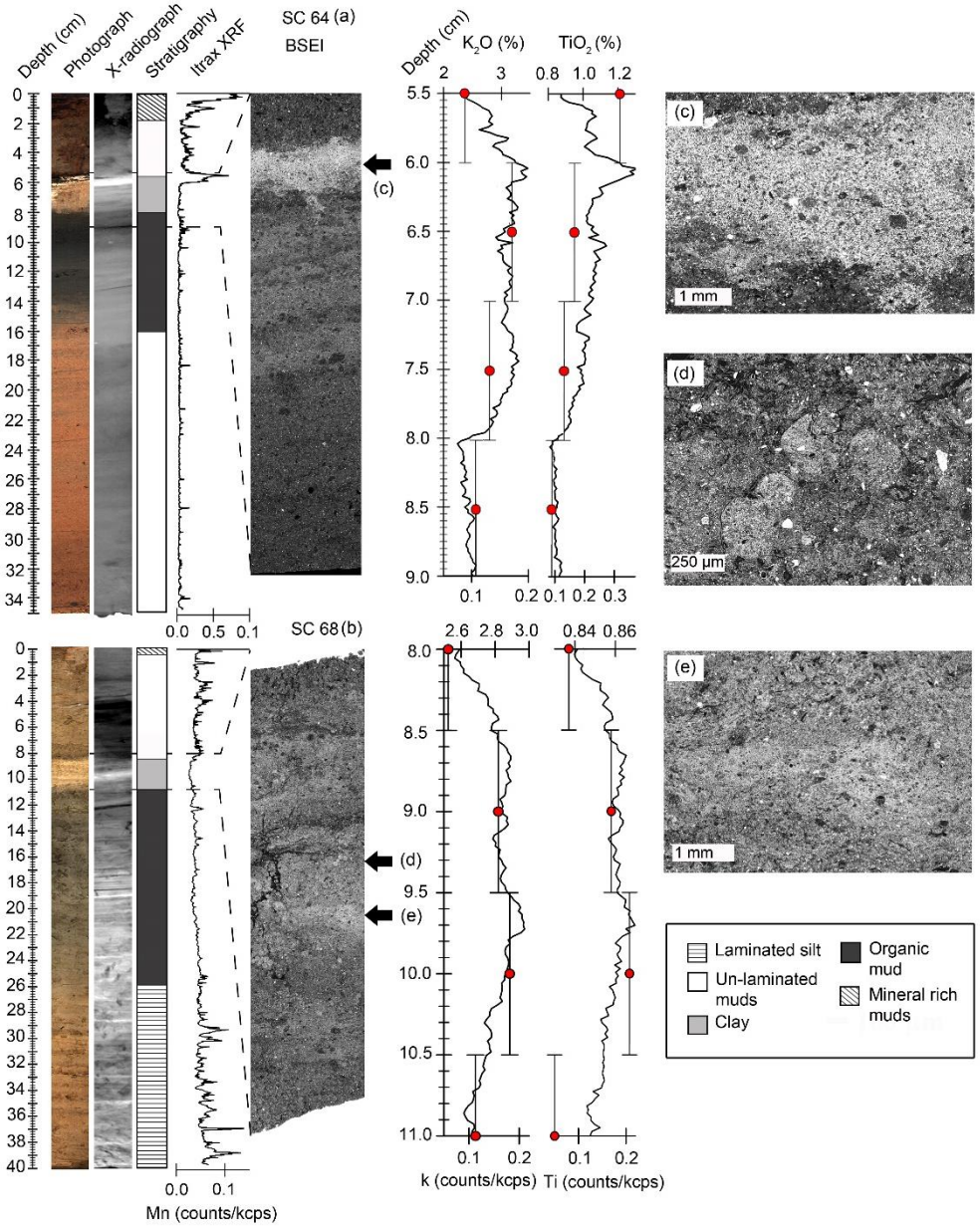

Figure 4-4**:** North Basin cores (**a**) SC64; (**b**) SC68 are shown with core depth (cm), core photograph, core x-radiograph and stratigraphy (and legend bottom right of the Figure). Black lines show the position of the Back Scatter Electron Image (BSEI) within the cores. BSEI are shown with depth (cm) and K, and Ti, ED-XRF geochemistry (element counts/ total kcps) for the BSEI interval is plotted by the black lines, and WD-XRF (%) are plotted as red dots with the error bars representing the sampling interval. Black arrows right of the BSEI show the location of the clay horizon in SC64 (**c**) and in SC68 (**e**), and more detailed bioturbation and clusters of pellets in SC68 (**d**).

In Core SC68 (Figure 4-4b), there is a colour change from grey (7.5Y 4/1) organic-rich mud to light brownish grey or dull orange clay-rich sediments (7.5YR 7/2 – 7/3) at 11 cm, with a further change at 10.5 cm to light orange (7.5YR 8/6). At 8.6cm the clay rich sediment upper boundary is marked by a colour change to dull yellow orange organic muds above (10YR 6/3) (Figure 4-4b). The X-radiograph shows a broad higher density (paler) interval corresponding to the pale yellow colour in the core surface but with a marked denser (paler) layer from 10.2 cm to 9.6 cm. BSEI show backscatter and clay content increases significantly between 9.8 and 9.5 cm (Figure 4-4 b), and pelletisation and redistribution of the clay-rich sediment indicates significant bioturbation of the interval (Figure 4-4 d and e). Clay content remains high to 9.2 cm then gradually decreases to a diatom-rich lamina at 8.5 cm (Figure 4-4b). Pellets are between 50 – 300 µm in diameter, and exhibit lithology and density of sediments from above and below, indicating redistribution of sediments by bioturbation (Figure 4-4c, e). The pale interval in the core is marked by elevated ED-XRF K and Ti from 10.5 – 8.5 cm with a peak in both at 9.8 – 9.5 cm corresponding to the palest (densest in the BSEI) sediment. Mn/Fe ratios values decrease and become less variable through the clay rich sediments reaching a low at 9.7 cm depth. ED line scan and elemental map data show similar results in elements associated with terrigenous detrital silt and clay (K) (Figure 4-5) peaking between 9.5 and 9.3 cm depth.

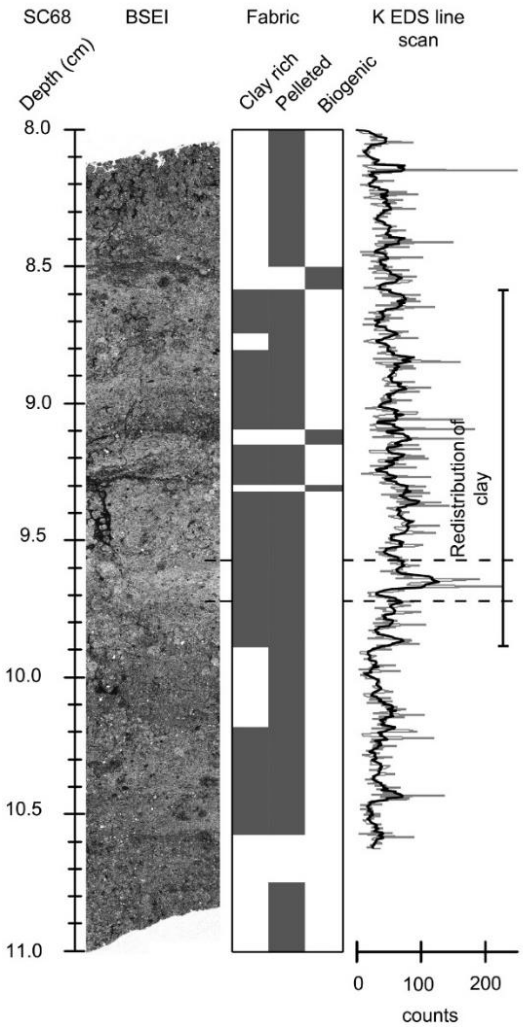

Figure 4-5: SC68 mass transport deposit (MTD) back scatter electron image, sediment fabric types, K ED line scan 5 point running average (black dots) and raw counts (grey line) with clay redistribution zone highlighted. Fabric types are determined from detailed analysis of backscatter electron imagery and optical microscopy. The figure highlights the extent to which the K enriched clay of the MTD has been vertically redistributed from the original deposit where the 5 point moving average K is highest (dotted line).

In both cores in the North Basin, the combined evidence from sediment fabrics and geochemistry is consistent with deposition of a distinct clay horizon followed by some bioturbative redistribution of the clay and this is discussed in more detail below. Independent ^{210}Pb and ^{137}Cs derived age models suggest that the clay horizons from both cores were deposited at the same time, with the SC64 clay horizon (6.2 – 5.6 cm depth) dating to 1979 (1974 – 1982) and the SC68 clay horizon (9.5 - 9.25 cm depth) to 1979 – 1980 (1973 – 1986).

4.3 Discussion

4.3.1 Origin of the clay horizon

In both cores SC64 and SC68, the pale clay appears as a relatively broad, 2 cm-thick horizon that is marked by elevated K and Ti over a similar depth range (Figure 4-4, Figure 4-5). However, the X-radiography and BSEI provide evidence for a thinner clay-rich compositional end-member (arrowed in Figure 4-4) which has evidently been redistributed by bioturbation. The BSEI microfabric analysis reveals clusters of pellets rich in detrital clay and fine silt throughout this broader 2 cm-thick interval (Figure 4-4, a). These pellets are consistent with evidence for vertical redistribution of sediments through bioturbation by conveyor belt feeding benthic organisms such as tubificid oligochaetes which have been observed in abundance in the profundal sediments of Windermere even in low oxygen conditions (Reynoldson 1987). Tubificid oligochaetes redistribute sediments vertically by burrowing, passing material through the digestive tract and depositing faecal pellets in mounds at the water sediment interface (McCall & Tevesz 1982; Dafoe et al. 2011) . Redistribution of sediments normally takes place over small vertical distances (2 – 9 cm) and 'blurs' sediment structure as opposed to completely removing original structures (McCall & Tevesz 1982). Furthermore, selective feeding can often result in the deposition of faecal pellets rich in clay and silt both above (Davis 1974; Ciutat et al. 2006) and slightly below (due to sediment slumping into burrows) (Fisher et al. 1980) the source sediment. Apart from tubificid oligochaetes, chironomid larvae are the other important component of the benthos and they create tubes and similarly sized faecal pellets (100 – 300 μm diameter) typically within the top 2 cm (Frouz et al. 2004; Nogaro et al. 2008). The overall microfabric and geochemical evidence therefore supports the bioturbative reworking of an originally compositionally pure clay end member.

The geochemical profile of Ti and K and microlithostratigraphy of the SC64 clay is consistent with erosion and re-deposition of the laminated pre-Holocene detrital clay, silt and organic-rich Holocene lake muds. The clay constitutes the finest material settling out of suspension after the mass flow event that generated a turbidity current that penetrated a large part of the North Basin of Windermere. The characteristic geochemical profile of Ti and K, and sediment microlithostratigraphy is comparable with typical examples of the finest grained section or "clay cap" commonly described from other lacustrine debrite – turbidite deposits (Gilli et al. 2003; Schlolaut et al. 2014).

The peak in Mn above the clay layer in SC64 (Fig. 5a) also supports this event bed origin. In many lakes with oxygenated bottom waters redox driven focusing causes sediments at the water sediment interface to became enriched in solid phase Mn, usually as Mn oxyhydroxides (Davison 1993). As has been identified in marine settings (Colley et al. 1984; Jarvis & Higgs 1987; Thomson et al. 1987), and under experimental conditions (Chaillou et al. 2007), burial of solid phase Mn by an MTD can inhibit oxygenation of the underlying sediment leading to the reduction of Mn into its mobile reduced Mn^{2+} ions and upwards migration in the pore waters. On reaching oxygenated sediments above the clay reduced Mn^{2+} would then be re-oxidised and precipitated as Mn oxyhydroxides (Fig. 9 d) (Davison 1993). A similar peak is not seen in SC68 since the deeper part of the basin was likely anoxic at this time (Pickering & Sutcliffe 2001), causing Mn to diffuse into the water column (Davison 1993). While this phenomena is well described in a marine setting its occurrence is poorly represented in a freshwater lake environments. Higher variability of Mn in core SC68 deeper than 25 cm is related to annual scale bottom water redox variability prior to the more eutrophic, and thus more intensely anoxic, mid-20th century.

As regards the source of the turbidite, the scarp of the Trout Beck mass flow deposit exposes both the Holocene organic muds and the distinctive late Pleistocene glacial laminated silt and clay facies (see Avery et al. (2017), for the overall stratigraphy) (Figs. 2c, d, 9) (Miller et al. 2013) allowing these sediments to be redistributed as part of the MTD.

4.3.2 Origins and timing of the Trout Beck debris flow and relation to clay

The absence of the pale clay horizon from the South Windermere basin suggests that it originated as an event deposit that affected the North basin only and a likely candidate for its origin is the Trout Beck debris flow (Figure 4-1). Analysis of high resolution photography (Figure 4-3) shows an erosional unconformity, followed by a debris lamina. These beds represent debris from the Trout Beck scarp wall failure, but unlike SC64 and SC68 there is no pale clay horizon. The absence of a clay cap is likely due to the shallow setting of core 53 near the origins of the slope failure since the main body of suspended sediment from which the clay settled would have been concentrated in the deeper parts of the basin below the zone of slope failure, as is commonly the case for such events (Van Daele et al. 2015).

The debris horizons are followed by 9 cm of organic mud. As ^{210}Pb and ^{137}Cs analysis was not done on core 53, the other cores from this basin provide us with a possible LSR. Using the LSR for SC68 (0.28 cm yr^{-1}) and SC64 (0.14 cm yr^{-1}) places the slope failure between 1950 and 1981. The size, relative position (1.7 km NNE of SC64, 3.2 km SE of SC68), and age of

the mass movements (Figure 4-1 and Figure 2-1) makes the Trout Beck scarp the most likely source of the MTD described in SC64 and SC68 which have been dated to 1979 (1978 – 1986) and 1979 – 1980 (1973 – 1986) respectively.

With the timing constrained, possible causes of the slope failure may be explored. Trigger mechanisms for slope failure in lacustrine settings include seismogenic activity; overloading of slopes due to rapid or increased sedimentation; flooding associated with catastrophic river discharge; lake level fluctuations; surface wave activity; terrestrial debris flow or rock fall from adjacent slopes; and anthropogenic activity. Flow data from the river Leven shows that the period 1978 to 1982 is a phase with above average, but not exceptional, winter outflow (National River Flow Archive, CEH, NERC – Figure 4-6). Sedimentological analysis shows that neither SC68 nor SC64 MTDs contain macro organic fragments or detrital sand and silt in amounts in excess of the average for Holocene muds. Furthermore, geochemical and microlithostratigraphic analyses show no evidence for a contemporary event in the South Basin or for other peak flow events, such as the exceptional 2008 – 2009 floods. There is therefore no evidence to support flooding as a trigger (Figure 4-6). Terrestrial slope failure is also not documented at this time.

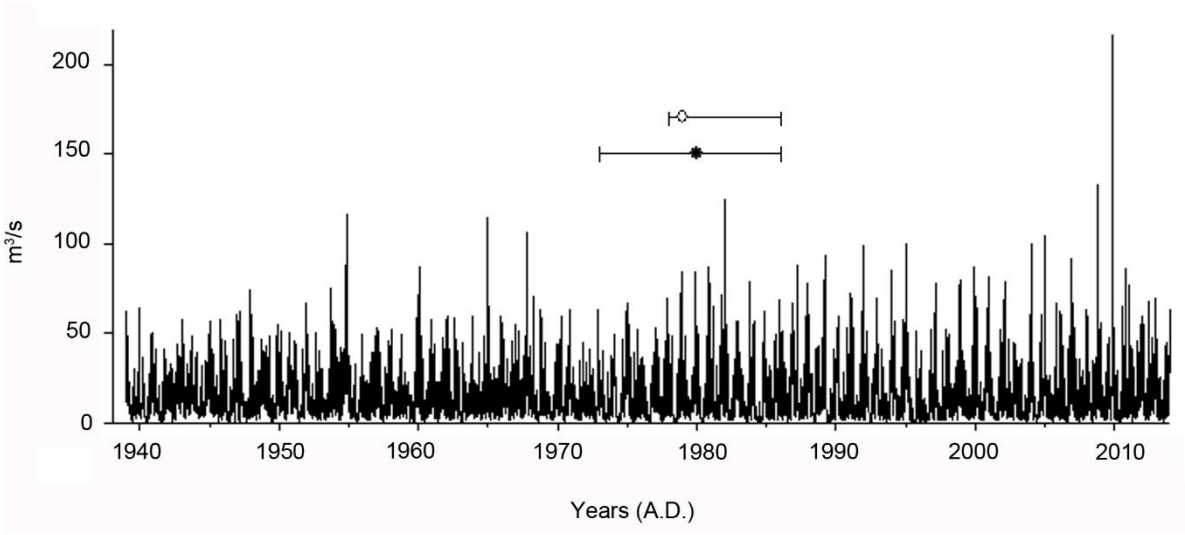

Figure 4-6: Black line shows river discharge data for the River Levin from 1939 – 2014. The black dot show the timing of the mass transport deposit (MTD) in SC68 and the white dot the timing of the MTD in SC64. Error bars on both show the machine error derived age range from ^{210}Pb dating.

4.3.3 The 1979 Carlisle Earthquake

The UK is an area of low to moderate seismological activity; however, recurrence relationship analysis of historical records shows that 4.7 ML earthquakes occur on average

every 10 years (Baptie et al. 2005; Musson & Sargeant 2007). On the 26th of December 1979 a 4.7 ML earthquake with an epicentre 13 km NNE of Carlisle, (70 km N of Windermere town) occurred. The earthquake was one of the largest in the UK in the last century and was followed by two aftershocks in early January 1980 each measuring 3.8 ML (King 1980; Musson & Henni 2002). The earthquake's effects were felt above 3 EMS (European Macroseismic Scale) over an area of 84 000 km^2, although intensity decreased rapidly to the south of the epicentre. Over much of the Lake District, the intensity was 4 EMS and data suggest that the intensity was 3 – 4 EMS in the Windermere and Kendal area (King 1980). The timing of the Carlisle earthquake, and its aftershocks (1979-1980), together with the lack of another contemporaneous mechanism suggest that it was a likely trigger of the Trout Beck delta fan failure and resulting mass transport deposits.

The Carlisle earthquake is the most likely cause of the Trout Beck delta fan slope failure and the resulting North Basin MTD. Previous earthquakes in the area similar in magnitude in 1901 (4.1 ML) and 1915 (4.0 ML) have, however, not left evidence on the same scale in the lake bed sediments since the clay layer is unique within these records (**Error! Reference ource not found.**). Palaeoseismic research demonstrates that some of the strongest historical earthquakes were not associated with slope failure (Talling 2014), but that even small earthquakes may cause considerable disruption if the sediment is destabilised by processes such as rapid sediment accumulation or biogenic gas production, prior to the event (Nisbet & Piper 1998; Girardclos et al. 2007). For example, although the 1865 Barrow-in-Furness earthquake was probably only in the range 2.5 – 3.5 ML, it produced spectacular and damaging liquefaction enhanced by saturated tidal sands (Musson 1998).

4.3.4 Slope preconditioning and failure

Biogenic gas build up as a result of sedimentary methanogenesis has been shown to intensify with increased organic matter input in eutrophic lakes systems (Kelly & Chynoweth 1981). The MTD overlays an organic-rich diatomaceous sediment thought to represent peak eutrophic conditions in the lake. Lake monitoring and previous sediment studies have shown seasonal cultural eutrophication of Windermere has occurred since the 19th century (Sabater & Haworth 1995; McGowan et al. 2012). Increased lake productivity as a result of additional nutrient loading and organic matter in-wash, is therefore likely to have led to increased biogenic gas in the sediments and reduced slope stability. However, Windermere has only been seasonally eutrophic since the mid-19th century meaning excess

biogenic gas production is likely to be restricted to at most the top 40 cm, reducing the impact of this as a slope failure trigger mechanism.

Increased sediment loading causes additional pore pressure further reducing slope stability especially in steep delta fan slopes (Girardclos et al. 2007). AMS radiocarbon age depth models from piston cores taken at corresponding sites to the gravity cores show that LSR have accelerated since the 19th century (pre-19th century LSR PC 68 = 0.03 cm yr^{-1}, PC 64 = 0.03 cm yr^{-1}). The Trout Beck delta fan has a slope angle of up to 7°, and while the Trout Beck catchment is relatively small in comparison to the Rothay/Brathay catchment to the North, the high elevation over a short distance and trapping efficiency of an intermediary smaller lake in the Rothay/Brathay catchment means the catchment is sedimentologically more important (Miller et al. 2014a). Thus, increased sediment loading may have contributed to slope destabilisation.

There is evidence of commercial dredging for sand and gravel in the lake particularly around the submerged Trout Beck delta fan leaving visible pot marks in the sediment (Figure 4-1). However, this activity ended in the early 1970s (Miller et al. 2013), and so while it was not likely to have led directly to the slope failure, it is entirely likely that this activity could have further destabilised the delta fan. It is therefore probable that a combination of biogenic gas production, increased sediment loading and anthropogenic activity such as dredging have led to a critical state where sediment failure may occur in the lead up to the 1979 Carlisle earthquake.

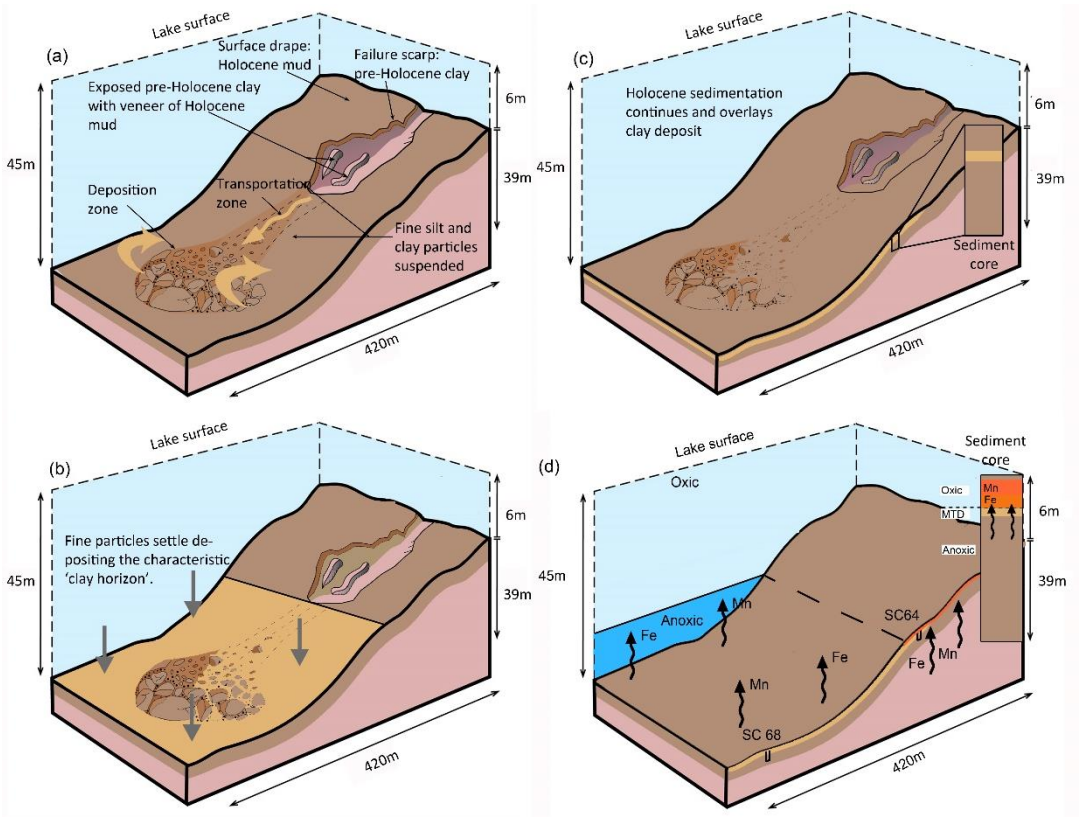

Figure 4-7: An illustration of the processes that generate the clay horizon in the North Basin of Windermere. (**a**) Trout Beck debris flow is triggered which removes Holocene mud from the slope and deposits it as a debris flow. The scarp failure exposes the pre-Holocene clays within the scarp. (**b**) Fine particle matter suspended in the water column below the level of the scarp settle over the North Basin of Windermere. (**c**) Mud continues to deposit on top of the clay horizon. (**d**) Mn – Fe lamination formation in deep anoxic and shallow oxic settings. On the left a schematic of SC68 shows Mn and Fe in solution being removed from the sediment pore water to the water column above in an anoxic bottom water environment. The right shows a schematic of SC64 with ventilated bottom water and a redox boundary within the sediment at which the reductively mobilised Mn and Fe are precipitated as oxyhydroxides above the MTD.

4.3.5 Likely event timeline

- Increased biogenic gas production as a result of increased productivity in the lake since the 19th century, combined with increased sediment loading and activities such as dredging, cause the steep-sided (7°) Trout Beck debris fan to become unstable.

- On the 26th of December 1979 an earthquake with an epicentre north of Carlisle occurs with an intensity was 3 – 4 EMS in the Windermere and Kendal area (King 1980), causing failure of the Trout Beck delta fan slope (Figure 4-1).
- Debris is transported as far as 1.7 km from the slope failure and fine-grained sediments (Holocene muds and glacial clay and fine silt) are suspended in a turbidity current that penetrates throughout large parts of the North Windermere Basin (Figure 4-7). Following this, the fine gained sediments settle out of suspension in order of density, covering the organic rich sediments of the North basin with at least 3.5 mm of clay rich sediment up to 3.2 km away. This yields a low-end estimate of 29.75 m3 of redeposited sediment in the North Basin.
- The clay horizon is variably vertically redistributed by bioturbation (Figure 4-4e). Microfabric analysis using BSEI and EDS analysis shows pelleting of the sediments suggesting that it was the result of conveyor belt feeding by tubificid oligochaetes and/or chironomids (**Error! Reference source not found.**).
- The MTD cuts off oxygen from the overlying water column, restricting the oxygenation of the underlying sediments causing a reducing environment. Dissolved Mn and Fe migrate up and form oxides-oxyhydroxides at the redox boundary of the sediment water interface now above the MTD. In shallower water depths (26.1 m SC64) oxygenation is prolonged enough to allow Mn and Fe oxides-oxyhydroxides to form, as shown by the post MTD peak in Mn:Fe in SC64 (Figure 4-7). In more profundal settings (SC68) a persistently anoxic environment prevents the formation of Mn and Fe oxides-oxyhydroxides (Figure 4-7).
- Organic rich sediment is deposited above the clay horizon at a rate of 0.28 cm yr-1 at SC68 and 0.14 cm yr-1 at SC64 (Figure 4-4a/b).

4.4 Conclusions

A combination of SEM sediment microfabric and geochemical analyses are used to identify event layers in the sediments of Windermere. These constitute the first evidence of seismic activity-induced mass transport deposits (MTD) preserved in lake sediments in the UK. Our microlithostratigraphic approach facilitated the identification of a MTD in two sediment cores (SC68, SC64) collected from Windermere's North Basin in 2014. Using a ^{210}Pb CF:CS age model, validated by ^{137}Cs profiles both MTDs were dated simultaneously to 1979 (1978 – 1986) and 1979 – 1980 (1973 – 1986).

Microfabric analysis using light and backscatter electron microscopy, and energy-dispersive X-ray microanalysis shows that the redistribution of sediments in faecal pellets through conveyor belt feeding by infaunal burrowers, has led to 'blurring' of the fine scale structure of the MTDs, especially in the more profundal SC68. Despite the redistribution of the original MTD clay, microstratigraphic techniques permit the identification of the initial MTD structure and accurate dating of the event. These results demonstrate that even if sediments are pelletised, event beds may nevertheless be detected using appropriate SEM microfabric and geochemical methods. The microlithostratigraphic analysis shows that the MTDs consist of reworked Holocene organic mud and Pleistocene age glacial detrital Ti- and K-rich clays. SC64 has a classic 'debrite – turbidite clay cap' profile and shows K and Ti distributions comparable with other examples of MTDs found in lacustrine settings (Schnellmann et al. 2005; Girardclos et al. 2007; Strasser et al. 2013; Schlolaut et al. 2014). The MTD also shows characteristic evidence for redox sensitive Mn redistribution.

The MTD origins are linked to a large recent subaqueous slope failure of the Trout Beck delta fan, and associated mass flow deposit that was identified by previous investigations (Miller et al. 2013). Exploration of historic records reveals the most likely cause of the Trout Beck mass flow event and subsequent North Basin MTD to be an 4.7 ML earthquake on the 26th of December 1979 with an epicentre 70 km North of Windermere. It is likely that recent increased biogenic gas production, sedimentation, and commercial dredging combined to destabilise sediments in the Trout Beck area effectively preconditioned the sediment to a critical state.

Chapter 5 Natural and anthropogenic inputs to and water-column and sediment redox history of Windermere since the 18th century

5.1 Introduction

Freshwater lakes represent a critical resource providing a wide range of services such as a municipal water source (Fowler et al. 2007), flood mitigation (Thampapillai & Musgrave 1985), fisheries or refuge for rare and protected species (Dudgeon et al. 2006; Maberly & Elliott 2012), and are often the basis for multimillion-pound tourism industry and associated employment (Maltby et al. 2011). Despite this, many of these lakes are subject to anthropogenic stressors such as cultural eutrophication caused predominantly by phosphorus (P) and nitrogen (N) enrichment (Richardson & Jørgensen 1996), and toxic heavy metal enrichment from industrial pollution (Förstner & Wittmann 2012). Collectively the economic impact of these anthropogenic stressors on lakes is estimated to be £75-114 m yr^{-1} in England and Wales alone (Pretty et al. 2003; Harvey et al. 2012). Furthermore, anthropogenic climate change has been linked to amplification and increased impact of these stressors (Williamson et al. 2009), making the restoration of freshwater lakes a priority. To this end current legislation, the European Union Water Framework Directive (WFD) (2000/06/EC), legally obliges stakeholders to return waterbodies to "good ecological and chemical status" with reference to pre-anthropogenic chemical, ecological and environmental conditions.

The interaction of physical, chemical and biological processes combine to generate a sedimentary record that enables the reconstruction of past lake conditions. Such palaeolimnological archives allow us to reconstruct the history of lake eutrophication and to assess the efficacy of lake restoration programs. Many lakes in industrialised areas near developing population centres have undergone similar histories over the past one to two centuries with progressive eutrophication and pollution driven by population increase, agricultural intensification and industrialisation. In the face of many lakes being subjected to remediation measures these activities often leave a legacy of sediments enriched in heavy metals and trace elements which are subject to redox (reduction–oxidation reaction) changes that may affect their stability and potentially cause them to be mobilised and form dangerous concentrations on the lake bed or even the lake waters. Furthermore, many lakes

vary seasonally with periods of summer stratification allowing depletion of oxygen in the hypolimnion that may lead to hypoxia or anoxia in the sediment and bottom waters. These rapid seasonal-scale redox changes may have major consequences for the redistribution of potentially toxic elements. Climate change is also exacerbating the situation since current warming promotes increased stratification and acts to further reduce dissolved oxygen concentrations. To effectively monitor and deal with such processes, it is necessary to obtain detailed geochemical records of lake sediments to quantify the history of inputs and to investigate the controls on mineral formation and dissolution.

The purpose of this study is to apply a multi-method geochemical and sediment fabric analysis to reconstruct the history of eutrophication and pollution in a major temperate lake system. A range of geochemical techniques together with scanning electron microscope imaging permit reconstruction of the sedimentary history and its relation to redox changes in the lake sediment and bottom waters. This combined approach also enables the identification of potential future hazards.

5.2 Results

5.2.1 Sediment fabrics and preservation of lamination

The range of sediment types and microfabrics observed is shown in Figure 5-1. Four end-member sediment types were recognized. Terrigenous silty clays were the dominant sediment type and these were interspersed with a more porous sediment type (paler in optical microscopy/ darker in BSEI). The more porous sediment commonly includes organic remains in the upper core intervals and either Fe or both Fe and Mn minerals in the lower pale brown mud of SC68 and in the near surface sediment. The middle dark muds were distinctly dark coloured also in optical microscopy. Fe and Mn mineral-rich sediments were present at or near the WSI.

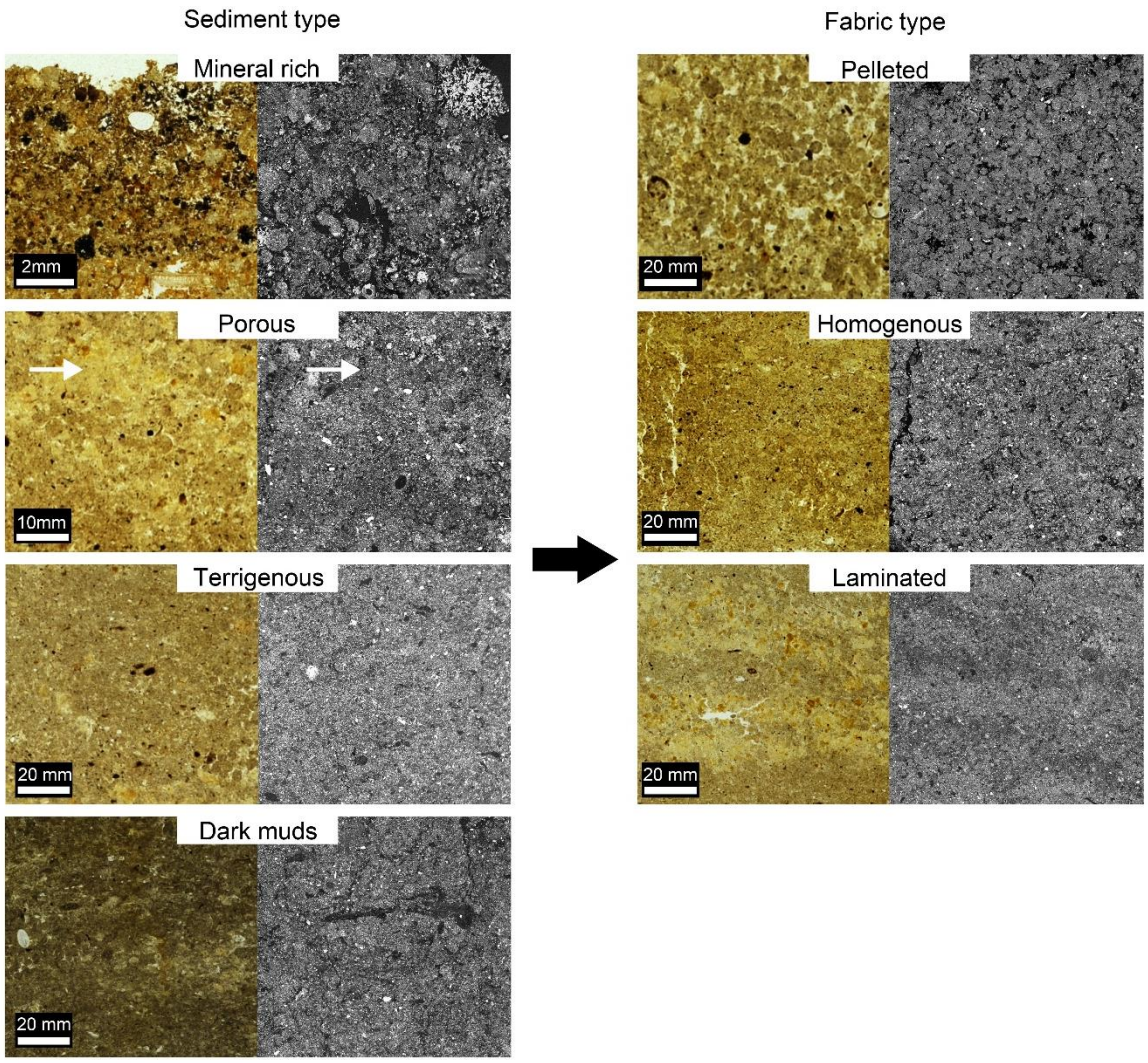

Figure 5-1: Detailed sediment and microfabric types as identified using optical thin section microscopy and back scatter electron imagery

The split core surfaces do not display any obvious lamination comparable to the regular macroscopic varves observed in many lake sediment cores (*e.g.* Zolitschka et al. (2015a). However, closer examination using a range of imaging techniques reveals the presence of a variety of lamina types at different levels in some of the cores. The X-radiographs show mm to cm-scale, bed-parallel density differences that is most prevalent in SC68 but also apparent in specific intervals in the other cores (Figure 5-2 and Figure 5-3). A combination of optical microscopy and BSEI showed a range of lamina types, the most common being 0.8 – 5.5 mm thick and comprises of alternations of detrital terrigenous and higher porosity laminae often with autochthonous organic material laminae with reduced detrital content. The high porosity laminae also often contain enrichments of Fe or both Fe and Mn. These laminae were logged using the BSEI complemented by SEM EDS analyses and by optical microscopy but the thicker examples are readily apparent in the itrax results, especially in SC68, where peaks of Fe and Mn are evident. Less common laminae include diatom ooze,

typically 1-2mm thick, and often by a single species and which occur only in SC68 and SC64 (Figure 5-1).

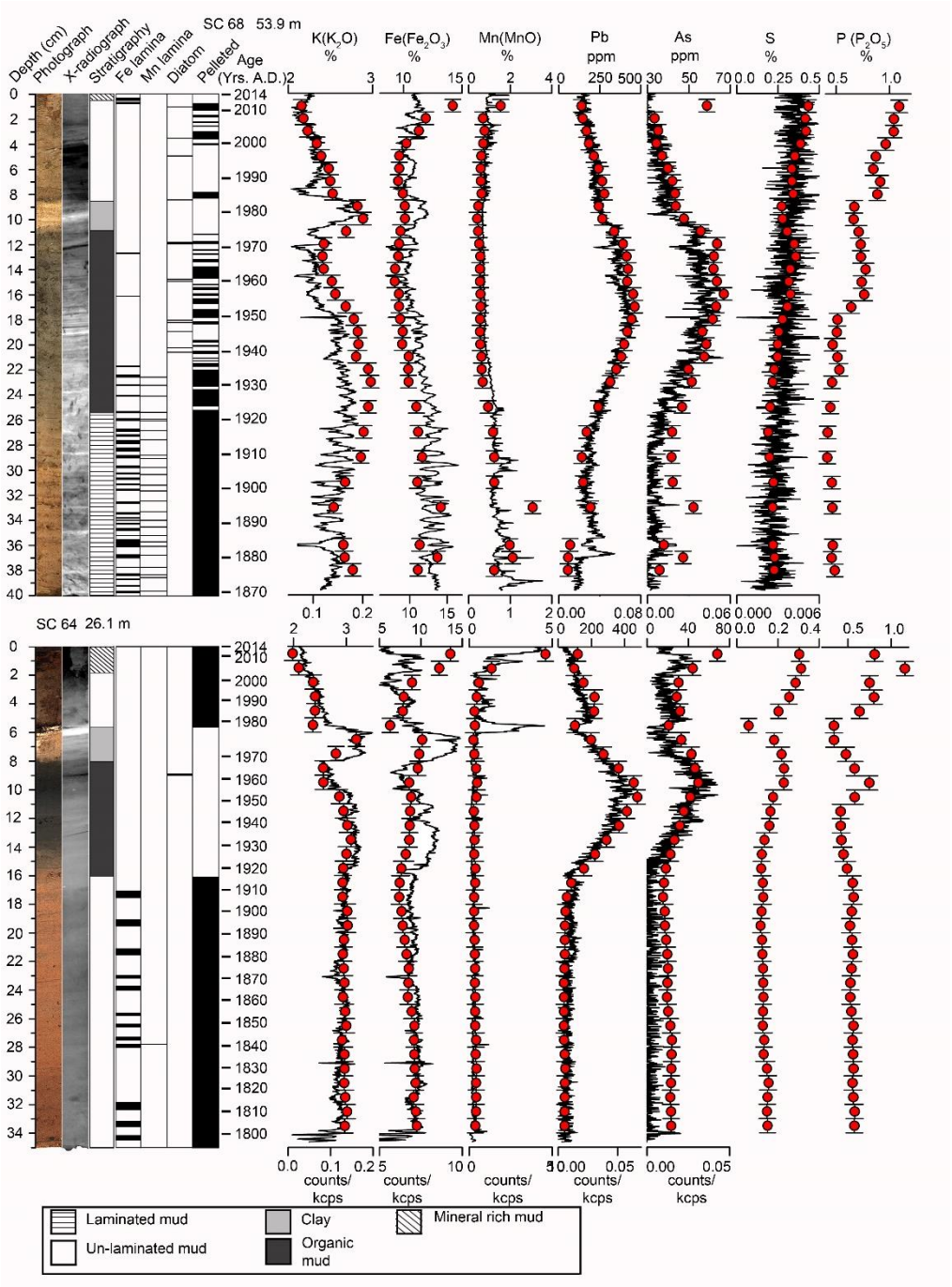

Figure 5-2: Stratigraphy log and geochemistry profiles for the North Basin cores SC68 and SC64. From left to right: Core depth (in cm), core photograph, core x-radiograph, lithostratigraphy (legend at the bottom), sediment fabric types (Fe or Mn laminae, diatom or pelleted layers), ^{210}Pb CF:CS LSR age depth model for the North Basin gravity cores (in years A.D.). On the right, geochemical itrax ED-XRF contents (black lines, lower scale) for K, Fe, Mn, , Pb, As, S and P and discrete WD-XRF concentrations (red dots, upper scale) for K_2O, Fe_2O_3, MnO,

1662 MnO/ Fe_2O_3, Pb, As, S and P_2O_5. Vertical errors of the WD-XRF are shown by
1663 the sampling interval. Water depths of each coring site is shown above the
1664 corresponding core.

1665

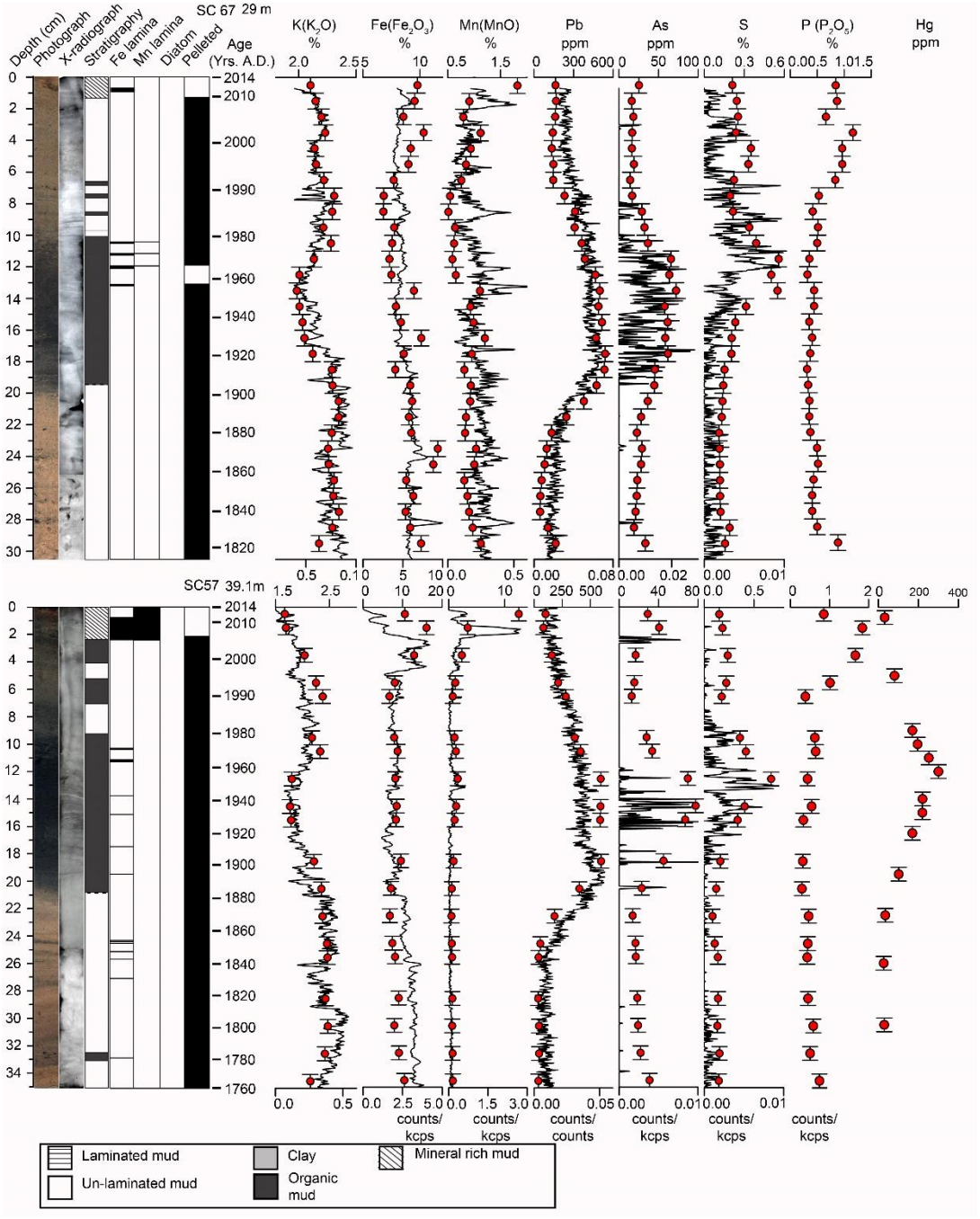

1666

1667 Figure 5-3: Stratigraphy log and geochemistry profiles for the South Basin cores SC67 and
1668 SC57. From left to right: Core depth (in cm), core photograph, core x-
1669 radiograph, lithostratigraphy (legend at the bottom), sediment fabric types (Fe
1670 or Mn laminae, diatom or pelleted layers), ^{210}Pb CF:CS LSR age depth model for
1671 the North Basin gravity cores (in years A.D.). On the right, geochemical itrax

ED-XRF contents (black lines, lower scale) for K, Fe, Mn, Pb, As, S and P and discrete WD-XRF concentrations (red dots, upper scale) for K_2O, Fe_2O_3, MnO, MnO/ Fe2O3, Pb, As, S, P_2O_5 and Hg. Vertical errors of the WD-XRF are shown by the sampling interval. Water depths of each coring site is shown above the corresponding core.

A common sediment feature observed in all four cores was pelletisation, with individual pellets ranging in size between 50- 350µm. The degree of pelletisation ranges from entirely pelleted to fully homogenous with no pelleting at all. The lower pale sediments of cores SC64, SC67 and SC57 are pelleted throughout and macroscopic burrowing is also apparent from the X-ray at this level in SC67. Only irregular Mn and Fe enriched zones are present in SC57 and SC64. In SC68, by contrast this section has only intermittent pelletisation and is regularly laminated with detrital terrigenous and higher porosity mm-scale laminae, which contain Fe and Mn minerals, some of which are visible in the x-radiograph. SEM and EDS analysis suggest that the Fe is present as amorphous and crystalline Fe-Mn (oxy)hydroxide Fe(Mn)(O)OH. Crystalline minerals occurred as subhedral platy agglomerates ranging in size between 50µm to 700µm. Some of these minerals include trace amounts of P (0.74 Wt.%) (Figure 5-4). Mn is also found in minerals which given this structure and the EDS line scan data (Figure 5-5) are most likely identified to be rhodochrosite $(Mn_{(0.98)}Ca_{(0.02)})CO_3$ (Figure 5-5). These minerals are present as individual minerals with a typical range of 2-10µm, but also occur as dense concentrations of individual rhombohedrals, of up to 60µm.

The occurrence of these minerals is recorded in Figure 5-2 and Figure 5-3. Mn occasionally takes the form of Mn oxyhydroxides in association with Fe oxyhydroxides in the lower pale sediments, but exclusively takes this form in the upper pale sediments. SC67 contains no mineral rich laminations through this interval. Instead broad cm scale changes in density seen in x-radiograph mark changes in detrital clay content in this interval.

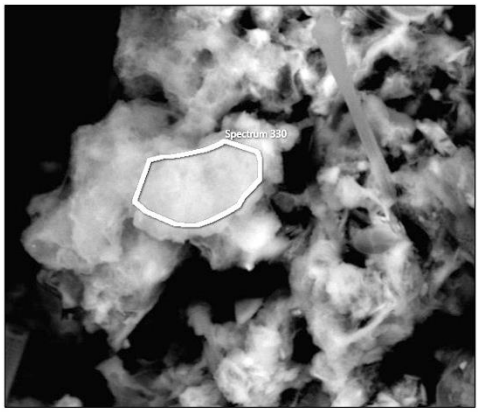

Element	Wt%
O	36.59
Mn	24.57
Fe	16.93
Si	11.30
Al	4.85
S	1.65
Ca	1.31
Mg	1.13
P	0.74
K	0.72
Ti	0.21

1698

1699 Figure 5-4 SEM image and EDS analysis of Fe and Mn oxyhydroxides from the sediment
1700 water interface from core SC57. Note, from the analysis, the co-occurrence of P.

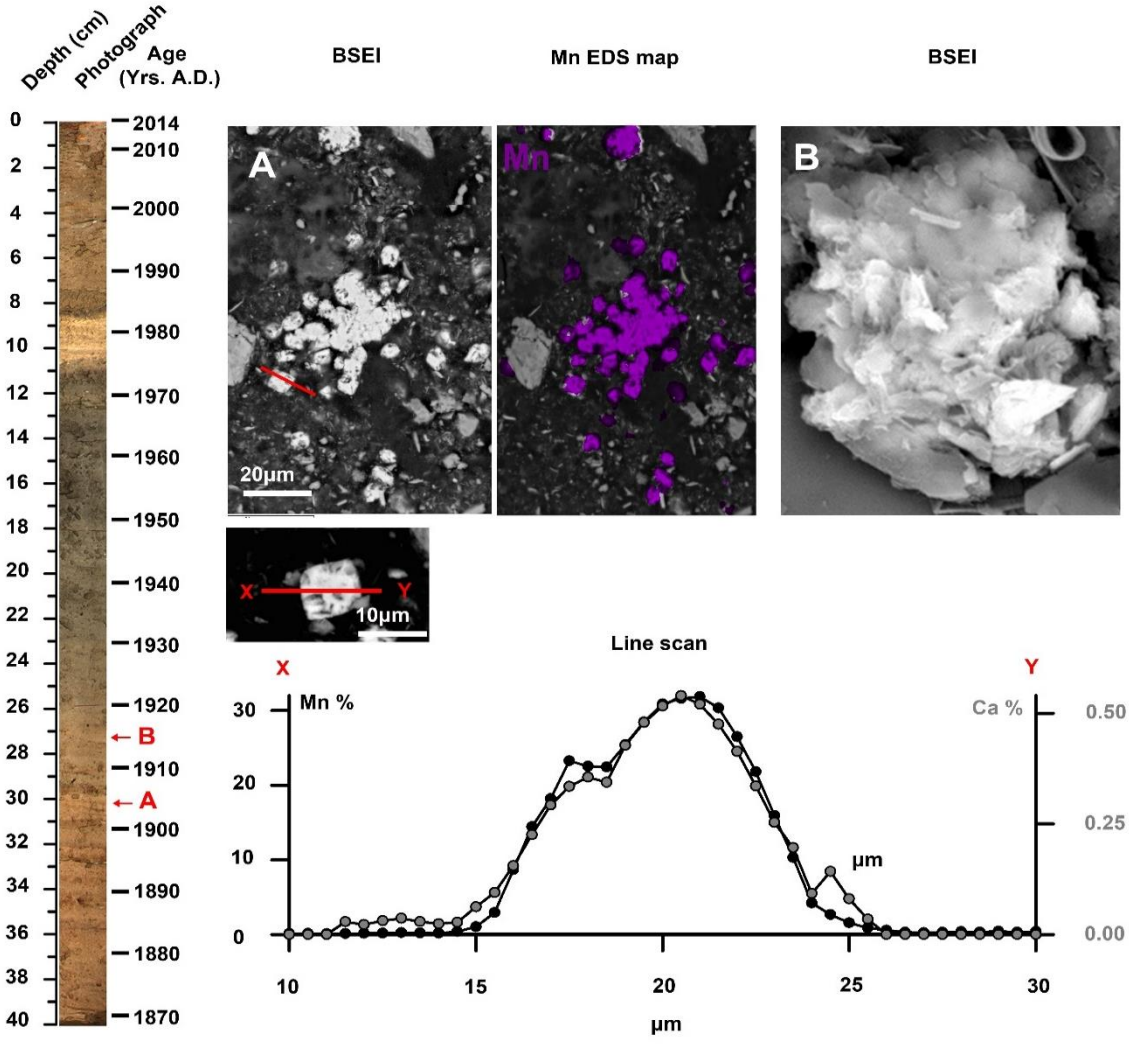

1701

1702 Figure 5-5 Core photograph of SC68 with depth and age showing the positon of
1703 rhodochrosite minerals shown in panel A, with corresponding EDS elemental
1704 map showing Mn highlighted in purple, and the position of mineral B. Lower
1705 panel shows the EDS line scan of Mn and Ca in mineral across x-y. Panel B

shows amorphous Fe oxyhydroxide, as determined by EDS from location indicated in panel A.

In the middle dark sediment in the North Basin in SC68, the level of pelletisation decreases further, the regular Fe and Mn laminae mainly cease by around the mid-1930s. Diatoms are abundant throughout this interval and discrete diatom laminae occur from around 1940. In SC64 the Fe and Mn banding also ceases in the dark sediment in which diatom laminae are only rarely seen. In contrast, in the South Basin these sediments lack diatom lamina and are partially or completely pelleted throughout. A few Fe-rich laminae are present in SC57 while both Fe and Mn laminae occur towards the top of the dark sediment in SC67.

In all cores except SC68 the upper paler sediments lack clear laminations and are pelleted although discrete Fe and Mn rich mineral zones are present in the surface few cm. In SC68 the pale upper sediments contain diatom laminae and are only intermittently pelleted. The core tops in all cores contain either a darker brown (Munsell colour: 10YR 3/3) or orange faint (Munsell colour: 5YR 4/6) mineral lamination. Geochemical analysis of this intervals show the Mn and Fe to be present in amorphous Fe-Mn oxyhydroxides associated with trace amounts of P. This sediment type becomes prominent simultaneously across both basins in 1979 – 1980.

5.2.2 Use of Mn and Fe content and mineralogy as redox indicators

Mn and Fe are sensitive redox indicators since both metals have soluble reduced ions in reducing conditions but on oxidation form solid oxyhydroxides (Davison 1993). Seasonal mixing in lakes that results in re-ventilation of bottom waters may generate precipitation of Fe and Mn oxyhydroxides in the water column, where bottom waters are anoxic (Naeher et al. 2013) or within bottom sediments with inward diffusion of oxygen from bottom waters. If sedimentation rates are sufficiently high, then Mn and Fe rich layers or laminae may be preserved even in permanently anoxic sediments (Naeher et al. 2013). Since Mn is slower to oxidise than Fe there is also the potential to gain insight into both the timing and the extent of oxygenation if mineral layers are preserved in the lake sedimentary record. In scenarios where reducing conditions in the sediment result in the dissociation of Mn oxyhydroxides there may still be the potential to preserve a record if rhodochrosite is formed (Yu et al. 2016). The Fe and Mn values from the itrax and WD-XRF analyses were therefore used as palaeo-redox indicators.

In SC68 through the pale brown mud (19th and early 20th centuries), Fe shows multi-annual variation and appears in anti-phase with peaks in K reflecting the alternating detritus-rich (rich in K) and pale Fe-rich laminae identified in SEM. Peaks in Mn, that are less frequent, may occur with, or immediately above the Fe peaks and generally have smaller concentrations. Moving up into the lower part of the dark sediment, these Fe and Mn peaks decrease and eventually cease to only recur in the top few cm of the core.

In the shallower SC64 there are fewer low-amplitude Fe peaks in the itrax in the lower pale sediment. Thereafter prominent Fe and Mn peaks occur above the 1980 pale clay horizon and, again, in the top few cm of the core. In the Southern Basin in SC57 there is irregular low amplitude variability with some Fe-peaks and little evidence of Mn fluctuations until the upper 5 cm when strong Fe and Mn peaks occur. In SC67 there is irregular moderate-amplitude variability in Mn with fewer peaks in Fe with the highest amplitude peaks occurring towards the upper part of the dark mud and irregularly also from there to the core top.

5.2.3 Combining sediment fabrics and Fe and Mn variability to reconstruct redox history

It is important first to clarify the significance of the pelletisation. In lake waters deeper than 20 m such structures would be produced mainly by tubificid oligochaetes or chironomid larvae (McCall & Tevesz 1982). The presence of pellets does not, however, necessarily imply oxic conditions since oligochaetes such as *Tubifex sp*. are known to survive in anoxic conditions (Famme & Knudsen 1985) and have been observed in abundance in the profundal sediments of Windermere even in anoxic conditions (Reynoldson 1987). Rather, here the extent of pelletisation is likely related to the relative degree and persistence of anoxia.

In the lower pale mud of the deep North Basin SC68, regular Mn-Fe mineral laminations occurring on a scale of 0.2-0.7 cm (compare to LSR – 0.29 cm yrs^{-1}) likely represent recurrent annual to multi-annual redox changes. The pattern is consistent with summer stratification and a reduction in bottom water oxygenation that promoted anoxia in the sediment that allowed the release and upwards diffusion of dissolved Fe and Mn ions. This was then followed by turnover in the autumn/winter that led to re-oxygenation of bottom waters and formation of the Fe and Mn oxides that precipitated at a redox boundary within the surficial sediment. The occurrence of Fe laminae without overlying Mn concentrations indicates that some overturning episodes were not of sufficient duration or intensity to

allow the slower-oxidising Mn to precipitate suggesting release of Mn to the water column. In the dark sediment from around 1920, in the deep North Basin these lake turnover indicators become less common and cease with first Mn and then Fe laminae disappearing other than for two isolated Fe laminae. This is consistent with the progressive development of more persistent stratification as well as sediment anoxia in the deep North Basin that enabled preservation of diatom laminae and there is only intermittent evidence of benthic activity in the form of pelletisation. In the shallower North Basin (SC64), the very rare Mn-laminae, the less common and broader Fe-rich zones and the maintained levels of pelletisation indicate rarer sediment anoxia until the change to the dark mud at around 1920 when pelleting ceased.

For much of the 18th and 19th century in both South Basin cores (SC67 and SC57) Fe and Mn remain stable except for a distinct peak in both in 1860-1878 in SC67. From the late 19th century in the deep South Basin (SC57) and from the early 20th century in the shallow South Basin (SC67) there is first elevated Fe, followed by decreasing values and a lowering in variability toward the middle and late 20th century. Following this in the late 20th to early 21st centuries both South Basin cores show a similar pattern, with Fe and Mn both showing stable or increased variability followed by a distinct enrichment first in Fe and then Mn at the top of the core.

5.2.4 Geochemical terrestrial input indicators

In SC68 through the 19th and 20th centuries, K shows inter-annual variability with peaks corresponding to increased density and clay content. Through the lower pale sediments in SC64 variability is markedly lower reflecting the fewer and less well defined changes in sediment fabric. In the South Basin K is elevated and varies on an inter-annual scale until the early 20th and the late 19th century in SC67 and SC57 respectively. The two cores also show further similarities in the mid-19th century where K values reduce before increasing again through the rest of the 19th century.

Through the dark mud in SC68 K decreases and becomes less variable to a low in the 1960s and 1970s. In SC64 values remain low in variability but increase at the base of the dark mud before also declining to a low in the 1960s-1970s. Both South Basin cores show a similar decline in overall values and variability with a low earlier in the 1950s-60s. After this values increase and variability becomes higher until the 1990s. In both North Basin cores there is a substantial short lived increase in K which corresponds to the clay horizon. Following this K values in all cores decline in/up to the top of the core.

5.2.5 Heavy metal and arsenic content

The overall pattern is one of increasing metal content of the sediments with the increase in Pb occurring earlier, followed by other metals (Cu, Zn, Supplementary figures: Figure 7-1, Figure 7-2, Figure 7-3 and Figure 7-4) and then arsenic, followed by a rapid decrease in all in the late 20th century. The overall timing of the increase is earlier in the South Basin with Pb increasing from around 1850 followed by the Zn, Cu and As between 1880 – 1890. In the North Basin, Pb increases from about 1910 with Zn, Cu and As in the next decade, showing less of a lag than in the South Basin. Mercury (Hg) (Figure 5-3), analysed only in SC57, follows Zn, Cu and As. Peak levels in heavy metals and As broadly occur between 1940-1970 in the North basin and between 1900 – 1980 in the South Basin. The lower pale muds in all cores generally show base line levels in all these elements except in SC68 where an earlier smaller increase in Pb occurs around 1890 – 1900 and peaks in As occurs around 1897/98 and 1880 concomitantly with spikes in Fe and Mn.

Above the clay horizon in the North Basin, from around 1980, Pb and (and Zn in SC64) decreases sharply to a low at the top of the core. In the South Basin Pb, Zn and Hg (Supplementary figures: Figure 7-3 and Figure 7-4) remain elevated and decrease less sharply to a low at the top of the core. In all cores As decreases to low variability before increasing sharply just below the water sediment interface.

5.2.6 Barium content and mineralogy

Barium (Ba) content (Supplementary figures: Figure 7-1, Figure 7-2, Figure 7-3 and Figure 7-4) is marked in all cores, except SC68, by peak values near the water sediment interface with maximum values of up to 2% in core SC57. Below this there are smaller increases above the peak in itrax K within the clay horizon in the North Basin cores, SC64 and SC68, and there are elevated levels within the upper part of the dark mud in SC68 and SC67. In SC68 Ba bulk geochemistry also shows high variability at the base of the core. SEM examination of sediment reveals the common presence of small, typically 2-12 μm crystals of barite that may occur in clusters or individually (Figure 5-6). SEM EDS analysis indicates that these have a normal barite $BaSO_4$ composition near the core top, but within the dark mud they contain Pb and so appear to be on the Barite ($BaSO_4$) - Anglesite ($PbSO_4$) solid solution. Individual crystals show zoning with Pb-enriched margins similar to those experimentally grown from aqueous solutions (Fernandez-Gonzalez et al. 2013). The barite – anglesite crystals are most abundant in SC57 and SC64 but occur in all cores and increase in abundance in the mid and upper part of the dark mud. Ba concentrations are particularly

enriched in the surface sediment attaining concentrations exceeding 2000 ppm in SC57. Here microlithostratigraphic analysis shows the presence of $BaSO_4$ in the water sediment interface (WSI) up to 35 µm appearing in clusters of well-defined minerals.

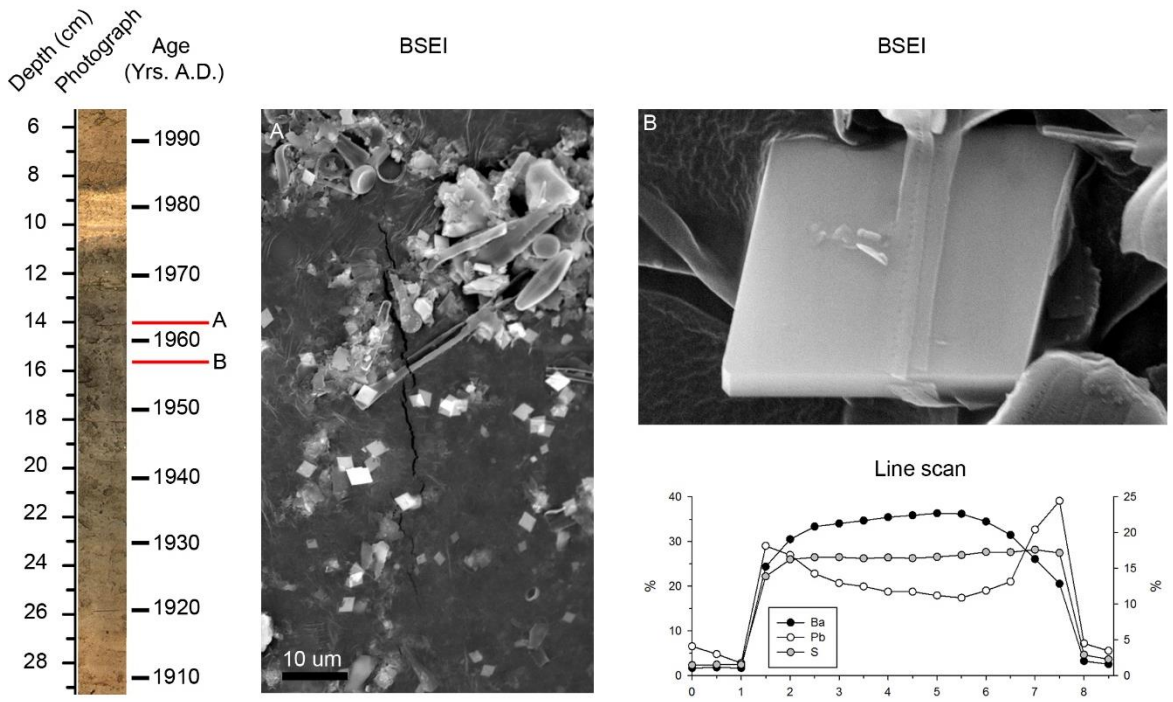

Figure 5-6: Core SC68 photograph along with depth and age showing the position of samples containing examples of (A) multiple barite-anglesite minerals, and (B, top) and individual barite-anglesite mineral. (B, bottom) Also shown is an EDS line scan of Pb, Ba and S in mineral B.

5.2.7 Phosphorous and Sulphur

Phosphorous (P) shows low variability in all cores before the early- mid 19th century. In the North Basin P increases through the 1950s and 60s, is reduced through the clay horizon and then continues to increase to the top of the core to values exceeding 1%. In the South Basin P increase occurs simultaneously in the late 1980s and peaks below the water sediment interface in the top 5 cm attaining values of 1-2%. SEM imaging of sediment and EDS analysis indicates an association of P with Fe-oxide particles (Figure 5-4).

Sulphur (S) in all cores shows low variability before the 20th century. In the North Basin S increases from the 1950s and 60s, to the top of the core, with exception of a low within the clay horizon. In the South Basin S increases simultaneously from around 1920 and data peaks within the dark mud from 1950-1980 before declining overall to the top of the core slightly lagging the decline in Pb, As, Zn and Hg.

5.2.8 Organic matter C and N content and isotopic composition

Six samples representing sediment endmember types in both basins were tested for calcium carbonate ($CaCO_3$), with all yielding results below the detection limit (4 counts). In both basins $\delta^{13}C$ and $\delta^{15}N$ increase through the lower pale mud to reach peak values in the upper part of the dark mud and then decrease through the upper pale mud to the core top (Figure 5-7). TOC, TN, and C/N decrease through the 19th century then increase in the 20th century with TOC and N reaching sustained higher values in the top part of the dark mud (1940-1980) before declining briefly, and then increasing to the core top (Figure 5-7).

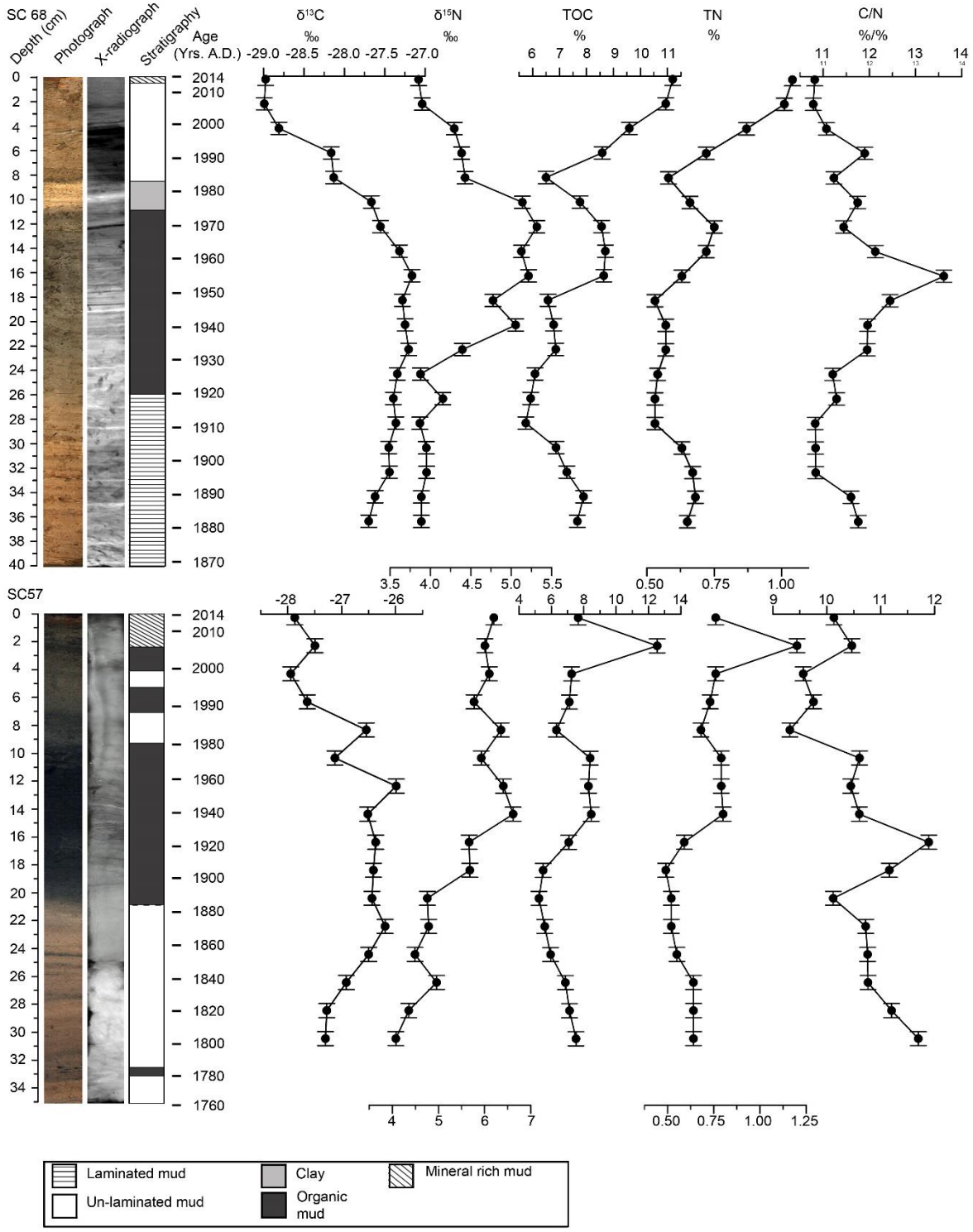

Figure 5-7: Stratigraphy log and organic chemistry profiles for the South Basin cores SC67 and SC57. From left to right: core depth (in cm), core photograph, core x-radiograph, lithostratigraphy (legend at the bottom), ^{210}Pb CF:CS LSR age depth model for the North Basin gravity cores (in years A.D.). On the right, chemical contents (black dots) for $\delta^{13}C$, $\delta^{15}N$, TOC, TN, C/N. Vertical errors are shown by the sampling interval.

5.2.9 Ordination analysis

Detrended correspondence analysis (DCA) of all the geochemical data and environmental/ climate data gave an axis 1 eigenvalue value of <0.2, suggesting a unimodal method was needed (Langdon et al. 2008). Canonical correspondence analysis (CCA) of SC68 for the period 1950 – 2014 and for selected annually averaged geochemistry and annual environment/climate parameters (Figure 5-8) firstly shows a clear negative relationship between the Pb and As, which dominate the dark sediment, and wind speed (annual, JJA and DJF) along the *x*-axis. Equally, distribution along the y-axis of the dark sediment is influenced by both winter and autumn rainfall. To a lesser extent, the upper pale unlaminated sediments show a positive relationship with annual water and air temperature. Comparison of individual elements with archival environmental/ climate (Figure 5-8B) also shows a clear negative relationship between As, and to a lesser extent Pb, and wind speed (annual, JJA and DJF). Although very weak K and Ba also show a negative relationship with summer precipitation, while Fe, and Mn share no significant relationship to any environmental or climate record.

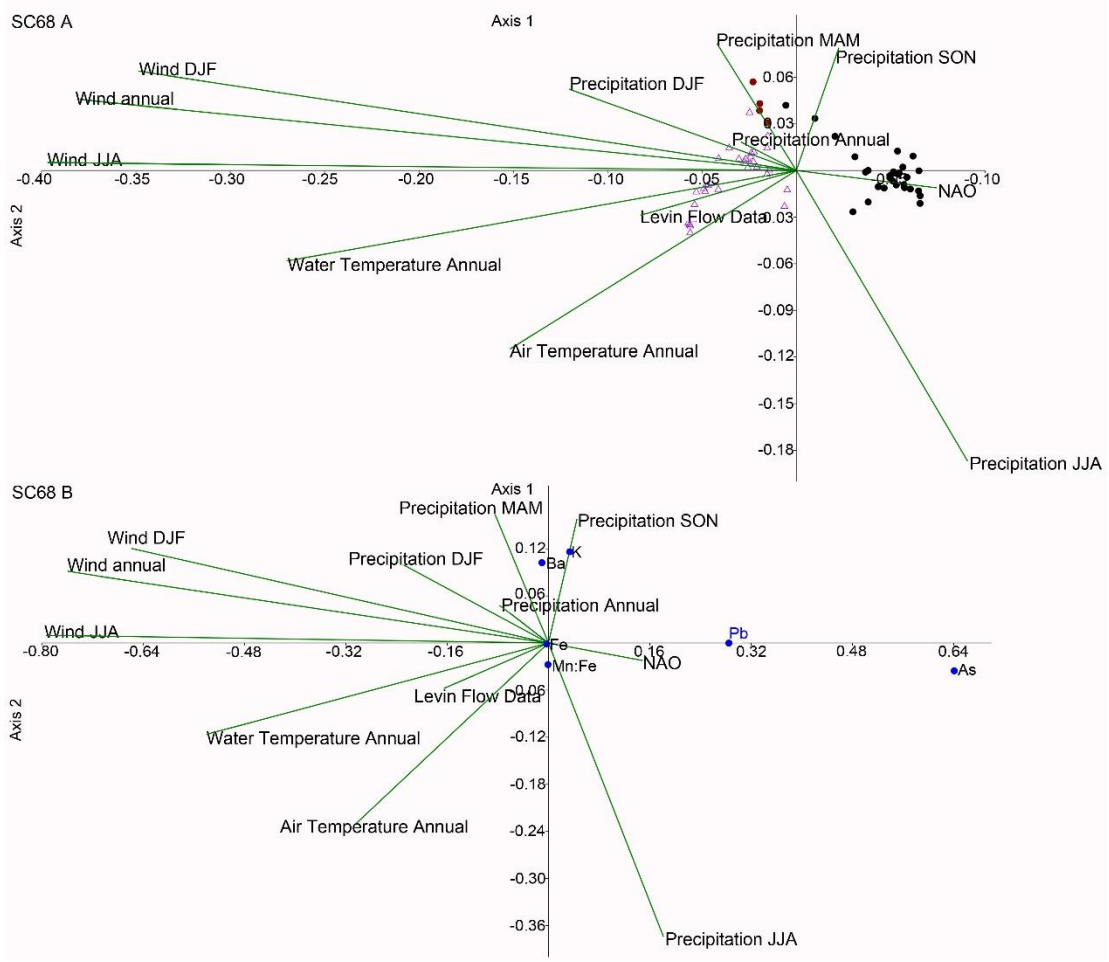

Figure 5-8: SC68 (A) and SC57 (B) climate and environment drivers of changes in sediment; CCA results 1946– 2014 environment (TP) and climate (air temperature, NAO, precipitation) comparison with organic matter / geochemistry

5.3 Discussion

5.3.1 Previous work on the source and fate of trace metals in Windermere lake waters

A quantitative assessment of inputs of selected trace elements (Fe, Mn, Al, Cu, Pb, and Zn) was undertaken between 1981-1983 (Hamilton-Taylor and Willis, 1990). Sewage effluents were found to contain the highest concentrations of dissolved and particulate metals as well as the highest labile particulate fractions. Fe, Mn and Al were mainly (> 90%) derived from river input while Cu, Pb and Zn were predominantly from atmospheric deposition or direct sewage discharges (Hamilton-Taylor and Willis, 1990). Studies on the association of metals with diatom blooms found a strong association of Zn with algal cycling leading to substantial delivery of Zn to the sediment by settling diatoms (Reynolds and Hamilton-Taylor, 1992). The river supply of ionic Mn^{2+} and Fe oxyhydroxides is enhanced by

derivation of inflow from smaller lakes that are subject to hypolimnetic anoxia with Cunsey Beck draining Esthwaite Water to the South Basin and the River Rothay draining Elterwater, Grasmere and Rydal Water to the North Basin (Hamilton-Taylor and Willis, 1990). Cores taken during the 1970s record a 1-2 cm surface brown layer with elevated Mn and Fe from the deep South Basin and increased bottom water Mn concentrations during thermal stratification in the 1970s indicate efflux of reduced Mn^{2+} from the sediment (Hamilton-Taylor et al. 1984).

5.3.2 The development of pollution and eutrophication in Windermere

5.3.2.1 The onset and increase in pollution

The first indications in the sediment of increased anthropogenic influence are some bands of dark sediment within the lower pale mud in the South Basin in SC57 in around 1850. In addition Pb content of both of the South Basin cores also starts to increase from 1850-1860 prior to other metals (Zn, Hg, Cu) and As which increase from 1880-1890 onwards. Although there was considerable mining and quarrying for metals in the Windermere catchment in the 19th century the periods of metal extraction do not coincide with increases in metal content in the lake sediment (Miller et al. 2014b). Double-spike Pb isotope analysis of Windermere sediments dating from the 1840s to the 1920s reveals a likely Pb source to be from Carboniferous coal, related to the launch of coal-fired steam ships from 1845 and the further expansion of their use following the opening of the Kendall to Windermere railway in 1847 (Miller et al. 2014b). The increase in Pb prior to other metals is also recorded in the sediments of the adjacent Blelham Tarn (Ochsenbein et al. 1983). The later increase in the other metals (Zn, Hg, Cu) and As from 1880-1990 coincides with increased sewage discharge from the rapidly increasing population centres around the lake (McGowan et al. 2012). Increasing values of the $\delta^{15}N$ of organic matter in the South Basin sediment also occur, in step with Zn, Hg, Cu, from this time. Elevation in $\delta^{15}N$ of organic matter can be attributed to a number of causes including increased algal productivity (Hodell & Schelske 1998) or the input of isotopically heavy nitrate from primary sewage or farm runoff (Meyers 1994).

5.3.2.2 Asynchrony between the South and North Basin

Other than a single pulse in the 1890s the increase in heavy metals and As in the North Basin occurs later at around 1910-1920 lagging the South Basin by 50 years (Pb) and 30 years (Zn, Cu, As). Changes in timing of heavy metal delivery between basins is unlikely to have

caused this delay as peaks in the probable sources of heavy metals (atmospheric deposition and sewage discharge) would have occurred almost synchronously on a catchment to regional scale. Algal productivity and eutrophication occur later in the North Basin, probably as a result of the larger volume, leading to greater dilution as well as a lower nutrient loading. Instead, it may be that the efficient delivery of the metals to the sediment was enhanced by increased productivity since sediment trap studies from Windermere show take up of Zn by diatoms (Reynolds & Hamilton-Taylor 1992). Furthermore, the extracellular polymeric substances (EPS) exuded by both diatoms and associated bacteria in lake "snow" aggregates (Schweitzer et al. 2001) are also efficient scavengers of trace metals (Bhaskar & Bhosle 2006; Comte et al. 2008).

5.3.2.3 Evidence of changing lake productivity from stable isotopes of carbon

In both basins $\delta^{13}C$ values of organic matter increase through the 19th and early 20th centuries reaching maximum values around 1950-1960 and then decrease to the surface with the most marked drop occurring around 1990. Phytoplankton preferentially take up the lighter ^{12}C isotope during photosynthesis, but in periods of sustained high productivity they will increasingly utilise the heavier isotope resulting in an increase $\delta^{13}C$ values (Schelske & Hodell 1995). This increase in $\delta^{13}C$ values in Windermere is consistent with steadily increasing algal productivity in the lake that reached peak values in the mid-20th century before mitigation strategies led to decreases. This trend also follows a common pattern in lakes influenced by adjacent population growth and agricultural development in the catchment (Schelske & Hodell 1995). The $\delta^{13}C$ values are around 1‰ heavier in the South Basin reflecting higher productivity and stronger eutrophication.

5.3.3 Changes in lake and sediment redox conditions with developing eutrophication.

The increase in metals in all cores and in the $\delta^{15}N$ of organic matter in SC68 and SC57 coincides with the transition from the lower pale brown muds to the dark mud indicating the onset of Fe reduction. A more detailed view of redox variation emerges from individual core records.

In the lower pale sediments of the deepest core, SC68, there are regular recurring lamina of Mn-rich and subjacent Fe-rich sediment. These indicate the development of sediment anoxia sufficient to reduce and mobilise these elements causing upwards diffusion towards a redox boundary in the sediment, where first Fe and subsequently Mn form oxy-

hydroxides. The regular occurrence of these laminae suggests quasi annual recurrence of reduced oxygen levels in the lake during the period of summer stratification that led to less oxygen penetration into the sediment and the development of sediment anoxia before the lake was re-ventilated in the November/ December mixing. However, as the colour changes from pale brown to grey these laminae become less common and largely cease. The decrease in the extent of pelletisation of the sediment is also consistent with progressively increasing hypoxia. In the lower pale brown muds of the shallower North Basin core, SC64, less distinct and less common Fe-rich layers occur with rare Mn laminae probably due to the greater intensity of bioturbation as indicated by thorough pelleting of the sediment.

In the 18th, 19th and early 20th century, South Basin cores contain no (SC67) or irregularly distributed Fe mineral laminations (SC57). The intermittent Fe lamination in the deep South Basin (SC57) is consistent with sediment anoxia developing reducing conditions sufficient to mobilise both Fe and Mn but with insufficient ventilation to re-oxidise the Mn. In the shallower South Basin core (SC67), at 29 m water depth, peak anoxia occurs between 1970 – 1980 marked by a cessation in pelletisation and the occurrence of paired Fe and Mn laminae indicating increased sediment anoxia but with seasonal turnover still sufficient to re-oxygenate the surface sediment leading to Fe and Mn precipitation. The late 1970s correspond to a period where monitoring of deep water dissolved oxygen concentrations in the South Basin recorded development of hypolimnetic anoxia in the later part of the stratified period (Hamilto-Taylor & Willis 1990).

5.3.4 Peak eutrophication, sediment anoxia and hypoxia of bottom waters

The upper part of the dark grey interval coincides with peak sediment heavy metal (Zn, Hg, Cu, and Pb) and metalloid (As) concentrations and the highest $\delta^{15}N$ of organic matter which together indicate maximum input from human sewage and agricultural run-off with timing of 1940 – 1980 in the North Basin and 1900 – 1980 in the South Basin. In both basins peak organic carbon contents are attained in 1950 – 1980 and this also coincides with some of the highest $\delta^{13}C$ values marking peak productivity. A coeval increase in diatom frustules in all cores and several preserved diatom bloom laminae in SC68 of near-monospecific concentrations of *Asterionella formosa* record the mass flux of blooms of this peak eutrophic species monitored in lake waters since 1946 (Maberly et al. 1994; Sabater & Haworth 1995; Barker et al. 2005). It is likely that the settling of these diatom blooms enhanced the flux of metals, especially Zn, to the sediments (Reynolds & Hamilton-Taylor 1992). Increasing diatom productivity and eutrophication were largely driven by marked increases in P

particularly in the South Basin together with concomitant increase in N in both basins from the mid-1960s that fuelled increases in the summer peak of algal production until phosphorus stripping was introduced in the main sewage treatment works (STW) inputting to the South Basin in 1991/ 1992 (Pickering, 2001).

Peak sediment anoxia is indicated in all cores with the most persistent in the deep North Basin (SC68) as evidenced by the intermittent absence of palletisation and the preservation of diatom ooze laminae which also suggest periodic bottom water anoxia, as measured at this time in the deep South Basin (Pickering & Sutcliffe 2001). The presence of Fe and Mn laminae and decrease in palletisation in SC67 indicate that enhanced sediment anoxia also extended to shallower zones of the lake at this time. These observations are consistent with episodic bottom water anoxia recorded in the deep South Basin and efflux of dissolved Mn from the sediment at this time (Hamilton-Taylor et al. 1984; Pickering & Sutcliffe 2001).

We find little evidence of authigenic pyrite from SEM observations so although the bottom sediments were anoxic, they were rarely sulphidic and there is no evidence for sulphate reduction and pyrite formation consistent with sulphur speciation studies in Windermere (Davison et al. 1985). However, increases in sulphur occur in the South Basin cores in the dark sediment in all cores contains common 2-20 µm barite crystals. The occurrence of the barite as euhedral crystals suggests a different mechanism of formation from that of the adjacent seasonally anoxic Esthwaite Water, where small (3-4 µm) spherical granules of barite form by biologically mediated formation within protozoa (Finlay et al. 1983; Smith et al. 2004). The origins of the Ba concentrations that led to the formation of the euhedral barite crystals in Windermere may be similar to those responsible for the build-up of bottom water concentrations of Ba in Lake Biwa where the hypolimnion has reducing conditions, but never zero dissolved oxygen concentrations (Sugiyama et al. 1992). In this case, during the period of stratification, enhanced anoxia within bottom sediments leads to the release of Fe and Mn into the oxic bottom waters where they are re-oxygenated to form hydrous oxides. The Mn oxyhydroxides have a strong affinity for Ba and result in draw down of Ba to the sediment. Although water column sulphate is low in freshwater lakes, bacterial oxidation of organic sulphur (Fakhraee et al. 2017) may have been important in producing the sulphate for barite formation.

Unlike the pure barite crystals in the near surface sediment the crystals in the dark sediment consistently contain Pb. The presence of barite-anglesite solid solution has not been reported before from lake sediments and has primarily been associated with mining waste and contaminated soils (Courtin-Nomade et al. 2008; Fernandez-Gonzalez et al. 2013).

5.3.5 Partial Recovery

From around 1980 the sediment colour changes back to pale brown in SC68 and SC67 and becomes less dark in SC64 and SC57. The colour change is more gradational in the shallow South Basin (SC67) but decreased sediment anoxia is also indicated by the resumption of pelletisation (enhanced benthic activity) and cessation of the Fe and Mn laminae, and in the deep South Basin (SC57) the Fe laminae also cease. The S content of both South Basin cores also decreases. The decline in heavy metals and As in this interval is likely due to the decline in atmospheric pollution, for example the marked decline in atmospheric Pb since peaks in the 1970s (Rippey & Douglas 2004).

The North Basin (SC68) shows a progressive decline in the $\delta^{15}N$ of organic matter indicating a diminishing contribution from isotopically heavy sewage but the persistence of diatom bloom laminae indicate maintenance of mass flux from the diatom blooms observed in the lake. On the other hand the $\delta^{15}N$ of organic matter in the South Basin (SC57) shows no such decline, highlighting continued influence of isotopically heavy sewage input. There is also a significant increase in organic carbon content in the North Basin.

Phosphate stripping was introduced in the main STW in 1991/ 1992 (McGowan et al. 2012), but phosphate contents in the sediment actually increase synchronously in all cores at this time and reach concentrations of 1-2% in the surface sediment. Microlithostratigraphic and EDS line scan analysis show P is associated with Fe oxyhydroxide.

CCA shows a negative relationship with wind speed and Pb and As. Following thermal stratification in summer wind is the primary driver of overturn and bottom water ventilation on Windermere (Jones et al. 2008). In years where wind was less strong, later or incomplete overturn in autumn would lead to prolonged low oxygen conditions at depth (Jones et al. 2008), which would lead to both higher preservation of organic matter (Lehmann et al. 2002) and increased sulphide production (Hodell & Schelske 1998).

5.3.6 Water Sediment Interface and topmost sediment

5.3.6.1 Mn, Fe and Ba

Microfabric and geochemical analyses shows that with the exception of SC67 the topmost sediment (1.5 – 3 cm) of all cores are enriched in Mn and Fe. This is consistent with upwards diffusion of reduced mobile Mn and Fe from the anoxic sediment and their subsequent precipitation at the redox boundary near the SWI as oxyhydroxides (Davison 1993). The

exceptional concentration of 12.5 wt. % MnO requires further explanation and suggests advection of Mn to the deep South Basin. The mechanism for this may be analogous to that identified in the Swiss Lake Baldaggersee where mobilisation of Mn leads to "geochemical focusing" of Mn (Figure 5-9) in to the deeper parts of the lake (Schaller & Wehrli 1996). A prerequisite for this to occur is for anoxic sediment to be in contact with an oxic water column, a situation which is apparently increasingly occurring during the stratified period in Windermere. A similar redox-driven "geochemical focusing" process is also invoked for Fe although this is less mobile with a tendency to precipitate more rapidly as oxyhydroxides (Schaller & Wehrli 1996).

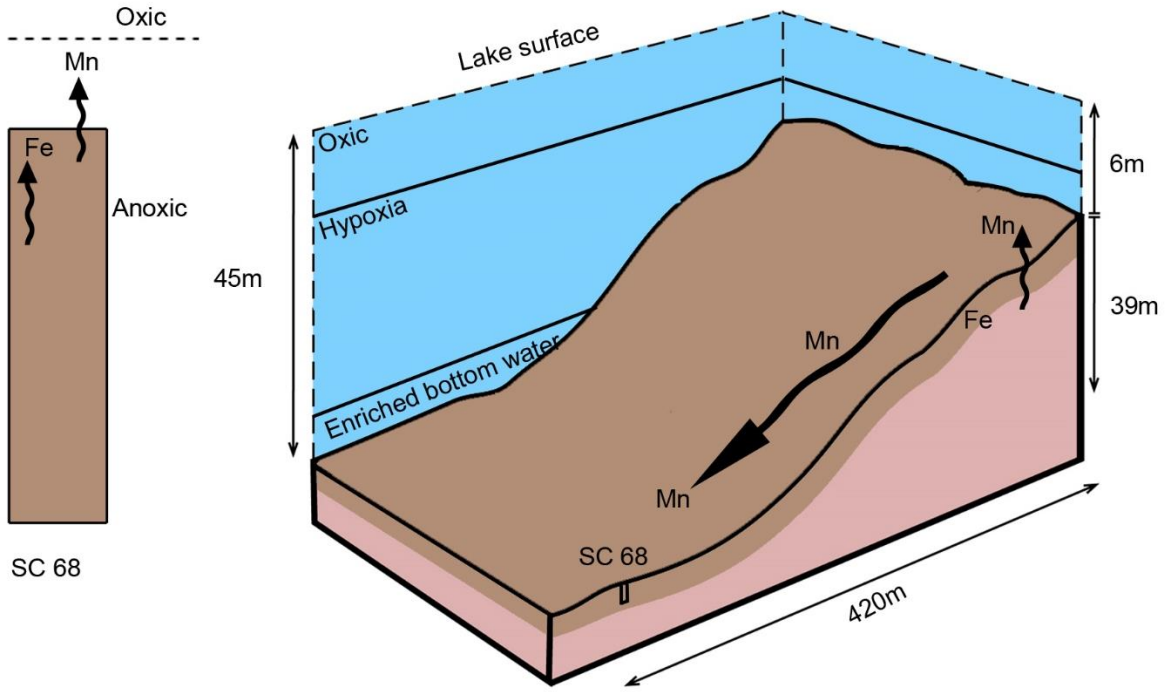

Figure 5-9: Schematic of Mn mobilisation and geochemical focusing in deep basin waters

The two cores that show the greatest Mn enrichment (SC 64 and SC57) also show significant Ba enrichment to values exceeding 2000 ppm in the deep South Basin. This association is consistent with the sequestration of Ba by Mn oxyhydroxides as documented from Lake Biwa (Sugiyama et al. 1992).

5.3.6.2 Arsenic

As is also relatively enriched in the surface sediments of SC68, SC64 and SC57 to values approaching 70 ppm (Figure 5-2 and Figure 5-3). As is readily adsorbed by Fe oxyhydroxides in sediment so the cycles of Fe and As are tightly coupled (Pierce & Moore 1982; Belzile & Tessier 1990; Dixit & Hering 2003; Couture et al. 2010). Field and experimental evidence indicate that As is also adsorbed by hydrous Mn oxide (Takamatsu et al. 1985).

As can become further enriched in surface sediments as result of sediment anoxia and Fe and Mn oxyhydroxides reduction, leading to arsenate reduction to arsenite, allowing for upward diffusion as an aqueous solution to the redox boundary. Here arsenite becomes adsorbed to more freshly formed Fe and Mn oxyhydroxides (Farmer & Lovell 1986; Dixit & Hering 2003). This can lead to concentrations in surfaces sediments far in excess of that delivered from the water column (Farmer & Lovell 1986) and has undoubtedly led to the enrichment of As in the surface sediments of Windermere. Furthermore, where a legacy of anthropogenic As pollution remains in deeper sediments, As can remain elevated in the

surface sediments long after exposure to anthropogenic sources of As have been reduced (Fabian et al. 2003). As is the case for Mn, As may be released to the water column during the stratified period where hypoxia develops in the hypolimnion.

5.3.7 Implications for future water quality and potential hazards

As many countries, the UK included, have failed to introduce formal Sediment Quality Standards (SQS) those set by the Canadian and Netherlands governments (Figure 5-10) are widely adopted as guidelines when considering sediments as dangerous to benthic life, human health and for remediation (Burton Jr 2002). The enrichment of Pb and As in the black sediments exceeds these standards in both the South Basin cores for Pb. Concentrations of As in all cores, except SC64 also exceed the SQS. This is concerning if these sediments where to be exposed to the water column hypoxic or dysoxic conditions where both Pb and As can become mobile (Hamilton-Taylor & Davison 1995). Evidence of MTD and slope failure scarps found in the distal lake slopes suggest that this is increasingly possible (Miller et al. 2013). What is more concerning is that in both North Basin cores As values at the WSI exceed both the Canadian and Netherlands governments SQS. As discussed Mn and As dissolution and migration under low oxygen conditions to the above water column is common in warm monomictic lakes during the Summer/ Autumn bottom water oxygen low (Jones et al. 2008). This would suggest that significant quantities of As are mobile and being released into the water column during Summer and Autumn months (El Bilali et al. 2002).

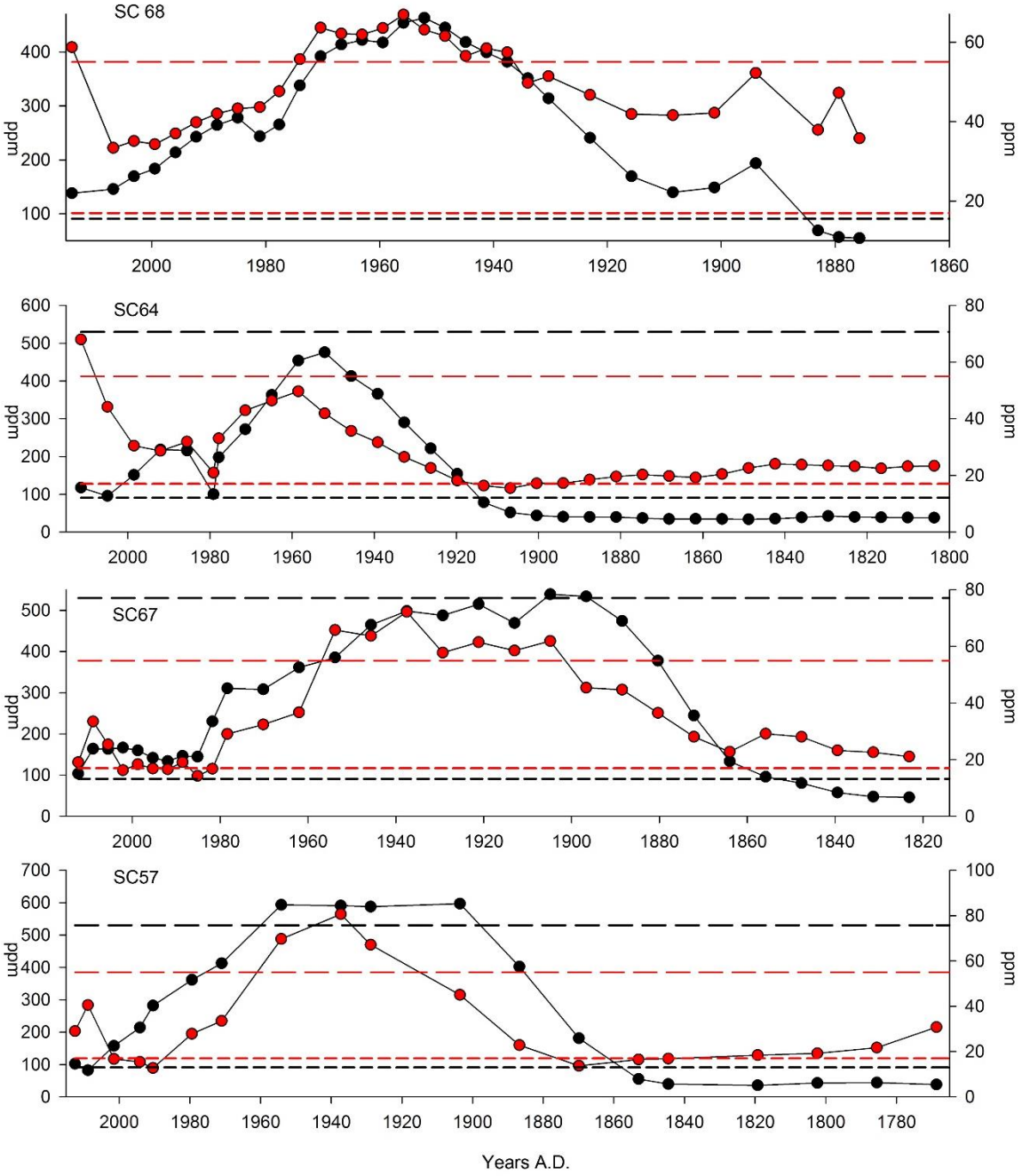

Figure 5-10: SC68 (a), SC64 (b), SC67 (c) and SC57 (d) Pb (black dots, left y-axis), As (red dots, right y-axis) concentrations over time along with Canadian (long dashes) and Netherlands (shorter dashes) sediment quality standards for Pb (black) and As (red).

Lake Biwa, Japan, shares some common physical and hydrological characteristics with Windermere and exhibits the seasonal release of Mn and As into the water column following the development of hypoxic conditions in a thermally stratified hypolimnion. Studies have linked these high levels of Mn and As in the bottom waters to mass fish mortality with Mn identified as the primary toxin (Itai et al. 2012). In Biwa there is

considerable enrichment in the surface (*ca.* 2 cm) of sediments of both Mn - 35,000 mg/kg (3.5%) and As - 300-350 mg/kg (Itai et al. 2012). The Mn and As in the Biwa (North Lake) sediments have evidently newly accumulated over the past 30 years and this has been partly related to inflow from the anoxic South Basin. In the case of Windermere there may be input of Mn and As from the seasonally anoxic Esthwaite Water. However, the closed cycle of dissolution and precipitation of Mn and As along with the constant addition of new Mn and As from allochthonous sources (geochemical focusing) to the deep basin, analogous to processes identified in the Swiss Baldaggersee (Schaller & Wehrli 1996) appears the most likely mechanism. The elevated Mn and As levels in Windermere not only pose a threat to human utilisation of the water, but also to the local fish such as the rare Arctic Char which migrate to the cooler bottom waters during summer months. Dissolved oxygen (DO) levels decrease in the hypolimnion during the period of stratification from April to October/December with arsenite and Mn being released into the bottom waters. This could lead to a building up to maximum concentrations through the stratification period, the very time that the Arctic Char migrate to bottom waters. There is currently extraction from Windermere for the NW England water supply during drought periods and these coincide with periods of stratification suggest risk of entrainment of Mn and As into drinking water.

5.4 Time line of events

18th and early 19th century: bottom waters are well-oxygenated and sediments host healthy benthic fauna, which pellet the sediments.

Mid-19th century: population increase and associated sewage discharge, coupled with intensified farming and agricultural runoff fuel increased algal production.

At SC57 (mid deep-South Basin) increased trace element input potentially from sewage and increased fossil fuel burning is incorporated into diatom skeletal matter (Hamilton-Taylor et al. 1984), and phytoplankton EPS (Bhaskar & Bhosle 2006; Comte et al. 2008), and hence accumulates on the lake bed.

Late-19th and early 20th century: eutrophic and low bottom water oxygen conditions cause reduced dark diatomatious (*Asterionella*) sediments to be deposited along with associated elevated trace metals in the South Basin. North Basin (SC68) Fe and Mn are precipitated annually as the redox conditions in the WSI alter with seasonal thermal stratification (Davison 1993).

As eutrophication intensifies and affects the larger less populated North Basin, the sediment quality deteriorates becoming enriched in heavy metals in the early 20th century. Annual Fe-Mn laminations become rarer and cease entirely by the 1930s.

Mid-20th century: Increased input of phosphate from sewage and runoff fuels eutrophication, causing intensification of diatom bloom activity and the deposition of near-monospecific diatom laminae in the sediment. Progressively oxygen depleted bottom waters cause sediments to become increasingly reduced with declining benthic activity, and pelleting, allowing for further trace element accumulation.

1979: A 4.7 ML earthquake north of Carlisle (Musson & Henni 2002) causes the slope failure of the Troutbeck delta fan, which deposits a clay rich MTD over the whole North Basin.

Late 20th century – early 21st century: North Basin - following the MTD the phasing out of leaded petrol and sewage treatment improvements, a reduction in eutrophic conditions leads to an improvement in sediment quality. Mn and Fe increase, and pelleting becomes more frequent indicating increasing bottom water oxygenation.

Modern day processes: Improvements in sediment quality, however, are only partial as sedimentary P and S continue to increase, diatom laminae continue to be deposited and TOC, TN and $\delta^{13}C$ indicate increased productivity and C from an increasing algal source.

Concentrating effects in the shallower and higher population in the South Basin, causes black high S sediments enriched in heavy metals to persist through the 20th century.

Despite P stripping being put in place at the South and North Basin sewage treatment works in 1991 and 1992 respectively (McGowan et al. 2012) sedimentary P increases through the 1990s to the top of the core through adsorption by Fe oxyhydroxides.

5.5 Conclusions

The sediments records have allowed for the reconstruction of a well dated timeline of events which show eutrophication, and associated effects on the sediments of Windermere, which began in conjunction with increased population and agricultural intensification in the mid-19th century. Differences in the physical properties and the population density between the two basins means that the eutrophication occurred in the South basin earlier and persisted longer. Peak eutrophication occurred in the mid-20th century in both basins and has been curtailed since then due to measures such as P stripping.

By tracking changes in the redox sensitive elements Mn and Fe the sediments also allowed for the reconstruction of bottom water ventilation regimes. As expected bottom water oxygenation, normally achieved following the autumn-winter over turn event, was lowest during the mid-20th century with peak eutrophication.

Heavy metal (Pb, Zn, Cu) and As enrichment of the sediments also coincides with peak eutrophic conditions in the lake. Sources may include fossil fuel burning or sewage but the delivery process to the sediment can potentially be linked to inclusion in diatom and or bacterial material. In the North Basin As enrichment at the surface still exceeds SQS set by the Netherlands and Canadian governments.

Persistent sediment anoxia, strengthened by hypoxic bottom waters during seasonal stratification, results in trace element mobilisation. Subsequent oxidation at the WSI or within the bottom waters causes enrichment of Mn, Fe, As, and Ba in the surficial sediment.

While the sediments of Windermere show a significant move towards improvement following peak eutrophic conditions geochemical and organic proxies show that, despite measures to prevent anthropogenic pollution, sediment quality is still lower than before the mid-19th century.

Chapter 6 Scanning Electron Microscope (SEM) methods reveal a history of seasonal-scale redox changes and diatom blooms in recent sediments from Windermere, UK.

6.1 Introduction

Lake sediments have the potential to act as important archives of environmental change driven by natural climate variability or anthropogenic forcing. Lakes with sufficiently high sedimentation rates can provide records on timescales of direct societal relevance and, in the case of annually laminated or varved lacustrine sediments, seasonal-scale temporal resolution is often attainable (Birks & Birks 2006; Zolitschka et al. 2015b). In such sequences, it is imperative to deploy the appropriate analytical methods to provide the best opportunity for maximising the available resolution. Seasonal forcing may translate to a sedimentary signal only if key prerequisites are met. These include: 1) a seasonally variable runoff of sufficient magnitude to deposit laminae of contrasting grain size; 2) a spring/ summer algal bloom that is adequately productive to generate a flux that forms a discrete lamina; 3) seasonal forcing that generates chemical changes that lead to the precipitation of minerals in identifiable layers, for example by the redox cycling of Mn and Fe. Thus a combination of imaging methods and analytical chemical techniques of sufficient resolution are required.

Most studies of varved lacustrine sequences rely on photographs or digital images of the split core surface or, for thinner varves, optical microscopy of thin sections of resin-embedded sediment to define the lamina boundaries and measure varve thickness. In some cases, however, laminations not visible on split core surfaces (so-called cryptic laminations) may be revealed by other imaging methods such as X-ray radiography (Edmondson & Allison 1970). In the Holocene and recent sediments recovered recently from Windermere, no obvious laminations were observed on split core surfaces and there were only occasional and irregular indications of laminations in X-radiographs.

Over the last decade, X-ray fluorescence core scanning (μ-XRF) has been increasingly applied to the analysis of varved sediments (Cuven et al. 2010; Naeher et al. 2013) and the ITRAX μ-XRF was used to analyse the Windermere cores. As detailed in chapter 3, in some

intervals this revealed mm-scale alternating peaks of Fe and Mn some of which did appear to coincide with potential lamina features in X-radiographs indicating the presence of potential "cryptic laminae" despite evidence for bioturbation.

The main geochemical and overall textural changes in the Windermere cores are discussed in chapter 5. The purpose of this Chapter is to document the lamina scale variability using a combination of SEM imaging and geochemical analysis with a view to maximising the temporal resolution of the records and so to resolve processes of seasonal or sub-seasonal origin.

6.2 Results

6.2.1 Lithostratigraphy

In all cores the top 2.4-0.5 cm is low porosity allochthonous detrital material and is abundant in authigenic minerals. The overall geochemistry and mineralogy is given in Chapter 5 whereas here, an account is given of the fine scale variability where lamina fabrics are observed. This Chapter focuses also on the detailed geochemistry and fabrics of the surface sediment.

6.2.2 Diatom ooze laminae

Microlithostratigraphic analysis shows the dark sediments and upper pale sediment in all cores to be abundant in diatom remains. In SC68 diatoms are observed to be concentrated in distinct laminae ranging in thickness from 0.2 to 1 mm (Figure 5-2 and Figure 6-1). Some 12 diatom ooze laminae occur in SC68 and single lamina is present in SC64 (Figure 5-2 and Figure 6-2). Imaging of stub samples taken from the laminae reveals that the laminae are comprised of near- monospecific concentrations of *Asterionella Formosa* in the dark mud, or *Aulacoseira* spp., in the upper pale mud (Figure 6-1).

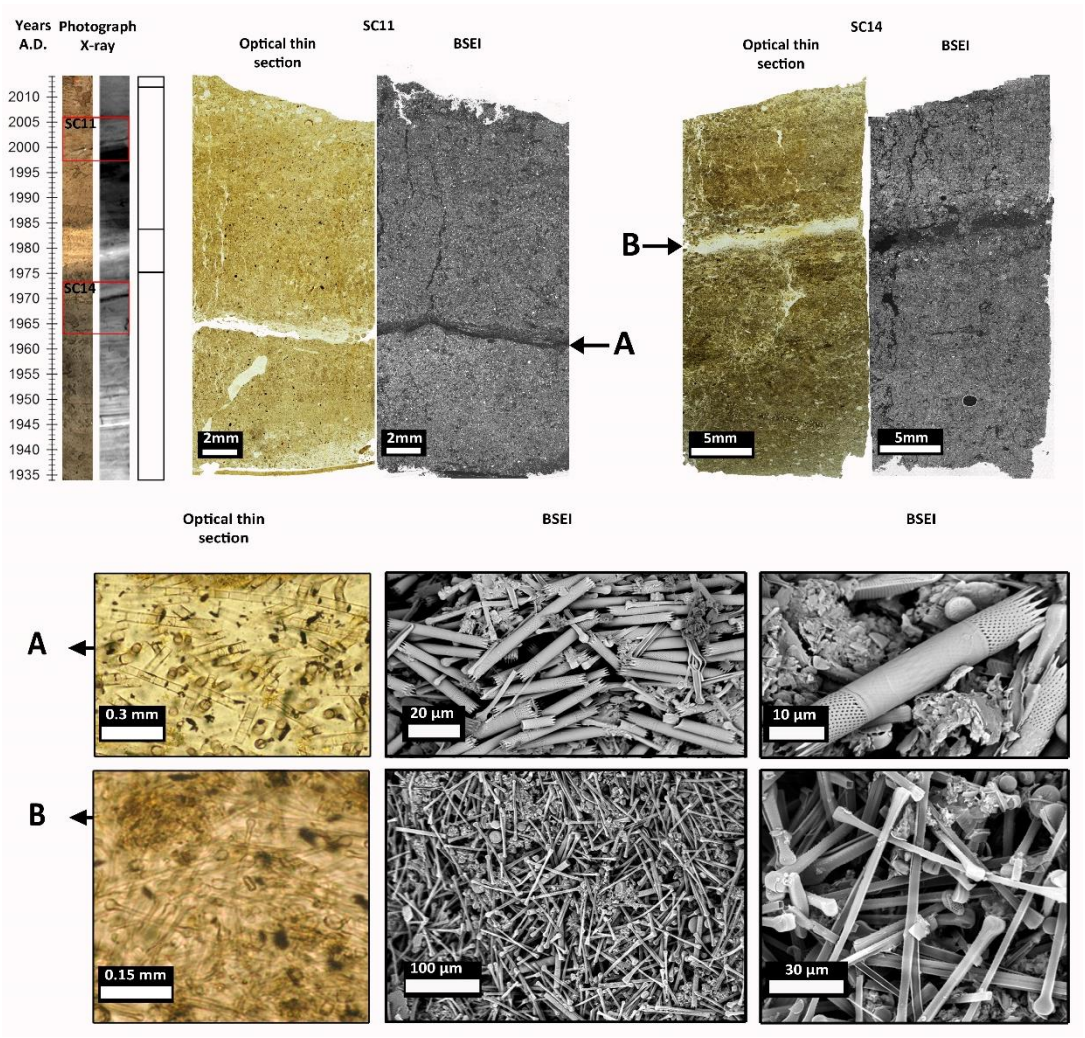

Figure 6-1: Position of Aulacoseira bloom lamina (A) within SC11 optical thin section and back scatter electron image (BSEI) and Asterionella bloom lamina (B) within SC14 optical thin section and BSEI, and detailed optical thin section and BSEI form both A and B.

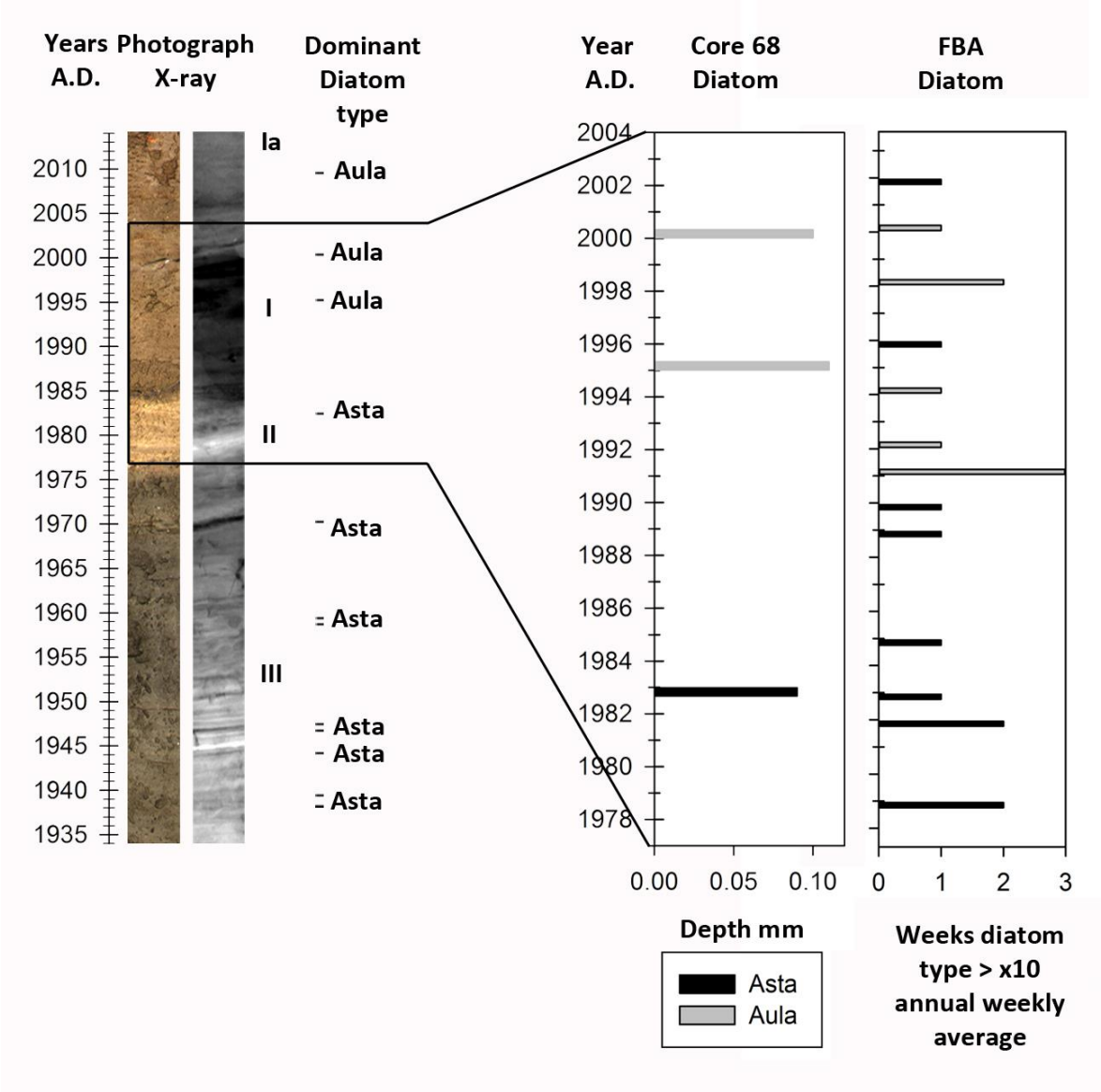

Figure 6-2: Comparison of sediment diatom record with FBA diatom record through the period 1977 – 2014. Asta = *asterionella* type diatom, Aula = *Aulacoseira* type diatom.

6.2.3 Diagenetic microfabric and mineral enrichment

To develop an integrated understanding of the inter-relationship of sediment microfabrics and chemical composition EDS line scans and elemental maps were produced in conjunction with optical and BSEI for a suite of thin sections from the topmost sediment of all cores and the lower pale brown sediments of SC68 (Figure 6-3, Figure 6-4, Figure 6-5 and Figure 6-7, Figure 6-8, Figure 6-9, Figure 6-10).

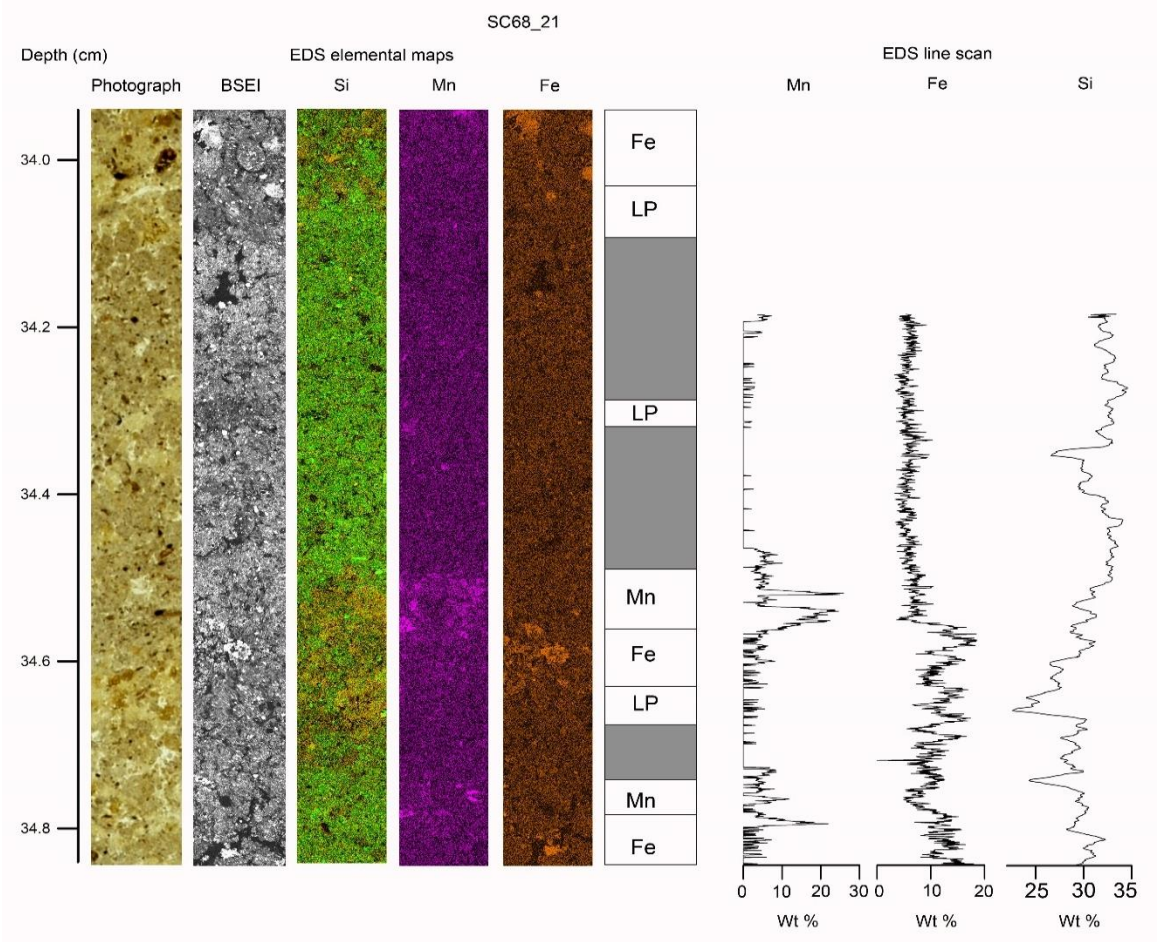

2275

2276 Figure 6-3: Optical thin section, back scatter electron image, mineral lamina log (LP=low
2277 porosity sediment, grey = mud), EDS map (Si, Mn and Fe) and EDS line scan
2278 (Si, Mn and Fe) of alternating laminae in slide SC 21 (core SC68)

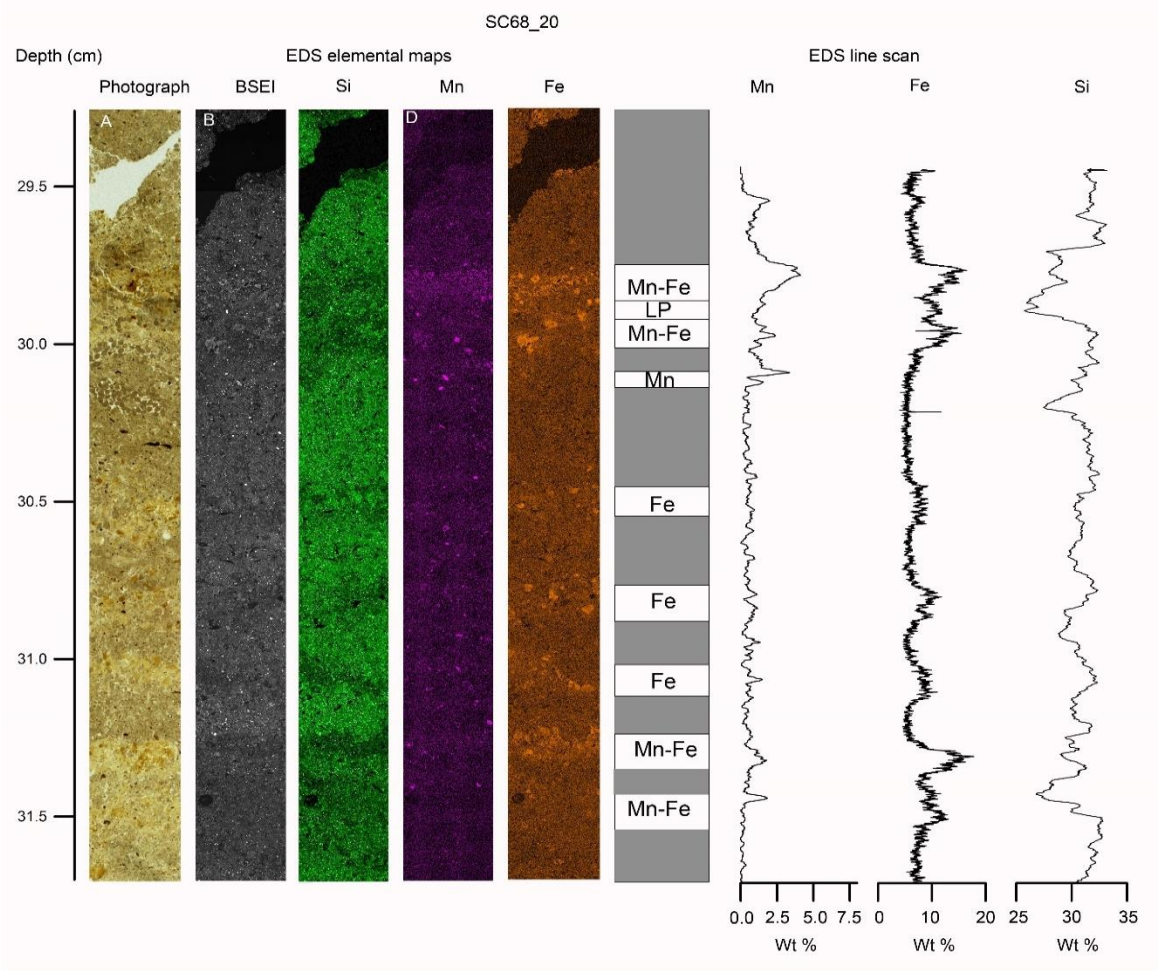

Figure 6-4 Optical thin section, back scatter electron image, mineral lamina log (LP=low porosity sediment, grey = mud), EDS map (Si, Mn and Fe) and EDS line scan (Si, Mn and Fe) of alternating laminae in slide SC 20 (core SC68)

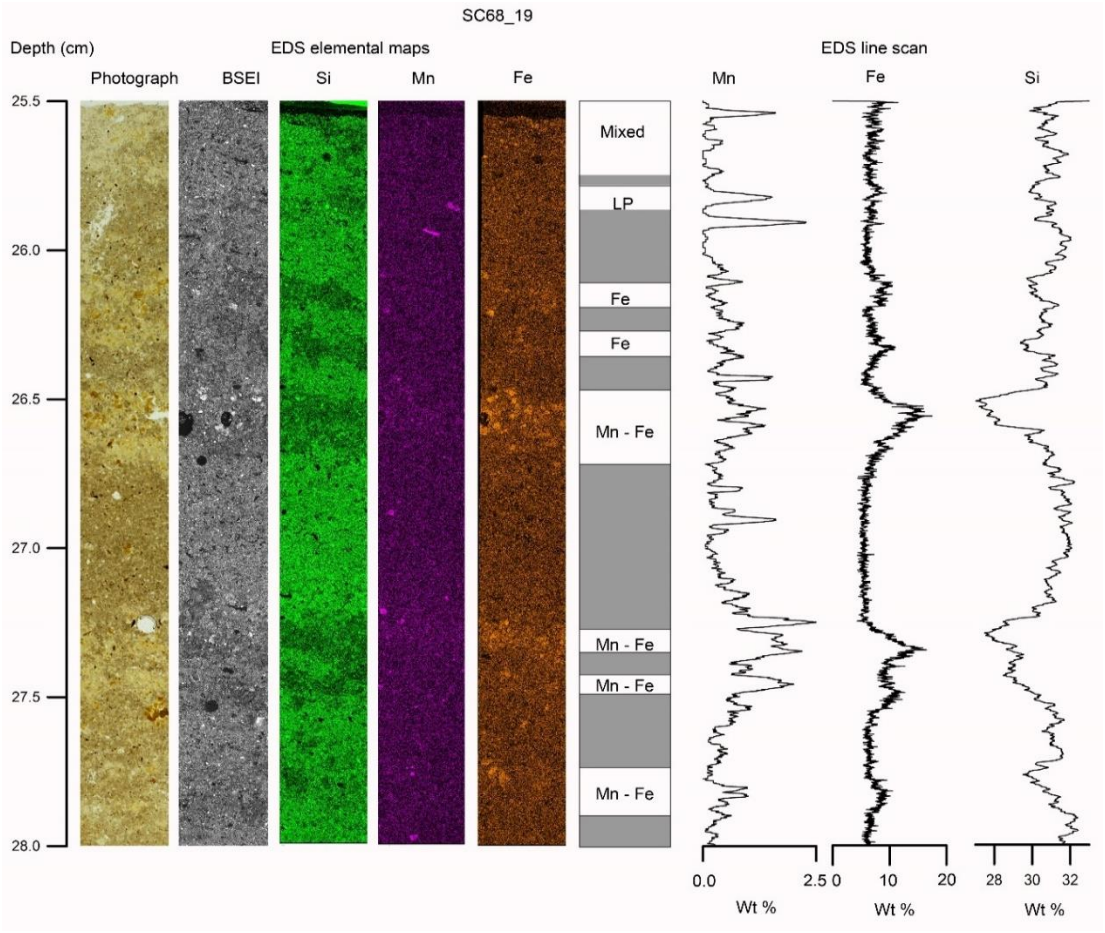

Figure 6-5 Optical thin section, back scatter electron image, mineral lamina log (LP=low porosity sediment, grey = mud), EDS map (Si, Mn and Fe) and EDS line scan (Si, Mn and Fe) of alternating laminae in slide SC 19 (core SC68)

6.2.4 Water Sediment Interface (WSI) micro scale geochemistry

Bulk sediment WD-XRF analysis of the topmost 1-2 cm shows major Mn enrichments in SC57 (12.5% MnO) and SC64 (4.5% MnO) with a lesser enrichment in SC68 (1.5% MnO). EDS elemental mapping and line scan analysis of SC57, SC64 and SC68 further indicates that the Mn enrichment is most concentrated in the top few mm (Figure 6-6). In SC64 the Mn enrichment is mainly confined to the uppermost 3 mm with subjacent enrichment in Fe and P from 3 – 5 mm, although more minor Fe and P elevations occur within the top 3 mm (Figure 6-8). In SC57, the Mn enrichment is most intense in the top 1 mm but continues down to 7 mm (Figure 6-10). In all three cores, Fe and P enrichments coincide with two distinct separate peak enrichments in SC57 and SC68. While SC67 shows simultaneous enrichment in Mn, Fe and P there are no distinct lamina formed by mineral bands associated with the WSI (Figure 6-7 and Figure 6-9).

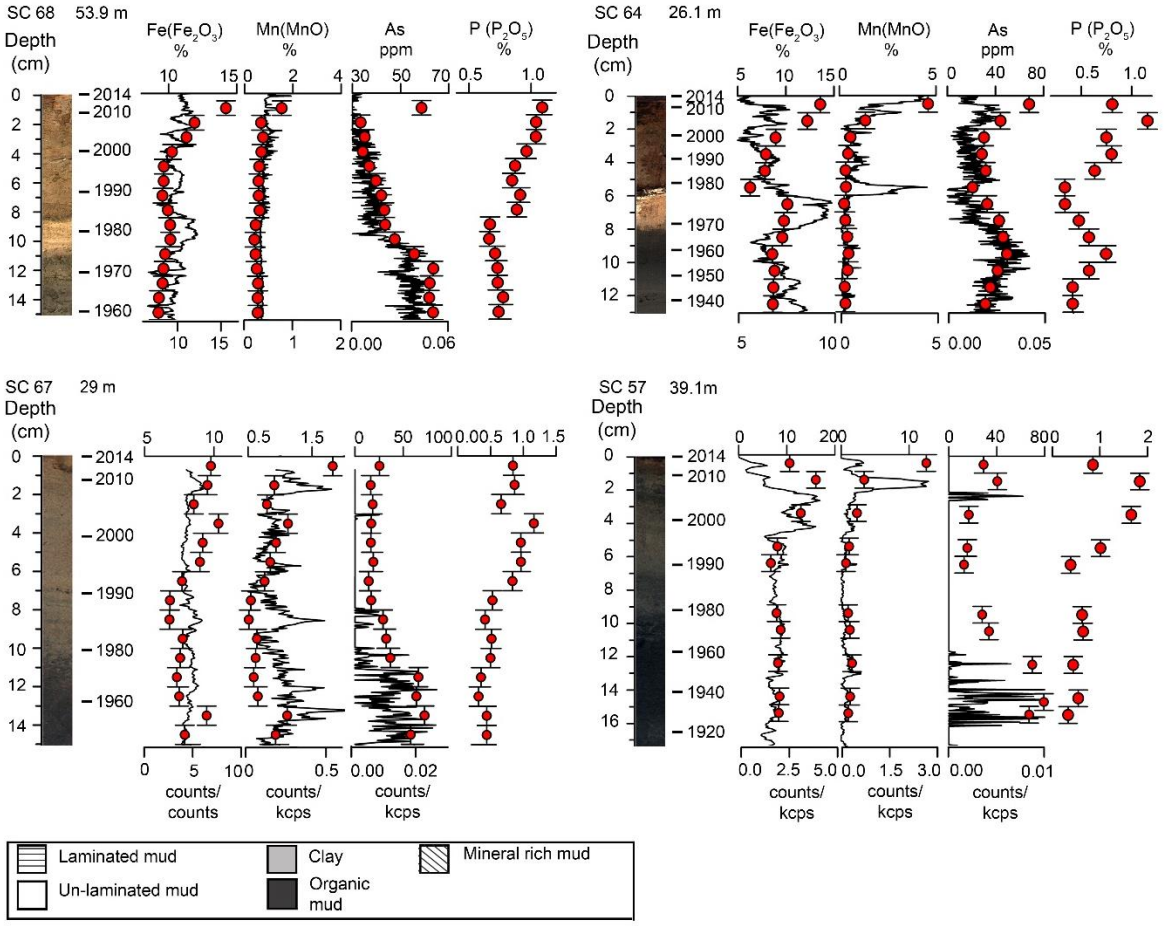

Figure 6-6 SC68, SC64, SC67 and SC57 Core photograph, X-radiograph, summary of lithostratigraphy and Mn, Fe, Pb, As, and P itrax (black line), WD-XRF (red dots) for upper most 15 cm showing mineral enrichment associated with the WSI

X-ray diffraction (XRD) analysis indicates that the Fe and Mn minerals in the surficial sediment are x-ray amorphous, consistent with the expected oxide/ hydroxide phases (Friedl et al. 1997).

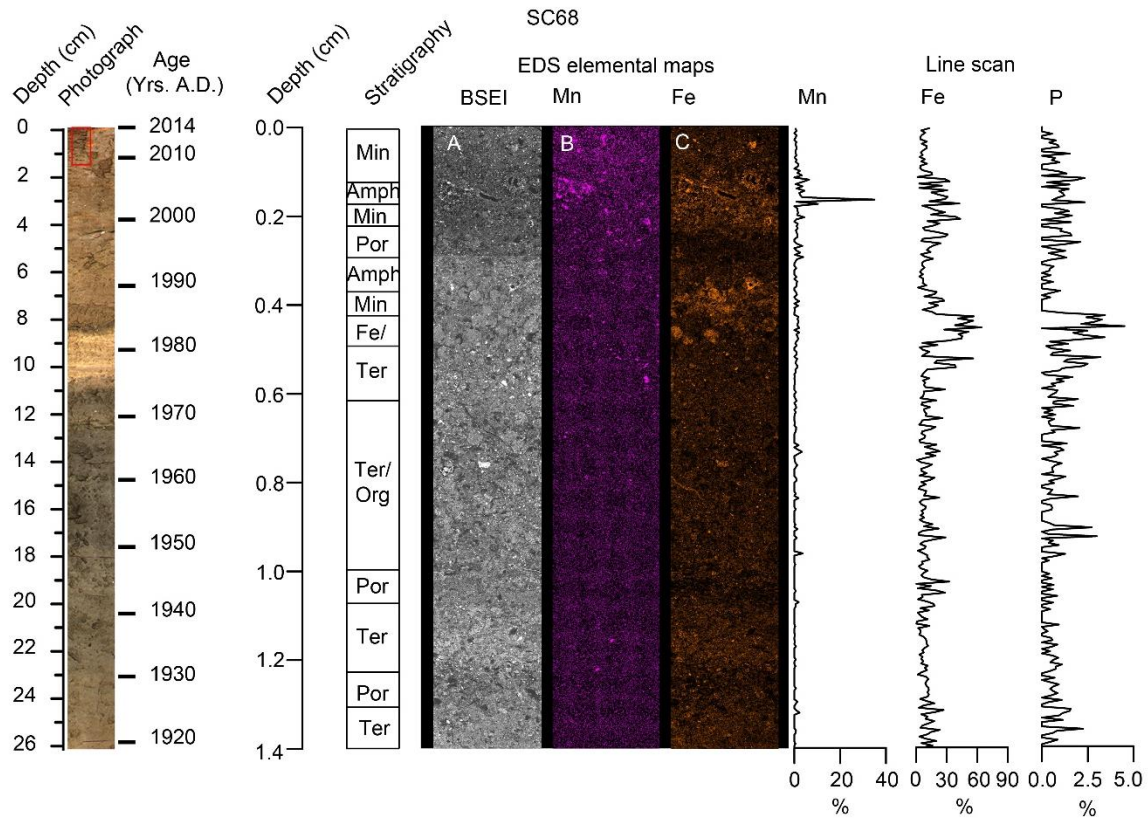

2307

2308 Figure 6-7 SC68 core photograph with age and depth showing the position of optical thin
2309 section, back scatter electron image, with core log (Ter = terrigenous debris, Org
2310 = organic debris, Por = porous, Amph = amorphous structure, Min = mineral
2311 with corresponding dominant element if identifiable), EDS map (Si, Mn and Fe)
2312 and EDS line scan (Si, Mn and Fe) of the water sediment interface.

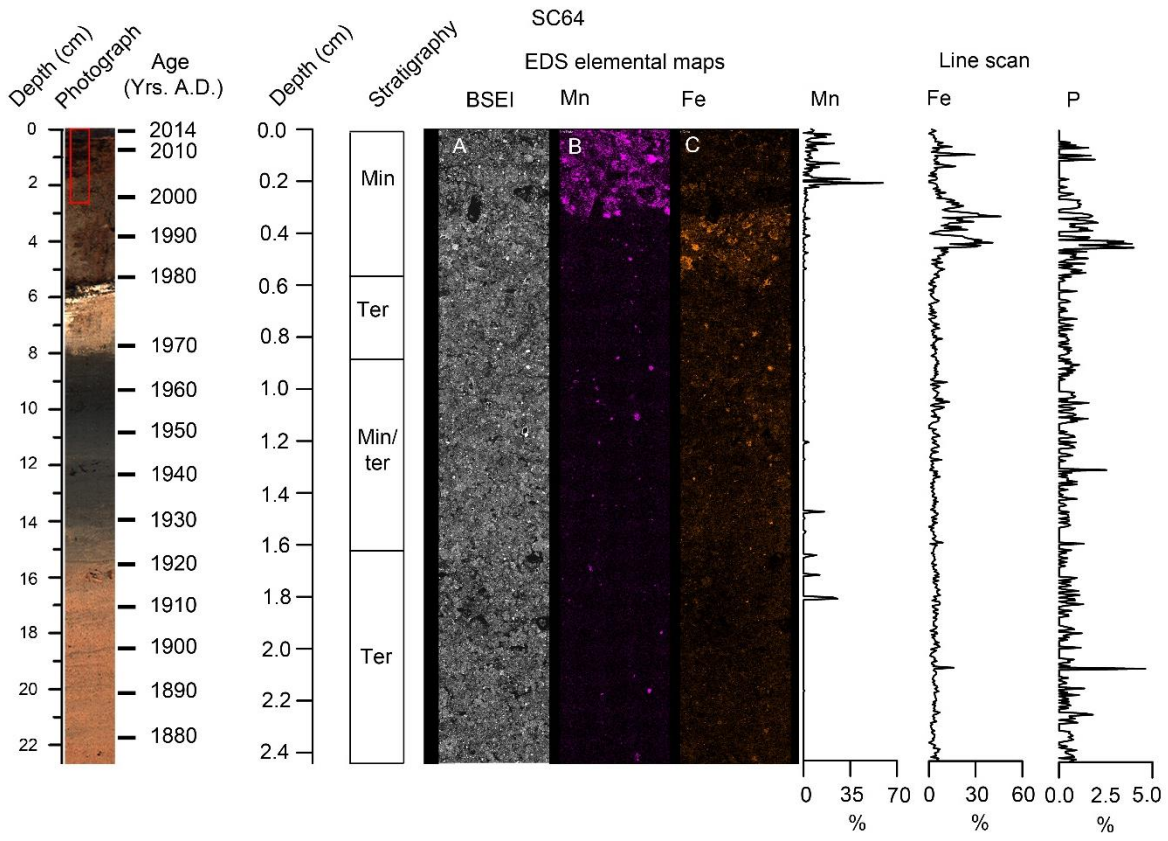

Figure 6-8 SC64 core photograph with age and depth showing the position of optical thin section, back scatter electron image, with core log (Ter = terrigenous debris, Org = organic debris, Por = porous, Amph = amorphous structure, Min = mineral with corresponding dominant element), EDS map (Si, Mn and Fe) and EDS line scan (Si, Mn and Fe) of the water sediment interface.

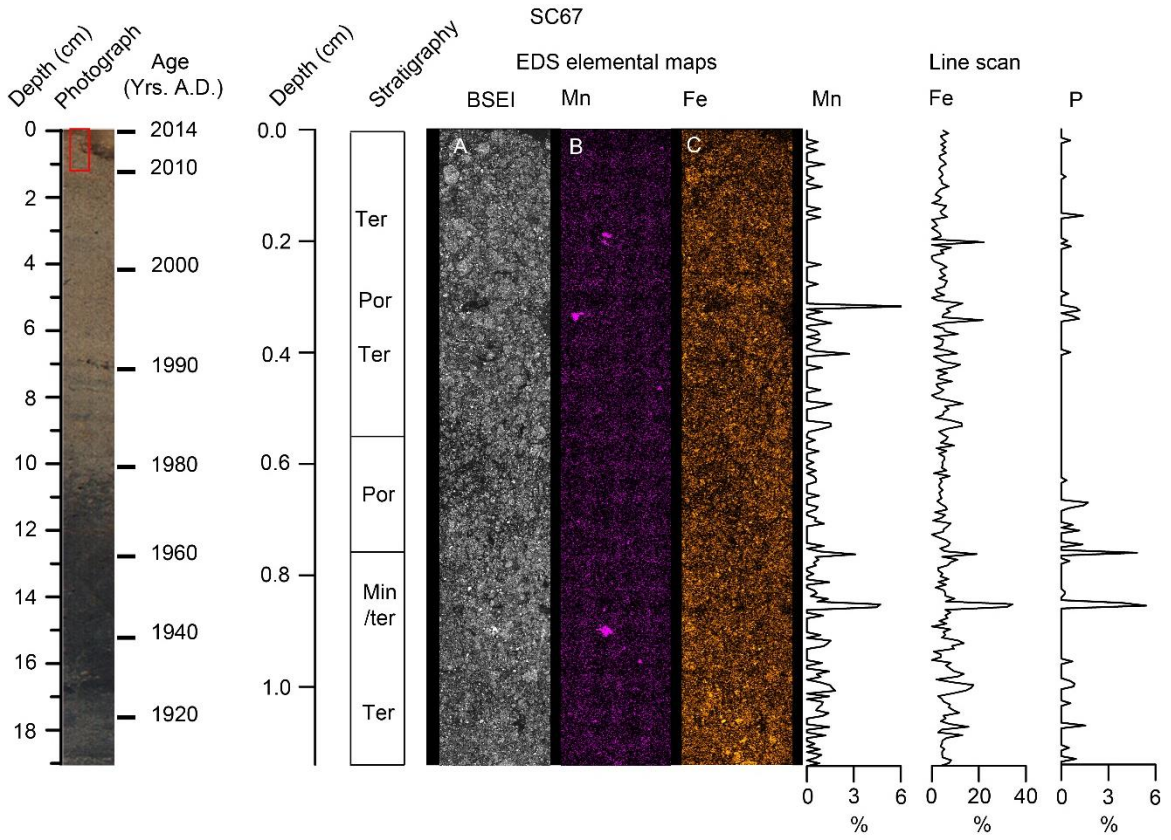

Figure 6-9 SC67 core photograph with age and depth showing the position of optical thin section, back scatter electron image, with core log (Ter = terrigenous debris, Org = organic debris, Por = porous, Amph = amorphous structure, Min = mineral with corresponding dominant element), EDS map (Si, Mn and Fe) and EDS line scan (Si, Mn and Fe) of the water sediment interface.

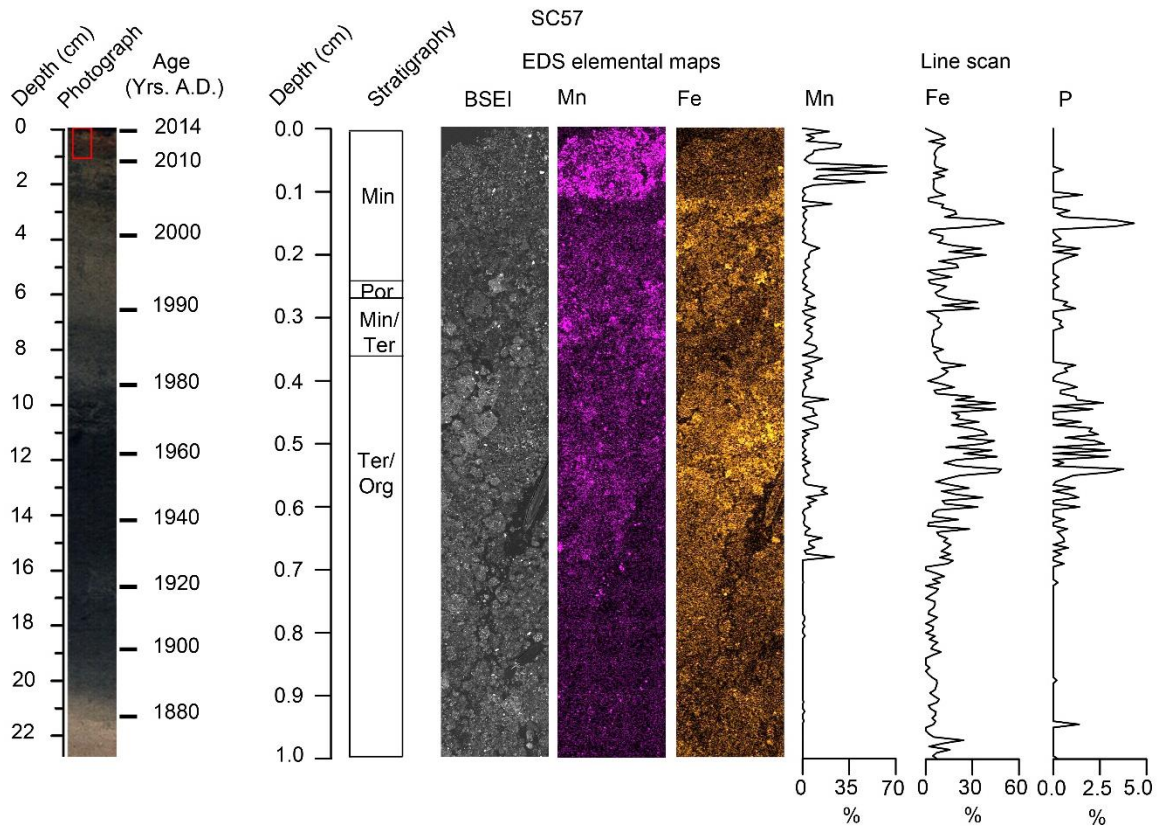

Figure 6-10 SC57 core photograph with age and depth showing the position of optical thin section, back scatter electron image, with core log (Ter = terrigenous debris, Org = organic debris, Por = porous, Amph = amorphous structure, Min = mineral with corresponding dominant element), EDS map (Si, Mn and Fe) and EDS line scan (Si, Mn and Fe) of the water sediment interface.

6.2.5 Fe & Mn enrichments in the lower pale brown laminated sediments of SC68

To further investigate the Fe-Mn enriched laminated sediments from the lower pale muds of SC68 three thin sections from the interval were more thoroughly investigated using combined BSEI and optical microscopy, and EDS elemental mapping and lines scans. In addition to Mn and Fe, Si is shown to indicate variation in detrital input.

The lower 1 cm of thin section SC21 shows three low porosity laminae spaced between 2 – 3.5 mm (Figure 6-3). Two contain both Mn and Fe with the Mn concentrations immediately above the Fe. A further low porosity lamina, indicated by darker BSEI and reduced Si, at 34.3 cm shows no Fe – Mn enrichment. Pelleting of the sediments is pervasive and the laminae are not observed in the optical photomicrograph. SC20 shows alternating terrigenous detrital material and Mn-Fe, as well as solely Fe, rich laminae with spacing 2 – 4 mm (Figure 6-4). Four low porosity Fe – Mn mineral rich laminae were identified, but

without clear zonation of Mn and Fe with three further Fe-rich laminae. The laminae are best defined in the lower part where the lower porosity Fe - Mn laminae are paler yellow in optical photomicrograph, darker in BSEI and are also defined by the Si (reduced counts) and Fe (higher counts) maps and line scans. Pelleting has again obscured some laminae structure and appears particularly intense in the upper part where the juxtaposition of dark and pale yellow pellets is consistent with more vertical redistribution of material than in the lower part where laminae are distinct.

In SC19 pelleting is less but has still resulted in some laminae being partially distorted (Figure 6-5). Within this thin section four Mn – Fe low porosity laminae, two Fe low porosity laminae and one none mineral low porosity lamina are shown by optical thin section, BSEI, and EDS elemental mapping. Line scan analysis highlights that what may have been considered singular large pale low porosity laminae at 27.28 – 27.5 cm depth and 25.5 – 25.75 cm have a more complex structure with two or three Mn-Fe rich sections. Here the mineral rich – detrital rich laminae couplets are between 0.14 and 0.8 cm but have an average of 0.24 cm width comparable with the LSR of 0.29 cm/ yr-1 for this core.

6.3 Discussion

6.3.1 Significance of diatom laminae and comparison with the FBA bloom record

A range of planktonic and benthic diatoms occur in the sediment but only two species form the distinct diatom ooze laminae, comprising of either *Asterionella formosa*, in the dark mud, or *Aulacoseira* spp., in the upper pale mud, in near-monospecific concentrations (Figure 6-1). These laminae evidently represent the mass sedimentation from diatom blooms. The increase in *Asterionella formosa* occurs in the dark mud, and its appearance has been related to the onset of eutrophication (Pennington 1973; Sabater & Haworth 1995). Diatom counts from bulk sediment through the dark mud show that *A. formosa* dominates the assemblage with concentrations ranging from 40 to 60% (Sabater & Haworth 1995). Water column sampling, undertaken every two weeks in Windermere since 1945, indicates some fluctuations in the abundance of *A. formosa* that have been related to competition with other planktonic diatoms (Maberly et al. 1994). In contrast to *A. formosa*, *Aulacoseira spp*. Dominance particularly in one species *Aulacoseira islandica* has only been detected in Windermere since 1988 (Canter & Haworth 2010). The water column surveys identify both *A. formosa* and *Aulacoseira* spp. to be abundant in the spring, acting as major contributors to the spring bloom (Feuchtmayr et al. 2012). However, other key spring bloom species are

also present including *Tabellaria flocculosa* and *Fragilaria crotonensis* with *T. flocculosa* identified as more abundant than *Aulacoseira* spp. (Feuchtmayr et al. 2012). The fact that the other spring bloom species do not form sediment laminae suggests that they may be less important for controlling flux than either *Asterionella formosa* or *Aulacoseira* spp.

Long-term phytoplankton records collected by the FBA from the southern part of the North Basin of Windermere were compared with the timing of monospecific diatom-bloom lamina in SC68 showing that specific diatom laminae can be matched to individual past diatom blooms which typically last 1 – 3 weeks (Figure 6-2). The lamina records show that *Aulacoseira* spp. have been the more dominant lamina-former since the early 1990s (Figure 6-1 and Figure 6-2). The installation of phosphate stripping to the Tower Wood STW in 1991/ 1992 has led to a decrease in eutrophication. This is therefore consistent with the view that *Asterionella formosa* may be the peak eutrophic species while *Aulacoseira subantarctica* thrives with moderate increases in nutrients but is disadvantaged by further enrichment (Gibson et al. 2003).

6.3.2 Redox driven geochemical lamination of Mn and Fe in the lower pale brown mud (SC68)

Laminae within the lower pale muds of SC68 may be comprised of Fe minerals, Mn minerals, and a combination of both or simply marked by relatively high porosity and reduced terrigenous sediment content relative to the more Si-rich intervening sediment. These are present throughout the interval despite the almost complete pelletisation of the sediment most likely by oligochaetes such as *Tubifex* sp. Given the bulk sedimentation rate through this interval of 0.28 cm/yr-1, the 2-4 mm spacing of these laminae argues for an annual origin. Windermere receives the majority of precipitation, and riverine input in the winter months (Pickering & Sutcliffe 2001) and so the terrigenous sediment (Si-rich) laminae likely correspond to this period of enhanced clastic sediment input. The intervening porous laminae that contain Mn and Fe minerals provide evidence for mobility of these redox-sensitive elements (Davison 1993) and suggest the following scenario. During the period of summer stratification, hypoxia developed in the water column promoting the development of anoxia within the sediment. This led to the successive reduction of Mn and Fe into their mobile reduced Mn^{2+} and Fe^{2+} ions and upwards migration in the pore waters. This migration would continue until they encountered the redox boundary in the sediment where Fe would be preferentially oxidised (Figure 6-11) reflecting the slower oxidation kinetics of Mn compared to Fe (Davison 1993). Evidence for

this differential oxidation is seen in SC68_21 (Figure 6-3) where Mn-rich laminae occur immediately above Fe-rich laminae. The return to full oxygenation of the surface sediments in Windermere is generated by the annual turnover which currently occurs in October in the South Basin and a little later, in December in the North Basin (Pickering & Sutcliffe 2001). This would re-oxygenate the surface sediment and promote the re-oxidation of the Fe and Mn.

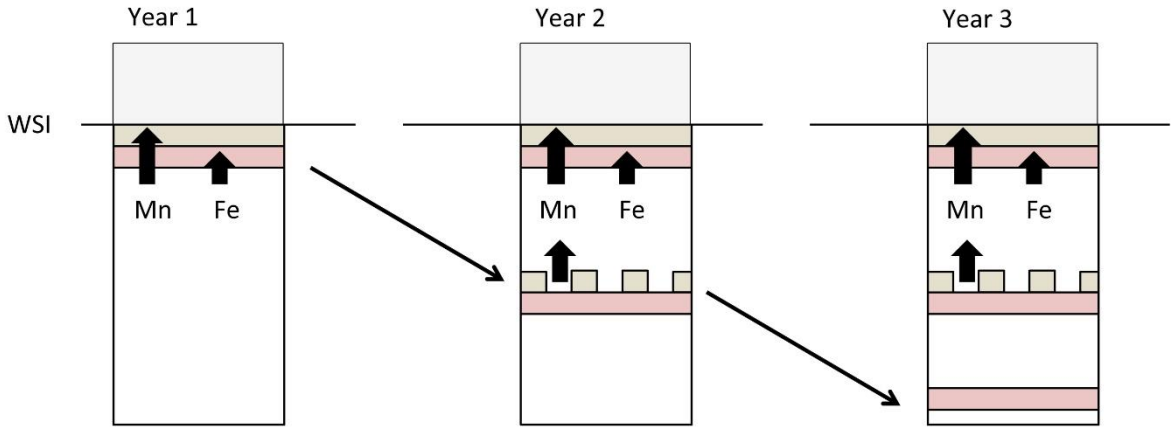

Figure 6-11 Preferential dissolution of Mn/ Fe layers. Year1 shows formation of Mn lamina and subjacent Fe lamina at the warmer sediment interface (WSI); Year 2 shows burial of the surface-formed layers with the reductive dissolution of Mn now feeding the Mn lamina forming at the surface; Year 3 shows complete dissolution of the Mn lamina formed in Year 1 with preservation only of the Fe lamina.

The occurrence of Mn mainly as rhodochrosite, and not as Mn oxyhydroxides as may be expected with Fe oxyhydroxides may be explained by the following mechanism. Mn oxyhydroxides that had formed in the sediment at the redox boundary underwent bacterial reduction as hypoxic conditions continued to develop through the stratified period. This led to an increase in alkalinity that promoted the formation of rhodochrosite. The rhodochrosite crystals contain impurities and inclusions of terrigenous sediment corroborating growth within the sediment. The presence of rhodochrosite a small proportion of some Mn oxyhydroxides and Fe oxyhydroxides is thus indicative of lowering bottom water oxygen during summer but not of persistently anoxic conditions. The less common occurrence of Mn laminae than Fe laminae may indicate efflux of Mn^{2+} from the sediment – see other scenario in Figure 6-12.

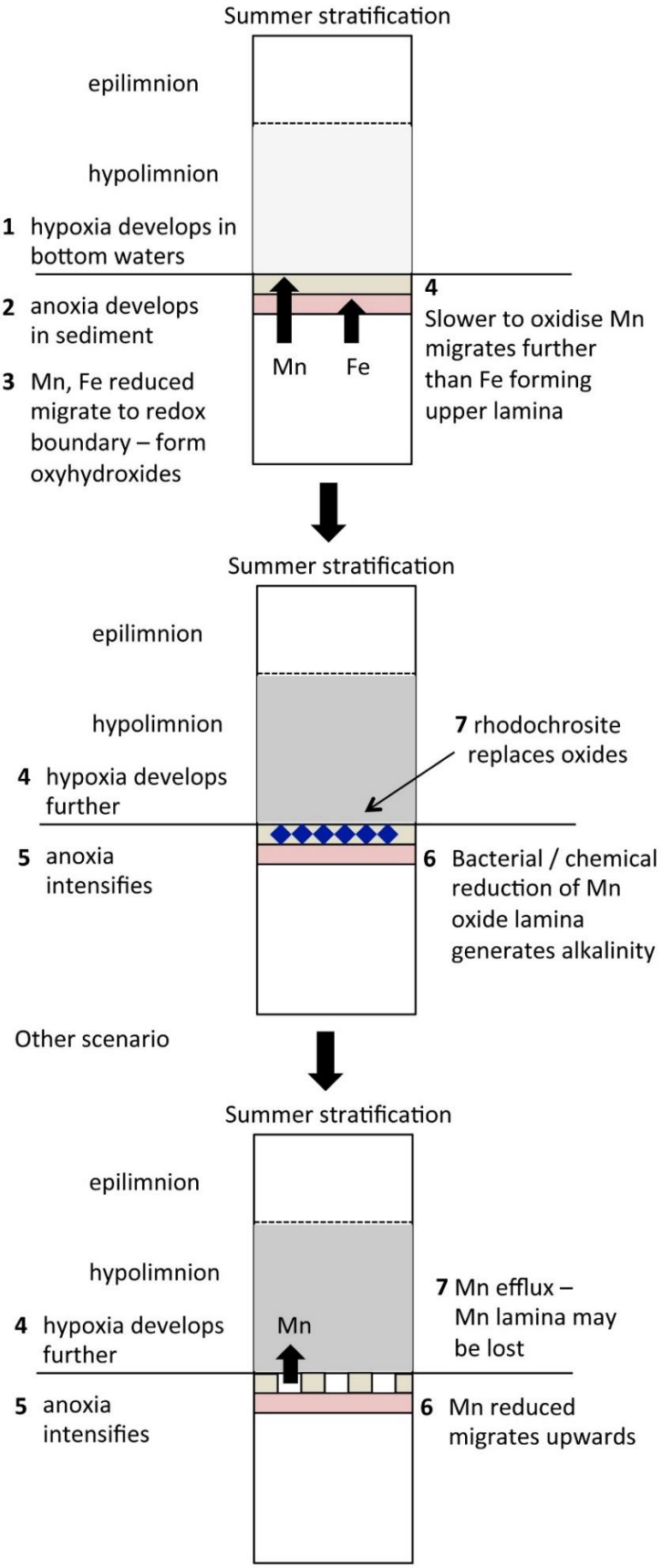

2432

2433 Figure 6-12 Processes in the surface sediment that generate the Fe and Mn laminae.

6.3.3 Redox driven mobility and of Mn and Fe and lamina formation near the water-sediment interface.

The fully quantitative WD-XRF and the itrax show enrichments of Mn and Fe in the top 1-3 cm of cores SC57, SC64 and SC68 and to a lesser extent in SC67 (Figure 6-6). The EDS line scan and elemental maps reveal that: in the 3 most enriched core tops a 1-2 mm Mn enriched zone is at the surface with most Fe enrichment between 1-2 mm below this (Figure 6-7, Figure 6-8 and Figure 6-10). The gravity cores were taken in April 2014, towards the end of the period of maximum ventilation following turnover in October – December 2013. Reductive mobilisation of Fe and Mn due to developing sediment anoxia in the previous stratified period in the summer of 2013 would have led to upwards migration of the mobile reduced ions. Thereafter, bottom water ventilation in the winter months was sufficient to oxidise first Fe and then the slower to oxidise Mn (Davison 1993; Dellwig et al. 2010) resulting in the Mn rich layer forming above the Fe layer at the water sediment interface. Similar to the Lake Baikal mineralisation (Och et al. 2012), albeit on smaller scales, there is generally a sharp boundary between the Mn and subjacent Fe layer. Distinct differences in the fine structure of the mineralisation between the different core tops helps to shed further light on the mechanisms of formation. In SC64 there is only a single Mn and Fe couplet with only a hint at some lower enrichments. The interval analysed incorporates around at least 10 years of sedimentation. This therefore suggests that reductive dissolution of both Mn and Fe oxides is progressive and effectively feeds the Mn and Fe enriched zone at the redox boundary near the sediment water interface leaving no trace of the annual hypoxia/ ventilation cycle in the sediment record. By contrast, in SC 57 and to a lesser extent in SC68 a legacy of Fe and Mn (SC57 only) layers are left in the sediment. The greater mobility of Mn relative to Fe is shown by the lesser preservation of the Mn layers. The evolution of these laminae during burial is shown schematically in Figure 6-12 where the scenario of dissolution of Mn laminae and preservation only of Fe lamina is given. A further scenario would be the reductive dissolution also of the Fe laminae resulting in no lamina preservation.

The cause of the "detachment" and preservation of these layers may relate to the overall kinetics of the redox reactions controlled by the relative timing and extent of anoxia development and the timing and degree of turnover ventilation. This evidence from the WSI indicates a clear distinction from the Lake Baikal Fe-Mn layers which generally form at a redox boundary within the sediment. The presence of the Mn in the surface layer

suggests that the redox boundary may have been at the WSI and that there may even have been a period of bottom water anoxia during the culmination of the stratified period.

The Mn and Fe lamina forming in the surface sediments represent precursors of the Fe-Mn laminae as found in the lower pale muds of SC68. The main difference is that the Mn in the near surface sediment appears to be in the form of X-ray amorphous oxyhydroxides and there is no evidence of rhodochrosite formation.

6.3.4 Evidence for Mn efflux from the sediment and geochemical focussing

The presence of high concentrations of Mn oxyhydroxides at the WSI suggests that there may have been significant Mn efflux from the sediment to the bottom waters. While Fe2+ is rapidly oxidised in the presence of oxygen with a half-life of minutes, by contrast, Mn2+ once in solution oxidises at much slower rates with a half-life of months or greater (Canfield et al. 2005). The upshot is that dissolved Mn may have persisted for significant periods even in the presence of oxygenated waters and this is corroborated by the detection of Mn in Windermere bottom waters during the 1970s/ 1980s (Hamilton-Taylor et al. 1984). While Mn is generally enriched in the core tops it is especially concentrated in the deep South Basin (SC57) with values of 12.5% MnO from WD-XRF and up to 60% Mn locally from EDS line scans. The origins of the Mn required to develop such concentrations may be explained by the "geochemical focussing" mechanism (Schaller & Wehrli 1996). This requires anoxic sediments to be in contact with an oxic water column whereby Mn efflux from the sediment generates a net flux to the deeper regions facilitated by the longer half-life of Mn2+ (Schaller & Wehrli 1996). The sediment concentrations and potential redox-driven mobilisation of the Mn to the water column may be hazardous to fish populations as documented from Lake Biwa, Japan (Itai et al. 2012). The deep South Basin core SC57 also has elevated concentrations of Ba and this may be driven by adsorption and scavenging by hydrous manganese oxides as documented from Lake Biwa (Sugiyama et al. 1992).

6.3.5 Iron – Phosphate coupling

EDS line scan analysis of thin sections and EDS from the WSI of cores SC64, SC68 and SC57 shows the association of P with Fe (Figure 6-8, Figure 6-9, Figure 5-4). Topographic imagery coupled with EDS spot analysis of WSI sediment also show an association between amorphous Fe and Mn oxyhydroxides and P. This suggests that P accumulation was driven by the complexation or adsorption of P onto Mn-Fe oxyhydroxides, a widely recognized process in lakes (Buffle et al. 1989; Davison 1993; Dellwig et al. 2010). Under anoxic

sediment conditions where Fe is reductively mobilised, then P is also mobilised until re-oxygenation when it is scavenged by Mn-Fe oxyhydroxides (Jensen et al. 1992; Søndergaard et al. 2003). Redox driven cycles of reflux can lead to geochemical focusing of P and mobilisation form deep sediments meaning that even where lakes have undergone remediation or preventative measures to reduce P the content can be enriched during periods of hypoxia (Søndergaard et al. 2003; Dellwig et al. 2010). As P is one of the main limits to phytoplankton growth, which reduce oxygen content of the isolated hypolimnion and lead to eutrophication, excess P release can have serious implications for chemical and ecological status of lakes already subject to anthropogenic stressors (Correll 1998; Christophoridis & Fytianos 2006).

6.4 Conclusion

The results of this study demonstrate that lake sediments that do not appear outwardly laminated and may even show bioturbation may nevertheless have the potential to provide seasonal-scale resolution with the application of the appropriate techniques. Scanning Electron Microscope (SEM)-led approaches applied to recent sediments from Windermere, England's largest natural lake, have revealed the preservation within the sedimentary record of a range of seasonal-scale processes. Individual seasonal blooms of diatom algae are preserved, some of which may be matched with lake water column records of bloom occurrence. Laminae on a millimetre-scale of Fe and Mn minerals were analysed from the surface sediments and from a pre-eutrophication interval from the deep North Basin. These record seasonal cycles of lake ventilation. During the summer stratified period anoxia develops in the sediment leading to reductive mobilisation of Mn and Fe. On oxidation at the WSI, that may be promoted by autumn/ winter (October – December) lake turnover and ventilation, the Mn and Fe oxides form distinct laminae, with the slower to oxidise Mn forming the upper layer. The subsequent burial of these laminae preserves a seasonally-resolved record of the extent of anoxia development and turnover in the lake and its sediments.

A range of allochthonous redox-driven processes that result in development of potentially hazardous As and Hg concentrations are also recognised. Analysis of cores from different depth zones provides evidence for redox-driven geochemical focussing of Mn in the deep South Basin to levels that may be hazardous to fish populations. Tight coupling of Fe and P further indicates the potential redox-driven release of P to the water column with implications for lake eutrophication.

2532

Chapter 7 **Conclusions**

Chapter 3 presents and discusses outline results from a piston core (PC68) collected from Windermere's deep North Basin in 2012. Using a multi-proxy approach, including itrax micro XRF analysis, the core was investigated for changes in Ti and K, terrigenous sediment input indicators, and Mn, a redox sensitive trace element. To complement this, changes in the organic component (TOC, TN, C/N, $\delta^{13}C$) were investigated, in addition to pollen and chironomid assemblages, in order to reconstruct environmental parameters and develop a chironomid inferred mean July temperature record. Further, optical thin and scanning electron microscopy (SEM) sections have been used in microlithostratigraphic analysis, and electron dispersive spectroscopy (EDS) thin section elemental mapping. The well dated sediment sequence shows the potential of the Windermere sediments to record phases of sediment in-wash, catchment and basin wide organic process and bottom water redox conditions, as well as record well-known climate excursions such as the Little Ice Age (LIA) and 4.2 k. yr. event. In addition, MTDs in the Early Holocene with distinct sedimentology and geochemistry, similar to MTDs in other lakes (Schlolaut et al. 2014) show the potential for Windermere sediments to record seismic activity.

Lake sediments commonly contain detrital layers that record past events such as floods or earthquakes, but these may be disturbed or partially destroyed by bioturbation. Chapter 4 used a novel combination of techniques to relate microscopic sediment fabric features to lake-basin scale processes. In addition to this, X- radiography and micro-XRF analyses of cores were complemented by backscattered electron imagery (BSEI) and energy dispersive X-ray microanalysis of resin-embedded sediment. Microfabric and geochemical methods allowed for the identification of clay-layer mass transport deposits (MTD) despite bioturbational mixing of the original end members. Two cores with robust radionuclide chronologies contained correlative clay layers dated to 1979 and 1979-1980 respectively. These clay layers represent the distal turbidite generated by a major MTD, identified from multibeam swath bathymetry and sediment grab sampling. A likely trigger for the mass flow is the 4.7 ML 1979 Carlisle earthquake. As historic seismic activity on a similar or even larger scale had not resulted in distal slope failure, it was concluded that the lake basin slope was likely preconditioned for failure by increased sedimentary biogenic gas production and increased sediment in-wash as a result of anthropogenic activities, coupled with sediment disruption and dredging. It was also found that MTDs can effect sensitive redox driven processes in the sediment and can result in geochemical focusing of potentially harmful Mn. Chapter 4 highlights the power of microstratigraphic techniques

in the recognition and characterisation of event layers in sediments where bioturbation has occurred.

Chapter 5 demonstrated the effectiveness of a multi-method geochemical and sediment fabric analysis applied to reconstruct the history of eutrophication and pollution of Windermere, the largest natural lake in England. The onset and development of eutrophication in the late 19th and early 20th centuries is marked by a change from pale brown to dark grey sediment, and increased lake productivity is indicated by an increase in the $\delta^{13}C$ values of organic matter. Increased flux of trace metals, including Pb, Zn, Cu, Hg, and As, was enhanced by incorporation and adsorption to settling diatom aggregates that formed near-monospecific laminae preserved in the sediment. Increasing values of the $\delta^{15}N$ of organic matter in the South Basin sediment also occurs, in step with Zn, Hg and Cu from this time, thus linking the metal enrichment to the input of isotopically heavy nitrate from human sewage or farm runoff. The recurrence of sediment anoxia increased and was most intense in the deep basin where benthic activity intermittently ceased. Strongly reducing conditions in the sediment promoted Fe-reduction and the formation of unusual Pb-bearing barite mineralisation, hitherto only described from toxic mine wastes and contaminated soils. From the late 20th century (1980) there is a partial recovery of oxic conditions, with pale sediment returning in some parts, but with elevated $\delta^{15}N$ of organic matter showing continued impacts of sewage discharge on the South Basin. Elevated concentrations of Mn, Fe, Ba, and As in the surficial sediment provide evidence for dynamic redox mobilisation of potentially toxic elements that may be released into the lake waters.

To complement broader scale geochemical analyses in chapter 5, a Scanning Electron Microscope (SEM)-led approach was applied to reconstructing seasonal-scale processes in chapter 6. Individual seasonal blooms of diatom algae preserved in the sediment were compared, and where possible matched with lake water column records of bloom occurrence from the Freshwater Biology Association (FBA). Fe and Mn mineral rich, millimetre-scale laminae were analysed from the surface sediments, and from a pre-eutrophication interval from the deep North Lake Basin. These record seasonal cycles of lake ventilation. During the summer stratified period anoxia develops in the sediment, leading to reductive mobilisation of Mn and Fe. On oxidation at the WSI, which may be promoted by autumn/winter lake turnover and ventilation, the Fe and Mn oxides form distinct laminae, with the slower to oxidise Mn forming the upper layer. The subsequent burial of these laminae preserves a seasonally-resolved record of the extent of anoxia development and turnover in the lake and its sediments. Analysis of cores from different

depth zones provides evidence for redox-driven geochemical focussing of Mn in the deep South Basin to levels that may be hazardous to fish populations. Tight coupling of Fe and P further indicates the potential redox-driven release of P to the water column, with implications for lake eutrophication.

7.1 Future work

7.1.1 Holocene microlithostratigraphy and geochemistry

Preliminary microlithostratigraphic, geochemical, and organic analyses have shown the potential of Windermere sediments in providing a high resolution palaeohydrological, and palaeoclimate proxy record (chapter 3). To complete the aim of providing a palaeoclimate and environment proxy record for the whole Holocene, future work will focus on continuing these analyses through the rest of PC68. Other coring sites show differences in sediment accumulation rates, and preliminary analysis of itrax XRF data from other piston cores (work not featured in this thesis) has shown differences in the geochemistry between the cores. To fully understand how climate and environment drivers affect sedimentary processes in both the North and South basins of the lake, a high resolution microlithostratigraphic and further geochemical work must also be carried out on the other piston cores from Windermere.

Specifically, chapters 4 – 6 highlight that detailed microlithostratigraphic analysis can shed light on redox driven processes on an annual to multi-annual scale. In the Holocene record, a possible link between changes in the ventilation regime of Windermere's deep North basin, organic material source and temperature was identified. Future work could therefore include the addition of detailed and higher resolution analysis through key sections of PC68 and other piston cores, to better understand these relationships, and potentially build a full reconstruction of bottom water ventilation for the Holocene.

7.1.2 MTDs

Although two MTDs in PC68 have already been investigated using a suit of analyses, there is potential for further geochemical and microlithostratigraphic work identifying additional MTDs in other piston cores. This may improve the understanding of the driving and triggering processes of MTDs in Windermere, and highlight the provenance of the deposits.

7.1.3 Chironomids

A preliminary study showed that chironomid inferred mean July temperature reconstructions are achievable in at least the deep North Basin sediments. To fully understand changes in the lithostratigraphy and geochemistry with relation to climate and environment, a more comprehensive chironomid study would need to be conducted on PC68. Moreover, additional chironomid studies in other cores could provide further validation of any future reconstructions, as well as potentially serving as a proxy for other palaeoenvironment parameters such as eutrophication (Lotter et al. 1998).

7.1.4 Recent sediment and redox driven processes

Cores were collected in April 2014, when it is likely that sediments were still well ventilated. As discussed in chapters 5 and 6 it is likely that, given the nature of mineral formation at the WSI and enrichment in trace and major elements such as P and Mn, seasonal dissolution of redox sensitive elements occurs at the WSI, especially in the shallower seasonally eutrophic South Basin. To assess the extent of element mobility during hypoxic conditions which form during the summer – early autumn thermal stratification, more gravity cores which capture the WSI interface at different times of year are required. This could have implication for lake management on Windermere, and provide a framework of methods for use in assessing redox sensitive elements in other lake basins affected by seasonal hypoxia. To help further understand redox driven diffusion within sediment gel probe sampling, which has been utilised successfully elsewhere to measure redox driven process, could be employed (Edenborn & Brickett 2002). To further augment such a study bottom landers could be deployed to measure bottom water conditions at different times of year.

Appendix A

Table 7: a compilation of previous palaeolimnological work from the Windermere catchment.

Title	Author	Date	Record length (Yrs. B.P.)	Coring Method	Chrono-logy	Sedimentology	Organic	Geo-chemistry	Biological proxy	Summary
Bathymetric surveys and lake deposits	C. H. Mortimer and E. B. Worthington	1938	~15000	Jenkin corer		Preliminary investigation			Pollen, Diatom	Preliminary study of lake sediments.
The Exchange of Dissolved Substances between Mud and Water in Lakes	C. H. Mortimer	1941	Recent/ surface muds	Jenkin corer				Mn, Fe (total and ferrous), SO_4, SO_1O_2, $CaCO_3$, Redox potential, pH,		Study of dissolved substances in the water and redox conditions in the mud of Windermere and Esthwaite Water

								conductivity,		
Lake sediments: the bottom deposits of the north basin of Windermere, with special reference to the diatom succession	W. Pennington	1943	~15000	Jenkin corer, Jenkin surface mud-sampler	Pollen	Water content, Wet density, Dry density, Particle size	LOI		Diatoms, Pollen, Plant remains	Identification of sediment facies representing major climate shifts since ~17 k.yr
Studies of the Post-Glacial History of British Vegetation. VII. Lake Sediments: Pollen Diagrams from the Bottom Deposits of the North Basin of Windermere	W. Pennington	1947	~15000	Jenkin corer	Pollen	Varve counting and measuring			Pollen, Plant remains	Identification of sediment facies representing major climate shifts since ~17 k.yr

Structures in the stratified late-glacial clays of Windermere, England	A. J. Smith (Smith 1959)	1959	late glacial	Mackereth Core Sampler						Description of structures in the stratified late-glacial clays showing post depositional disturbance
Sedimentary Studies in Lake Windermere	P. W. Holms	1964	Glacial – modern	Freshwater Biological Association Automatic Surface Sampler (short core), Mackereth cores		particle-size analyses, flocculation		Mineralogy		Identification of sediment depositional processes through time
Sedimentary studies of late quaternary material in	P. W. Holmes	1967	Glacial – modern	Freshwater Biological Association		particle-size analyses, flocculation		Mineralogy		Identification of sediment depositional

Windermere lake (Great Britain)				Automatic Surface Sampler (short core), Mackereth cores						processes through time
Mercury in lake sediments: a possible indicator of technological growth	Aston, S.R., Bruty, D., Chester, R. and Padgham, R.C.	1973	1430	Mackereth Core Sampler		Basic description		Hg		Heavy metal enrichment
The recent sediments of Windermere	W. Pennington	1973	~200	Jenkin surface mud-sampler, Mini-Mackereth piston corer	^{137}Cs	Water content, Dry weight	LOI, TC, TN		Diatom, Pollen	Description of the recent sediment facies and comparison with other limnologic records in Cumbria

Palaeolimnology and Palaeomagnetism	R. Thompson	1973	~16000	?	Radiocarbon	NRM				Development of a British archaeomagnetic record.
Enrichments of zinc, lead, and copper in recent sediments of Windermere, England	J. Hamilton-Taylor	1979	~150	?	Marker layers and published sedimentation rates		TS	Fe, Mn, Al, Zn, Pb, and Cu - atomic absorption spectrophotometry		Zn, Pb, and Cu greatly enriched over the past 130 years. Metal sources and transport mechanisms within the lake are discussed.
Lake sediment record of the geomagnetic secular variation in Britain during Holocene times	R. Thompson	1981	~17000	Mackereth Corer and Mini Mackereth Corer	Palaeomagnetism	NRM				Further development of a British archaeomagnetic record.

Sedimentary record of polycyclic aromatic and aliphatic hydrocarbons in the Windermere catchment	P. A. Cranwell, V. K. Koul	1989	~300	?	^{210}pb		C, H, N, C:N	polycyclic aromatic and aliphatic hydrocarbons		Increase in both polycyclic aromatic and aliphatic hydrocarbons through the 20th century until 1975. Post 1975 a decrease occurs attributed to the replace of coal with oil and gas, but remains 10 x higher than pre industrial levels.
An assessment of recent trophic changes in Windermere South Basin	S. Sabater, E. Y. Haworth	1995	150>	Piston core	^{210}pb, ^{226}Ra, ^{137}Cs,		LOI		Chlorophyll and carotenoids -	Transition from 'normal' sedimentation to black ooze and high

(England) based on diatom remains and fossil pigments					^{134}Cs and ^{241}Am				Cyanobacteria. Diatoms	anthropogenic influence
Changing nutrient levels in Grasmere, English Lake District, during recent centuries	P. A. Barker, J. M. Pates, R. J. Payne, R. M. Healey	2005	~300	Mackereth cores,	^{210}Pb, ^{137}Cs. ^{226}Ra	magnetic susceptibility	LOI,		TP_{diatom}	Eutrophication from 1855, anthropogenic influence peak 1970-80s, improvement since 1990
A multiproxy palaeolimnological study of climate and nutrient impacts on Esthwaite Water, England over the past 1200 years	X. Dong, H. Bennion, R. W. Battarbee, C. D. Sayer	2011	1200	Mini-Mackereth piston corer & percussion piston corer	^{210}Pb and ^{14}C	Median Grain Size	TC	ICP-AES: Al, Na, K	TP_{diatom}	MWP AD 880 – 1350 LIA AD 1350 – 1880 Modern - >nutrients <climate influence on sedimentology

Humans and climate as drivers of algal community change in Windermere since 1850	S. Mᶜgowan, P. Barker, E. Y. Haworth, P. R. Leavitt, S. C. Maberly, J. Pates	2012	150>	Mini-Mackereth corer	^{210}Pb	Dry density	LOI, $\delta^{13}C$, $\delta^{15}N$		Pigment - UVR	Anthropogenic influence begins N. Basin 1890 AD, S. Basin 1860 AD Increased to ~1940s where levels were maintained
Deglacial history of glacial lake Windermere, UK: implications for the central British and Irish Ice Sheet	L. J. W. Pinson, M. E. Vardy, J. K. Dix, T. J. Henstock, J. M. Bull, S. E. Maclachlan	2012	~17600	Seismic reflectance		Seismic reflectance				Identification of seismic facies representing major climate shifts of the past 17.6 k.yr

Contrasting effects of nutrients and climate on algal communities in two lakes in the Windermere catchment since the late 19th century	H. L. Moorhouse, S. Mcgowan, M. D. Jones, P. Barker, P. R. Leavitt, S. A. Brayshaw, E. Y. Haworth	2014	150>	Mackereth cores	^{210}pb, ^{137}Cs ^{241}Am	Dry density	LOI, TC, $\delta^{13}C$, $\delta^{15}N$		Pigment - UVR	Increase in anthropogenic influence from 1970. 1990 > algal community invers to winter precipitation
A 500 Year Sediment Lake Record of Anthropogenic and Natural Inputs to Windermere (English Lake District) Using Double-Spike Lead Isotopes, Radiochronology, and	H. Miller, I. W. Croudace, J. M. Bull, C. J. Cotterill, J. K. Dix,R. N. Taylor	2014	500	Uwitec Piston corer	^{210}pb, ^{137}Cs			WD-XRF, itrax		Heavy metal pollution in recent sediments of Windermere

Sediment Microanalysis										

Appendix B

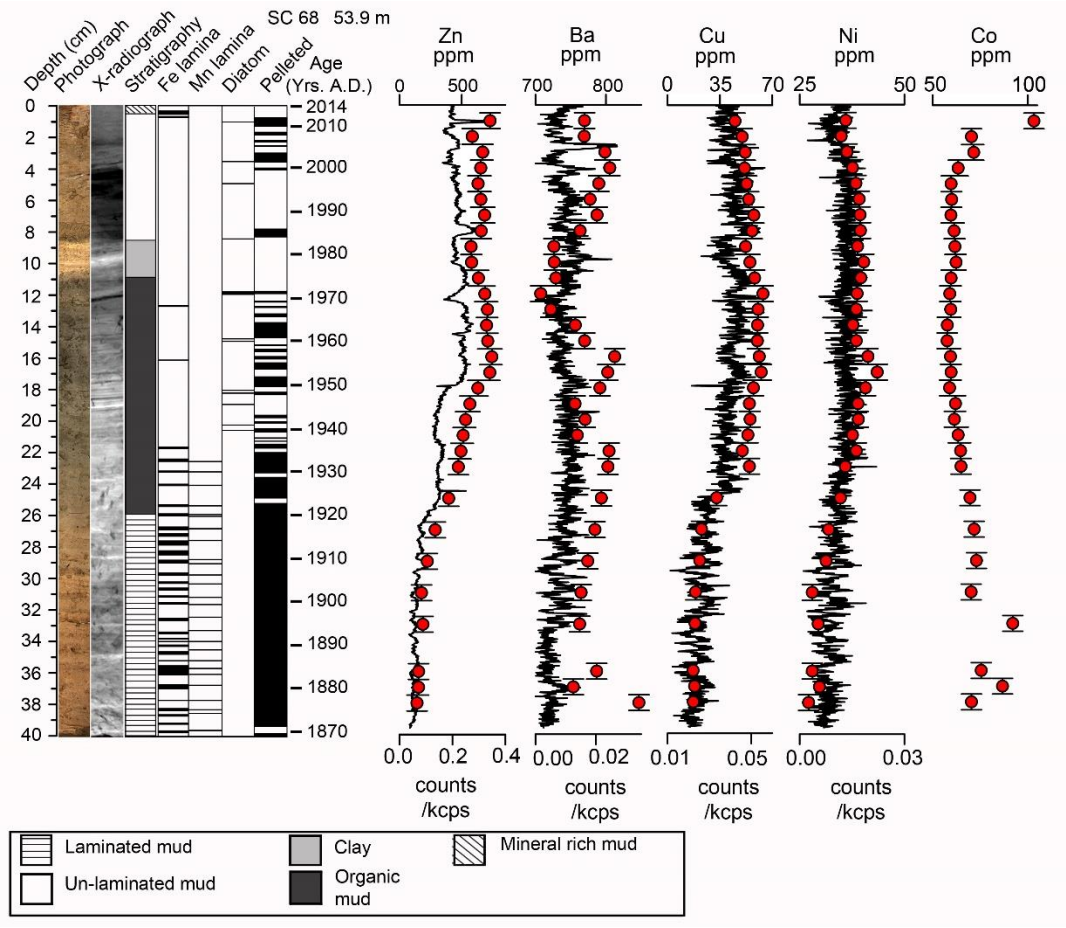

Figure 7-1: Stratigraphy and geochemistry for North Basin Cores SC68. Core depth in cm, core photograph, core x-radiograph, lithostratigraphy, sediment fabric types, ^{210}Pb CF:CS LSR age depth model for the North Basin gravity cores. For geochemistry black lines show itrax ED-XRF Zn, Ba, Cu, Ni and Co (lower scale). Red dots show discrete WD-XRF data for Zn, Ba, Cu, Ni and Co (titles in brackets, upper scales). Vertical errors of the WD-XRF are show the sampling interval. Water depths of each coring site is shown above the corresponding core.

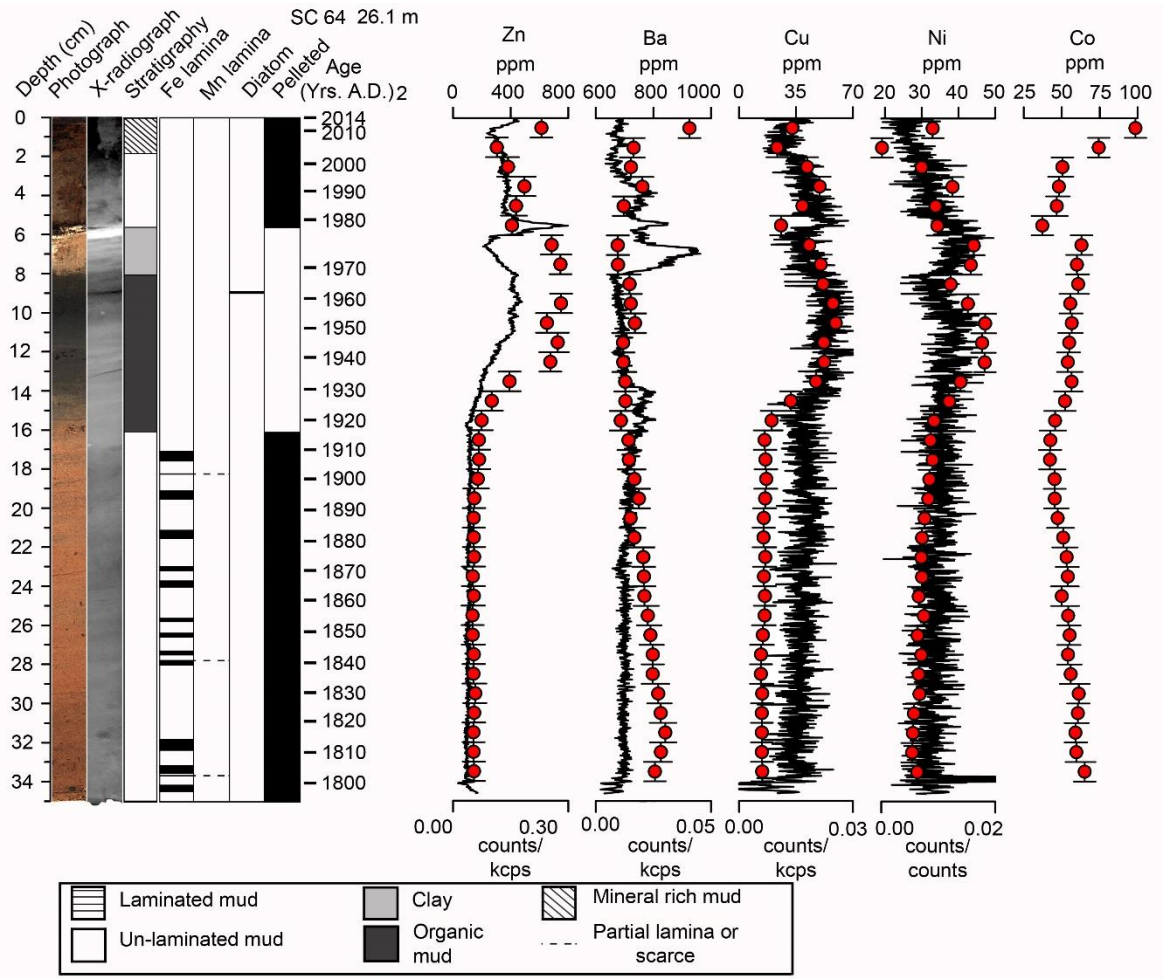

Figure 7-2: Stratigraphy and geochemistry for North Basin Cores SC64. Core depth in cm, core photograph, core x-radiograph, lithostratigraphy, sediment fabric types, ^{210}Pb CF:CS LSR age depth model for the North Basin gravity cores. For geochemistry black lines show itrax ED-XRF Zn, Ba, Cu, Ni and Co (lower scale). Red dots show discrete WD-XRF data for Zn, Ba, Cu, Ni and Co (titles in brackets, upper scales). Vertical errors of the WD-XRF are show the sampling interval. Water depths of each coring site is shown above the corresponding core.

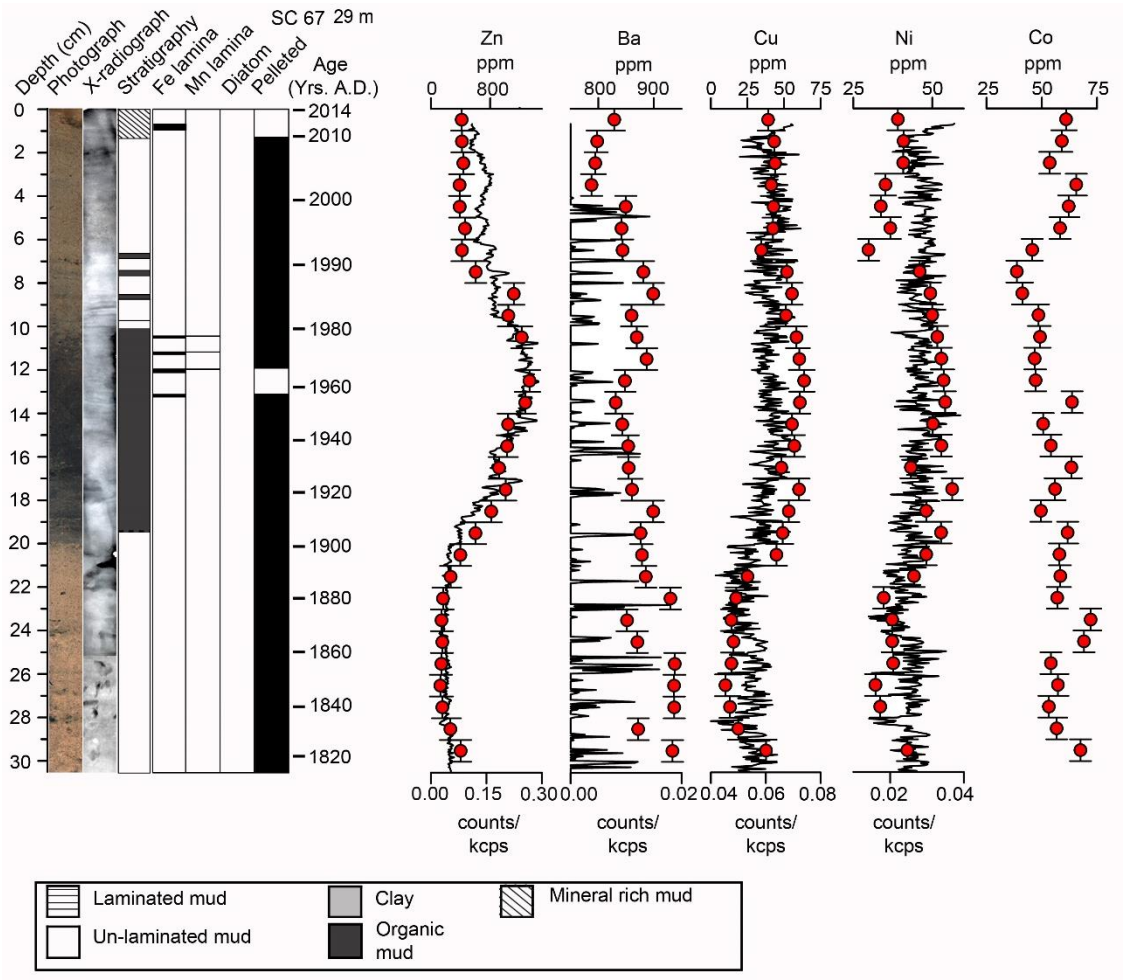

Figure 7-3: Stratigraphy and geochemistry for North Basin Cores SC67. Core depth in cm, core photograph, core x-radiograph, lithostratigraphy, sediment fabric types, ^{210}Pb CF:CS LSR age depth model for the North Basin gravity cores. For geochemistry black lines show itrax ED-XRF Zn, Ba, Cu, Ni and Co (lower scale). Red dots show discrete WD-XRF data for Zn, Ba, Cu, Ni and Co (titles in brackets, upper scales). Vertical errors of the WD-XRF are show the sampling interval. Water depths of each coring site is shown above the corresponding core.

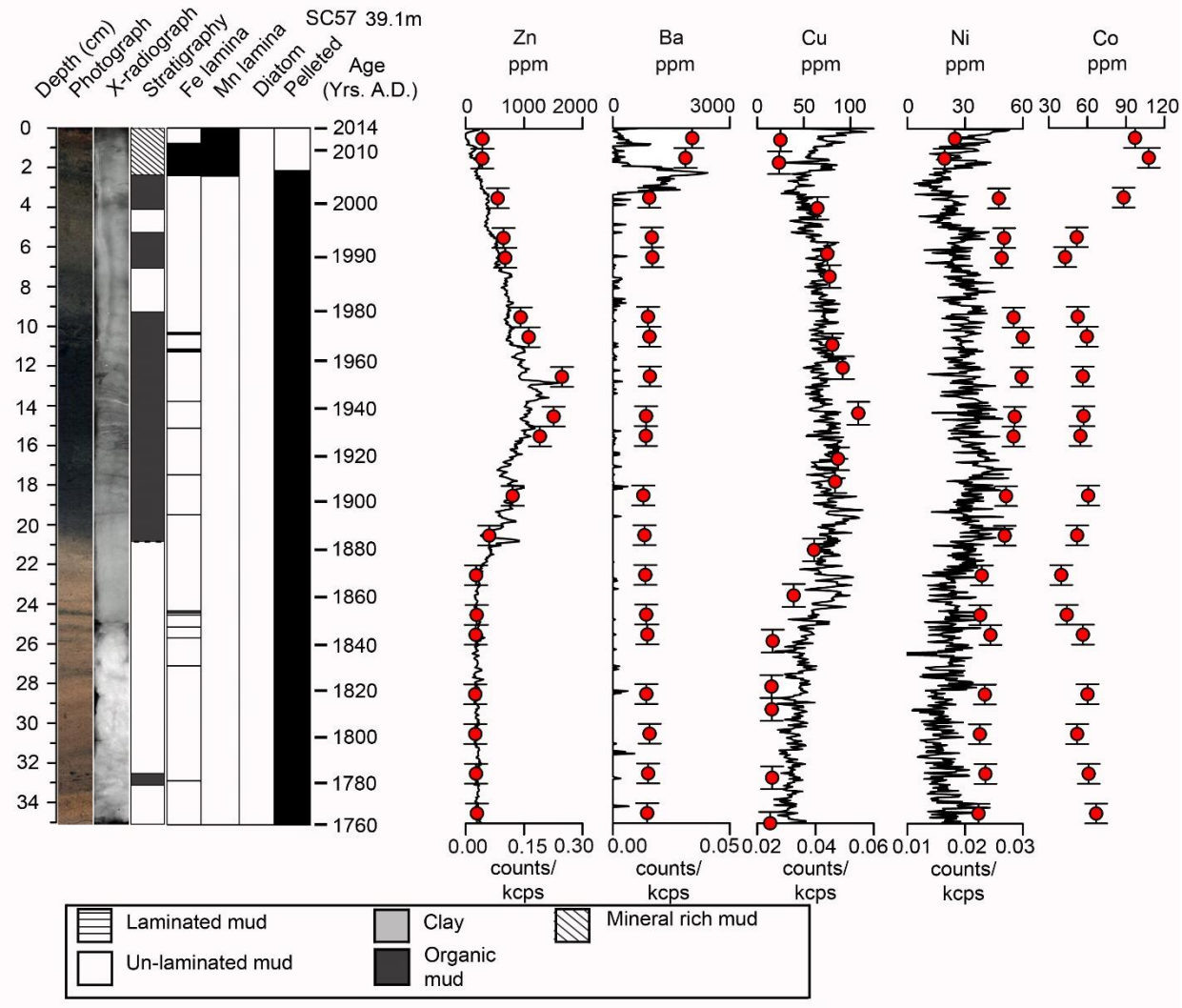

Figure 7-4: Stratigraphy and geochemistry for North Basin Cores SC57. Core depth in cm, core photograph, core x-radiograph, lithostratigraphy, sediment fabric types, ^{210}Pb CF:CS LSR age depth model for the North Basin gravity cores. For geochemistry black lines show itrax ED-XRF Zn, Ba, Cu, Ni and Co (lower scale). Red dots show discrete WD-XRF data for Zn, Ba, Cu, Ni and Co (titles in brackets, upper scales). Vertical errors of the WD-XRF are show the sampling interval. Water depths of each coring site is shown above the corresponding core.

Appendix C

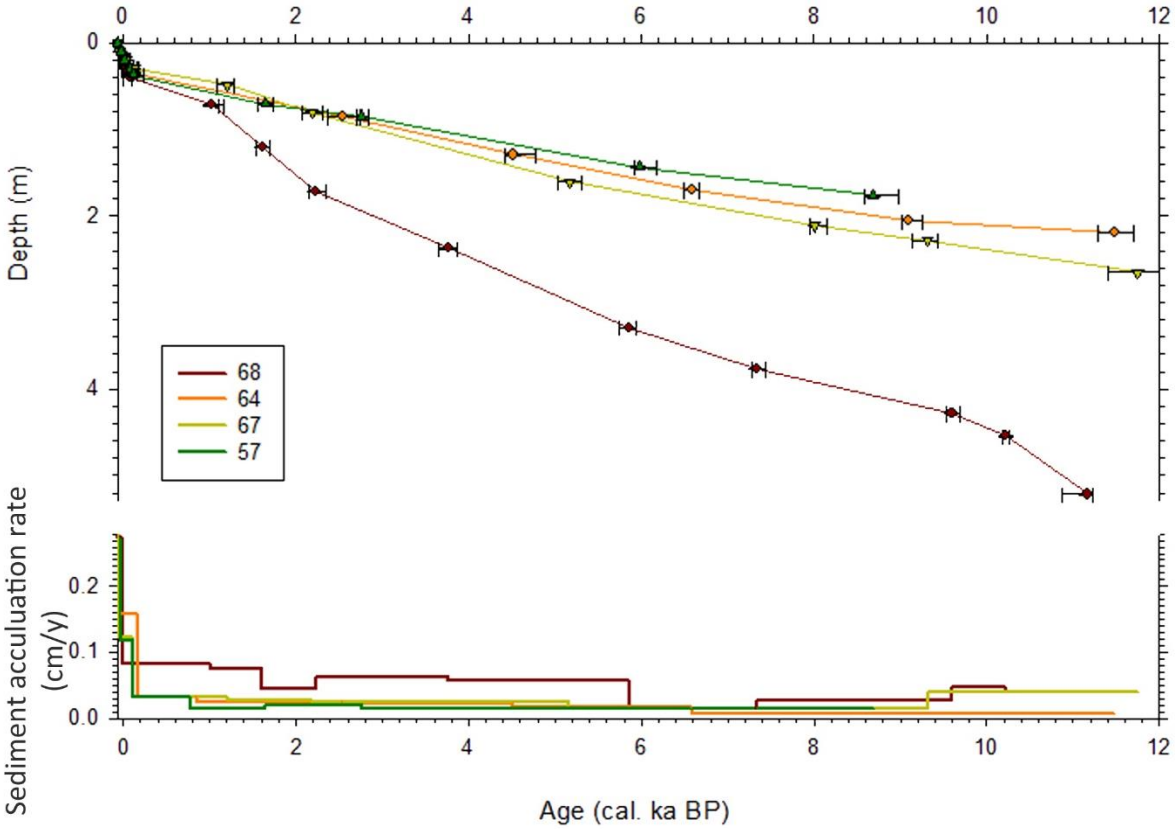

Figure 7-5 Age depth model and sedimentation rates for the four piston cores shown in the legend.

Appendix D

Table 8: Typical Detection Limits in routine XRF analysis using the 4kW Rh end window X-ray tube

Element	X-Ray line	Possible interferences*	** L.L.D. (ppm)
As	As Lb		3
Ba	Ba Lb	Ce, high As	8
Bi	Bi La	W	3
Br	Br Ka		3
Ce	Ce Lb		6
Cl	Cl Ka		50
Cr	Cr Ka	V	4
Cu	Cu Ka	Cu from the tube	2
Ga	Ga Ka		2
I	I Ka		2
La	La Ka		5
Mo	Mo Ka		3
Ni	Ni Ka		2
Nb	Nb Ka	Y	2
P	P Ka		20
Pb	Pb Lb	Bi	2
Rb	Rb Ka	high U	1
S	S Ka		30
Sb	Sb Ka		3
Se	Se Ka		1
Sn	Sn Ka		3

Sr	Sr Ka		2
Th	Th La	High Pb	3
U	U La	High Rb, high Br	3
V	V Ka		3
W	W Lb	High Zn, Ga	8
Y	Y Ka	Rb	1
Zn	Zn Ka		2
Zr	Zr Ka	Sr	2

The detection limits are calculated assuming a count-time of 100 seconds on the background.
*

Note that these interferences are dealt with automatically. **

Reference list

Alley, R.B. 2000. The Younger Dryas cold interval as viewed from central Greenland. *Quaternary Science Reviews*, **19**, 213-226.

Alley, R.B., Mayewski, P.A., Sowers, T., Stuiver, M., Taylor, K.C. & Clark, P.U. 1997. Holocene climatic instability: A prominent, widespread event 8200 yr ago. *Geology*, **25**, 483-486.

Ambrosetti, W. & Barbanti, L. 1999. Deep water warming in lakes: an indicator of climatic change. *Journal of Limnology*, **58**, 1-9.

Appleby, P. 2002. Chronostratigraphic techniques in recent sediments. *Tracking environmental change using lake sediments*, 171-203.

Appleby, P. 2008. Three decades of dating recent sediments by fallout radionuclides: a review. *The Holocene*, **18**, 83-93.

Appleby, P. & Oldfield, F. 1978. The calculation of lead-210 dates assuming a constant rate of supply of unsupported 210Pb to the sediment. *Catena*, **5**, 1-8.

Appleby, P., Richardson, N. & Nolan, P. 1991. ^{241}Am dating of lake sediments. *Hydrobiologia*, **214**, 35-42.

Appleby, P., Richardson, N., Nolan, P. & Oldfield, F. 1990. Radiometric dating of the United Kingdom SWAP sites. *Philosophical Transactions of the Royal Society of London B: Biological Sciences*, **327**, 233-238.

Aston, S., Bruty, D., Chester, R. & Padgham, R. 1973. Mercury in lake sediments: a possible indicator of technological growth. *Nature*, **241**, 450-451.

Avery, R.S., Xuan, C., Kemp, A.E., Bull, J.M., Cotterill, C.J., Fielding, J.J., Pearce, R.B. & Croudace, I.W. 2017. A new Holocene record of geomagnetic secular variation from Windermere, UK. *Earth and Planetary Science Letters*, **477**, 108-122.

Axford, Y., Losee, S., Briner, J.P., Francis, D.R., Langdon, P.G. & Walker, I.R. 2013. Holocene temperature history at the western Greenland Ice Sheet margin reconstructed from lake sediments. *Quaternary Science Reviews*, **59**, 87-100.

Baier, J., Negendank, J.F. & Zolitschka, B. 2004. Mid-to Late Holocene lake ecosystem response to catchment and climatic changes—a detailed varve analysis of Lake Holzmaar (Germany) *The Climate in Historical Times*. Springer, 195-208.

Balistrieri, L.S., Murray, J.W. & Paul, B. 1995. The geochemical cycling of stable Pb, 210 Pb, and 210 Po in seasonally anoxic Lake Sammamish, Washington, USA. *Geochimica et Cosmochimica Acta*, **59**, 4845-4861.

Ballantyne, C.K., Sandeman, G.E., Stone, J.O. & Wilson, P. 2014. Rock-slope failure following Late Pleistocene deglaciation on tectonically stable mountainous terrain. *Quaternary Science Reviews*, **86**, 144-157, http://doi.org/10.1016/j.quascirev.2013.12.021.

Baptie, B., Ottemoller, L., Sargeant, S., Ford, G. & O'Mongain, A. 2005. The Dudley earthquake of 2002: A moderate sized earthquake in the UK. *Tectonophysics*, **401**, 1-22.

Barker, P.A., Wilby, R. & Borrows, J. 2004. A 200-year precipitation index for the central English Lake District. *Hydrological Sciences Journal*, **49**.

Barker, P.A., Pates, J., Payne, R. & Healey, R. 2005. Changing nutrient levels in Grasmere, English Lake District, during recent centuries. *Freshwater Biology*, **50**, 1971-1981.

Baskaran, M., Bianchi, T. & Filley, T. 2016. Inconsistencies between ^{14}C and short-lived radionuclides-based sediment accumulation rates: Effects of long-term remineralization. *Journal of Environmental Radioactivity*.

Battarbee, R.W. & Bennion, H. 2011. Palaeolimnology and its developing role in assessing the history and extent of human impact on lake ecosystems. *Journal of Paleolimnology*, **45**, 399-404.

Belzile, N. & Tessier, A. 1990. Interactions between arsenic and iron oxyhydroxides in lacustrine sediments. *Geochimica et Cosmochimica Acta*, **54**, 103-109.

Bennett, K.D. & Birks, H.J.B. 1990. Postglacial history of alder (Alnus glutinosa (L.) Gaertn.) in the British Isles. *Journal of Quaternary Science*, **5**, 123-133.

Bennion, H. & Battarbee, R. 2007. The European Union water framework directive: opportunities for palaeolimnology. *Journal of Paleolimnology*, **38**, 285-295.

Benoit, G. & Hemond, H.F. 1990. Polonium-210 and lead-210 remobilization from lake sediments in relation to iron and manganese cycling. *Environmental Science & Technology*, **24**, 1224-1234.

Benoit, G. & Hemond, H.F. 1991. Evidence for diffusive redistribution of 210Pb in lake sediments. *Geochimica et Cosmochimica Acta*, **55**, 1963-1975.

Berger, A. & Loutre, M.-F. 1991. Insolation values for the climate of the last 10 million years. *Quaternary Science Reviews*, **10**, 297-317.

Bhaskar, P. & Bhosle, N.B. 2006. Bacterial extracellular polymeric substance (EPS): a carrier of heavy metals in the marine food-chain. *Environment International*, **32**, 191-198.

Birks, H.H. & Birks, H.J.B. 2006. Multi-proxy studies in palaeolimnology. *Vegetation history and Archaeobotany*, **15**, 235-251.

Björck, S., Rundgren, M., Ingolfsson, O. & Funder, S. 1997. The Preboreal oscillation around the Nordic Seas: terrestrial and lacustrine responses. *Journal of Quaternary Science: Published for the Quaternary Research Association*, **12**, 455-465.

Bradley, R.S. 1999. Chapter 9: Pollen analysis. *In*: Bradley, R.S. (ed) *Paleoclimatology, Reconstructing Climates of the Quaternary*. Academic Press, **68**, 357-396.

British Geological Survey 2010. UK historical earthquake database. . http://quakes.bgs.ac.uk/historical/.

Brooks, S.J. & Birks, H. 2000a. Chironomid-inferred Late-glacial air temperatures at Whitrig Bog, Southeast Scotland. *Journal of Quaternary Science*, **15**, 759-764.

Brooks, S.J. & Birks, H. 2000b. Chironomid-inferred late-glacial and early-Holocene mean July air temperatures for Kråkenes Lake, western Norway. *Journal of Paleolimnology*, **23**, 77-89.

Buffle, J., De Vitre, R., Perret, D. & Leppard, G.G. 1989. Physico-chemical characteristics of a colloidal iron phosphate species formed at the oxic-anoxic interface of a eutrophic lake. *Geochimica et Cosmochimica Acta*, **53**, 399-408.

Burke, I.T. & Kemp, A.E. 2004. A mid-Holocene geochemical record of saline inflow to the Gotland Deep, Baltic Sea. *The Holocene*, **14**, 940-948.

Burthe, S.J., Henrys, P.A., Mackay, E.B., Spears, B.M., Campbell, R., Carvalho, L., Dudley, B., Gunn, I.D., *et al.* 2016. Do early warning indicators consistently predict nonlinear change in long-term ecological data? *Journal of Applied Ecology*, **53**, 666-676.

Burton Jr, G.A. 2002. Sediment quality criteria in use around the world. *Limnology*, **3**, 65-76.

Canfield, D.E., Kristensen, E. & Thamdrup, B. 2005. The iron and manganese cycles. *In*: Southward, A.J., Tyler, P.A., Young, C.M. & Fuiman, L.A. (eds) *Aquatic Geomicrobiology*, **48**, 269-312.

Canter, H.M. & Haworth, E.Y. 2010. The occurrence of two new plankton diatom populations in the English Lake District: Aulacoseira islandica. *Freshwater Forum*.

Catalan, J., Pla-Rabés, S., Wolfe, A.P., Smol, J.P., Rühland, K.M., Anderson, N.J., Kopáček, J., Stuchlík, E., *et al.* 2013. Global change revealed by palaeolimnological records from remote lakes: a review. *Journal of Paleolimnology*, **49**, 513-535.

Chaillou, G., Anschutz, P., Dubrulle, C. & Lecroart, P. 2007. Transient states in diagenesis following the deposition of a gravity layer: dynamics of O 2, Mn, Fe and N-species in experimental units. *Aquatic Geochemistry*, **13**, 157-172.

Christophoridis, C. & Fytianos, K. 2006. Conditions affecting the release of phosphorus from surface lake sediments. *Journal of environmental quality*, **35**, 1181-1192.

Ciutat, A., Weber, O., Gérino, M. & Boudou, A. 2006. Stratigraphic effects of tubificids in freshwater sediments: a kinetic study based on X-ray images and grain-size analysis. *Acta Oecologica*, **30**, 228-237.

Claris, P., Quartermaine, J. & Woolley, A. 1989. The Neolithic quarries and axe factory sites of Great Langdale and Scafell Pike: a new field survey. *Proceedings of the Prehistoric Society*. Cambridge University Press, 1-25.

Colley, S., Thomson, J., Wilson, T. & Higgs, N. 1984. Post-depositional migration of elements during diagenesis in brown clay and turbidite sequences in the North East Atlantic. *Geochimica et Cosmochimica Acta*, **48**, 1223-1235.

Comte, S., Guibaud, G. & Baudu, M. 2008. Biosorption properties of extracellular polymeric substances (EPS) towards Cd, Cu and Pb for different pH values. *Journal of hazardous materials*, **151**, 185-193.

Coombes, P.M., Chiverrell, R.C. & Barber, K.E. 2009. A high-resolution pollen and geochemical analysis of late Holocene human impact and vegetation history in southern Cumbria, England. *Journal of Quaternary Science: Published for the Quaternary Research Association*, **24**, 224-236.

Coope, G. & Pennington, W. 1977. *The Windermere interstadial of the late Devensian*.

Correll, D.L. 1998. The role of phosphorus in the eutrophication of receiving waters: a review. *Journal of environmental quality*, **27**, 261-266.

Courtin-Nomade, A., Soubrand-Colin, M., Marcus, M.A. & Fakra, S.C. 2008. Evidence for the incorporation of lead into barite from waste rock pile materials. *Environmental Science & Technology*, **42**, 2867-2872, http://doi.org/10.1021/es702822k.

Couture, R.-M., Gobeil, C. & Tessier, A. 2010. Arsenic, iron and sulfur co-diagenesis in lake sediments. *Geochimica et Cosmochimica Acta*, **74**, 1238-1255.

Cranwell, P. & Koul, V. 1989. Sedimentary record of polycyclic aromatic and aliphatic hydrocarbons in the Windermere catchment. *Water Research*, **23**, 275-283.

Croudace, I. & Williams-Thorpe, O. 1988. A low dilution, wavelength-dispersive X-ray fluorescence procedure for the analysis of archaeological rock artefacts. *Archaeometry*, **30**, 227-236.

Cuven, S., Francus, P. & Lamoureux, S.F. 2010. Estimation of grain size variability with micro X-ray fluorescence in laminated lacustrine sediments, Cape Bounty, Canadian High Arctic. *Journal of Paleolimnology*, **44**, 803-817.

Dafoe, L.T., Rygh, A.L., Yang, B., Gingras, M.K. & Pemberton, S.G. 2011. A new technique for assessing tubificid burrowing activities, and recognition of biogenic grading formed by these oligochaetes. *Palaios*, **26**, 66-80.

Damon, P.E., Donahue, D., Gore, B., Hatheway, A., Jull, A.T., Linick, T., Sercel, P., Toolin, L., *et al.* 1989. Radiocarbon dating of the Shroud of Turin. *Nature*, **337**, 611-615.

Davis, B.A., Brewer, S., Stevenson, A.C. & Guiot, J. 2003. The temperature of Europe during the Holocene reconstructed from pollen data. *Quaternary Science Reviews*, **22**, 1701-1716.

Davis, R.B. 1974. Stratigraphic effects of tubificids in profundal lake sediments. *Limnol. Oceanogr*, **19**, 466-488.

Davison, W. 1993. Iron and Manganese in Lakes. *Earth-Science Reviews*, **34**, 119-163, http://doi.org/Doi 10.1016/0012-8252(93)90029-7.

Davison, W., Lishman, J. & Hilton, J. 1985. Formation of pyrite in freshwater sediments: Implications for C/S ratios. *Geochimica et Cosmochimica Acta*, **49**, 1615-1620.

Davison, W., Hilton, J., Hamilton-Taylor, J., Kelly, M., Livens, F., Rigg, E., Carrick, T. & Singleton, D. 1993. The transport of Chernobyl-derived radiocaesium through two freshwater lakes in Cumbria, UK. *Journal of Environmental Radioactivity*, **19**, 125-153.

Dean, J.M., Kemp, A.E.S., Bull, D., Pike, J., Patterson, G. & Zolitschka, B. 1999. Taking varves to bits: Scanning electron microscopy in the study of laminated sediments and varves. *Journal of Paleolimnology*, **22**, 121-136, http://doi.org/10.1023/a:1008069514445.

Dellwig, O., Leipe, T., März, C., Glockzin, M., Pollehne, F., Schnetger, B., Yakushev, E.V., Böttcher, M.E., *et al.* 2010. A new particulate Mn–Fe–P-shuttle at the redoxcline of anoxic basins. *Geochimica et Cosmochimica Acta*, **74**, 7100-7115.

Dixit, S. & Hering, J.G. 2003. Comparison of arsenic (V) and arsenic (III) sorption onto iron oxide minerals: implications for arsenic mobility. *Environmental Science & Technology*, **37**, 4182-4189.

Dong, X., Bennion, H., Battarbee, R.W. & Sayer, C.D. 2012. A multiproxy palaeolimnological study of climate and nutrient impacts on Esthwaite Water, England over the past 1200 years. *The Holocene*, **22**, 107-118.

Dudgeon, D., Arthington, A.H., Gessner, M.O., Kawabata, Z.-I., Knowler, D.J., Lévêque, C., Naiman, R.J., Prieur-Richard, A.-H., *et al.* 2006. Freshwater biodiversity: importance, threats, status and conservation challenges. *Biological reviews*, **81**, 163-182.

Eastwood, W.J., Leng, M.J., Roberts, N. & Davis, B. 2007. Holocene climate change in the eastern Mediterranean region: a comparison of stable isotope and pollen data from Lake Gölhisar, southwest Turkey. *Journal of Quaternary Science*, **22**, 327-341.

Edenborn, H. & Brickett, L. 2002. Determination of manganese stability in a constructed wetland sediment using redox gel probes. *Geomicrobiology Journal*, **19**, 485-504.

Edmondson, W.T. & Allison, D.E. 1970. Recording Densitometry of X-Radiographs for Study of Cryptic Laminations in Sediment of Lake-Washington. *Limnology and Oceanography*, **15**, 138-+.

Edwards, K.J. & Whittington, G. 2001. Lake sediments, erosion and landscape change during the Holocene in Britain and Ireland. *Catena*, **42**, 143-173.

El Bilali, L., Rasmussen, P., Hall, G. & Fortin, D. 2002. Role of sediment composition in trace metal distribution in lake sediments. *Applied geochemistry*, **17**, 1171-1181.

Elmore, A., Wright, J.D. & Southon, J. 2015. Continued meltwater influence on North Atlantic Deep Water instabilities during the early Holocene. *Marine Geology*, **360**, 17-24.

Fabian, D., Zhou, Z., Wehrli, B. & Friedl, G. 2003. Diagenetic cycling of arsenic in the sediments of eutrophic Baldeggersee, Switzerland. *Applied geochemistry*, **18**, 1497-1506.

Fakhraee, M., Li, J. & Katsev, S. 2017. Significant role of organic sulfur in supporting sedimentary sulfate reduction in low-sulfate environments. *Geochimica et Cosmochimica Acta*, **213**, 502-516.

Famme, P. & Knudsen, J. 1985. Anoxic survival, growth and reproduction by the freshwater annelid, Tubifex sp., demonstrated using a new simple anoxic chemostat. *Comparative Biochemistry and Physiology Part A: Physiology*, **81**, 251-253.

Farmer, J. & Lovell, M. 1986. Natural enrichment of arsenic in Loch Lomond sediments. *Geochimica et Cosmochimica Acta*, **50**, 2059-2067.

Farmer, J.G., Eades, L.J. & Graham, M.C. 1999. The lead content and isotopic composition of British coals and their implications for past and present releases of lead to the UK environment. *Environmental Geochemistry and Health*, **21**, 257-272.

Fernandez-Gonzalez, A., Carneiro, J., Katsikopoulos, D. & Prieto, M. 2013. Thermodynamic properties of the (Ba,Pb)SO4 solid solution under ambient conditions: Implications for the behavior of Pb and Ra in the environment. *Geochimica Et Cosmochimica Acta*, **105**, 31-43, http://doi.org/10.1016/j.gca.2012.11.042.

Feuchtmayr, H., Thackeray, S.J., Jones, I.D., De Ville, M., Fletcher, J., James, B. & Kelly, J. 2012. Spring phytoplankton phenology - are patterns and drivers of change consistent among lakes in the same climatological region? *Freshwater Biology*, **57**, 331-344, http://doi.org/10.1111/j.1365-2427.2011.02671.x.

Finlay, B.J., Hetherington, N.B. & Davison, W. 1983. Active Biological Participation in Lacustrine Barium Chemistry. *Geochimica Et Cosmochimica Acta*, **47**, 1325-1329, http://doi.org/Doi 10.1016/0016-7037(83)90071-6.

Fisher, J., Lick, W., McCall, P. & Robbins, J. 1980. Vertical mixing of lake sediments by tubificid oligochaetes. *Journal of Geophysical Research: Oceans*, **85**, 3997-4006.

Förstner, U. & Wittmann, G.T. 2012. *Metal pollution in the aquatic environment*. Springer Science & Business Media.

Fowler, H., Kilsby, C. & Stunell, J. 2007. Modelling the impacts of projected future climate change on water resources in north-west England. *Hydrology and Earth System Sciences Discussions*, **11**, 1115-1126.

Friedl, G., Wehrli, B. & Manceau, A. 1997. Solid phases in the cycling of manganese in eutrophic lakes: New insights from EXAFS spectroscopy. *Geochimica et Cosmochimica Acta*, **61**, 275-290.

Frouz, J., Lobinske, R.J. & Ali, A. 2004. Influence of Chironomidae (Diptera) faecal pellet accumulation on lake sediment quality and larval abundance of pestiferous midge Glyptotendipes paripes. *Hydrobiologia*, **518**, 169-177.

George, D., Maberly, S. & Hewitt, D. 2004. The influence of the North Atlantic Oscillation on the physical, chemical and biological characteristics of four lakes in the English Lake District. *Freshwater Biology*, **49**, 760-774.

Gibson, C.E., Anderson, N.J. & Haworth, E.Y. 2003. Aulacoseira subarctica: taxonomy, physiology, ecology and palaeoecology. *European Journal of Phycology*, **38**, 83-101.

Gilli, A., Anselmetti, F.S., Ariztegui, D. & McKenzie, J.A. 2003. A 600-year sedimentary record of flood events from two sub-alpine lakes (Schwendiseen, Northeastern Switzerland) *Lake Systems from the Ice Age to Industrial Time*. Springer, 49-58.

Girardclos, S., Schmidt, O.T., Sturm, M., Ariztegui, D., Pugin, A. & Anselmetti, F.S. 2007. The 1996 AD delta collapse and large turbidite in Lake Brienz. *Marine Geology*, **241**, 137-154.

Goldstein, J.I., Newbury, D.E., Echlin, P., Joy, D.C., Lyman, C.E., Lifshin, E., Sawyer, L. & Michael, J.R. 2003. Quantitative X-ray analysis: the basics *Scanning Electron Microscopy and X-ray Microanalysis*. Springer, 391-451.

Goslar, T., Kuc, T., Ralska-Jasiewiczowa, M., Rózánski, K., Arnold, M., Bard, E., van Geel, B., Pazdur, M., *et al.* 1993. High-resolution lacustrine record of the Late Glacial/Holocene transition in Central Europe. *Quaternary Science Reviews*, **12**, 287-294.

Gracia, E., Lamarche, G., Nelson, H. & Pantosti, D. 2013. Preface: Marine and Lake Paleoseismology. *Natural Hazards and Earth System Sciences*, **13**, 3469-3478, http://doi.org/10.5194/nhess-13-3469-2013.

Grove, J.M. 2001. The initiation of the "Little Ice Age" in regions round the North Atlantic *The Iceberg in the Mist: Northern Research in pursuit of a "Little Ice Age"*. Springer, 53-82.

Hage, S., Hubert-Ferrari, A., Lamair, L., Avşar, U., El Ouahabi, M., Van Daele, M., Boulvain, F., Ali Bahri, M., *et al.* 2017. Flow dynamics at the origin of thin clayey sand lacustrine turbidites: Examples from Lake Hazar, Turkey. *Sedimentology*.

Hamilto-Taylor, J. & Willis, M. 1990. A quantitative assessment of the sources and general dynamics of trace metals in a soft-water lake. *Limnology and oceanography*, **35**, 840-851.

Hamilton-Taylor, J. 1979. Enrichments of zinc, lead, and copper in recent sediments of Windermere, England. *Environmental Science & Technology*, **13**, 693-697.

Hamilton-Taylor, J. & Davison, W. 1995. Redox-driven cycling of trace elements in lakes *Physics and chemistry of lakes*. Springer, 217-263.

Hamilton-Taylor, J., Willis, M. & Reynolds, C. 1984. Depositional fluxes of metals and phytoplankton in Windermere as measured by sediment traps. *Limnology and oceanography*, **29**, 695-710.

Hammer, Ø., Harper, D. & Ryan, P. 2001. Paleontological statistics software: Package for education and data analysis. *Palaeontologia Electronica*.

Harvey, D., Thompson, N., Charles, S. & Hubbard, C. 2012. *Farming and Farm Forestry in the Lake District: A report for the Lake District National Park Partnership Farming and Forestry Task Force.* Centre for Rural Economy, Newcastle University.

Hodell, D.A. & Schelske, C.L. 1998. Production, sedimentation, and isotopic composition of organic matter in Lake Ontario. *Limnology and oceanography*, **43**, 200-214.

Holmes, P.W. 1964. *Sedimentary studies in Lake Windermere.* University of London.

Holmes, P.W. 1968. Sedimentary studies of late quaternary material in Windermere Lake (Great Britain). *Sedimentary Geology*, **2**, 201-224.

Horiuchi, K., Minoura, K., Hoshino, K., Oda, T., Nakamura, T. & Kawai, T. 2000. Palaeoenvironmental history of Lake Baikal during the last 23000 years. *Palaeogeography, Palaeoclimatology, Palaeoecology*, **157**, 95-108.

Ince, J. 1996. Late-glacial and early Holocene vegetation of Snowdonia. *New Phytologist*, **132**, 343-353.

IPCC 2014. *Climate Change 2014–Impacts, Adaptation and Vulnerability: Regional Aspects*. Cambridge University Press.

Itai, T., Hayase, D., Hyobu, Y., Hirata, S.H., Kumagai, M. & Tanabe, S. 2012. Hypoxia-induced exposure of isaza fish to manganese and arsenic at the bottom of Lake Biwa, Japan: experimental and geochemical verification. *Environmental Science & Technology*, **46**, 5789-5797.

Jansen, E., Andersson, C., Moros, M., Nisancioglu, K.H., Nyland, B.F. & Telford, R.J. 2008. The Early to Mid-Holocene Thermal Optimum in the North Atlantic. *Natural Climate Variability and Global Warming: A Holocene Perspective*, 123-137.

Jarvis, I. & Higgs, N. 1987. Trace-element mobility during early diagenesis in distal turbidites: late Quaternary of the Madeira Abyssal Plain, N Atlantic. *Geological Society, London, Special Publications*, **31**, 179-214.

Jenkin, P.M. 1942. Seasonal changes in the temperature of Windermere (English Lake District). *The Journal of Animal Ecology*, 248-269.

Jensen, H.S., Kristensen, P., Jeppesen, E. & Skytthe, A. 1992. Iron: phosphorus ratio in surface sediment as an indicator of phosphate release from aerobic sediments in shallow lakes. *Hydrobiologia*, **235**, 731-743.

Joannin, S., Magny, M., Peyron, O., Vannière, B. & Galop, D. 2014. Climate and land-use change during the late Holocene at Lake Ledro (southern Alps, Italy). *The Holocene*, **24**, 591-602.

Johnsen, S.J., Dahl-Jensen, D., Gundestrup, N., Steffensen, J.P., Clausen, H.B., Miller, H., Masson-Delmotte, V., Sveinbjörnsdottir, A.E., *et al.* 2001. Oxygen isotope and palaeotemperature records from six Greenland ice-core stations: Camp Century, Dye-3, GRIP, GISP2, Renland and NorthGRIP. *Journal of Quaternary Science*, **16**, 299-307.

Johnson, T.C. 1984. Sedimentation in large lakes. *Annual Review of Earth and Planetary Sciences*, **12**, 179-204.

Jones, I.D., Winfield, I.J. & Carse, F. 2008. Assessment of long-term changes in habitat availability for Arctic charr (Salvelinus alpinus) in a temperate lake using oxygen profiles and hydroacoustic surveys. *Freshwater Biology*, **53**, 393-402.

Jones, P., Jonsson, T. & Wheeler, D. 1997. Extension to the North Atlantic Oscillation using early instrumental pressure observations from Gibraltar and South-West Iceland. *International Journal of climatology*, **17**, 1433-1450.

Jones, V., Hodgson, D. & Chepstow-Lusty, A. 2000. Palaeolimnological evidence for marked Holocene environmental changes on Signy Island, Antarctica. *The Holocene*, **10**, 43-60.

Juckes, M.N., Allen, M.R., Briffa, K.R., Esper, J., Hegerl, G.C., Moberg, A., Osborn, T.J. & Weber, S. 2007. Millennial temperature reconstruction intercomparison and evaluation. *Climate of the Past*, **3**, 591-609.

Kelly, C.A. & Chynoweth, D.P. 1981. The contributions of temperature and of the input of organic matter in controlling rates of sediment methanogenesis. *Limnology and oceanography*, **26**, 891-897.

Kelly, T.J., Hardiman, M., Lovelady, M., Lowe, J.J., Matthews, I.P. & Blockley, S.P. 2017. Scottish early Holocene vegetation dynamics based on pollen and tephra records from Inverlair and Loch Etteridge, Inverness-shire. *Proceedings of the Geologists' Association*, **128**, 125-135.

Kemp, A.E., Pearce, R.B., Pike, J. & Marshall, J.E. 1998. Microfabric and microcompositional studies of Pliocene and Quaternary sapropels from the eastern Mediterranean. *Proceedings of the Ocean Drilling Program Scientific Results*. Ocean Drilling Program, 349-364.

Kemp, A.E.S., Dean, J., Pearce, R.B. & Pike, J. 2001. Recognition and analysis of bedding and sediment fabric features. *In*: Last, W.M. & Smol, J.P. (eds) *Tracking Environmental Change Using Lake Sediments. Volume 2: Physical and Geochemical Methods*. Kluwer Academic Publishers, Dordrecht, 7-22.

King, G. 1980. A fault plane solution for the Carlisle earthquake, 26 December 1979. *Nature*, **286**, 142-143.

Klaminder, J., Appleby, P., Crook, P. & Renberg, I. 2012. Post-deposition diffusion of ^{137}Cs in lake sediment: Implications for radiocaesium dating. *Sedimentology*, **59**, 2259-2267.

Kremer, K., Simpson, G. & Girardclos, S. 2012. Giant Lake Geneva tsunami in ad 563. *Nature Geoscience*, **5**, 756-757.

Krinsley, D.H., Pye, K., Boggs Jr, S. & Tovey, N.K. 2005. *Backscattered scanning electron microscopy and image analysis of sediments and sedimentary rocks*. Cambridge University Press.

Lang, B., Bedford, A., Brooks, S.J., Jones, R.T., Richardson, N., Birks, H.J.B. & Marshall, J.D. 2010. Early-Holocene temperature variability inferred from chironomid assemblages at Hawes Water, northwest England. *The Holocene*, **20**, 943-954.

Langdon, P., Barber, K. & Lomas-Clarke, S. 2004. Reconstructing climate and environmental change in northern England through chironomid and pollen analyses: evidence from Talkin Tarn, Cumbria. *Journal of Paleolimnology*, **32**, 197-213.

Langdon, P.G., Holmes, N. & Caseldine, C.J. 2008. Environmental controls on modern chironomid faunas from NW Iceland and implications for reconstructing climate change. *Journal of Paleolimnology*, **40**, 273-293.

Legendre, P. & Legendre, L. 1998. Numerical ecology: second English edition. *Developments in environmental modelling*, **20**.

Lehmann, M.F., Bernasconi, S.M., Barbieri, A. & McKenzie, J.A. 2002. Preservation of organic matter and alteration of its carbon and nitrogen isotope composition during simulated and in situ early sedimentary diagenesis. *Geochimica et Cosmochimica Acta*, **66**, 3573-3584.

Lotter, A.F., Birks, H.J.B., Hofmann, W. & Marchetto, A. 1998. Modern diatom, cladocera, chironomid, and chrysophyte cyst assemblages as quantitative indicators for the reconstruction of past environmental conditions in the Alps. II. Nutrients. *Journal of Paleolimnology*, **19**, 443-463.

Lowag, J., Bull, J., Vardy, M., Miller, H. & Pinson, L. 2012. High-resolution seismic imaging of a Younger Dryas and Holocene mass movement complex in glacial lake Windermere, UK. *Geomorphology*, **171**, 42-57.

Lowe, J.J. & Walker, M.J. 2014. *Reconstructing quaternary environments*. Routledge.

Maberly, S. 2008. The response of Windermere to external stress factors: phosphorus load from wastewater treatment works.

Maberly, S. & Elliott, J. 2012. Insights from long-term studies in the Windermere catchment: external stressors, internal interactions and the structure and function of lake ecosystems. *Freshwater Biology*, **57**, 233-243.

Maberly, S., Hurley, M.A., Butterwick, C., Corry, J., Heaney, S., Irish, A., Jaworski, G., Lund, J., *et al*. 1994. The rise and fall of Asterionella formosa in the South Basin of Windermere: analysis of a 45-year series of data. *Freshwater Biology*, **31**, 19-34.

Maberly, S., De Ville, M., Thackeray, S., Feuchtmayr, H., Fletcher, J., James, J., Kelly, J., Vincent, C., *et al*. 2011. A survey of the lakes of the English Lake District: The Lakes Tour 2010.

Macklin, M.G. & Lewin, J. 2003. River sediments, great floods and centennial-scale holocene climate change. *Journal of Quaternary Science*, **18**, 101-105.

Magny, M., Bégeot, C., Guiot, J. & Peyron, O. 2003. Contrasting patterns of hydrological changes in Europe in response to Holocene climate cooling phases. *Quaternary Science Reviews*, **22**, 1589-1596.

Maltby, E., Ormerod, S., Acreman, M., Dunbar, M., Jenkins, A., Maberly, S., Newman, J., Blackwell, M., *et al.* 2011. Freshwaters: openwaters, wetlands and floodplains [chapter 9].

Mann, M.E., Zhang, Z., Rutherford, S., Bradley, R.S., Hughes, M.K., Shindell, D., Ammann, C., Faluvegi, G., *et al.* 2009. Global signatures and dynamical origins of the Little Ice Age and Medieval Climate Anomaly. *Science*, **326**, 1256-1260.

Marcott, S.A., Shakun, J.D., Clark, P.U. & Mix, A.C. 2013. A reconstruction of regional and global temperature for the past 11,300 years. *Science*, **339**, 1198-1201.

Mayewski, P.A., Rohling, E.E., Stager, J.C., Karlén, W., Maasch, K.A., Meeker, L.D., Meyerson, E.A., Gasse, F., *et al.* 2004. Holocene climate variability. *Quaternary Research*, **62**, 243-255.

McCall, P.L. & Tevesz, M.J. 1982. The effects of benthos on physical properties of freshwater sediments *Animal-Sediment Relations*. Springer, 105-176.

McCarroll, D., Loader, N.J., Jalkanen, R., Gagen, M.H., Grudd, H., Gunnarson, B.E., Kirchhefer, A.J., Friedrich, M., *et al.* 2013. A 1200-year multiproxy record of tree growth and summer temperature at the northern pine forest limit of Europe. *The Holocene*, **23**, 471-484.

McColl, S.T. 2012. Paraglacial rock-slope stability. *Geomorphology*, **153**, 1-16, http://doi.org/10.1016/j.geomorph.2012.02.015.

McDougall, S., Hilton, J. & Jenkins, A. 1991. A dynamic model of caesium transport in lakes and their catchments. *Water Research*, **25**, 437-445.

McGowan, S., Barker, P., Haworth, E.Y., Leavitt, P.R., Maberly, S.C. & Pates, J. 2012. Humans and climate as drivers of algal community change in Windermere since 1850. *Freshwater Biology*, **57**, 260-277.

Meyer-Jacob, C., Bindler, R., Bigler, C., Leng, M.J., Lowick, S.E. & Vogel, H. 2017. Regional Holocene climate and landscape changes recorded in the large subarctic lake Torneträsk, N Fennoscandia. *Palaeogeography, Palaeoclimatology, Palaeoecology*, **487**, 1-14.

Meyers, P.A. 1994. Preservation of elemental and isotopic source identification of sedimentary organic matter. *Chemical Geology*, **114**, 289-302.

Meyers, P.A. & Lallier-Vergès, E. 1999. Lacustrine sedimentary organic matter records of Late Quaternary paleoclimates. *Journal of Paleolimnology*, **21**, 345-372.

Meyers, P.A. & Teranes, J.L. 2002. Sediment organic matter. *Tracking environmental change using lake sediments*, 239-269.

Miller, H. 2014. *Lake bed environments, modern sedimentation and the glacial and post-glacial history of Windermere, UK.* PhD, University of Southampton.

Miller, H., Cotterill, C.J. & Bradwell, T. 2014a. Glacial and paraglacial history of the Troutbeck Valley, Cumbria, UK: integrating airborne LiDAR, multibeam bathymetry, and geological field mapping. *Proceedings of the Geologists' Association*, **125**, 31-40.

Miller, H., Croudace, I.W., Bull, J.M., Cotterill, C.J., Dix, J.K. & Taylor, R.N. 2014b. A 500 year sediment lake record of anthropogenic and natural inputs to Windermere (English Lake District) using double-spike lead isotopes, radiochronology, and sediment microanalysis. *Environmental Science & Technology*, **48**, 7254-7263.

Miller, H., Bull, J.M., Cotterill, C.J., Dix, J.K., Winfield, I.J., Kemp, A.E. & Pearce, R.B. 2013. Lake bed geomorphology and sedimentary processes in glacial lake Windermere, UK. *Journal of Maps*, **9**, 299-312.

Mills, P.C. 1983. Genesis and diagnostic value of soft-sediment deformation structures—a review. *Sedimentary Geology*, **35**, 83-104.

Moorhouse, H.L., McGowan, S., Jones, M.D., Barker, P., Leavitt, P.R., Brayshaw, S.A. & Haworth, E.Y. 2014. Contrasting effects of nutrients and climate on algal communities in two lakes in the Windermere catchment since the late 19th century. *Freshwater Biology*, **59**, 2605-2620.

Morner, N.A. 2005. An interpretation and catalogue of paleoseismicity in Sweden. *Tectonophysics*, **408**, 265-307, http://doi.org/10.1016/j.tecto.2005.05.039.

Mortimer, C. & Worthington, E. 1938. Bathymetric surveys and lake deposits.

Mortimer, C.H. 1942. The exchange of dissolved substances between mud and water in lakes. *The Journal of Ecology*, 147-201.

Müller, A. 2001. Geochemical expressions of anoxic conditions in Nordåsvannet, a land-locked fjord in western Norway. *Applied geochemistry*, **16**, 363-374.

Musson, R. 1998. The Barrow-in-Furness earthquake of 15 February 1865: liquefaction from a very small magnitude event. *pure and applied geophysics*, **152**, 733-745.

Musson, R. & Henni, P. 2002. The felt effects of the Carlisle earthquake of 26 December 1979. *Scottish Journal of Geology*, **38**, 113-125.

Musson, R. & Sargeant, S. 2007. Eurocode 8 seismic hazard zoning maps for the UK. *Nottingham, UK, British Geological Survey*, **CR/07/125N**, 62.

Naeher, S., Gilli, A., North, R.P., Hamann, Y. & Schubert, C.J. 2013. Tracing bottom water oxygenation with sedimentary Mn/Fe ratios in Lake Zurich, Switzerland. *Chemical Geology*, **352**, 125-133, http://doi.org/10.1016/j.chemgeo.2013.06.006.

Nisbet, E.G. & Piper, D.J. 1998. Giant submarine landslides. *Nature*, **392**, 329-330.

Nogaro, G., Mermillod-Blondin, F., Montuelle, B., Boisson, J.-C. & Gibert, J. 2008. Chironomid larvae stimulate biogeochemical and microbial processes in a riverbed covered with fine sediment. *Aquatic Sciences-Research Across Boundaries*, **70**, 156-168.

Och, L.M., Müller, B., Voegelin, A., Ulrich, A., Göttlicher, J., Steiniger, R., Mangold, S., Vologina, E.G., *et al.* 2012. New insights into the formation and burial of Fe/Mn accumulations in Lake Baikal sediments. *Chemical Geology*, **330**, 244-259.

Ochsenbein, U., Davison, W., Hilton, J. & Haworth, E. 1983. The Geochemical Record of Major Cations and Trace Metals in a Productive Lake; Analysis of Thinly Sliced Sediment Samples Characterised by Diatom Stratigraphy. *Archiv fur Hydrobiologie*, **98**.

Oldfield, F., Richardson, N., Appleby, P. & Yu, L. 1993. 241Am and 137Cs activity in fine grained saltmarsh sediments from parts of the NE Irish Sea shoreline. *Journal of Environmental Radioactivity*, **19**, 1-24.

Overpeck, J.T., Otto-Bliesner, B.L., Miller, G.H., Muhs, D.R., Alley, R.B. & Kiehl, J.T. 2006. Paleoclimatic evidence for future ice-sheet instability and rapid sea-level rise. *Science*, **311**, 1747-1750.

Parker, A.G., Goudie, A.S., Anderson, D.E., Robinson, M.A. & Bonsall, C. 2002. A review of the mid-Holocene elm decline in the British Isles. *Progress in Physical Geography*, **26**, 1-45.

Parker, J.E. & Maberly, S.C. 2000. Biological response to lake remediation by phosphate stripping: control of Cladophora. *Freshwater Biology*, **44**, 303-309.

Pearsall, W.H. & Pennington, W. 1973. The Lake District: a landscape history. *London: Collins 320p.-Illus., maps.. Geog*, **1**.

Pennington, W. 1943. Lake sediments: the bottom deposits of the north basin of Windermere, with special reference to the diatom succession. *New Phytologist*, **42**, 1-27.

Pennington, W. 1947. Studies of the post-glacial history of British vegetation. VII. Lake sediments: Pollen diagrams from the bottom deposits of the North Basin of Windermere. *Philosophical Transactions of the Royal Society of London B: Biological Sciences*, **233**, 137-175.

Pennington, W. 1973. The recent sediments of Windermere. *Freshwater Biology*, **3**, 363-382.

Pennington, W., Cambray, R., Eakins, J. & Harkness, D. 1976. Radionuclide dating of the recent sediments of Blelham Tarn. *Freshwater Biology*, **6**, 317-331.

Pickering, A.D. & Sutcliffe, D. 2001. *Windermere: restoring the health of England's largest lake*. Freshwater Biological Association.

Pierce, M.L. & Moore, C.B. 1982. Adsorption of arsenite and arsenate on amorphous iron hydroxide. *Water Research*, **16**, 1247-1253.

Pinson, L.J., Vardy, M.E., Dix, J.K., Henstock, T.J., Bull, J.M. & Maclachlan, S.E. 2013. Deglacial history of glacial lake Windermere, UK: implications for the central British and Irish Ice Sheet. *Journal of Quaternary Science*, **28**, 83-94.

Piovano, E.L., Córdoba, F.E. & Stutz, S. 2014. Limnogeology in Southern South America: an overview. *Latin American journal of sedimentology and basin analysis*, **21**, 65-75.

Plaza-Morlote, M., Rey, D., Santos, J., Ribeiro, S., Heslop, D., Bernabeu, A., Mohamed, K., Rubio, B., *et al.* 2017. Southernmost evidence of large European Ice Sheet-derived freshwater discharges during the Heinrich Stadials of the Last Glacial Period (Galician Interior Basin, Northwest Iberian Continental Margin). *Earth and Planetary Science Letters*, **457**, 213-226.

Prentice, I.C. 1985. Pollen representation, source area, and basin size: toward a unified theory of pollen analysis. *Quaternary Research*, **23**, 76-86.

Pretty, J.N., Mason, C.F., Nedwell, D.B., Hine, R.E., Leaf, S. & Dils, R. 2003. Environmental costs of freshwater eutrophication in England and Wales. ACS Publications.

Putyrskaya, V., Klemt, E., Röllin, S., Astner, M. & Sahli, H. 2015. Dating of sediments from four Swiss prealpine lakes with 210 Pb determined by gamma-spectrometry: progress and problems. *Journal of Environmental Radioactivity*, **145**, 78-94.

Rasmussen, S.O., Vinther, B.M., Clausen, H.B. & Andersen, K.K. 2007. Early Holocene climate oscillations recorded in three Greenland ice cores. *Quaternary Science Reviews*, **26**, 1907-1914.

Rautio, M., Mariash, H. & Forsström, L. 2011. Seasonal shifts between autochthonous and allochthonous carbon contributions to zooplankton diets in a subarctic lake. *Limnology and oceanography*, **56**, 1513-1524.

Reimer, P.J., Bard, E., Bayliss, A., Beck, J.W., Blackwell, P.G., Ramsey, C.B., Buck, C.E., Cheng, H., *et al.* 2013. IntCal13 and Marine13 radiocarbon age calibration curves 0–50,000 years cal BP. *Radiocarbon*, **55**, 1869-1887.

Renssen, H., Seppä, H., Heiri, O., Roche, D., Goosse, H. & Fichefet, T. 2009. The spatial and temporal complexity of the Holocene thermal maximum. *Nature Geoscience*, **2**, 411-414.

Reynolds, G. & Hamilton-Taylor, J. 1992. The role of planktonic algae in the cycling of Zn and Cu in a productive soft-water lake. *Limnology and oceanography*, **37**, 1759-1769.

Reynoldson, T.B. 1987. The role of environmental factors in the ecology of tubificid oligochaetes-an experimental study. *Ecography*, **10**, 241-248.

Richardson, K. & Jørgensen, B.B. 1996. Eutrophication: definition, history and effects. *Eutrophication in coastal marine ecosystems*, 1-19.

Rippey, B. & Douglas, R.W. 2004. Reconstructing regional-scale lead contamination of the atmosphere (1850–1980) in the United Kingdom and Ireland using lake sediments. *Global biogeochemical cycles*, **18**.

Ritchie, J.C. & McHenry, J.R. 1990. Application of radioactive fallout cesium-137 for measuring soil erosion and sediment accumulation rates and patterns: a review. *Journal of environmental quality*, **19**, 215-233.

Rohling, E.J. & Pälike, H. 2005. Centennial-scale climate cooling with a sudden cold event around 8,200 years ago. *Nature*, **434**, 975-979.

Roland, T.P., Caseldine, C., Charman, D., Turney, C. & Amesbury, M. 2014. Was there a '4.2 ka event'in Great Britain and Ireland? Evidence from the peatland record. *Quaternary Science Reviews*, **83**, 11-27.

Rowland, C.S. 2015. *Land Cover Map 2015.* Centre for Ecology & Hydrology.

Sabater, S. & Haworth, E.Y. 1995. An assessment of recent trophic changes in Windermere South Basin (England) based on diatom remains and fossil pigments. *Journal of Paleolimnology*, **14**, 151-163.

Schaller, T. & Wehrli, B. 1996. Geochemical-focusing of manganese in lake sediments—an indicator of deep-water oxygen conditions. *Aquatic Geochemistry*, **2**, 359-378.

Schelske, C.L. & Hodell, D.A. 1995. Using carbon isotopes of bulk sedimentary organic matter to reconstruct the history of nutrient loading and eutrophication in Lake Erie. *Limnology and oceanography*, **40**, 918-929.

Schimmelmann, A., Lange, C.B., Schieber, J., Francus, P., Ojala, A.E. & Zolitschka, B. 2016. Varves in marine sediments: A review. *Earth-Science Reviews*, **159**, 215-246.

Schlolaut, G., Brauer, A., Marshall, M.H., Nakagawa, T., Staff, R.A., Ramsey, C.B., Lamb, H.F., Bryant, C.L., *et al.* 2014. Event layers in the Japanese Lake Suigetsu 'SG06'sediment core: Description, interpretation and climatic implications. *Quaternary Science Reviews*, **83**, 157-170.

Schnellmann, M., Anselmetti, F.S., Giardini, D. & Mckenzie, J.A. 2005. Mass movement-induced fold-and-thrust belt structures in unconsolidated sediments in Lake Lucerne (Switzerland). *Sedimentology*, **52**, 271-289.

Schweitzer, B., Huber, I., Amann, R., Ludwig, W. & Simon, M. 2001. α-and β-Proteobacteria control the consumption and release of amino acids on lake snow aggregates. *Applied and Environmental microbiology*, **67**, 632-645.

Simpson, J.H., Lucas, N.S., Powell, B. & Maberly, S.C. 2015. Dissipation and mixing during the onset of stratification in a temperate lake, Windermere. *Limnology and oceanography*, **60**, 29-41.

Sirocko, F., Dietrich, S., Veres, D., Grootes, P.M., Schaber-Mohr, K., Seelos, K., Nadeau, M.-J., Kromer, B., *et al.* 2013. Multi-proxy dating of Holocene maar lakes and Pleistocene dry maar sediments in the Eifel, Germany. *Quaternary Science Reviews*, **62**, 56-76.

Smith, A.J. 1959. Structures in the stratified late-glacial clays of Windermere, England. *Journal of Sedimentary Research*, **29**.

Smith, E., Hamilton-Taylor, J., Davison, W., Fullwood, N.J. & McGrath, M. 2004. The effect of humic substances on barite precipitation-dissolution behaviour in natural and synthetic lake waters. *Chemical Geology*, **207**, 81-89, http://doi.org/10.1016/j.chemgeo.2004.02.005.

Smol, J.P. 2010. The power of the past: using sediments to track the effects of multiple stressors on lake ecosystems. *Freshwater Biology*, **55**, 43-59.

Solanki, S.K., Usoskin, I.G., Kromer, B., Schüssler, M. & Beer, J. 2004. Unusual activity of the Sun during recent decades compared to the previous 11,000 years. *Nature*, **431**, 1084-1087.

Søndergaard, M., Jensen, J.P. & Jeppesen, E. 2003. Role of sediment and internal loading of phosphorus in shallow lakes. *Hydrobiologia*, **506**, 135-145.

Stow, D.A. 1984. Anatomy of debris-flow deposits. *Hay, WW, and Sibuet, JC, et al.(1984). Initial Reports, Deep Sea Drilling Project: Washington, DC, US Government Printing Office*, **75**, 801-807.

Strasser, M., Monecke, K., Schnellmann, M. & Anselmetti, F.S. 2013. Lake sediments as natural seismographs: A compiled record of Late Quaternary earthquakes in Central Switzerland and its implication for Alpine deformation. *Sedimentology*, **60**, 319-341, http://doi.org/10.1111/sed.12003.

Stucchi, M., Rovida, A., Capera, A.G., Alexandre, P., Camelbeeck, T., Demircioglu, M., Gasperini, P., Kouskouna, V., *et al.* 2013. The SHARE European earthquake catalogue (SHEEC) 1000–1899. *Journal of Seismology*, **17**, 523-544.

Stuiver, M. & Reimer, P.J. 1993. Extended 14C data base and revised CALIB 3.0 14C age calibration program. *Radiocarbon*, **35**, 215-230.

Sturm, M. & Matter, A. 1978. *Turbidites and varves in Lake Brienz (Switzerland): deposition of clastic detritus by density currents*. Wiley Online Library.

Sugiyama, M., Hori, T., Kihara, S. & Matsui, M. 1992. A Geochemical Study on the Specific Distribution of Barium in Lake Biwa, Japan. *Geochimica Et Cosmochimica Acta*, **56**, 597-605, http://doi.org/Doi 10.1016/0016-7037(92)90084-V.

Takamatsu, T., Kawashima, M. & Koyama, M. 1985. The role of Mn2+-rich hydrous manganese oxide in the accumulation of arsenic in lake sediments. *Water Research*, **19**, 1029-1032.

Tallantire, P.A. 2002. The early-Holocene spread of hazel (Corylus avellana L.) in Europe north and west of the Alps: an ecological hypothesis. *The Holocene*, **12**, 81-96.

Talling, P.J. 2014. On the triggers, resulting flow types and frequencies of subaqueous sediment density flows in different settings. *Marine Geology*, **352**, 155-182.

Thampapillai, D.J. & Musgrave, W.F. 1985. Flood damage mitigation: A review of structural and nonstructural measures and alternative decision frameworks. *Water Resources Research*, **21**, 411-424.

Thompson, R. 1973. Palaeolimnology and palaeomagnetism. *Nature*, **242**, 182-184.

Thompson, R. 1981. Lake sediment record of the geomagnetic secular variation in Britain during Holocene times. *Geophysical Journal International*, **65**, 703-725.

Thomson, J., Colley, S., Higgs, N., Hydes, D., Wilson, T. & Sørensen, J. 1987. Geochemical oxidation fronts in NE Atlantic distal turbidites and their effects in the sedimentary record. *Geological Society, London, Special Publications*, **31**, 167-177.

Tipping, R. 1995. Holocene evolution of a lowland Scottish landscape: Kirkpatrick Fleming. Part II, regional vegetation and land-use change. *The Holocene*, **5**, 83-96.

Tylmann, W., Bonk, A., Goslar, T., Wulf, S. & Grosjean, M. 2016. Calibrating 210 Pb dating results with varve chronology and independent chronostratigraphic markers: problems and implications. *Quaternary geochronology*, **32**, 1-10.

Van Daele, M., Moernaut, J., Silversmit, G., Schmidt, S., Fontijn, K., Heirman, K., Vandoorne, W., De Clercq, M., *et al.* 2014. The 600 yr eruptive history of Villarrica Volcano (Chile) revealed by annually laminated lake sediments. *Geological Society of America Bulletin*, **126**, 481-498.

Van Daele, M., Moernaut, J., Doom, L., Boes, E., Fontijn, K., Heirman, K., Vandoorne, W., Hebbeln, D., *et al.* 2015. A comparison of the sedimentary records of the 1960 and 2010 great Chilean earthquakes in 17 lakes: Implications for quantitative lacustrine palaeoseismology. *Sedimentology*, **62**, 1466-1496.

Vardy, M.E., Pinson, L.J., Bull, J.M., Dix, J.K., Henstock, T.J., Davis, J.W. & Gutowski, M. 2010. 3D seismic imaging of buried Younger Dryas mass movement flows: Lake Windermere, UK. *Geomorphology*, **118**, 176-187.

Vincent, P.J., Lord, T.C., Telfer, M.W. & Wilson, P. 2011. Early Holocene loessic colluviation in northwest England: new evidence for the 8.2 ka event in the terrestrial record? *Boreas*, **40**, 105-115.

Von Gunten, H. & Moser, R. 1993. How reliable is the210Pb dating method? Old and new results from Switzerland. *Journal of Paleolimnology*, **9**, 161-178.

Walker, M., Johnsen, S., Rasmussen, S.O., Popp, T., Steffensen, J.P., Gibbard, P., Hoek, W., Lowe, J., *et al.* 2009. Formal definition and dating of the GSSP (Global Stratotype Section and Point) for the base of the Holocene using the Greenland NGRIP ice core, and selected auxiliary records. *Journal of Quaternary Science*, **24**, 3-17.

Walker, M.J., Berkelhammer, M., Björck, S., Cwynar, L.C., Fisher, D.A., Long, A.J., Lowe, J.J., Newnham, R.M., *et al.* 2012. Formal subdivision of the Holocene Series/Epoch: a Discussion Paper by a Working Group of INTIMATE (Integration of ice-core, marine and terrestrial records) and the Subcommission on Quaternary Stratigraphy (International Commission on Stratigraphy). *Journal of Quaternary Science*, **27**, 649-659.

Wanner, H., Mercolli, L., Grosjean, M. & Ritz, S. 2015. Holocene climate variability and change; a data-based review. *Journal of the Geological Society*, **172**, 254-263.

Wanner, H., Solomina, O., Grosjean, M., Ritz, S.P. & Jetel, M. 2011. Structure and origin of Holocene cold events. *Quaternary Science Reviews*, **30**, 3109-3123.

Wilby, R., O'hare, G. & Barnsley, N. 1997. The North Atlantic Oscillation and British Isles climate variability, 1865–1996. *Weather*, **52**, 266-276.

Wilhelm, B., Arnaud, F., Sabatier, P., Magand, O., Chapron, E., Courp, T., Tachikawa, K., Fanget, B., *et al.* 2013. Palaeoflood activity and climate change over the last 1400 years recorded by lake sediments in the north-west European Alps. *Journal of Quaternary Science*, **28**, 189-199.

Williamson, C.E., Saros, J.E., Vincent, W.F. & Smol, J.P. 2009. Lakes and reservoirs as sentinels, integrators, and regulators of climate change. *Limnology and oceanography*, **54**, 2273-2282.

Wilson, P. 2005. Paraglacial rock-slope failures in Wasdale, western Lake District, England: morphology, styles and significance. *Proceedings of the Geologists Association*, **116**, 349-361.

Wilson, P. & Smith, A. 2006. Geomorphological characteristics and significance of Late Quaternary paraglacial rock-slope failures on Skiddaw Group terrain, Lake District, northwest England. *Geografiska Annaler Series a-Physical Geography*, **88a**, 237-252.

Wimble, G., Wells, C.E. & Hodgkinson, D. 2000. Human impact on mid-and late Holocene vegetation in south Cumbria, UK. *Vegetation history and Archaeobotany*, **9**, 17-30.

Winfield, I. & Fletcher, J. 2014. Windermere monthly temperatures 1946-2012. *NERC Environmental Information Data Centre* https://doi.org/10.5285/453fdf49-7328-42ec-94b7-1cebf06c51e2.

Wood, J. & Walton, J.K. 2016. *The Making of a Cultural Landscape: The English Lake District as Tourist Destination, 1750-2010*. Routledge.

Woodbridge, J., Fyfe, R.M., Roberts, N., Downey, S., Edinborough, K. & Shennan, S. 2014. The impact of the Neolithic agricultural transition in Britain: a comparison of pollen-based land-cover and archaeological 14 C date-inferred population change. *Journal of Archaeological Science*, **51**, 216-224.

Woolway, R.I., Maberly, S.C., Jones, I.D. & Feuchtmayr, H. 2014. A novel method for estimating the onset of thermal stratification in lakes from surface water measurements. *Water Resources Research*, **50**, 5131-5140.

Young, N.E., Briner, J.P., Rood, D.H., Finkel, R.C., Corbett, L.B. & Bierman, P.R. 2013. Age of the Fjord Stade moraines in the Disko Bugt region, western Greenland, and the 9.3 and 8.2 ka cooling events. *Quaternary Science Reviews*, **60**, 76-90.

Yu, C., Virtasalo, J.J., Österholm, P., Burton, E.D., Peltola, P., Ojala, A.E., Hogmalm, J.K. & Åström, M.E. 2016. Manganese accumulation and solid-phase speciation in a 3.5 m thick mud sequence from the estuary of an acidic and Mn-rich creek, northern Baltic Sea. *Chemical Geology*, **437**, 56-66.

Zolitschka, B. 1998. A 14,000 year sediment yield record from western Germany based on annually laminated lake sediments. *Geomorphology*, **22**, 1-17.

Zolitschka, B., Francus, P., Ojala, A.E. & Schimmelmann, A. 2015a. Varves in lake sediments–a review. *Quaternary Science Reviews*, **117**, 1-41.

Zolitschka, B., Francus, P., Ojala, A.E.K. & Schimmelmann, A. 2015b. Varves in lake sediments - a review. *Quaternary Science Reviews*, **117**, 1-41.